UNIVERSIDADE DE LISBOA

FACULDADE DE FARMÁCIA

Microencapsulated lipid nanoparticles for pulmonary delivery of biopharmaceutical agents

Diana Patrícia Rodrigues Gaspar

Orientador: Professor Doutor António José Leitão das Neves Almeida
Co-orientadores: Professora Doutora María del Carmen Remuñán López
Professor Doutor Pablo Antelo Taboada

Tese especialmente elaborada para obtenção do grau de Doutor em Farmácia na especialidade de Tecnologia Farmacêutica

2017

UNIVERSIDADE DE LISBOA

FACULDADE DE FARMÁCIA

Microencapsulated lipid nanoparticles for pulmonary delivery of biopharmaceutical agents

Diana Patrícia Rodrigues Gaspar

Orientador: Professor Doutor António José Leitão das Neves Almeida
Co-orientadores: Professora Doutora María del Carmen Remuñán López
Professor Doutor Pablo Antelo Taboada

Tese especialmente elaborada para obtenção do grau de Doutor em Farmácia na especialidade de Tecnologia Farmacêutica

Júri

Presidente:
Doutora Matilde da Luz dos Santos Duque da Fonseca e Castro, Professora Catedrática e Directora da Faculdade de Farmácia da Universidade de Lisboa

Vogais:
Doutora María del Carmen Remuñán-López, Titular de Universidad da Facultad de Farmacia da Universidad de Santiago de Compostela, Espanha, orientadora
Doutor Domingos de Carvalho Ferreira, Professor Catedrático da Faculdade de Farmácia da Universidade do Porto
Doutora Ana Margarida Moutinho Grenha, Professora Auxiliar da Faculdade de Ciências e Tecnologia da Universidade do Algarve
Doutora Helena Maria Cabral Marques, Professora Associada com Agregação da Faculdade de Farmácia da Universidade de Lisboa
Doutor Jorge Manuel Barreto Vítor, Professor Auxiliar da Faculdade de Farmácia da Universidade de Lisboa
Doutora Maria Manuela de Jesus Guilherme Gaspar, Investigadora Auxiliar da Faculdade de Farmácia da Universidade de Lisboa

2017

↠ Nothing is impossible,

the word itself says *I'm possible*! ↞

Audrey Hepburn

Table of Contents

Acknowledgements

A realização desta dissertação de doutoramento contou com importantes apoios e incentivos sem os quais não se teria tornado uma realidade e aos quais estarei eternamente grata. Foram, sem dúvida 4 anos intensos, de muita aprendizagem, com altos e baixos, sucessos e insucessos, mas que me tornaram na pessoa a nível pessoal e profissional que sou hoje. Uma tese de doutoramento é muitas vezes descrita como um esforço solitário, no entanto, os meus agradecimentos provam exactamente o contrário.

I would like to express my special appreciation and thanks to my supervisor Professor Dr. António José Leitão das Neves Almeida, he has been a tremendous mentor for me. First, I would like to thank him for believing in me 4 years ago and for all the discussions, for all the opportunities and suggestions to improve my work, and for encouraging my research and for allowing me to grow as a research scientist. His advice on both research as well as on my career have been invaluable. He enabled to broadening my scientific horizons, always providing me with the conditions necessary to complete this work.

Quiero también expresar mi mayor gratitud a mis co-directores, la Profesora Carmen Remuñán-López y el Profesor Pablo Taboada, por acogerme en su laboratorio durante mis estancias en Santiago de Compostela, por sus consejos, su paciencia, por toda la ayuda prestada, por su apoyo en momentos de desánimo y por brindarme todas las herramientas necesarias para culminar esta tesis con éxito.

I would like to extend my special acknowledgment to Doutora Lídia Gonçalves for the unreserved assistance she provided at several levels of this research project and for her insightful comments and encouragement, but also for the hard question which incented me to widen my research from various perspectives.

I acknowledge to the Biochemistry and Human Biology Department and, in particular, I am extremely grateful to Professor Jorge Vítor for the reception in his lab and for the guidance, planning and critical revision of the plasmid studies of this thesis.

I would like to extend my special acknowledgment to Joana Vital for her scientific support and guidance, for having me host and integrated in her lab always in a good mood.

To Professor Ana Grenha and Doutora Manuela Gaspar for their vast knowledge and scientific discussions, as well as being always available to clarify my doubts. They have been very encouraging and supportive, and I express my gratitude to them.

To Eng.Carla Eleutério for all the help provided in HPLC studies.

The members of the Pharmaceutical Technology Department have contributed immensely to my personal and professional time. The group has been a source of friendships as well as good advice and collaboration. I would like to thank, and without particular order, to: Joana Marto, Maria Paisana, Joana Pinto, João Quintas, Vasco Faria, Rui Lopes, Inês Ferreira, Paulo Roque Lino, Marco Cavaco, Bruna Kreutzer, Adeoye Oluwatomide, Beatriz Silva, Joana Bicho, Giuliana Mancini, Carina Peres, Vanessa Sainz, Ana Matos, Liliana Aranha, Barbara Gregori, Lara Figueiredo, André Sá Couto, Nélio Drummond, Ana Costa, Maritza Culma, Mamen Leiva Arrabal and Mariana Dalagnol. It was a pleasure working with all of you! I know that many friends have passed outside the walls of the laboratory.

To iMed.ULisboa Postgraduate Students Commission members, in special to Pedro Rodrigues, Adriano Gigante, Gisela Santos and Tânia Genebra, for the sleepless nights we were working together before meetings and for all the fun we have had in the last years. No doubt belonging to this commission was an added value for me at personal and professional level.

To the board and other members of the Department of Galenic Pharmacy and Pharmaceutical Technology for the best conditions in a scientific and rich environment.

To Dra. Ana Salgado and Mrs. Fernanda Carvalho thank you for the good welcome, continued availability for your concern and good wishes.

To all Chemical Biology and Toxicology Group members, I thank you for the warm welcome they received us in *their space* and how they made us feel *at home*. I would like to thank, and without particular order, to: Sérgio Camões, Bernardo Antunes, Joana Rodrigues, Madalena Cipriano, Inês Vieira da Silva, Professor Fátima Cabral, Professor Ana Bettencourt, Professor Joana Miranda and Professor Nuno Oliveira.

Me gustaría, también, agradecer al resto de los Profesores e investigadores del Departamento de Farmacia y Tecnología Farmaceútica su tiempo y colaboración cuando lo he necesitado, su amabilidad y su disponibilidad. A todos mis colegas y amigos de Santiago de Compostela, pues han sido muchos los momentos inolvidables que he pasado

ahí. ¡Os echo de menos desde que me marché de Santiago! ¡Me habéis acogido desde el primer día, han sido meses de fiesta, de tapas, de amistad y claro, de trabajo y cooperación en el laboratorio! Ana Cadete e Sofia Mendes, obrigada por me fazerem sentir um pouco mais perto de casa quando as saudades apertavam e por todos os passeios que demos pela Galiza! ¡A Inés Fernández Piñeiro, por todos los momentos juntas y todas las risas que me ha sacado! A todos los demás: Andrea Pensado, Jesús Álvarez, Estefanía y Cristina Fernández Paz, Carmen Remuñán Martínez, Carmen García Candeira, Kristin Hölzel, Jacopo Bianchino, Luca Zecchin, Isa Rial, Lidia Pereiro, Patricia Díaz Rodríguez, Luis Díaz, Clara, Rosalía y Helena Rouco Taboada (que por el destino nos volvimos a cruzar en Lisboa). Muchas gracias por vuestro cariño y por tantos y tantos momentos juntos! De manera especial quiero agradecer a Rafael Romero toda la dedicación, los consejos y la ayuda que siempre me ha proporcionado.

Al personal de microscopía electrónica y confocal (CACTUS): Ramiro Barreiro, Raquel Antón, María José Pazos y Mercedes Rivas Cascallar, por toda la amistad, el conocimiento que me han ofrecido en las diferentes técnicas de microscopía, todas las horas pasadas delante de los microscopios y, los bollos de crema que hemos comido juntos.

Una mención especial merecen mis primeras compañeras de piso, Ana Puga y Maria de Matos, que fueron mis pilares en los primeros días en Santiago. Sé que siempre podré contar con vosotras aunque el destino se tuerza y nos lleve por caminos diferentes. Con vosotras las risas tienen otro sentido.

À Covilhã, que será sempre a cidade da minha vida. Obrigada por me ter tornado na pessoa que sou hoje. E como diz a música: *Junto à serra onde faz frio, embalada num berço de lã, ocupaste o meu vazio, oh minha Doce Covilhã!* Obrigada por todas as amizades que nesta cidade construí. E em especial, à Cindy, Dani e Li. Obrigada pela amizade de cada uma, de maneira diferente e em momentos distintos, mas também pelo convívio e interajuda durante todo este percurso. Que seja para sempre a nossa amizade.

À minha amiga Ana Catarina Lima, agradeço de forma especial, pela amizade, bons momentos e por todo o apoio na adaptação à vida de Santiago de Compostela e nos momentos mais difíceis, especialmente nos *tropeços* da vida! Ainda bem que o mundo é minúsculo e nos fez reencontrar em Santiago! Agradeço também por ser *a amiga que está sempre lá* mesmo que a distância também esteja! Agradeço ao João Ferreira, uma boa

aquisição nestes últimos anos, que esteja onde estiver, está sempre disponível quer para me ajudar, quer para me ouvir pacientemente!

Aos meus Pais, Joaquim e Lucinda, agradeço por tudo! *Tudo* não cabe numa folha de papel mas inclui a paciência, o carinho, o apoio constante, mesmo nos momentos de maior desânimo, a força que sempre me transmitiram quando havia quilómetros de distância entre nós e a confiança que sempre depositaram em mim! Obrigada por acreditarem e me fazerem acreditar que tudo seria possível! Obrigada por sempre me deixarem *voar*!

Estendo ainda o meu Muito Obrigada à minha família, Avós, Tios e Tias e Primas, Gabriela, Inês Margarida e Inês Maria, pela amizade, pelo vosso constante apoio e força, mas também pelos momentos de alegria e cumplicidade partilhados. Obrigada por me ensinarem desde cedo a festejar as pequenas vitórias.

Um agradecimento especial à minha Afilhada, Ritinha, por ter sido a minha maior alegria e força durante estes anos que, com um sorriso, uma brincadeira ou carinho, nos momentos mais complicados, me ajudou a prosseguir e concluir esta etapa da minha vida.

A Deus por ser o meu porto de abrigo nas horas de desânimo e inquietação e por ser o meu confidente nas horas de sucesso.

Last, the work presented here was supported by a grant (SFRH/BD/89520/2012) from Fundação para a Ciência e Tecnologia (FCT, Portugal).

Thank you all!

Um bem-haja a todos!

¡Muchas gracias!

Abstract

A key point in the administration of biopharmaceuticals is the recognition of appropriate, effective, safe and biocompatible nanocarriers allowing overcoming extracellular and intracellular biological barriers without loss of drug stability and adequate therapeutic response at the target sites. Since their description by Rainer Müller in the early 1990's, solid lipid nanoparticles (SLN) have been developed as an effective colloidal drug carrier. Under optimized conditions, SLN can be produced for the entrapment of lipophilic or hydrophilic drugs with the essential requirements for an optimum nanoparticulate carrier. Its colloidal size and the controlled release behaviour allow protection and management when administered by parenteral and non-parenteral routes (e.g., oral, nasal and pulmonary).

The pulmonary route has gained interest to the non-invasive administration of biopharmaceuticals on account of the promising anatomical features of the lung, particularly its large absorptive epithelial surface area, low thickness and avoiding the first-pass effect. The lung region where the particles are deposited depends on their aerodynamic diameter. The complex structure of the respiratory tree and the natural defence mechanisms of the lung are fundamental aspects for the design of a proper pulmonary delivery system.

Although pulmonary delivery of nanoparticles has an unquestionable interest, it still requires a complex setup and an aerosolization technique, due to their low inertia and small size, which hindering the deposition in the lung, facilitating the exhalation with air. A promising alternative is the formulation of nanoparticles in inhalable microspheres that ensure their release after pulmonary administration. Microspheres have recently been proposed for pulmonary inhalation as dry powders, since they can be designed to achieve appropriate morphological and aerodynamic characteristics. Previous studies have shown that polymeric nanocarriers loaded in microparticulate systems present a great potential for pulmonary delivery of therapeutic macromolecules and genetic material. These microspheres act only as *inert vehicles* of the nanoparticles, which remain unaltered after the spray-drying process, not affecting the properties or the release profile of the encapsulated active agents, thus constituting a suitable microparticulate carrier for the pulmonary delivery of drug-containing nanoparticles.

In this context a research project has been designed to explore the application and versatility of these micro-nanostructured systems as carriers for therapeutic drugs/proteins and genetic material. The SLN containing an anti-tuberculosis drug, a model peptide or a model plasmid (rifabutin, papain and pEGFP-C1, respectively) were formulated and optimized. Then, for pulmonary administration, SLN were spray-dried using common pharmaceutical excipients (mannitol and trehalose). The integrity and stability of all biomacromolecules studied were not affected by the SLN and microspheres formulation and preparation procedures, which were then considered as suitable for the encapsulation of labile therapeutic molecules. Particularly mannitol and trehalose and the SLN themselves acted as stabilizers of the pharmaceutics during spray-drying. The prepared spray-dried powders displayed good flow and aerosolization properties for pulmonary administration and exhibited high deposition in the lower regions of the respiratory tract determined through a twin-stage liquid impinger, Moreover, the spray-drying process preserved the peculiar nanoparticles features after their disintegration from dry microspheres, exhibiting a sustained release profile of antibiotic and peptide after contact with an aqueous medium containing a lung surfactant. Studies in cell cultures and animal models have revealed the biocompatibility and ability of these nanoparticles to promote the absorption of drugs and peptides through pulmonary epithelium, as well as their excellent potential in gene therapy.

In conclusion, all the results obtained in this experimental work showed the interest of these systems as vehicles for the pulmonary administration of antibiotic drugs and therapeutic proteins and nucleic acids.

Keywords: Microspheres, pulmonary administration, solid lipid nanoparticles, spray-drying.

Resumen

La vía pulmonar presenta un gran interés para la administración no invasiva de biofármacos. Los dispositivos inhaladores de polvo seco, que presentan la ventaja de su esterilidad y estabilidad a largo plazo, revisten hoy un gran interés para la aerosolización pulmonar de fármacos. La liberación pulmonar de nanopartículas presenta un incuestionable interés pero también requiere una compleja puesta a punto y una técnica de aerosolización precisa ya que las nanopartículas individuales, por su baja inercia inherente al pequeño tamaño, no se depositan de manera eficaz en los pulmones sino que son fácilmente exhaladas con el aire. Una alternativa muy prometedora consiste en la formulación de nanopartículas en microesferas fácilmente aerosolizables y que garanticen su liberación tras su administración pulmonar. Desde la primera descripción por Müller, las nanopartículas lipídicas sólidas (SLN) preparadas ya sea com lípidos fisiológicos o lípidos utilizados como excipientes farmacéuticos, han atraído una creciente atención como eficaz transportador coloidal de fármacos. Bajo condiciones optimizadas, SLN pueden ser producidos para incorporar/asociar un amplio abanico de moléculas terapéuticas (fármacos lipofílicos o hidrofílicos, péptidos, proteínas, DNA, siRNA).

En este trabajo de tesis se desarrolló una nueva plataforma de liberación consistente en sistemas nanotransportadores microencapsulados, con indiscutible potencial para la administración pulmonar de antibióticos, macromoléculas terapéuticas y material genético. Las SLN, elaboradas a partir de lípidos sólidos, utilizando el método de dispersión-fusión fueron posteriormente encapsuladas en microesferas de manitol y trehalosa mediante un procedimiento de atomización-secado, resultando en sistemas micro-nanoestructurados (polvos secos) con propiedades superficiales, estructurales y aerodinámicas adecuadas para administración pulmonar. Las microesferas únicamente actúan como vehículos inertes de las SLN, que permanecen inalteradas tras el proceso de co-atomización y son fácilmente recuperadas intactas en medio acuoso, no viéndose afectado su tamaño, carga superficial ni perfil de liberación de la biomacromolécula encapsulada. Con el objeto de explorar la aplicación y versatilidad de estos sistemas micro-nanoestructurados como vehículos de antibióticos, proteínas terapéuticas y material genético, se procedió a investigar la asociación y liberación de un fármaco utilizado contra la tuberculosis (rifabutina), de un péptido modelo (papaína) y un plásmido modelo (pEGFP-C1). Se comprobó que las biomacromoléculas no habían visto afectada su

estabilidad por su procesado mediante las técnicas de dispersión-fusión y atomización. El procedimiento resulta interesante para la encapsulación de moléculas terapéuticas lábiles, actuando tanto el manitol y la trehalosa como las propias SLN como estabilizantes de los biofármacos durante la atomización. Los polvos obtenidos por atomización mostraron propiedades adecuadas de flujo y aerosolización para administración pulmonar, depositándose de manera elevada en las regiones inferiores del tracto respiratorio, preservando las peculiares características de las nanopartículas después de su desintegración a partir de microesferas secas. Además, el proceso de secado por pulverización no alteró las características de las SLN nativas, exhibiendo un perfil de liberación sostenida de antibiótico y péptido después del contacto con un medio acuoso que contenía un tensioactivo pulmonar. Estudios realizados en cultivos celulares y modelos animales, han revelado la biocompatibilidad y capacidad de estas nanopartículas de promover la absorción de medicamentos y péptidos a través de lo epitelio pulmonar, así como su excelente potencial en terapia génica. La interacción *in vitro* de las nanopartículas fluorescentes con los macrófagos demostró que los macrófagos representan una de las vías de eliminación de nanopartículas del pulmón.

En definitiva, el conjunto de los resultados obtenidos en este trabajo experimental pone de manifiesto el interés de estos sistemas como vehículos para la administración pulmonar de fármacos y proteínas terapéuticas.

Palabras-claves: Administración pulmonar, atomización, microesferas, nanopartículas lipídicas sólidas.

Resumo

Um ponto-chave na administração de substâncias activas é a formulação de nanotransportadores apropriados, eficazes, seguros e biocompatíveis, que permitam transpor barreiras biológicas extracelulares e intracelulares sem perda da estabilidade e resposta terapêutica do fármaco até atingir os locais alvo. Desde a sua primeira descrição por Rainer Müller no princípio da década de 1900, as nanopartículas lipídicas sólidas (SLN) têm sido estudadas como um eficaz transportador coloidal dos mais variados tipos de fármacos, incluindo moléculas de natureza peptídica e material genético. As SLN são preparadas com lípidos fisiológicos e tensioactivos que permitem a sua estabilização. Sob condições optimizadas, as SLN podem incorporar fármacos lipofílicos ou hidrofílicos e o seu tamanho coloidal e comportamento de libertação controlada permitem a protecção das moléculas encapsuladas após administração por vias não parentéricas e parentéricas.

Nos últimos anos, a via pulmonar tem ganho interesse na administração não invasiva de substâncias activas. A região pulmonar onde as partículas são depositadas depende sobretudo do seu diâmetro aerodinâmico. Por outro lado, a estrutura complexa da árvore respiratória, bem como os mecanismos naturais de defesa do pulmão, são aspectos fundamentais para a formulação de um sistema para administração pulmonar adequado. Neste contexto, os dispositivos de inalação de pó seco apresentam vantagens, como a sua fácil esterilização e estabilidade a longo prazo e, por isso, têm ganho um enorme interesse na aerossolização de fármacos. Também a administração pulmonar de nanopartículas tem ganho um interesse inquestionável. No entanto, devido à sua baixa inércia e tamanho reduzido, as nanopartículas apresentam dificuldades de deposição nos pulmões, favorecendo a sua exalação. Assim, a formulação de nanopartículas em microesferas inaláveis, que asseguram a sua libertação após a administração pulmonar mantendo as características primárias, tem sido amplamente investigada. Estudos anteriores demostraram que nanopartículas poliméricas microencapsuladas apresentam um grande potencial na libertação pulmonar de macromoléculas terapêuticas. Para tal, as nanopartículas são incorporadas em microesferas através de um processo de secagem por atomização (*spray-drying*), resultando em sistemas micro-nanoestruturados (pó seco) com adequadas propriedades estruturais e aerodinâmicas para administração pulmonar. Estas microesferas são constituídas por excipientes inertes e não-tóxicos e autorizados pelas agências regulamentares, actuando como veículo inerte das nanopartículas e como

termoprotectores das nanopartículas. Por outro lado, os nanotransportadores devem-se manter inalterados após o processo de atomização, não afectando as propriedades físico-químicas ou o perfil de libertação dos agentes activos encapsulados.

Assim sendo, o objetivo geral deste projeto centra-se no desenvolvimento de novos sistemas micro-nanoestruturados compostos por SLN encapsuladas em microesferas de manitol e trealose com propriedades adequadas para a administração pulmonar de substâncias activas. As substâncias activas usadas foram um antibiótico tuberculostático, uma proteína modelo e um plasmídeo, respectivamente, rifabutina (RFB), papaína (PAP) e pEGFP-C1. Para a sua incorporação nas SLN, diferentes métodos de associação foram usados. No caso da RFB, este antibiótico foi encapsulado na própria matriz lipídica durante a formulação das SLN. Por outro lado, a PAP foi adsorvida à superfície das nanopartículas enquanto o plasmídeo ficou confinado entre duas camadas poliméricas com carga positiva que por sua vez estavam adsorvidas à carga negativa da superfície das SLN. Nestes últimos dois casos, as moléculas foram associadas às SLN após a sua formulação. Os fármacos modelos incorporados nos diferentes nanoveículos foram utilizados com o intuito de caracterizar intensivamente as novas formulações desenvolvidas, e compreender os mecanismos de libertação, assim como estudar a sua eficácia terapêutica *in vitro* e *in vivo*.

Dois diferentes tipos de SLN foram formulados e optimizados pela técnica de homogeneização de alta pressão a altas temperaturas, um à base de dibe-henato de glicerilo e outro de triestearato de glicerilo. Esta técnica apresenta a vantagem de não usar solventes orgânicos nem necessitar da aplicação de ultrassonicação. Em seguida, as nanopartículas foram caracterizadas em termos físico-químicos e de estabilidade, concluindo-se que as SLN apresentam um tamanho na escala nanométrica, com uma polidispersão homogénea, carga superfície dependente do método de associação da substância activa sem perda de estabilidade física e actividade da própria molécula terapêutica. Estudos de citotoxicidade e de internalização em linhas celulares pulmonares relevantes (A549, Calu-3 e em monócitos diferenciados em macrófagos) confirmaram a biocompatibilidade das nanopartículas e revelaram ainda que as SLN apresentam capacidade de internalização por macrófagos.

Numa fase seguinte, as SLN, através da técnica de atomização, foram microencapsuladas usando manitol e trealose como excipientes. As propriedades aerodinâmicas de densidade, tamanho, fluidez e humidade residual foram avaliadas, apresentando

resultados aceitáveis para administração pulmonar. Estudos de deposição e de aerossolização revelaram que os pós, quando administrados por um dispositivo adequado, apresentam características apropriadas para serem depositados na zona alveolar.

As SLN contendo RFB demonstraram ter uma elevada eficiência de encapsulação do antibiótico, próxima da solubilidade do fármaco na matriz lipídica. Por análise térmica observou-se que a RFB encontra-se dissolvida na matriz das nanopartículas, que as nanoformulações eram estáveis quando sujeitas a altas temperaturas e que, após arrefecimento, recuperavam o seu tamanho nanométrico e a sua morfologia esférica e compacta. As SLN foram facilmente internalizadas por monócitos humanos, sendo uma característica importante, uma vez que o bacilo da Tuberculose (TB) é um parasita intracelular alojado nos macrófagos alveolares. Após incubação das SLN-RFB com células pulmonares, não foi observada citotoxicidade, confirmando assim que as SLN são potenciais sistemas transportadores para a administração pulmonar de fármacos anti-TB.

Numa fase posterior, estas RFB-SLN foram encapsuladas em microesferas de mannitol e trealose por um processo de secagem por atomização, resultando em pós secos com propriedades aerodinâmicas e estruturais adequadas para administração pulmonar. Esta técnica de microencapsulação permite superar os problemas de estabilidade das formulações de nanopartículas líquidas, bem como atingir a zona alveolar após inalação. A análise estrutural por microscopia electrónica de varrimento e por microscopia de confocal indicou que as microesferas são esféricas com limites bem definidos e que as SLN foram eficientemente encapsulados nas microesferas, apresentando uma distribuição homogénea dentro das microesferas. A caracterização física por calorimetria de titulação isotérmica demonstrou que as SLN têm maior afinidade para o manitol do que para a trealose durante o processo de atomização, favorecendo as interacções entre as SLN e o manitol. Após dissolução *in vitro* das microesferas de manitol e trealose, as SLN permitiram a libertação da RFB ao final de 24 h de incubação em meio contendo o tensioactivo pulmonar (> 95% de libertação no caso das SLN microencapsuladas em manitol e cerca de 80% para as SLN microencapsuladas em trealose). As micro-nanoformulações mantiveram a actividade intracelular anti-TB da RFB. Estudos *in vivo* demonstraram que os pós são eficazes para administração pulmonar da RFB, reduzindo o índice de crescimento da infecção nos órgãos estudados. Desta forma, confirma-se que as SLN microencapsuladas são uma plataforma promissora para a administração pulmonar de antibióticos terapêuticos, podendo contribuir para a melhoria do tratamento da TB.

Numa etapa posterior, foi utilizado um processo de adsorção para associar uma proteína modelo, PAP, à superfície das SLN de dibe-henato de glicerilo e de triestearato de glicerilo, previamente optimizadas com o intuito de serem passíveis de administração pulmonar. A adsorção da PAP à superfície das SLN segue uma isotérmica de adsorção do tipo Freundlich sobre o intervalo de concentrações estudado, sugerindo um modelo de multicamadas de proteína na superfície das SLN através da interação eletrostática entre os grupos amina da PAP e a carga negativa das SLN. O processo de adsorção, bem como o processo de microencapsulação das PAP-SLN em manitol e trealose, foram confirmados por diferentes técnicas de caracterização de superfície. Os pós obtidos por atomização, para além de possuírem características aceitáveis para deposição pulmonar, permitiram também manter a actividade enzimática da PAP. Em conjunto, estes resultados são um indicador encorajador da utilização das SLN microencapsuladas como transportadores de proteínas para administração pulmonar.

Por forma a analisar a versatilidade das SLN de dibe-henato de glicerilo e de triestearato de glicerilo como transportadores de material genético, estas dispersões foram modificadas com um polímero catiónico, o quitosano (CS). Posteriormente, o plasmídeo modelo (pEGFP-C1) foi incorporado à superfície das SLN e protegido pelas camadas de CS. Os nanosistemas policatiónicos demonstraram ter uma afinidade elevada para o plasmídeo, proporcionando protecção ao pEGFP-C1 encapsulado quando sujeito à degradação por endonuclease específicas. As nanoformulações demonstraram baixa citotoxicidade celular e uma elevada taxa de transfecção em células pulmonares. As SLN modificadas foram atomizadas com manitol e trealose, formando microesferas com características adequadas para administração de genes ao nível pulmonar. Por sua vez, estas microesferas garantiram a estabilidade, protecção e funcionalidade do pEGFP-C1.

No geral, estes resultados evidenciam a versatilidade das SLN como veículos transportadores seguros e eficazes de substâncias activas para o desenvolvimento de sistemas de libertação ao nível pulmonar, podendo ser utilizados em abordagens terapêuticas inovadoras.

Palavras-chaves: Administração pulmonar, microesferas, nanopartículas lipídicas sólidas, secagem por atomização.

List of Abbreviations and Acronyms

ACI	Andersen cascade impactor
AFM	Atomic force microscopy
CFU	Colony-forming units
CLSM	Confocal laser scanning microscopy
CS	Chitosan
d_{aer}	Aerodynamic diameter
DL	Drug loading
DLS	Dynamic light scattering
DMSO	Dimethylsulfoxide
DOX	Doxorubicin
DPI	Dry powder inhaler
DPPC	1,2-dipalmitoyl-*sn*-glycero-3-phosphocholine
DSC	Differential scanning calorimetry
EE	Encapsulation efficiency
FPF	Fine particle fraction
FTIR	Fourier transform infrared spectroscopy
GFP	Green fluorescent protein
HPLC	High-performance liquid chromatography
HPMC	Hydroxypropyl methylcellulose
HSH	High shear homogenization
ITC	Isothermal titration calorimetry
LD	Laser diffractometry
LDC	Lipid drug conjugate
MAC	*Mycobacterium avium-intracellulare* complex
MMAD	Mass median aerodynamic diameter
m.p.	Melting point
MSLI	Multistage liquid impinger
MTS	(3-(4,5-dimethylthiazol-2-yl)-5-(3-carboxymethoxyphenyl)-2-(4-sulfophenyl)-2H-tetrazolium)
MTT	3-(4,5-dimethyl-2-thiazolyl)-2,5-diphenyl-2H-tetrazolium bromide
MW	Molecular weight
NGI	Next-generation impactor
NLC	Nanostructured lipid carriers
PAP	Papain
PBCA	Poly(butylcyanoacrylate)
PBS	Phosphate buffered saline
PCL	Poly(caprolactone)
PCS	Photon correlation spectroscopy
pDNA	Plasmid DNA
PEG	Poly(ethylene glycol)
PI	Polydispersity index
pKa	Dissociation constant
PLGA	Poly (lactic-*co*-glycolic acid)
PMA	Phorbol 12-myristate 13-acetate
PVA	Poly(vinyl alcohol)
PY	Production yield
RFB	Rifabutin

SCF	Supercritical fluids
SDS	Sodium dodecyl sulphate
SEM	Scanning electron microscopy
SFD	Spray-freeze-drying
SLN	Solid lipid nanoparticles
TB	Tuberculosis
TEM	Transmission electron microscopy
$\mathbf{T_{inlet}}$	Inlet temperature
$\mathbf{T_{outlet}}$	Outlet temperature
TPP	Tripolyphosphate
TSLI	Twin-stage liquid impinger
URF	Relative fluorescence unit
XPS	X-ray photoelectron spectroscopy

$\Delta \mathbf{H}_i^{\boldsymbol{i}}$	Enthalpy
$\Delta \mathbf{S}_i^{\boldsymbol{i}}$	Entropy
$\mathbf{K}^{\boldsymbol{i}}$	Binding constant
$\boldsymbol{n}^{\boldsymbol{i}}$	Stoichiometry
$\boldsymbol{\rho}$	Density

List of Figures

Chapter 1

Chapter 2

Chapter 3

Chapter 4

Chapter 5

List of Tables

Chapter 1

Chapter 2

Chapter 3

Chapter 4

Chapter 5

Aims and Organization of the Thesis

Over the last years, absorption of therapeutic macromolecules administered by pulmonary route has received great attention. The large alveolar surface area suitable for drug absorption, low thickness epithelial barrier, extensive vascularization and relatively low proteolytic activity compared to other administration routes, together with the absence of the first-pass effect, make the pulmonary delivery an outstanding target. However, the issue for a reliable and specific lung protein delivery is the design of adequate carrier systems. The delivery of biopharmaceuticals as dry powders with suitable characteristics for inhalation presents advantages when compared with liquid formulations, for instance where stability and patient compliance are concerned.

Microspheres have been proposed for pulmonary administration because they can be designed to achieve appropriate morphological and aerodynamic characteristics for that purpose. The success of the inhaled particles depends mostly on their size and density, and hence, aerodynamic diameter (d_{aer}). The respirable fraction of these powders, generally the fraction of particles with an d_{aer} ranging from 1 to 5 μm, should be as high as possible to guarantee a maximum deposition in the deep lung and, consequently, a systemic adsorption.

The main objective of this doctoral thesis, which began 1st January 2013, was the investigation of microencapsulation of solid lipid nanoparticles (SLN) as a hybrid particulate delivery system for pulmonary delivery of different kinds of biopharmaceutical agents, such as, low molecular weight drugs, proteins and nucleic acids. It involved the study and optimization of SLN formulation containing the three model drugs, the feasibility of the spray-drying technique for SLN microencapsulation, as well as the *in vitro* and *in vivo* performance of the resulting dry powders.

The emphasis of this research work was put on the development and in-depth characterization of microencapsulated SLN in a dry powder form intended for pulmonary administration with therapeutic purposes. This microencapsulation technique allowed improving the nanoparticles efficiency for inhalation. In addition, the versatility of these developed lipidic carriers was also investigated as carriers of drugs, proteins and peptides or nucleic acids through different association mechanisms of the biopharmaceuticals in the nanoparticles.

All the research and scientific work results from a joint partnership between the Faculty of Pharmacy, University of Lisbon, Portugal and the Faculty of Pharmacy and the Faculty of Physics, University of Santiago de Compostela, Spain. The financial support of the entire research project was given through a PhD grant (SFRH/BD/89520/2012) by Portuguese Foundation for Science and Technology, between January 2013 and December 2016. The experimental work that supports this thesis was performed at the Departamento de Farmácia Galénica e Tecnologia Farmacêutica of the Faculty of Pharmacy, University of Lisbon, at the Departamento de Farmacología, Farmacia y Tecnología Farmaceútica, Faculty of Pharmacy, University of Santiago de Compostela and at the Departamento de Física de la Materia Condensada, Faculty of Physics, University of Santiago de Compostela.

The present thesis is divided into 6 chapters. The first chapter corresponds to the general introduction of the thesis. The following 4 chapters provide detailed information on the obtained experimental results and their discussion. The last chapter compiles the final remarks and the future perspectives in the context of this research project. The chapters of this thesis are all based on peer-reviewed papers, either published or submitted for publication. The following paragraphs summarize the content of each chapter.

↠ *Chapter 1* reviews the literature on microencapsulation of nanoparticles intended for pulmonary administration, describing the suitable aerodynamic characteristics of these hybrid particles for lung delivery of biopharmaceuticals, such as drugs, proteins and genetic material. It also analyzes and discusses the potential and the future directions for inhalation therapy using dry powders composed of microencapsulated nanoparticles.

↠ *Chapter 2* describes the formulation, optimization and characterization of rifabutin (RFB)-loaded SLN prepared by a hot high shear homogenization technique, using glyceryl dibehenate and glyceryl tristearate as the lipidic phase. Studies included morphology and stability analysis, physical characterization, *in vitro* cytotoxicity tests and *in vitro* release, as well as, *in vitro* uptake.

↠ *Chapter 3* reports the microencapsulation studies of the previous developed RFB-loaded SLN via spray-drying using the biocompatible and safe excipients, mannitol and trehalose. The optimal dry powder formulations were selected and fully characterized in terms of morphology by microscopy techniques, aerodynamic and powder flow properties

(for instance, d_{aer}, density, moisture residual content), as well as *in vitro* deposition studies using a twin-stage liquid impinger (Ph. Eur. 2.9.18. Apparatus A). *In vitro* drug release from the nanoparticles and from the SLN-containing microparticles (i.e. dry powders) was also evaluated, as well as bacteriological studies aiming to evaluate the RFB activity throughout the formulation procedures. *In vivo* studies using a murine model were performed to establish the effective drug dose by the inhalation route.

↠ *Chapter 4* comes in the sequence of the previous chapters, now applying the formulation strategy to a model protein molecule (papain). This enzyme was associated to the preformed SLN using adsorption procedure, to avoid the harsh temperature and agitation conditions involved in the nanoencapsulation procedure. The protein-loaded SLN were then microencapsulated in mannitol or trehalose microparticles using spray-drying. Full characterization was performed in terms of morphology, adsorption process and molecular interactions between the protein and the nanoparticles. Furthermore, a complete physical characterization of the obtained dry powders was also done.

↠ *Chapter 5* describes the formulation and characterization studies of dry powders composed by hybrid microencapsulated SLN containing a model plasmid for pulmonary administration. The model plasmid (pEGFP-C1) was associated to chitosan-coated SLN. The nanoparticle structure consisted of a lipidic core coated with two polymeric layers between which the plasmid was entrapped. After microencapsulation by spray-drying, the physical and aerodynamic characteristics of both complex structured dry powders systems were studied to evaluate their potential for pulmonary applications. *In vitro* characterization included transfection in relevant pulmonary cell lines (Calu-3 and A549). pEGFP-C1 stability and integrity studies after nanoformulation and subsequent microencapsulation was also performed in order to highlight this strategy for pulmonary delivery of genetic material.

↠ *Chapter 6* describes the general discussion and main conclusions of the developed work, focusing on the current limitations and the future perspectives of the formulation strategy herein investigated and proposed.

This page was intentionally left blank.

Chapter 1

General introduction - Particle engineering by nanoparticle microencapsulation for pulmonary delivery

This chapter is partially based on the following publication:
Gaspar DP, Faria V, Quintas J and Almeida AJ. *Targeted delivery of lipid nanoparticles by means of surface chemical modification.* 2016. *Accepted for publication*.

This page was intentionally left blank.

Abstract

The lung offer a large surface area for absorption, rich blood circulation, high permeability and limited proteolytic activity when compared with other administration routes, which makes it an ideal route for non-invasive administration of therapeutics. Localized delivery shows great promise not only in the treatment of respiratory diseases (such as asthma, tuberculosis (TB), influenza, cystic fibrosis), but also reduces the systemic toxicity. Alternatively, systemic drug delivery can be achieved by targeting the alveolar region where the active agents can be absorbed through a thin layer of epithelial cells and into the systemic circulation, leading to enhanced permeability, a rapid onset of action and avoidance of first-pass metabolism. Nanotechnology has potential in the development of novel and effective delivery systems of drugs for pulmonary administration. Different strategies have been utilized for pulmonary delivery of therapeutics, including the use of lipid-based delivery systems (liposomes, solid lipid nanoparticles), polymeric matrix and polysaccharide particulates (poly(lactic-co-glycolic acid), poly (caprolactone), cynoacrylates, gelatin, chitosan, alginate), biocompatible metallic inorganic particles (iron, gold, zinc), among others. Due to their extremely small sizes, the nanoparticles suffer many problems related to their surface and thermal stability, shape preservation, handling and others. It is therefore an important challenge to overcome these issues by developing larger particles (e.g., on the micrometer scale) in which the characteristics from the included nanocarriers are preserved. One approach to this is to trap nanoparticles in a micrometer-sized inert matrix. A novel particulate form incorporating nanoparticles into micron-scale structures has been engineered through suitable techniques, such as spray-drying, spray-freeze-drying and supercritical fluid technology, aiming to overcome the problems of storing and delivering nanoparticles to the lung. This chapter highlights various microencapsulated nanoparticles approaches in the form of lipids, polymers, metals, polysaccharides, or emulsions based for pulmonary drug delivery with proper aerodynamic characteristics for this purpose that could provide an increased biological efficacy and better local and systemic action.

Graphical Abstract

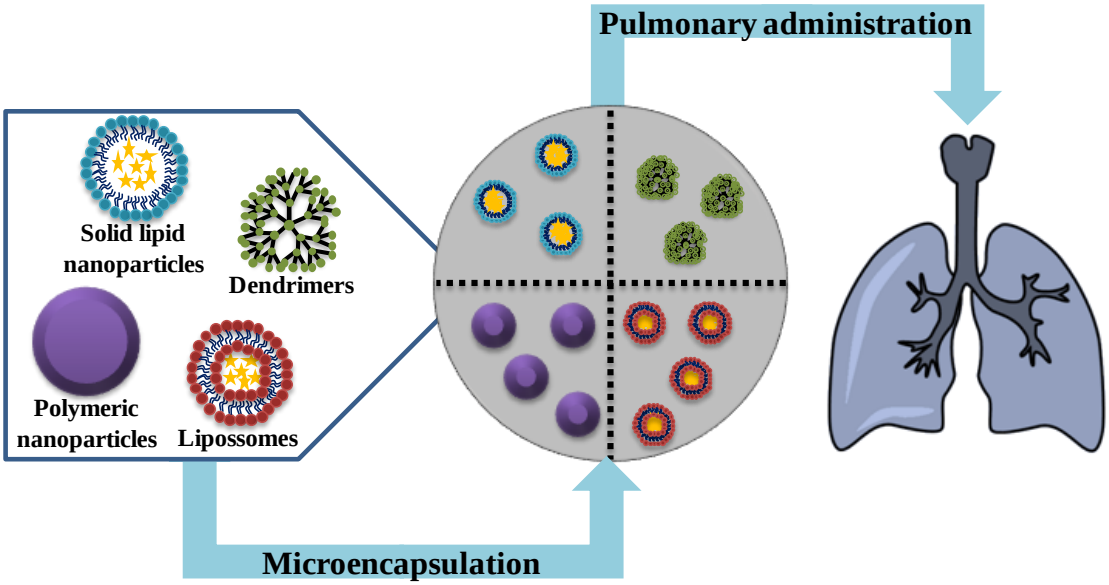

1.1. Drug delivery systems based on nanoparticles

Particulate systems have been widely used as drug delivery carriers to prevent or treat a variety of diseases. In the particular case of pharmaceutical applications, the discovery of new active substances (e.g. peptides, proteins and nucleic acids) brings new challenges related to the needs of overcoming the deficient solubility/stability of a large number of these substances of both synthetic and biotechnological origin, as well as of improving the efficiency and safety profiles of *old drugs* as a way to extend their therapeutic and commercial value [1, 2]. The microencapsulation or nanoencapsulation of drugs into optimized particles is opening new opportunities. In general terms, encapsulation is the process to confine active agents in envelopes of polymeric, lipid or other protective materials, generally in a particulate form, in order to confer protection, control the release and/or even target the molecules to the site of action [3-5]. Its application to medicine and pharmacy has been extensively studied for taste masking, entrapment of irritant or unstable drugs and for sustained and site-specific release of drugs.

The development of nanoparticles for drug delivery began in the 1960s by Birrenbach and Speiser [6]. The nanoparticles are most commonly referred as solid colloidal particles ranging in size from 1 to 1000 nm (1 μm). Moreover, nanoparticles have the potential to revolutionize a wide range of medical diagnostic and therapeutic interventions such as diagnostic imaging, implantable devices and, of particular interest in this review, drug delivery [7]. Due to their small sizes, the nanostructures exhibit unique physicochemical and biological properties (e.g., an enhanced reactive area as well as an ability to cross cell and tissue barriers) that make them a favorable material for biomedical applications. Their nanosize also promotes a uptake by cells more easily than larger particles [8]. They transport the therapeutic macromolecule to the site of action, thus its influence on healthy tissues and cells and undesirable side effects can be minimized. They also protect the drug from rapid degradation or clearance and enhance drug concentration in target tissues, therefore lower doses of drug are required [8].

In fact, nanoparticles can be used to deliver hydrophilic drugs, hydrophobic drugs, proteins, biological macromolecules and nucleic acids via a number of routes [9]. Additionally, several strategies have been proposed to regulate the association and, consequently, the drug release, playing with the materials used to produce the nanoparticles as well as with their structural design. For example, drugs can be entrapped

in the nanocarrier matrix, encapsulated in a nanoparticle core, surrounded by a shell-like membrane, chemically conjugated to the nanoparticle matrix (e.g. covalent bonds, electrostatic interactions, among others) or bound to the particle's surface by adsorption [8-10]. Besides the nanostructures, they can be formulated for targeted delivery to the lymphatic system, brain, arterial walls, lung, liver, spleen, or made for long-term systemic circulation [9]. After reaching the target site, the nanoparticles can release the associated therapeutic agent in a controlled manner which depends on their nature, pH, osmotic gradient and the surrounding environment [8].

The nanoparticles used for medical applications must be biocompatible, biodegradable and non-toxic. Undesirable effects associated to nanoformulations strongly depend on their hydrodynamic size, shape, surface chemistry, administration route, interaction with the immune system and residence time in the bloodstream. Nanoparticulate systems as different as liposomes, solid lipid nanoparticles (SLN), polymeric nanoparticles, metallic nanoparticles or dendrimers have been used as drug carriers for routes of administration such as oral, transdermal, intravenous, subcutaneous and pulmonary [4].

In addition to their controlled or triggered release properties, nanoparticles can also be designed to afford longer circulation times, reducing unwanted distribution and promoting targeting to the site of action. The ability to provide specific drug delivery to target sites is among the characteristics of an ideal drug delivery system. In this context, nanoparticles functionalization, resulting in a stealth surface avoiding the opsonisation phenomenon (adhesion of serum proteins at the nanoparticles surface), is necessary to increase circulation times by escaping the mononuclear phagocyte system. For example, nanoparticles may be conjugated, grafted or coated with hydrophilic polymers, e.g. poly(ethylene glycol) (PEG) (strategy called as PEGylation), affording steric stabilization, conferring stealth properties and being the most frequent and successful approach to delay the circulation time of nanoparticulate systems and protein drugs in the blood flow [11, 12]. Moreover, with the aim to improve targeting, the nanoparticles surface can also be functionalized using specific ligands (aptamers, peptides, antibodies/antibody fragments, small molecules, among others) (Figure 1.1) [5].

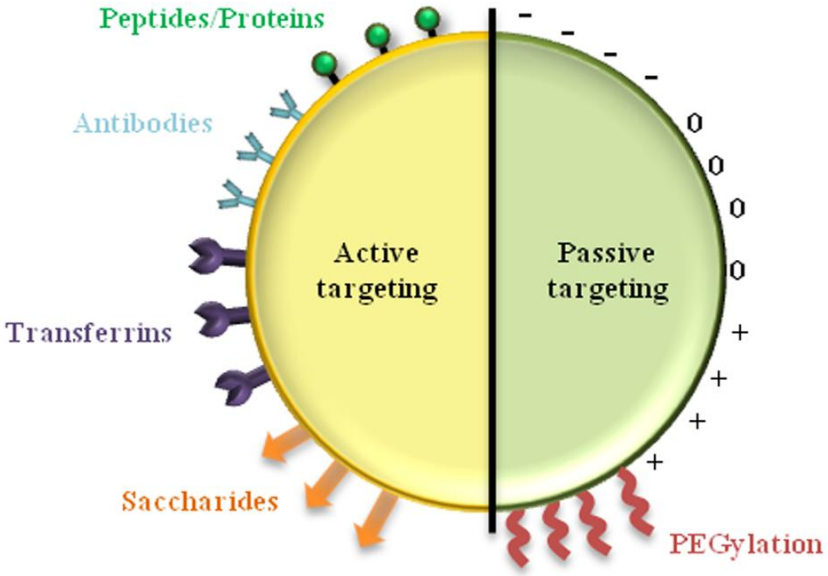

Figure 1.1: Surface functionalization of nanoparticles with the aim to increase residence time in the blood, to reduce nonspecific distribution and to target tissues or specific cells. The chemistry at surface and bulk levels, as well as the physical features such as size, porosity, surface topography, shape and compartmentalization should be carefully considered during the design/optimization and targeting of particulate systems for biomedical applications [5].

The first nanoparticles licensed as a medicine was AmBisome® (Astellas Pharma), a liposomal amphotericin B formulation for the treatment of fungal infections, which led to the development of other successful liposomal nanoformulations, intended mainly for cancer treatment and infectious diseases, such as Doxil®/Caelyx® (doxorubicin (DOX), Janssen-Cilag) [13], Myocet® (DOX, Teva B.V.), Daunoxome® (daunorubicine, Galen Limited), Marqibo® (vincristine, Talon Therapeutics Inc.), Mepact® (mifamurtide, Takeda), Abelcet® (amphotericin B, Sigma-Tau Pharmaceuticals) and Depocyt® (cytarabine, Sigma-Tau Pharmaceuticals). More recently paclitaxel formulated as albumin-nanoparticles has been marketed for the treatment of metastatic breast cancer (Abraxane®, Celgene Corporation), while DOX-loaded polyalkylcyanoacrylate nanoparticles are in phase III clinical trials for the treatment of the multidrug resistant hepatocarcinoma (Transdrug®, Bioalliance) [14].

However, currently available nanoparticulate formulations have not been able to enhance the activity for many active substances, with the exception of Abraxane® and Endorem® (dextran-stabilised superparamagnetic iron oxide nanoparticles, Guerbet). According to Couvreur [14], these failures may be caused by: (i) poor drug loading (DL) capacity impeding a pharmacologically suitable concentration at the target site, or the quantity of particles required is too high, leading to unwanted adverse reactions; (ii) too quick release i.e. burst release of the active substance after administration, generally corresponding to the immediate release of the drug that is located at the particle surface, leading to an early release before reaching the site of action; (iii) polymer cytotoxicity after internalization into cells, and (iv) the need of a large-scale production of polymeric nanoparticles which also reduces the current relevance of these carrier systems in the market.

1.2. Types of nanoparticles

The nanoparticles exist in a wide variety of natures, sizes, shapes and compositions, including metals and inorganic particles, such as gold, silver, and metal oxides, polymer-based materials, such as poly (lactic-*co*-glycolic acid) (PLGA) and lipid-based particles, such as liposomes, SLN and nanoemulsions (Figure 1.2) [7, 15, 16]. Each substance exhibits its own inherent physicochemical properties, e.g. surface charge, hydrophilicity/hydrophobicity, solubility, size, shape and tendency to aggregation, which can be engineered to trigger different biological responses. Furthermore, in drug delivery it is crucial to evaluate the nanocarrier's biocompatibility to ensure safe drug release and minimize cytotoxicity [7]. The description of the several types of nanoparticles is out of the scope of the present thesis, which is focused only on lipid-based nanoparticles.

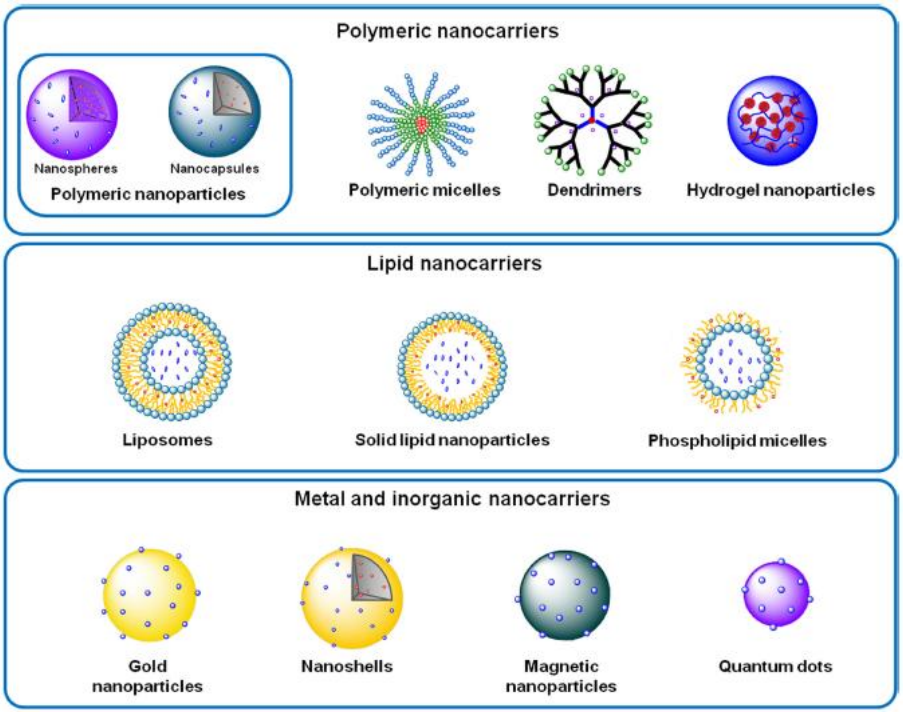

Figure 1.2: Different types of nanoparticles commonly used for biomedical applications [17].

1.2.1. Liposomes

Liposomes have been the first system investigated as colloidal drug carriers about 40 years ago [18]. They are spherical bilayers vesicles composed of phospholipids (phosphatidylcholine, phosphatidylglycerol, phosphatidylethanolamine and phosphatidylserine) and steroids (e.g., cholesterol) or other surfactants, and they are formed spontaneously when certain lipids are dispersed in an aqueous media by sonication [8, 19]. Liposomes have been reported to improve the pharmacokinetic properties of drugs and the therapeutic index of chemotherapeutic agents, reduce unwanted side effects and increase *in vitro* and *in vivo* anticancer activity [8]. Indeed they were the first marketed nanoformulation (as such), being introduced in 1990 (AmBisome®, Astellas Pharma). However, limitations of liposomes include low encapsulation efficiency (EE), rapid leakage of water-soluble drug in the presence of blood components and poor storage stability. Stability and structure integrity of liposomes after administration can be conferred by their surface functionalization by attaching polymers, such as poly (methacrylic acid-co-stearyl methacrylate). On the other hand, the

circulation time of liposomes in the blood can be enhanced by adding PEG chains or by surface conjugation of antibodies or ligands, such as lectins [8, 19].

There are many examples of liposomal drug formulations, such as anticancer drugs, neurotransmitters (serotonin), antibiotics, anti-inflammatory and anti-rheumatic drugs [8]. Despite their advantages, the unresolved problem of using drug delivery systems based on liposomes arises from their accumulation in cells (liver macrophages) outside the target tissues and the unpredictable effects dependent on the active agent they carry [8]. Applications of liposomes include transdermal drug delivery to enhance skin permeation of drugs with high molecular weight (MW) and poor water solubility [20] or chemotherapeutic drug delivery in cancer treatment [21], drug delivery to the lung by nebulisation [22], ocular drug delivery [23] and the treatment of parasitic infections. Other vesicular structures similar to liposomes have emerged mainly intended for transdermal delivery, including transferosomes, ethosomes, niosomes and marinosomes [24-26]. Briefly, transferosomes are developed by incorporation of surfactant molecules, such as sodium chlorate into liposomes, while ethosomes are liposomes presenting a high ethanol content (up to 45%). Niosomes are vesicles developed from non-ionic surfactants and marinosomes are liposomes produced from a natural marine lipid extract containing a high poly (unsaturated) fatty acid ratio [19].

1.2.2. Nanoparticles based on solid lipids

The use of micro- and nanoparticles made of solid lipids was first reported by Speiser *et al.* [27], who described the production of *lipid nanopellets* intended for oral drug delivery. The technique then developed involved the cooling of an emulsion prepared with molten lipids. In 1993, Domb proposed a similar procedure to prepare the so-called *lipospheres* [28]. But it was in the mid 1990s, that lipid-based nanoparticles (SLN) emerged as an effective alternative particulate carrier system, prepared with solid physiological lipids used as common pharmaceutical excipients and stabilized by surfactants [29-31]. Initially, the two main formulation/preparation techniques described for producing SLN were the high-pressure homogenisation and the microemulsion-based technique, described by Müller and Lucks [32] and by Gasco [33], respectively. In contrast to most polymeric nanoparticulate systems, SLN formulation techniques do not necessarily need to use organic solvents minimizing the toxicological risk [34]. Their colloidal dimensions and

controlled release profiles allow both drug protection and improved administration by several routes. Moreover, the main manufacturing processes proposed for SLN are easy to scale up and the resulting formulations often withstand terminal sterilization [35-41]. Different solid mono-, di- and triacylglycerols have been exploited to produce SLN, such as tripalmitin, cetyl palmitate, glyceryl distearate, trimyristin, stearic acid and glyceryl stearate [42].

SLN have received increased attention over the last years, because they present good physical stability and biocompatibility, provide drug protection, allow controlled (fast or sustained) and targeted drug release depending on the incorporation model [35-37, 39-41, 43, 44]. Regarding the drug incorporation within the SLN, there are three models: (a) homogenous matrix, (b) drug-enriched shell and (c) drug-enriched core [39, 42, 45-48], as represented in Figure 1.3. The type of model depends basically on the formulation components (lipid, lipophilic or hydrophilic active compound and surfactant) and the production conditions [40, 45, 46]. In the first model, the drug is molecularly and homogeneously dispersed in the lipid matrix of the particles. Hence, drug release occurs via diffusion from the solid lipid matrix and/or by degradation of lipid matrix. As consequence of their structure, this type of SLN can show controlled release properties. In case of the second model (drug-enriched shell), the drug is concentrated on the outer shell of the nanoparticles [40, 42, 48]. An outer shell enriched with active compound can be obtained when phase separation occurs during the cooling process from the liquid oil droplet to the formation of a SLN, since the lipid precipitates first forming a practically compound-free lipid core [40, 48, 49]. This model is not suitable for prolonged drug release, nonetheless it may be used to obtain a burst release of the drug [40, 42]. In contrast to drug-enriched shell model, drug-enriched core model is formed when precipitation of the drug is faster than lipid during cooling of the nanoemulsion. Generally, prolonged drug release is observed from these SLN [40, 42, 48, 49].

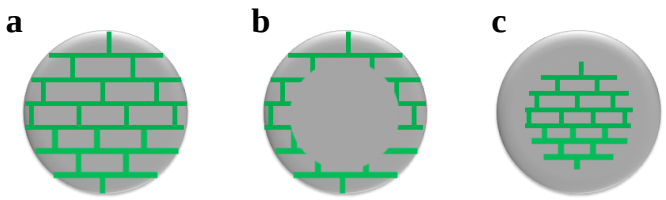

Figure 1.3: Models of incorporation of drugs (green) into SLN: (a) Type I - homogeneous matrix, (b) Type II - drug-enriched outer shell, and (c) Type III - drug-enriched core with lipid shell (adapted from [40]).

Several studies have been developed on the pulmonary delivery of SLN as local and systemic delivery nanocarriers for molecules [50]. Pandey and Khuller [51] investigated the chemotherapeutic potential of SLN associating rifampicin, pyrazinamide and isoniazid against Tuberculosis (TB), and verified the sustained-release of drugs from the SLN *in vitro* and *in vivo*. Liu *et al.* [50] developed a novel nebulizer-contained insulin-SLN for pulmonary delivery. They observed that SLN could be successfully applied as a pulmonary carrier system for insulin, providing a systemic delivery of protein. Deposition and clearance of SLN were studied by Videira *et al.* [52, 53] after inhalation of aerosolized particles using gamma-scintigraphy imaging analysis. It was visualized that a few minutes post deposition, inhaled SLN translocated to regional lymph nodes indicating that pulmonary route can be an efficient via to deliver SLN to the lymphatic system.

However, potential disadvantages such as insufficient loading capacity, drug expulsion after polymorphic transition during storage and relatively high water content of the dispersions (70-99.9%) have been reported for SLN. The DL capacity of conventional SLN is limited by the solubility of drug in the molten lipid, the structure of the lipid matrix and the polymorphic state of the lipid matrix [29, 47, 54-56]. If the lipid matrix consists of similar molecules, a perfect crystal with few imperfections is formed. Since incorporated drugs are located between fatty acid chains, between the lipid layers and also in crystal imperfections, a highly ordered crystal lattice cannot accommodate large amounts of drug [42, 55]. Expulsion of encapsulated drug molecules may be observed during storage, which leads to limited DL capacity of SLN. Therefore, amount of encapsulated drug and drug release profile of SLN may change throughout storage time [42, 57] as a consequence of the transition to a highly ordered lipid matrix. Immediately

after production, lipids crystallize partially in higher energy modifications (α, β′) with more imperfections in the crystal lattice [58-60]. The preservation of the α-modification during storage and transformation after administration (e.g. by temperature changes) could lead to a triggered and controlled release and has recently been investigated for topical formulations [61]. If, however, a polymorphic transition to β takes place during storage, the drug will be expelled from the lipid matrix and it can then neither be protected from degradation nor released in a controlled manner.

In order to overcome some observed limitations of conventional SLN, modifications of the lipid structure have been introduced resulting in the so-called nanostructured lipid carriers (NLC) and lipid drug conjugate (LDC) [49, 62-64] (Figure 1.4). The aim was the development of a nanoparticulate lipid carrier with increased payload while preventing drug expulsion.

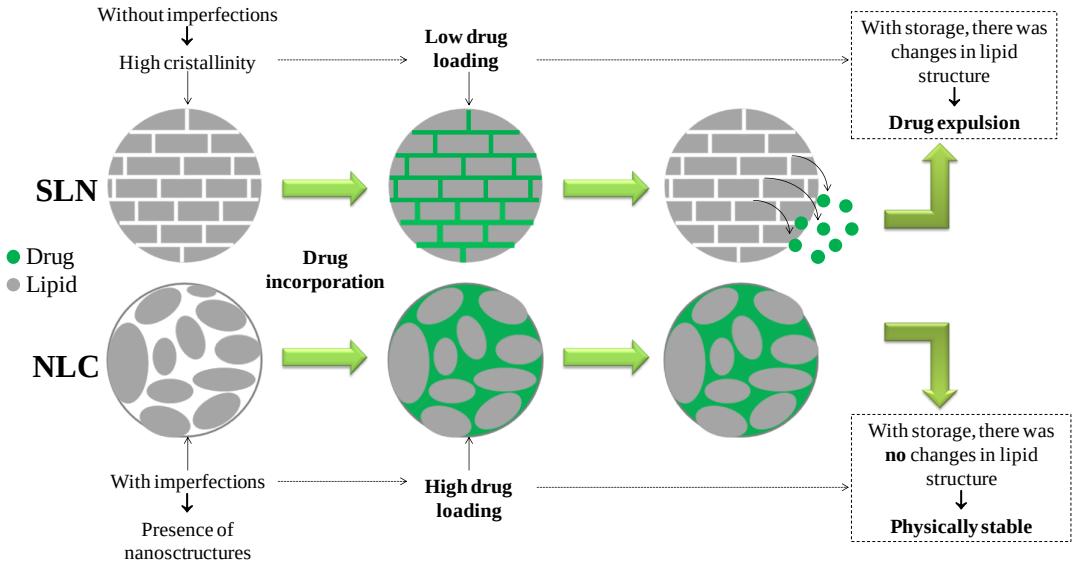

Figure 1.4: SLN *versus* NLC. The main difference between SLN and NLC is the fact that the concept of the latter is performed by nanostructuring the lipid matrix, in order to increase the DL and to prevent leakage, conferring more flexibility for drug release modulation. This goal is achieved by mixing solid lipids with liquid lipids in NLC instead of highly purified lipids with relatively similar molecules in SLN. The result is a less-ordered lipid matrix with many imperfections, which can accommodate a higher amount of drug.

The NLC are composed of blends of solid and liquid lipids, improving DL and drug retention during storage [40]. The resulting nanoparticulate matrix shows a melting point (m.p.) depression compared to the raw lipid while the particles still present a solid matrix at body temperature [65]. Actually, by conferring the lipid matrix a less ordered structure, the DL capacity is enhanced while the drug loss during storage is minimized by preventing the formation of perfect crystals [46].

However, the main drawback of SLN is their reduced ability to carry hydrophilic drugs, which will preferentially partition to the outer aqueous phase during the production process. As a consequence, only highly potent low dose hydrophilic drugs may be encapsulated in SLN [29, 39, 65, 66]. For this reason LDC were developed aiming at increasing the loading capacity for hydrophilic drugs [39, 64, 65]. The preparation of LDC involves drug-lipid conjugation (e.g. by salt formation or covalent binding) and the so-formed insoluble drug-lipid conjugate will be processed with an aqueous surfactant solution to a nanoformulation using a method suitable for SLN preparation [39, 65].

Overall, these three lipid-based nanosystems have been used for the incorporation of drugs with an enormous range of applications, such as diagnosis, prevention and treatment of diseases, as well as drug delivery by different administration routes (oral, rectal, topical, pulmonary, ocular, nasal, nose-to-brain and parenteral) [57, 67-69] (Table 1.1).

Table 1.1: Examples of bioactive compounds incorporated into lipid nanoparticles (adapted from [70]).

Encapsulated drug	Lipid	Advantages	Nanosystem	Ref
3'-Azido-3'-deoxythymide palmitate	Trilaurin	Stable after autoclaving, lyophilisation and rehydration	SLN	[71]
5-Fluorouracil	Dynasan 114 and Dynasan 118	Prolonged release in simulated colonic medium	SLN	[72]
Apomorphine	Glyceryl monostearate, polyethylene glycol monostearate	Enhanced the bioavailability *in vivo*	SLN	[73]
Ascorbyl palmitate	Imwitor 400 and Labrafil M1944	Viscoelastic measurements is appropriate for topical application	NLC	[74]
Baclofen	Stearic acid	Significantly higher drug concentrations in plasma	SLN	[75]
Benzyl nicotinate	Dynasan 116	Increased oxygenation in the skin	SLN	[76]
Calcitonin	Trimyristin	Improvement of the efficacy of such carriers for oral delivery of proteins	SLN	[77]
Camptothecin	Monostearin and Soybean Oil 788	Stable and high performance delivery system	NLC	[78, 79]
Clozapine	Trimyristin, tripalmitin and tristearin	Improvement of bioavailability	SLN	[80]
Cyclosporin A	Glyceryl monostearate and glyceryl palmitostearate	Controlled release	SLN	[81, 82]
Cytarabine	Stearic acid	Provided sustained drug release, stability and improved cytotoxicity	LDC	[83]
Dexamethasone	Compritol 888 ATO	Drug delivery topical use	SLN	[84]
Diazepam	Compritol 888 ATO and Imwitor 900K	Prolonged release	SLN	[85]
Diminazenediaceturate	Mixture of stearic- and palmitic acid	Improvement of loading capacity for hydrophilic drugs for brain delivery	LDC	[64, 86]
Doxorubicin	Glyceryl caprate	Enhanced apoptotic death	SLN	[87]

Table 1.1: Continuation.

Encapsulated drug	Lipid	Advantages	Nanosystem	Ref
Gonadotropin release hormone	Monostearin	Prolonged release	SLN	[88]
Hydrocortisone	Monoglyceryde, chain length of the fatty acid moiety	SLN stable with release properties	SLN	[45]
Ibuprofen	Stearic acid, trilaurin, tripalmitin	Stable formulation and negligible cell cytotoxicity	SLN	[89]
Idarubicin	Emulsifying wax	Potential to deliver anticancer drugs	SLN	[90]
Insulin	Stearic acid, octadecyl alcohol, cetyl palmitate, glyceryl monostearate, glyceryl palmitostearate, glyceryl tripalmitate, glyceryl behenate	Promising for oral delivery of proteins	SLN	[91]
Ketoprofen	Mixture of beeswax and carnauba wax	SLN with beeswax content exhibited faster drug release as compared carnauba wax	SLN	[92]
Lopinavir	Compritol 888 ATO	Bioavailability enhanced	SLN	[93]
Methotrexate	Stearic acid	Enhanced bioavailability and reduced drug associated gastrointestinal toxicity even in higher doses recommended for anticancer therapy	LDC	[94]
Nimesulide	Glyceryl behenate, palmitostearate, glyceryl tristearate	Sustained drug release	SLN	[95]
Oryzalin	Tripalmitin	Stable SLN after autoclaving and improvement of tolerability and therapeutic index of dinitroanilines	SLN	[35]
Penciclovir	Glyceryl monostearate	Provide a good skin targeting	SLN	[96]
Progesterone	Monostearin, stearic acid and oleic acid	Potential DDS for oral administration	NLC	[97, 98]
Repaglinide	Glyceryl monostearate and tristearin	Toxicity indicated that the SLN were well tolerated	SLN	[99, 100]

Table 1.1: Continuation.

Encapsulated drug	Lipid	Advantages	Nanosystem	Ref
Salbutamol sulphate	Monostearin and PEG2000	Formulation accelerate release of hydrophilic small molecule drugs	SLN	[101]
Tetracycline	Glyceryl monostearate and stearic acid	Sustained release	SLN	[102]

SLN: solid lipid nanoparticles; NLC: nanostructured lipid carriers; LDC: lipid drug conjugate; DDS: drug delivery systems; PEG: polyethylene glycol.

As shown in Table 1.2, only a few solid lipid-based nanoformulations are approved for human use, while there are some lipid-based drug product candidates currently in clinical trials, as described in Table 1.3 [103, 104].

Table 1.2: Lipids used in marketed lipid nanoparticles formulations (adapted from [67]).

Lipid name	Examples of marketed products	Company
Glyceryl palmitostearate	Xifaxan®	Salix Pharmaceuticals Inc.
Cetyl palmitate	Azelex®	Allergan
Stearic acid	Viokace™	Aptalis Pharma Inc.
Tripalmitin	Survanta®	Abbot
Caprylic/capric triglycerides	Avodart™	Glaxo SmithKline
Lauroyl polyoxylglycerides	Lipofen®	Cipher Pharmaceuticals Inc.
Glyceryl monostearate / glyceryl monopalmitate	Terramycin®	Pfizer
Soy lecithin	Baycip®	Bayer
Squalene	Cutanova	Dr.Rimpler Gmb

Table 1.3: Examples of targeted lipid nanoparticles formulations currently in clinical trials (adapted from [103, 104]).

Drug	Target	Disease	Phase	Company
ALN-VSP02	KSP and VEGF	Solid tumours	I	Alnylam Pharmaceuticals
SiRNA-EphA2-DOPC	EphA2	Advanced tumours	I	MD Anderson Cancer Center
Atu027	PKN3	Solid tumours	I	Silence Therapeutics
TKM-100201	VP24, VP35, Zaire Ebola-polymerase	Ebola-virus infection	I	Tekmira Pharmaceutical
PRO-040201	ApoB	Hypercholesterolaemia	I	Tekmira Pharmaceutical
TKM-080301	PLK1	Tumours	I	Tekmira Pharmaceutical
ALN-PCS02	PCSK9	Hypercholesterolaemia	I	Alnylam Pharmaceuticals
ALN-TTR02	TTR	Transthyretin-mediated amyloidosis	II	Alnylam Pharmaceuticals

KSP: kinesin spindle protein; VEGF: vascular endotelial growth factor; EphA2: erythropoietin-producing hepatocellular receptor tyrosine kinase class A2; PKN3: protein kinase N3; VP24: viral protein 24; VP35: viral protein 35; ApoB: apolipoprotein B; PLK1: polo-like kinase 1; PCSK9: proprotein convertase subtilisin/kesin type 9; TTR: transthyretin.

1.3. Inhaled drug delivery through nanoparticles

Mucosal routes for systemic drug administration present a great advantage in comparison to the parenteral routes, since they are non-invasive. Thus, development of suitable non-injectable delivery systems for mucosal drug administration could significantly enhance patient compliance, thereby leading to increased therapeutic benefits [105]. Among the mucosal routes, pulmonary administration has attracted remarkable scientific and biomedical interest in recent years for the treatment of systemic diseases, such as diabetes mellitus [106]. Aside from this, drugs are generally delivered to the respiratory tract for the treatment or prophylaxis of airways diseases, such as bronchial asthma and cystic fibrosis. The administration of a drug at its site of action can result in a rapid onset of activity, which may be highly desirable, for instance when delivering broncho-dilating drugs for the treatment of asthma. Additionally, smaller doses can be administered locally compared to those delivered by the oral or parenteral routes, thereby reducing the potential incidence of adverse systemic effects and reducing drug costs. The pulmonary route is also useful when a drug is poorly absorbed or when it is rapidly metabolized orally [107, 108]. Systemic delivery can be achieved through pulmonary administration, offering the advantage of bypassing the first pass effect in the liver, as well as offering a large alveolar area available for absorption with an extensive vascularization, a low thickness epithelium and low extracellular and intracellular enzyme activities. The high permeability of the epithelial barrier, the low proteolytic activity and the thinner mucus layer compared to the gastrointestinal mucosa, also make the airways suitable for both local and systemic applications [109-112].

Besides, many drugs, including hydrophilic high MW compounds, have demonstrated to be absorbed by the pulmonary route. However, their bioavailabilities are still low. The drugs administered by the pulmonary route must overcome important obstacles [113, 114] since the structure of the airways also prevents the entry airborne foreign particles, promoting their efficient removal [107]. These obstacles include the complex structure of the respiratory tree itself and the lung defense mechanisms (e.g., mucociliary clearance, lung surfactant) that oppose to drug absorption.

In order to overpass the bioavailability limitation, nanoparticulate carriers arise as promising pulmonary drug delivery system [112-114]. An ideal pulmonary carrier system designed with a specific size, density and surface properties for lung drug delivery can

play a key role in increasing the drug therapeutic index by the following mechanisms: (i) improving lung deposition and the amount of drug that reaches the site of action (either extracellular or intracellular) and, as a consequence, decreasing adverse effects due to non-specific drug delivery to non-target tissues; (ii) protecting the therapeutic macromolecule and improving its *in vivo* stability and (iii) reducing clearance and prolonging the drug residence time at its site of action. In a study performed by Kawashima *et al.* [115], insulin-loaded PLGA nanoparticles were prepared to be administered in guinea pig lung. They demonstrated a significant reduction in blood glucose level, with a prolonged effect over 48 h as compared to insulin solution. Additionally, insulin-loaded nanoparticles using a different polymer, poly(butyl cyanoacrylate), delivered to the lung of rats were shown by Zhang *et al.* [116] to extend the duration of a hypoglycaemic effect over 20 h (glucose level below 80% of the original levels) as compared to pulmonary administration of insulin solution.

Although nanoparticles are most often delivered to the airways by nebulization, these nanocarriers present technical issues, being unfeasible for pulmonary administration. For example, nanoparticles stored in an aqueous medium will, over time, suffer polymer hydrolysis or lipid transitions with significant loss of drug. Moreover, solution instability is another concern owing to particle agglomeration and settling, as well as a consequence of the small size and strong particle-particle interactions, leading to poor functionality of the nebulizer and, consequently, poor delivery efficiency due to exhalation of low-inertia nanoparticles [4, 7, 16, 17]. To prepare nanoparticles for ultimate commercial use, lyophilisation has been explored as a means to provide a storage form that can be rehydrated to deliver nanoparticles in suspension. There are, however, a number of drawbacks to lyophilisation, including the lengthy process time required for drying, low energy efficiency, high cost of purchasing and maintaining the equipment, and sensitivity of the product to freezing and various other processing-related stresses. Moreover, resuspension may be difficult and the retention, post-hydration, of the same nanoparticles size requires the use of stabilizers during the freeze-drying process [117]. These limitations have led to the search for next-generation drying methods that can be applied to therapeutics as will discussed in the following sections.

1.4. Deposition of inhaled particles in the respiratory tract

The deposition of inhaled particles in the airways is dependent, mainly, on the formulation, the delivery device and the patient's physiological characteristics (e.g., breathing patterns and clinical status) [107, 112]. There are three principal mechanisms that lead to particles pulmonary deposition: inertial impaction, gravitational sedimentation and Brownian diffusion, which are associated with the particle aerodynamic diameter (d_{aer}) [118] (Figure 1.5). The d_{aer} is the most appropriate measure of aerosol particle size, because it relates to particle dynamic behaviour and describes the main mechanisms of aerosol deposition [119]. Indeed, the d_{aer} is measured taking into account the geometric diameter and the density of the inhaled particles, which is defined as the diameter of a sphere of unit density characterized by the same settling velocity in air as the particle aerosol being measured [112, 120], as depicted by the following equation:

$$d_{aer}(\mu m) = d_{geo}\sqrt{\frac{\rho_e}{\lambda \rho_s}} \qquad \text{(Eq. 1.1)}$$

where d_{geo} is the particle geometric diameter, ρ_s is 1 g/cm^3, ρ_e is the effective particle density in the same unit as ρ_s and λ is the dynamic shape factor of the particle. This shape factor is theoretically defined as 1 for spherical particles.

The inertial impaction occurs during the passage through the oropharynx and large conducting airways (i.e. upper tracheobronchial regions) and is the dominant deposition mechanism for particles larger than 5 µm. When the d_{aer} of particles ranges from 1 to 5 µm, they are subject to sedimentation by gravitational force that occurs in smaller airways and respiratory bronchioles. Sedimentation is influenced by breath-holding. Particles with an d_{aer} of less than or equal to approximately 1 µm are deposited significantly by diffusion, based on the Brownian motion, and then exhaled. This diffusion is of little significance for particles >1 µm [10, 107, 118, 119, 121, 122].

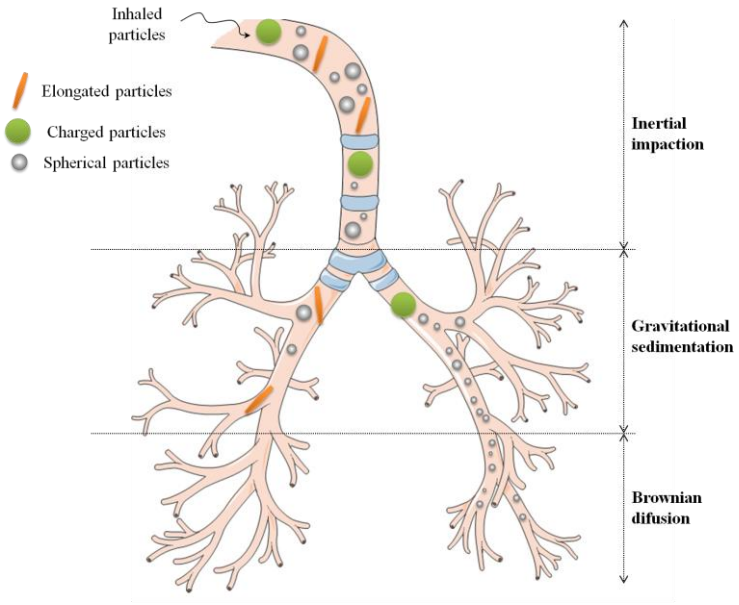

Figure 1.5: Mechanisms involved in particle deposition in the different regions of airways. Electrostatic deposition is seen for charged particles and interception for elongated-shaped particles (adapted from [111, 123]).

Thereby, a successful deposition into deep lung requires the particles be small enough to avoid deposition by inertial impaction on upper airways and can pass through the lower airways, while being large enough to avoid exhalation. So, the optimal particle size for achieving delivery deep into alveolar region has been established to be an d_{aer} between 1 and 5 µm, as summarized in Figure 1.6 [110, 118, 124]. For these reasons, one of the metrics used to quantify the performance of an inhalable powder is the determination of the fine particle fraction (FPF), which is usually defined as the percentage of particles that are smaller than 5 µm of d_{aer} that can potentially achieve alveolar deposition [125].

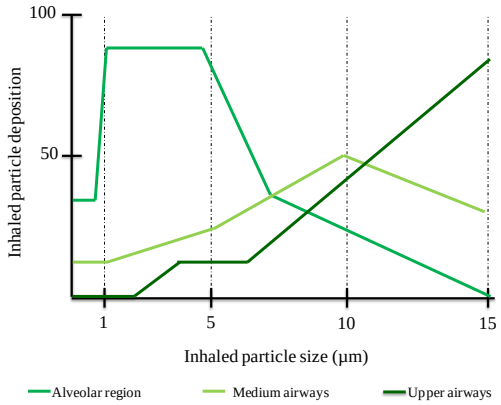

Figure 1.6: Effect of particle size on the deposition of aerosol particles in the human respiratory tract. Larger particles deposit in the airways or mouth and throat, whereas smaller particles deposit in the alveolar region. Particles <1 µm can be exhaled, thereby reducing deep lung deposition. This representation considers for a slow inhalation and a 5-second breath hold (adapted from [124]).

Regarding the practical aspects, values for d_{aer} of particles can be determined *in vitro* with cascade impactors based on particle impaction principles. Several methods are used to evaluate the aerodynamic performance of inhalable powder involving the following equipments: (i) twin-stage liquid impinger (TSLI); (ii) multistage liquid impinger (MSLI); (iii) Andersen cascade impactor (ACI) and (iv) next-generation impactor (NGI) (Figure 1.7) [126-128].

These impactors were calibrated to separate the particles according to the d_{aer} in different stages, predicting the deposition patterns of particulate drug carriers in the respiratory tract. They operate on the principle of internal impaction, i.e. particle separation is provided on the basis of difference in inertia (a function of particle size and velocity). The TSLI is relatively easy to use as it operates on the principle of liquid impingement to divide the dose emitted from the inhaler into non-respirable and respirable fractions, having only two stages. The MSLI is a five-stage system while the ACI consists of 8 stages. Both are constructed in a pattern such that larger particles will impact upon particular stage collection plate as the aerosol stream passes through, whereas relatively smaller particles will be carried in the air stream and pass to the next impaction stage. Further, the NGI was developed in 2000 and it comprises seven stages with a micro-orifice collector [126, 127].

Apart from this, cascade impactors should not be considered as *in vitro* simulators of lung, chiefly due to the divergence in the flow rate when compared with that of a human lung. Since a cascade impactor functions with a constant flow rate but human lung have a varying flow rate due to the breathing cycle [126].

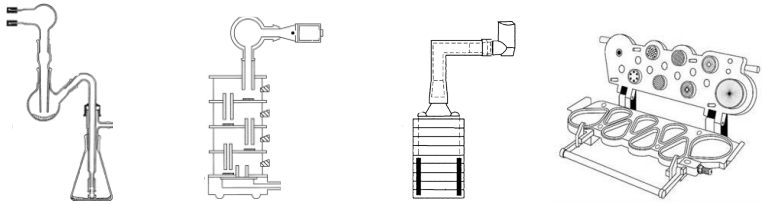

Figure 1.7: Schematic of cascade impactor systems evaluated for dry powder inhaler (DPI) testing. Several aerodynamic particle size measuring devices are available but the most commonly used in pharmaceutical aerosols are the liquid impingers, including the (A) twin-stage liquid impinger (TSLI) and the (B) multi-stage liquid impinger (MSLI), and the inertial impactors, including the (C) Andersen cascade impactor (ACI) and, more recently, the (D) next generation impactor (NGI).

1.5. Fate of inhaled particles in the lung

The fate of inhaled particles depends on various factors, such as regional distribution in the lung and particle size, because deposition within the lung is a complex function of absorption and non-absorptive clearance mechanisms [118, 123]. In order to succeed the pulmonary delivery of any therapeutic molecule, many obstacles and lung defense mechanisms that could hinder the path of foreign substances must be overcome, such as the effect of the airways' structure (e.g., mucus barrier), mucociliary clearance and phagocytosis by alveolar clearance (Figure 1.8) [122, 129-131]. Once inhaled particles are deposited onto the lining of the respiratory tract, they first contact the mucous layer within the airways or the surfactant-lining fluid layer within the alveolar region. Then, the inhaled carriers that are soluble in these fluids and mucus undergo chemical dissolution *in situ* or binding to proteins and may be eventually cleared into blood and lymphatic circulation. Insoluble particles may undergo physical translocation and they are subjected

at several post-defense mechanisms, including the mucocilliary escalator transport, phagocytosis by macrophages and endocytosis [118, 132].

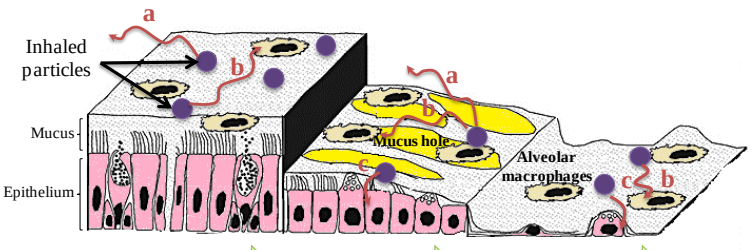

	Trachea, bronchi	Bronchioli	Alveoli
Soluble particles	- Coughing - Mucociliary escalator - Chemical binding - Pinocytosis	- Pinocytosis - Mucociliary escalator - Chemical binding	- Pinocytosis - Endocytosis - Difussion
Insoluble particles	- Coughing - Mucociliary escalator - Coughing	- Endocitosys - Mucociliary escalator	- Phagocytosis - Endocytosis

Figure 1.8: Clearance mechanisms of inhaled particle in the bronchi, bronchioles and the alveolar region. (a) clearance via mucociliary escalator, (b) uptake by macrophages and (c) trans-epithelial clearance (adapted from [131]).

In detail, particles that penetrate the lower respiratory tract but are not solubilized immediately may adhere to the epithelial lining and be cleared more slowly. However, the shortened drug action associated with the relatively rapid clearance represents a significant challenge to drug delivery to the lung. Particles of large volume diameter, such as porous particles, usually show a better bioavailability than solid particles of the same volume diameter either because of their improved dissolution rate (due to the larger specific surface area) which is advantageous for immediate release, or because of their size-related delaying effect on the phagocytic clearance, which can afford sustained action up to several days [133]. Indeed the mucociliary escalator dominates nanoparticles clearance from the upper airways, since nanoparticles that consist of slowly dissolving or insoluble materials in the airway mucus will be partly moved by action of the ciliated epithelial cells pushing the mucus along with the nanoparticles that deposited on the airway walls to the larynx, where they are swallowed to the gastro-intestinal tract or excreted through the mouth [107, 118]. A specific case can be made for ultrafine nanoparticles (<150 nm), which exhibit different interactions with both the trachea-

bronchial and alveolar epithelia [133]. While the mucociliary escalator is the most efficient mechanism of clearance in the upper airways, particles are predominantly cleared by macrophage phagocytosis and lymphatic uptake and, afterwards, by epithelial endocytosis in the alveoli, which promotes a systemic effect [52, 107, 118]. Another possible fate for inhaled particles is not a generally recognized mechanism because it appears to be distinct for particles and involves their uptake by sensory nerve endings embedded in airway epithelia, followed by axonal translocation to ganglionic and central nervous system structures [132].

1.6. Techniques for nanoparticles microencapsulation by particle engineering

Since nanoparticles are within a nanosize range which is not suitable for deep lung delivery, the major challenge for pulmonary delivery of nanoparticles is to find a proper carrier system and a suitable microencapsulation technique. Several researchers have prepared microcarrier systems to improve the delivery of nanoparticles to the alveolar area. In this context, the main goal of particle engineering is to design particles with desirable characteristics such as narrow size distribution, improved dispersibility, good drug stability, optimized bioavailability, sustained release and/or specific targeting, taking into account inhaler design and drug delivery requirements [133]. Different strategies to engineer micrometric nanoparticles-based dry powders have recently been explored: (a) nanoparticles on coarse inert carrier; (b) nanoparticle self-assembling (*Trojan* particles or porous nanoparticle-aggregate particles) and (c) nano-embedded microparticles (Figure 1.9) [112].

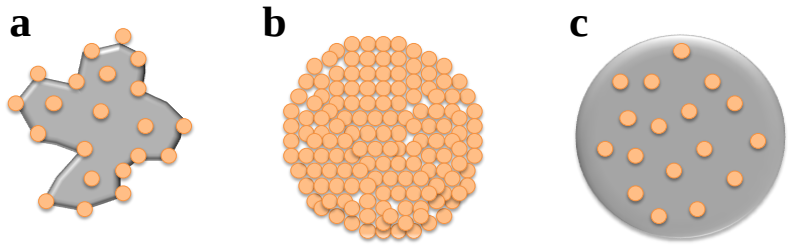

Figure 1.9: Nanoparticle-based inhaled dry powders can be obtained by: (a) adsorption on coarse inert carriers, (b) *Trojan* particles (nanoparticles-aggregate particles) or (c) embedding nanoparticles into an inert microparticle (adapted from [112]).

Among these, self-assembly of nanoparticles or their embedding within an inert microcarrier have been extensively investigated and, probably, represent the most promising technological approach. Thereby, the following sections will focus on microencapsulated nanoparticles using suitable techniques with the aim of improving nanoparticles handling and stability, obtaining dry powders with proper aerodynamic properties for pulmonary administration [110, 134]. Spray-drying and spray-freeze-drying (SFD) are the most common techniques to provide suitable aerodynamic characteristics to nanoparticles with their microencapsulation in inert excipients.

1.6.1. Spray-drying

The spray-drying technology was first described 150 years ago by Percy in a patent entitled "Improvement in drying and concentrating liquid substances by atomizing" [135]. Its growth took place during the 20th century for the milk powder production, which still represents one of its major application [136]. Since the early 1940s [114, 137], it has been widely used as a procedure to transform an emulsion, suspension, dispersion or liquid into a micron-scale dry powder product [55, 108, 138-140]. Currently, some inhaled therapeutics had been successfully manufactured by spray-drying, being the most well-known marketed inhalation products: Pulmosol™ (Nektar/Pfizer), PulmoSphere™ (Novartis) and TechnoSphere® (Mannkind) [141].

The spray-drying technique allows converting a suspension of nanoparticles into dry powder of non-aggregated nanoparticles dispersed in a matrix microsphere composed by excipients, such as sugars, surfactants and/or carbohydrates [110, 120]. It can also be employed as an alternative procedure to lyophilisation, since it is a faster and cheaper method than lyophilisation and provides better dry powders characteristics for inhalation [138]. It is particularly advantageous because it can be easily scaled to an industrial level [108]. Essentially, the typical spray-drying process comprises four fundamental steps: (i) atomization of feed into a spray, (ii) spray-air contact, (iii) drying of spray and (iv) separation of dried product from the drying air. First, this technique involves the preparation of a formulation by mixing the nanocarriers with an excipient solution before spray-drying. This solubilized liquid formulation is spray-dried into a spray of fine droplets and then brought into contact with the hot drying gas, typically air, in a drying chamber, promoting the evaporation of the volatile phase and forming dry particles under

controlled temperature and air-flow conditions. Dried particles then pass to a cyclone, where particles separation occurs, according their properties (such as size) under centrifugal and/or gravitational force and the product is collected in a reservoir. The schematic spray-drying process is depicted in Figure 1.10. An important feature of this process is that it is suitable for labile molecules because spray-drying conditions expose biological molecules only for a few milliseconds to seconds in the spray-dryer chamber, maintaining the integrity of the molecule. The type of spray-dryer, the inlet temperature (T_{inlet}), the most suitable air-flow pattern, the drying chamber design and the feed-flow rate are selected according to the drying characteristics of the product and powder requisites [108, 142-144].

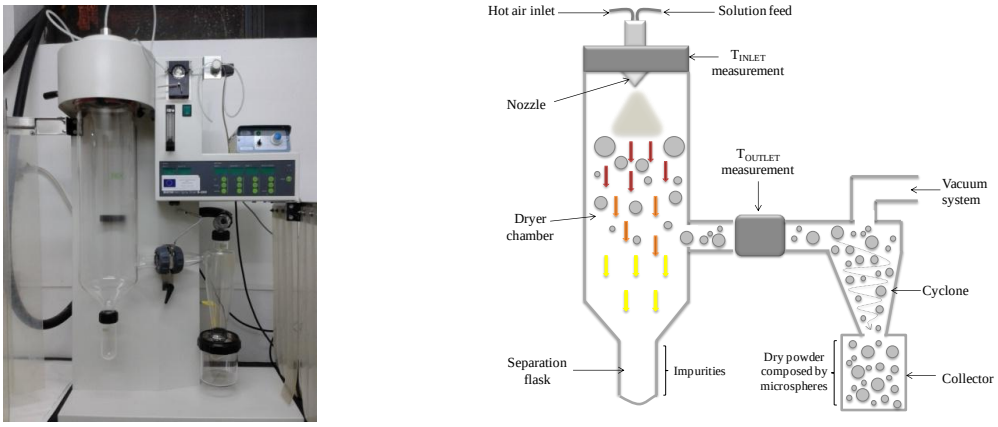

Figure 1.10: Büchi® Mini spray-dryer B-290 apparatus used in this research work (left) and spray-dryer apparatus scheme (right).

Droplet drying starts instantaneously after atomization and particle formation happens by influence of two simultaneous phenomena: evaporation rate of the solvent while the solutes diffuse towards the droplet centre. Therefore, the particles morphology will be defined by two main driving forces: the solvent evaporation rate and the solute diffusion rate (Figure 1.11) [145-147]. In detail, the solvent evaporation rate is dependent on the T_{inlet} and outlet temperature (T_{outlet}) of the spray-drying process and the relative saturation profiles at the inlet of the drying chamber as well as at the outlet of the drying chamber. On the other hand, the solute diffusion rate is dependent on the solute properties and solid contents in the suspension. Usually, during a fast drying, where the evaporation rate is higher than the diffusion rate, the droplet life time is shorter, and the solute molecules do not have time to diffuse towards the droplet centre. This phenomenon leads to the

formation of a spherical and hollow particle or even open-hole or fragmented particles. Contrary, during a slow drying, the solute molecules are able to migrate to the droplet centre, giving rise to the formation of full solid particles, spherical particles or wrinkly particles [145, 146]. Apart of this, the raw material properties conjugated with the drying kinetics involved during the particle formation will mainly dictate the aerodynamic properties of the inhalable powders, such as particle size, density, morphology, surface roughness, flowability and residual water content.

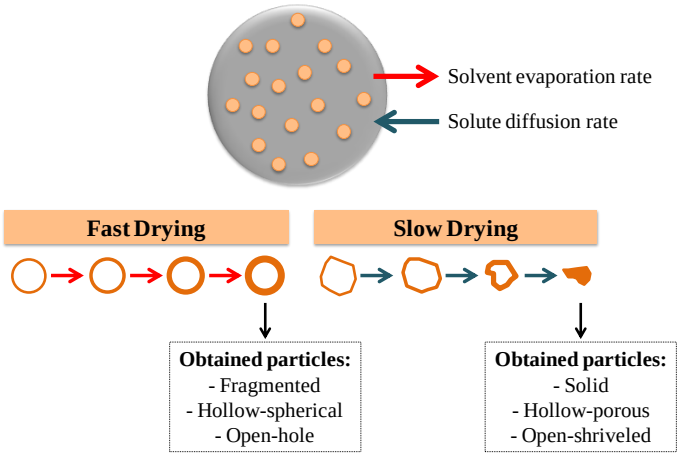

Figure 1.11: Scheme of particle formation from spray-drying process (adapted from [145, 146]).

Therefore, the product yield of spray-drying is another important feature that can be affected by the process parameters. The mass yield is determined by the amount of solids pumped into the spray-drying unit and the mass of particles collected. For laboratory-scale, the yield is often low, between 20-50%, depending on the feed solution composition and spray-drying operating parameters. However, industrial-scale spray-dryers can produce yields of up to 100%, due to higher wall deposits, since air residence times and radial distances from the atomiser to the drying chamber wall are shorter [108, 148]. Other limitation of this microencapsulation process is inherent to the fact that it can be caused particle aggregation due to high temperatures, shear forces and partial melting of the particles when it is spray-drying sensitive nanoparticles, SLN for instance [55, 138, 139]. Thus, a reduction of temperature effects can be achieved by spraying alcoholic instead of aqueous nanoparticles dispersions, due to lower necessary T_{inlet} [55, 139]. But then, the inconvenient will be the use of organic solvents and the remaining organic

solvents in the particles. This possible aggregation may also be avoided by including dispersibility enhancers such as leucine in the formulations for spray-drying [108].

The spray-drying of lipid-based nanoparticles was first investigated and reported by Freitas and Müller [149]. In those studies, trehalose, mannitol, lactose, sorbitol, glucose and mannose were used as spray-drying excipients. In addition, spray-drying was also performed with ethanol and methanol in order to reduce the required T_{inlet}. It was found that mannitol, lactose and trehalose resulted in fine grained powders, while sorbitol, glucose and mannose were unsuitable as spray-drying excipients due to high moisture content and low yield of the resulting powders. Trehalose was identified as the optimum spray-drying excipient, since SLN were easily re-dispersed upon exposure to an aqueous environment without any change in size. In another initial attempt, Kawashima *et al.* [150] used ultrafine hydroxypropylmethyl cellulose phthalate nanospheres to improve the aerosolization properties of a dry powder for inhalation of a hydrophobic drug. Authors prepared drug-loaded nanospheres and then spray-dried the resulting suspension to obtain a dry powder using lactose as excipient. They demonstrated that the dry powder had desirable inhalation properties through *in vitro* inhalation test using a TSLI apparatus. Tsapis *et al.* [151] produced large spray-dried porous carriers of nanoparticles, presenting extremely thin walled structures. For that, two different lipidic surfactants, 1,2-dipalmitoyl-*sn*-glycero-3-phosphocholine (DPPC) and 1,2-dimyristoyl-*sn*-glycero-3-phophoethanolamine and lactose were added to the nanoparticles. Although the spray-dried powder presented suitable characteristics for pulmonary delivery, it could only be re-dissolved in a mixture of ethanol/water. Poly(butylcyanoacrylate) (PBCA) and gelatin nanoparticles containing FITC-dextran were spray-dried by Sham *et al.* [152], resulting in a mixture of particles with hollow cores and continuous matrix. The distribution of the different nanoparticles in the resulting micron-sized particles varied, with gelatin nanoparticles mostly uniformly dispersed, while PBCA nanoparticles clustered in the lactose carrier matrix. The size of the gelatin nanoparticles of the dry powder increased after re-dispersion, in contrast with the size of PBCA nanoparticles that remained approximately the same. Nanoparticles of a hydrophilic model drug, terbutaline sulphate, were successfully entrapped within hydrophobic DPPC microspheres that exhibited a favourable FPF of 46.5±1.8% and mass median aerodynamic diameter (MMAD) of 3.93±0.12 μm [153]. Taking into account the advantages of spray-drying as a valuable technique for producing dry powders adequate for pulmonary delivery, Grenha *et al.*

[154] developed chitosan (CS)/tripolyphosphate (TPP) nanoparticles that promoted peptide absorption across mucosal surfaces. Then, they subjected these nanoparticles to a spray-drying microencapsulation process using typical aerosol excipients, such as mannitol and lactose, producing microspheres as carriers of insulin-loaded nanoparticles to the lung. The results showed that the obtained microspheres were mostly spherical and possessed appropriate aerodynamic properties for pulmonary delivery. These nanoparticles showed a good protein loading capacity (65-80%), providing the release of 75-80% insulin within 15 min, and can be easily recovered from microspheres after contact with an aqueous medium with no significant changes in size and zeta potential values. The plasmatic glucose levels following intratracheal administration revealed that the microencapsulated insulin-loaded CS nanoparticles induced a more pronounced and prolonged hypoglycemic effect compared to the controls (insulin solution, suspension of insulin loaded CS/TPP nanoparticles or mannitol microspheres including insulin) [110]. In later studies, the same authors formulated a new drug delivery system consisting of complexes formed between CS/TPP nanoparticles and phospholipids, named as lipid/CS nanoparticles (L/CS-nanoparticles) complexes. These protein-loaded L/CS-nanoparticles were microencapsulated by spray-drying using mannitol as excipient, corroborating the previous results concerning aerodynamic behaviour and the recovery of nanoparticles from the mannitol microspheres upon incubation in aqueous medium. Furthermore, the microencapsulation process did not have any effect on the insulin release profile [155]. Based on the same research line, Al-Qadi *et al.* [156] reported the preparation of a nanoparticle-based dry powder consisting of hybrid CS/hyaluronic acid nanoparticles by ionotropic gelation. Using mannitol as carrier, these nanoparticles were successfully microencapsulated presenting suitable aerodynamic and disintegration properties, corroborating the previous studies. Based on previous studies [154], recently, Rodrigues *et al.* [157], produced CS/carrageenan/TPP nanoparticles containing bovine serum albumin as a model protein, which were successfully microencapsulated by spray-drying in an aqueous suspension of L-leucine. The aerosol properties showed suitable FPF and MMAD suggesting a good deposition in the respiratory bronchiolar region of the lung [158].

Chougule *et al.* [159, 160] also investigated the feasibility of spray-dried liposomes encapsulating amiloride hydrochloride and dapsone. Two different excipients were identified as suitable liposomal carriers, mannitol and hydrolyzed gelatin. *In vivo* studies

involving intratracheal instillation demonstrated a prolonged drug activity and a slow pulmonary clearance of these liposomal dry powders. The encapsulation of superoxide dismutase in liposomes and the subsequent spray-drying with sucrose, lactose and trehalose were studied by Lo *et al.* [161]. Sucrose was capable of preserving the activity of the encapsulated drug and resulted in the highest aerosolization efficiency despite the high moisture content in the resulting particles. In addition to therapeutic drugs, plasmid DNA (pDNA) has also been encapsulated in liposomes, followed by spray-drying with lactose and trehalose [162]. In this study, the activity of the pDNA was not affected by the spray-drying process, while the post-mixing of spray-dried particles with CS was reported as resulting in increased surface roughness of the particles, thus improving the emitted dose compared to particles not modified with CS.

Regarding the re-dispersion ability of nanoparticles from microspheres, Tewa-Tagne *et al.* [163] investigated the effect of different excipients on the re-dispersibility of the spray-dried poly(caprolactone) (PCL) nanocapsules. They observed that lactose and mannitol were the most suitable excipients to produce microparticles that are readily wetted yielding immediate aqueous re-dispersion. Tomoda *et al.* [164] investigated the effect of the T_{inlet} on the re-dispersibility of rifampicin-loaded PLGA nanoparticles and established that at high T_{inlet}, PLGA nanoparticles undergo aggregation leading to poorly re-dispersed nano-aggregates, in contrast to spray-drying at a lower T_{inlet}. Unfortunately, spray-drying at a lower temperature resulted in insufficiently dried nano-aggregates with high moisture content and d_{aer} unsuitable for inhalation. In order to overcome these limitations, L-leucine was added as spray-drying excipient, producing large hollow nanoparticulate aggregates. They observed that particles are more capable of re-dispersing into individual nanoparticles in an aqueous environment than the first ones [164]. In another study, rifampicin-PLGA nanoparticles microencapsulated in mannitol showed a good *in vitro* aerosol performance and an *in vivo* imaging suggested that the rifampicin-PLGA nanoparticles were recognized by alveolar macrophages, increasing drug uptake [165].

In order to evaluate the feasibility of microparticles containing SLN for pulmonary drug delivery, a hybrid system was designed containing thymopentin-loaded glyceryl monostearate SLN microencapsulated in mannitol and leucine [166]. The obtained microparticles showed a high aerosolization efficiency and SLN could be easily recovered from the microparticles without significant changes on their innate

characteristics and their drug release behaviour. Pharmacokinetic and pharmacodynamic studies showed the bioavailability and therapeutic efficacy of thymopentin were remarkably strengthened after pulmonary administration, compared to the i.v. thymopentin solution [166]. Pourshahab *et al.* [167] prepared isoniazid-loaded CS/TPP nanoparticles atomized with some excipients, such as lactose, mannitol and maltodextrin alone or in combination with leucine. Spray-dried particles with lactose in the presence of leucine resulted in the production of inhalable powders with the highest FPF (≈ 45%). A dry powder formulation based on cationic lipid-modified PLGA nanoparticles, intended for delivery of siRNA, had been reported [168]. Herein, the spray-drying process, using mannitol as an excipient, did not affect the physicochemical properties of the readily re-dispersible nanoparticles. Most importantly, the siRNA activity was preserved throughout the spray-drying process. As X-ray powder diffraction analysis demonstrated that mannitol remained in a crystalline state upon spray-drying with PLGA nanoparticles, it was hypothesized that it might exert its stabilizing effect by sterical inhibition of the interactions between adjacent nanoparticles [168]. Ungaro *et al.* [169] developed PLGA nanoparticles embedded in an inert microcarrier made of lactose. Results showed that the spray-drying of the nanoparticles microencapsulated in lactose yielded particles with promising flow and aerosolization properties, while preserving the nanoparticles properties. Nonetheless, *in vivo* biodistribution studies showed that poly(vinyl alcohol) (PVA)-modified alginate/PLGA nanoparticles reached the deep lung, while CS-modified nanoparticles were found in great amounts in the upper airways [169].

The aforementioned investigations performed in this area indicated the pulmonary delivery of nanoparticles formulated as dry powders, using a spray-drying technique, is a promising and feasible strategy for the treatment of lung diseases with potential systemic therapeutic effects, reducing possible side effects. However, the use of polymeric colloidal drug carriers in pulmonary formulations is often limited by the unknown toxicity of the carrier in the lung, and even biodegradable polymers have not yet undergone any thorough toxicity testing for ensuring safe delivery via the lung. It has been suggested that lipids have a faster biodegradation rate and higher tolerability in the lung compared to most polymer-based particles [133]. So, lipid-based nanoparticles emerged as a good strategy as alternative to others colloidal systems for pulmonary purposes. Table 1.4 summarizes the published studies on pulmonary delivery of nanoparticles using dry powder carriers produced by spray-drying.

Table 1.4: Summary of pulmonary delivery of microencapsulated nanoparticles using dry powder carriers developed by a spray-drying process.

NPs type	NPs size (nm)	Carrier microparticle	Microparticle size (µm)	Drug	Ref
Hydroxypropylmethyl cellulose phthalate	ca. 52	Lactose	0.6-9.3	Pranlukast	[150]
Carboxylate-modified PS and Nyacol 9950 colloidal silica	PS NPs: 25, 170, 1000 Nyacol NPs: 100	Large porous particles, NPs attached to each other	4.0±0.2	–	[151]
Gelatin and *iso*-butyl cyanoacrylate	173-242	Lactose	2.5±2.6	–	[152]
Terbutaline sulfate with sorbitan monostearate	ca. 238	DPPC, glyceryl behenate, tripalmitin and hydrogenated palm oil	3.9±0.1	Terbutaline sulfate	[153]
PBCA	126±20	Lactose monohydrate	2.2±0.4	Ciprofloxacin	[170]
CS	388-419	Lactose	2.0±3.0	Insulin	[154]
CS/hyaluronic acid	173-233	Mannitol	2.6±0.1	-	[156]
Polyacrylate and silica	20-170	Phosphatidylcholine from fat free soybean lecithin	2.9±1.0	-	[171]
Polyacrylate (PMMA-MeOPEGMa)	50-220	Phospholipid (S100)	ca. 3	Salbutamol sulfate, aspirin	[172]
Polyacrylate, polystyrene and silica	5-150	Lactose	ca. 10	-	[173]
PCL	ca. 300	Sugars (mannitol, lactose, maltodextrine) and polymers (PVP, HPC, HPMC)	n.d.	-	[163]
SPC, hydrogenated SPC and SPC:cholesterol lipossomes	n.d.	Lactose	3.5-7.0	Atropine sulfate	[174]
DPPC and cholesterol liposomes	137±15 and 198±15	Mannitol and hydrolyzed gelatin	2.3±0.1 and 2.4±0.1	Amiloride hydrochloride and dapsone	[159, 160]

Table 1.4: Continuation.

NPs type	NPs size (nm)	Carrier microparticle	Microparticle size (µm)	Drug	Ref
DPPC, DMPC, DSPC and DPPG liposomes	150-200	Sucrose, lactose and trehalose	2.1±0.1-4.0±1.1	Superoxide dismutase	[161]
PLGA	ca. 400	Trehalose and lactose	2.5-6.0	Rifampicin	[164]
PLGA	195±4	L-leucine	4.2±0.1	Rifampicin	[175]
PLGA	ca. 213	Mannitol	2.1-3.2	Rifampicin	[165]
n.d.	n.d.	CS/mannitol	2.8–3.3	Honokiol	[176]
Glyceryl monostearate	ca. 147	Mannitol and L-leucine	4.1±0.1	Thymopentin	[166]
CS	241-449	Lactose, mannitol and maltodextrin alone or in combination with leucine	2.4-12.7	Isoniazid	[167]
PLGA	221-243	CS-grafted-PEG or CS	3.1-3.9	Curcumin	[177]
Cationic lipid-modified PLGA	207-261	Mannitol	3.7±0.2	siRNA	[168]
PLGA NPs modified with CS, alginate and PVA	250-300	Lactose	PVA-Alg NEM: 3.3±0.3 CS-Alg NEM: 3.7±0.4	Tobramycin	[169]
CS/carrageenan/TPP	ca. 300	Mannitol	1.8±0.1	BSA	[157]
PGA-co-PDL NPs with a cationic surfactant DMAB	129±6	L-leucine	2.8±0.2	BSA	[158]

NPs: nanoparticles; PS: polystyrene; DPPC: dipalmitoyl phosphatidylcholine; PBCA: poly (butylcyanoacrylate); CS: chitosan; PMMA-MeOPEGMa: poly(methyl methacrylate)-methoxy(polyethylene glycol)methacrylate; PCL: poly(caprolactone); PVP: poly(vinylpyrrolidone); HPC: hydroxyproplycellulose; HPMC: hydroxypropylmethylcellulose; SPC: soybean phosphatidylcholine; DMPC: dimyristoyl phosphatidylcholine; DSPC: distearoyl phosphatidylcholine; DPPG: dipalmitoyl phosphatidyl glycerol; PLGA: poly(d,l-lactide-*co*-glycolide); PEG: polyethylene glycol; siRNA: small interfering RNA; PVA: poly(vinyl alcohol); Alg: alginate; NEM: nano-embedded micro-particles; TPP: tripolyphosphate; BSA: bovine serum albumin; PGA-co-PDL: poly(glycerol adipate-co-ω-pentadecalactone); DMAB: didodecyldimethylammonium bromide; n.d.: no data.

1.6.2. Spray-freeze-drying

Although spray-drying is a convenient method to convert nanoparticulate suspensions into dry powders, the exposure of some heat sensitive nanoparticles formulations (including drugs and excipients) to the high temperatures involved in the process (>100°C) may be not ideal. For example, the use of low m.p. polymers or solid lipids, such as PCL and Precirol® ATO 5 may preclude the use of spray-drying [15, 178]. To overcome these limitations, the formulation of microencapsulated nanoparticles by SFD is employed as a viable alternative to spray-drying [179]. The SFD is a process that includes two-steps, i.e. atomization into a cryogen followed by lyophilisation, whereby the active material and excipients are sprayed into a freezing medium, such as liquid nitrogen, and then lyophilised (Figure 1.12). For that, SFD requires the selection of suitable cryoprotectants to reduce degradation of the active substance [108]. In detail, the first step involves channeling of the nanoparticles suspension through a nozzle to be atomized into tiny droplets. As the nanoparticles suspension is atomized into droplets, the cold temperature provided by the cryogen (i.e. liquid nitrogen) is sufficient to freeze the water molecules present within the air-borne droplets. The droplets are then completely frozen when immersed in the liquid nitrogen. The rapid freezing allows the water molecules to freeze into ice crystals that are interspersed among the dissolved or suspended materials (i.e. nanoparticles and freeze-drying excipients). Excess liquid nitrogen is subsequently removed from the slurry containing the frozen droplets by evaporation or decanting. Liquid nitrogen evaporation is carried out by holding the slurry at a temperature between its boiling point and the m.p. of ice (i.e. between -196°C and 0°C) to ensure the droplets remain frozen while the liquid nitrogen is being evaporated. To obtain dry powders, the ice crystals are removed from the frozen droplets via sublimation in the lyophilisation stage. This step is carried out below the triple point of water to prevent the melting of ice crystals into liquid water that can destroy the solid structure of the nano-aggregates. As the ice crystals in the frozen droplets are sublimed interstitially, the frozen droplets retain their size and do not shrink. The SFD produces particles having larger geometric diameter compared to spray-drying, in which the atomized droplets shrink due to convective evaporation of the aqueous medium. Furthermore, due to the interstitial sublimation, particles produced by SFD exhibit highly porous structures attributed to the presence of voids previously occupied by the sublimed ice crystals [15, 179, 180].

In SFD of nanoparticles suspension, freeze-drying excipients need also to be included in the formulation to: (i) function as cryoprotective agents protecting the nanoparticles from the sub-zero temperature, and (ii) facilitate re-dispersion of the nano-aggregates back into primary nanoparticles, so that the nanoparticles can perform their intended therapeutic functions. Aqueous re-dispersibility is an important characteristic as they must readily dissociate into primary nanoparticles upon exposure to the lung interstitial fluid, as discussed further. In this regard, excipient inclusion prevents the nanoparticles from irreversible coalescence upon freezing caused by mechanical stresses exerted by the ice crystal formation. The presence of excipients leads to the formation of *excipient bridges* that interconnect the nanoparticles preventing direct inter-nanoparticle contacts upon freezing [179].

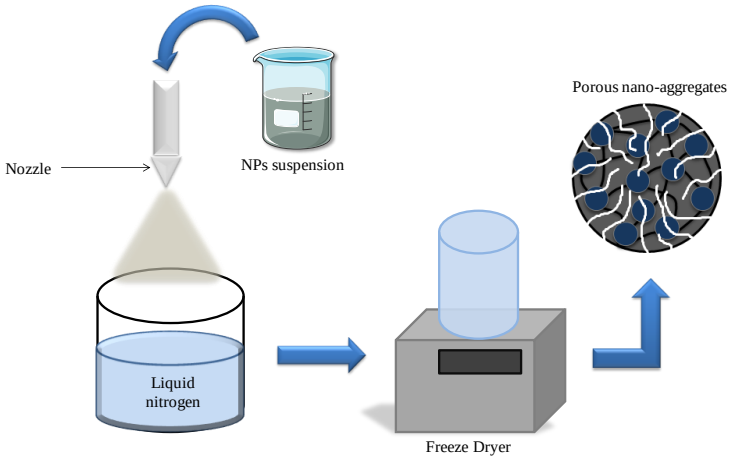

Figure 1.12: Schematic representation of the SFD technique to transform nanoparticulate suspension into porous dry powders aerosol of nano-aggregates (NPs: nanoparticles).

The SFD was primarily employed to produce dry powder proteins as the sub-zero temperature, unlike the high temperature, does not affect adversely protein structures and functions [179]. In a recent study, a suspension of DOX-loaded PBCA nanoparticles was converted by SFD into inhalable dry powder aerosol using lactose as a carrier. Upon dispersion in aqueous medium, the PBCA nanoparticles were easily recovered from the microcarriers. The cytotoxicity of DOX-nanoparticles was demonstrated to be higher than the corresponding free-DOX due to the higher uptake of DOX-loaded nanoparticles by

the cancer cells. The porosity of the nano-aggregates produced by SFD is evident from the large geometric diameter (≈10 µm) and the suitable d_{aer} for inhalation (approximately 3.5 µm) [181]. This technique was also employed to produce a dry powder of liposomal ciprofloxacin, where lactose was also used as carrier [182]. The resulting SFD particles had a reduced particle mass and the liposomal ciprofloxacin was reconstituted when the dry powder aggregates were immersed in an aqueous medium [182].

In another study, a dry powder for inhalation containing insulin-loaded liposomes incubated with different lyoprotectants (lactose, sucrose, mannitol and glucose) were produced by the SFD process for a best preservation of the entrapped drug in the liposome bilayers [183]. The same authors developed another novel inhaled dry powder composed by insulin-loaded SLN, which provided prolonged drug release, improved stability and effective inhalation [184]. Cheow *et al.* [179] produced a dry powder of drug-loaded thermally sensitive PCL nanoparticles using SFD and mannitol and PVA as excipients. Importantly, the particles produced by SFD exhibited significantly higher aqueous re-dispersibility than those produced by spray-drying, supporting the suitability of SFD as a method for producing solid-dosage-form of thermally sensitive nanoparticles. In addition, the dry powders exhibited large, porous and spherical morphologies with good flowability and effective aerosolization [179].

Overall, the nanocomposite microcarriers produced by SFD presented larger specific surface areas and lower densities than their corresponding nanoparticles-microparticles produced by spray-drying, conferring better aerodynamic characteristics to the particles. The authors have been concluded that the SFD into cooled air proved to be an efficient technique to prepare nanoparticles microencapsulated for pulmonary delivery while maintaining the stability of the original nanoparticulate formulation [185].

Table 1.5 shows a summary of pulmonary delivery of microencapsulated- nanoparticles suspensions using SFD.

Table 1.5: Summary of pulmonary delivery of nanoparticle suspensions microencapsulated using SFD process.

NPs type	NPs size (nm)	Carrier microparticle	Carrier microparticle size (µm)	Drug	Ref
PBCA	173±43	Lactose	10±4	Doxorubicin	[181]
DMPG	<600	Lactose	ca. 2.8	Ciprofloxacin	[182]
PCL	290±40	Mannitol and PVA	ca. 5	Levofloxacin	[179]
PLGA, EDRL and EC for polymeric NPs. Miglyol® 812, Kolliphor® HS15 and soybean lecithin for LNC. Witepsol® H15 for SLN.	PLGA: 81.7±11.5 EDRL: 78.3±19.2 EC: 111.4±10.2 LNC: 36.2±2.6 SLN: 441.7±7.5	Maltodextrin and trehalose for polymeric and lipid NPs, respectively	9.3-62.3	-	[185]

NPs: nanoparticles; PBCA: poly (butylcyanoacrylate); DMPG: dimyristoyl phosphatidylglycerol; PCL: poly(caprolactone); PVA: poly (vinyl alcohol); PLGA: poly (DL-lactide-co-glycolide); EDRL: Eudragit® RL; EC: ethyl cellulose; LNC: lipid nanocapsules; SLN: solid lipid nanoparticles.

1.6.3. Other microencapsulation techniques

In addition to the most popular particle engineering techniques described above, there are some other methods that are not as well explored, such as milling and supercritical fluids (SCF) technology, or even alternative methods for preparing micron-sized drug particles that have been proposed, such as solvent evaporation, liquid-liquid emulsion and emulsion/coacervation techniques [186].

1.6.3.1. Milling

The traditional method for producing active drug particles within the respirable range involves high-intensity combination, usually in a fluid-energy (air-jet) mill [187]. Regarding milling technique, there are many different types of mills, but only a few are able to mill powders to the acceptable particle size range of 1-5 μm for pulmonary administration. The two main used types of mills are ball mills and fluid-energy mills, such as the jet mill, which is a well-established procedure used to produce dry powders intended for inhalation [119].

Jet milling is the most useful technique, because the reduction of the particle size occurs via high velocity particle-particle collisions. Coarse particles are introduced into the milling chamber and air or nitrogen, fed through nozzles at high pressure, accelerates the solid particles to sonic velocities, inducing collision and fractures between them. While flying around the mill, larger particles are subjected to higher centrifugal forces and are forced to the outer perimeter of the chamber. Small particles exit the mill through the central discharge stream. Depending on the pressure and powder feed rate, particles with diameters down to approximately 1 μm can be produced [119].

A ball mill is essentially a rotating cylinder loaded with drug and *milling media* (i.e., balls that grind the drug between each other as they tumble inside the mill). Ball milling is very slow and the process is poorly scalable, which is why tumbling-ball mills are only used for laboratory-scale [119]. However, strong mechanical processing, such as milling, has been shown to affect the crystallinity of the material [187]. The micronization process leads to small, irregularly shaped flat particles and extensive flat surfaces promote large contact areas, resulting in increased adhesion between the particles, leading that micronized powders show poor flow properties [188].

However, this can be viewed as an old process, providing only limited opportunity for control over potentially important particle characteristics such as size, shape and morphology. Intense milling might also cause unwanted changes in the physicochemical properties of the material. As a consequence the micronized material has intrinsically poor flow properties, leading to upstream processing problems, for example when filling the reservoir of a DPI, or a unit dose container such as a capsule or blister. Furthermore, cohesive micronized drug particles are generally resistant to redispersion following administration. It may not be suitable for fragile molecules and more complex engineered structures, such as porous/hollow particles and nanoaggregates, or for surface-modified, coated or encapsulated materials.The pharmaceutical industry has proposed several formulation strategies to allow these cohesive aggregates to be used in DPI. However, until now, classical milling processes are not suitable for the production of hybrid microencapsulated nanoparticles for pulmonary purposes.

1.6.3.2. Supercritical fluids technology

The SCF technology is a relatively recent particle engineering technology that can be used to manufacture respirable drug particles that are intrinsically more uniform in terms of crystallinity, morphology, particle size distribution and shape. It uses compressed gases or liquids above their critical pressures and temperatures. Several gases have been used (e.g. nitrogen), but carbon dioxide, because of its accessible critical point at 31°C and 74 bar, low cost and low toxicity, is the most widely used solvent in SCF processes. Its critical temperature makes SCF suitable for processing heat-labile solutes at conditions close to room temperature [187, 189]. The added advantage of this technology is the ability of supercritical solvents to be efficiently separated by decompression from organic co-solvents and solid powders, facilitating a single-step, clean and solvent recyclable production. Since SCF are gases under ambient conditions, a key benefit of this process is the elimination of the harvesting and drying stages even a very small amount of water is used as a co-solvent [186]. Furthermore, fine drug particles produced by means of SCF presented better flow properties and are more dispersible following discharge from a DPI device. In fact, it has been demonstrated that salmeterol xinafoate particles produced by SCF have higher respirable fractions (defined as the percentage of the drug dose emitted from an inhaler that is within the respirable range) than those produced by conventional crystallization and micronization [187, 190].

The SCF technology involves three main processes: (i) precipitation from supercritical solutions composed of supercritical fluid and solutions, where particles are formed as the result of rapid expansion of a supercritical fluid containing a dissolved solute; (ii) precipitation from gas saturated solutions, which involves rapid dispersion and mixing of the drug solution with the supercritical fluid, typically in a coaxial spray arrangement and extraction of the solvent into the supercritical fluid, leading to high supersaturation ratios and (iii) precipitation from saturated solutions using supercritical fluid as antisolvent, which relies on the capacity of a supercritical fluid to act as an antisolvent and cause precipitation within a liquid solution or droplet [187, 189, 191].

Other advantages can be noted depending on the chosen process configuration: high purity of products, control of crystal polymorphism, possibility of processing thermolabile molecules, single-step process, easy downstream processing and environmentally acceptable technology [191]. Nevertheless, scale-up of these techniques is limited by particle aggregation and nozzle blockage caused expansion cooling. It is also limited to molecules that are soluble in carbon dioxide [189]. However, all techniques allow production of inhalable particles with a significant increase in FPF compared to jet-milled products [133, 192].

Among the drugs that have been successfully processed by SCF technology, there are many active substances relevant for pulmonary administration such as anti-asthmatic drugs, antibiotics and peptides [186, 192-194]. For example, cyclosporine was precipitated as nanospheres and dispersible in budesonide crystals with an d_{aer} between 1 and 2 µm for dry powder formulations [189].

Particle engineering using this type of technology is the subject of intense research in the pharmaceutical industry [193, 195]. Despite its potential, SCF is still an emerging technology that is not much exploited in DPI products. As happens with milling processes, the nanoparticles microencapsulation by means of SCF technology is not yet developed and there are no studies about this research area of interest.

1.7. Nanoparticles recovery after microencapsulation

In addition to the specific aerodynamic requirements of the inhaled particles, the nanoparticles-containing micron-sized formulations obtained by microencapsulation techniques must readily dissociate into the primary nanoparticles upon depositing in the lung interstitial fluid in order to retain the benefits of the original nanoparticles (i.e., availability of internalization and improvement of drug absorption, increased dissolution rate, sustained and prolonged release) [110, 114, 120, 154, 156, 196] (Figure 1.13). Furthermore, the re-dispersed nanoparticles must remain colloidally stable to prevent aggregation in the lung. For this purpose, the process for microencapsulation typically employs a wide range of pharmaceutical excipients. Hence, the ability of the nanoparticles to readily redisperse in an aqueous medium depends on the strength of the nanocarriers binding force as well as the degree of particle wetting (i.e., the excipient solubility in the lung interstitial fluid) [120].

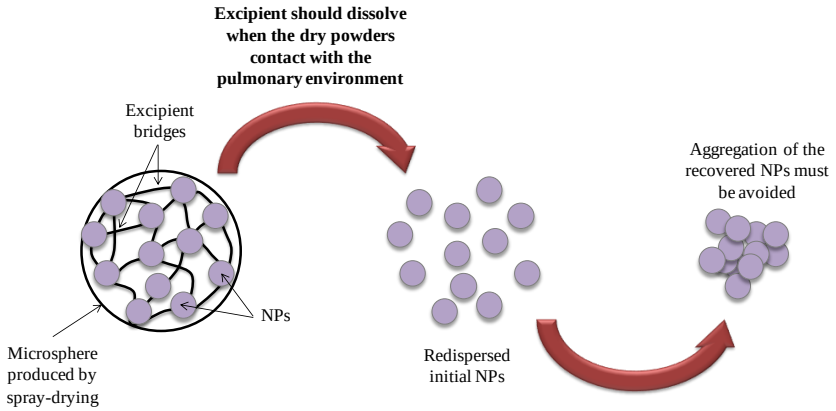

Figure 1.13: *Excipient bridges* govern the nanoparticles redispersability (NPs: nanoparticles).

Polymers, surfactants, carbohydrates and sugars (e.g., sorbitol, lactose, mannose) are widely used as the excipients for DPI, since they are approved by the main regulatory agencies (FDA and EMA) [112, 114, 120, 197]. This is due to their non-toxic, readily degradable properties after administration as well as their chemical and physical stability [111, 114, 198]. During the process, these substances act as drying excipients that protect the structural integrity of the nanoparticles, avoiding coalescence upon exposure to high

temperature and forming the so-called *excipient bridges* that occupy the interstitial space between the nanoparticles, hence preventing the nanoparticles from forming irreversible interparticle fusion upon heating above their glass transition or melting temperature [120, 196].

Despite the small number of excipients that are authorized for pulmonary delivery, a variety of new excipients is under investigation. Since lung have limited buffer capacity, only compounds that are biocompatible or endogenous to the lung and that are easily metabolized or cleared can be used in inhaled formulations [111]. Among the inert excipients available for nanoparticles microencapsulation, lactose is the first choice and the most commonly used in marketed DPI, being the only excipient used in DPI marketed in the USA. It has an established safety and stability profile, may be processed by different manufacturing techniques with tight controls over purity and physical properties, is easily available at different grades and is inexpensive. It is conceived that the fine particles of lactose reaching the lung are rapidly absorbed and metabolized by the intestinal epithelium and are mainly excreted in urine. Furthermore, lactose swallowed at the levels present in inhaled preparations is unlikely to present problems even in patients with lactose intolerance. However, a high number of excipients are under study, such as mannitol and trehalose [112].

1.8. Conclusions

Recent advances in inhalation therapy have brought considerable biomedical interest in the development of novel particle technologies for pulmonary drug formulation. This is due to the specific physiological environment of the lung as an absorption and treatment organ. Inhaled nanoparticulate therapy holds great potential for treating diseases that require direct lung delivery with reduced drug dosage and dosing frequency, leading to less systemic side effects and improved patient compliance. However their small size can bring some administration problems. Formulating nanoparticles into dry powder aerosols of micron-sized particles provides stability, ease of handling and delivery from simple inhalers. It is also demonstrated that dry powder delivery systems allow the absorption of molecules into the systemic circulation. Pulmonary drug delivery offers tremendous opportunities to improve drug therapies systemically and locally using advanced drug

delivery systems like nanoparticles. Nanotoxicological aspects of inhaled drug delivery systems have to be considered and *in vitro* methods can be established to ensure safety.

In the light of current literature data, it can be concluded that microencapsulated nanoparticles are very promising systems for sustained delivery of conventional and biotech drugs in the lung.

1.9. References

1. Peppas, N.A. Historical perspective on advanced drug delivery: how engineering design and mathematical modeling helped the field mature. Adv. Drug Deliv. Rev., 2013, 65 (1), 5-9.

2. De Koker, S.; De Cock, L.J.; Rivera-Gil, P.; Parak, W.J.; Velty, R.A.; Vervaet, C.; Remon, J.P.; Grooten, J.; De Geest, B.G. Polymeric multilayer capsules delivering biotherapeutics. Adv. Drug Deliv. Rev., 2011, 63 (9), 748-761.

3. Bao, G.; Mitragotri, S.; Tong, S. Multifunctional nanoparticles for drug delivery and molecular imaging. Annu. Rev. Biomed. Eng., 2013, 15 (1), 253-282.

4. Lima, A.C.; Alvarez-Lorenzo, C.; Mano, J.F. Design Advances in Particulate Systems for Biomedical Applications. Adv. Healthc. Mater., 2016, 5 (14), 1687-1723.

5. Gaspar, D.; Faria, V.; Quintas, Q.; Almeida, A. Targeted Delivery of Lipid Nanoparticles by Means of Surface Chemical Modification. Curr Org Chem, 2016, Accepted for publication.

6. Birrenbach, G.; Speiser, P. Polymerized micelles and their use as adjuvants in immunology. J. Pharm. Sci., 1976, 65 (12), 1763-1766.

7. Naahidi, S.; Jafari, M.; Edalat, F.; Raymond, K.; Khademhosseini, A.; Chen, P. Biocompatibility of engineered nanoparticles for drug delivery. J. Control. Release, 2013, 166 (2), 182-194.

8. Wilczewska, A.Z.; Niemirowicz, K.; Markiewicz, K.H.; Car, H. Nanoparticles as drug delivery systems. Pharmacol. Rep., 2012, 64 (5), 1020-1037.

9. Hans, M.; Lowman, A. Biodegradable nanoparticles for drug delivery and targeting. Curr. Opin. Solid St. M., 2002, 6 (4), 319-327.

10. Sung, J.C.; Pulliam, B.L.; Edwards, D.A. Nanoparticles for drug delivery to the lungs. Trends Biotechnol., 2007, 25 (12), 563-570.

11. Singh, R.; Lillard, J.W. Nanoparticle-based targeted drug delivery. Exp. Mol. Pathol., 2009, 86 (3), 215-223.

12. Byrne, J.D.; Betancourt, T.; Brannon-Peppas, L. Active targeting schemes for nanoparticle systems in cancer therapeutics. Adv. Drug Deliv. Rev., 2008, 60 (15), 1615-1626.

13. Barenholz, Y.C. Doxil® - the first FDA-approved nano-drug: lessons learned. J. Control. Release, 2012, 160 (2), 117-134.

14. Couvreur, P. Nanoparticles in drug delivery: past, present and future. Adv. Drug Deliv. Rev., 2013, 65 (1), 21-23.

15. Cheow, W.; Hadinoto, K. Preparations of dry-powder therapeutic nanoparticle aerosols for inhaled drug delivery. J. Aerosol Res., 2010, 25 (2), 155-165.

16. Colson, Y.L.; Grinstaff, M.W. Biologically responsive polymeric nanoparticles for drug delivery. Adv. Mater., 2012, 24 (28), 3878-3886.

17. Conniot, J.; Silva, J.M.; Fernandes, J.G.; Silva, L.C.; Gaspar, R.; Brocchini, S.; Florindo, H.F.; Barata, T.S. Cancer immunotherapy: nanodelivery approaches for immune cell targeting and tracking. Front. Chem., 2014, 2 (1), 105-132.

18. Mozafari, M.R. Liposomes: an overview of manufacturing techniques. Cel. Mol. Biol. Lett., 2005, 10 (4), 711.

19. Ochekpe, N.A.; Olorunfemi, P.O.; Ngwuluka, N.C. Nanotechnology and drug delivery part 2: nanostructures for drug delivery. Trop. J. Pharm. Res., 2009, 8 (3), 275-287.

20. Qiu, Y.; Gao, Y.; Hu, K.; Li, F. Enhancement of skin permeation of docetaxel: a novel approach combining microneedle and elastic liposomes. J. Control. Release, 2008, 129 (2), 144-150.

21. Jia, Y.; Joly, H.; Omri, A. Liposomes as a carrier for gentamicin delivery: development and evaluation of the physicochemical properties. Int. J. Pharm., 2008, 359 (1), 254-263.

22. Zaru, M.; Mourtas, S.; Klepetsanis, P.; Fadda, A.M.; Antimisiaris, S.G. Liposomes for drug delivery to the lungs by nebulization. Eur. J. Pharm. Biopharm., 2007, 67 (3), 655-666.

23. Budai, L.; Hajdú, M.; Budai, M.; Gróf, P.; Béni, S.; Noszál, B.; Klebovich, I.; Antal, I. Gels and liposomes in optimized ocular drug delivery: studies on ciprofloxacin formulations. Int. J. Pharm., 2007, 343 (1), 34-40.

24. Moussaoui, N.; Cansell, M.; Denizot, A. Marinosomes®, marine lipid-based liposomes: physical characterization and potential application in cosmetics. Int. J. Pharm., 2002, 242 (1), 361-365.

25. Barry, B.W. Novel mechanisms and devices to enable successful transdermal drug delivery. Eur. J. Pharm. Sci., 2001, 14 (2), 101-114.

26. Barry, B.W. Is transdermal drug delivery research still important today? Drug Discov. Today, 2001, 6 (19), 967-971.

27. Speiser, P., Lipidnanopellets als Trägersystem für Arzneimittel zur peroralen Anwendung. EP 0167825, 1990.

28. Domb, A.J.; Bergelson, L.; Amselem, S., Lipospheres for controlled delivery of substances. US Patent 5188837 A, 1996.

29. Schwarz, C.; Mehnert, W.; Lucks, J.; Müller, R. Solid lipid nanoparticles (SLN) for controlled drug delivery. I. Production, characterization and sterilization. J. Control. Release, 1994, 30 (1), 83-96.

30. Siekmann, B.; Westesen, K. Submicron-sized parenteral carrier systems based on solid lipids. Pharm. Pharmacol. Lett., 1992, 1 (3), 123-126.

31. Müller, R.; Mehnert, W.; Lucks, J.-S.; Schwarz, C.; Zur Mühlen, A.; Meyhers, H.; Freitas, C.; Rühl, D. Solid lipid nanoparticles (SLN): an alternative colloidal carrier system for controlled drug delivery. Eur. J. Pharm. Biopharm., 1995, 41 (1), 62-69.

32. Müller, R.; Lucks, J., Arzneistoffträger aus festen lipidteilchen, feste lipidnanosphären (SLN). German P4131562.6, 1996.

33. Gasco, M.R., Method for producing solid lipid microspheres having a narrow size distribution. US Patent 5 250 236, 1993.

34. Almeida, A.; Souto, E. Solid lipid nanoparticles as a drug delivery system for peptides and proteins. Adv. Drug Deliv. Rev., 2007, 59 (6), 478-490.

35. Lopes, R.; Eleutério, C.; Gonçalves, L.; Cruz, M.; Almeida, A. Lipid nanoparticles containing oryzalin for the treatment of leishmaniasis. Eur. J. Pharm. Sci., 2012, 45 (4), 442-450.

36. Nguyen, H.; Hwang, I.; Kweon, D.; Park, H. Enhanced payload of lipid nanocarriers using supersaturated solution prepared by solvent-mediated method. J. Microencapsul., 2013, 30 (7), 657-666.

37. Pandey, R.; Ahmad, Z. Nanomedicine and experimental tuberculosis: facts, flaws, and future. Nanomed.: Nanotechnol., 2011, 7 (3), 259-272.

38. Mancini, G.; Lopes, R.M.; Clemente, P.; Raposo, S.; Gonçalves, L.; Bica, A.; Ribeiro, H.M.; Almeida, A.J. Lecithin and parabens play a crucial role in tripalmitin-based lipid nanoparticle stabilization throughout moist heat sterilization and freeze-drying. Eur. J. Lipid Sci. Tech., 2015, 117 (12), 1947-1959.

39. Wissing, S.; Kayser, O.; Müller, R. Solid lipid nanoparticles for parenteral drug delivery. Adv. Drug Deliv. Rev., 2004, 56 (9), 1257-1272.

40. Souto, E.; Almeida, A.; Müller, R. Lipid nanoparticles (SLN®, NLC®) for cutaneous drug delivery: structure, protection and skin effects. J. Biomed. Nanotechnol., 2007, 3 (4), 317-331.

41. Vitorino, C.; Carvalho, F.; Almeida, A.; Sousa, J.; Pais, A. The size of solid lipid nanoparticles: An interpretation from experimental design. Colloid. Surface B, 2011, 84 (1), 117-130.

42. Das, S.; Chaudhury, A. Recent advances in lipid nanoparticle formulations with solid matrix for oral drug delivery. AAPS PharmSciTech, 2011, 12 (1), 62-76.

43. Silva, A.; González-Mira, E.; García, M.; Egea, M.; Fonseca, J.; Silva, R.; Santos, D.; Souto, E.; Ferreira, D. Preparation, characterization and biocompatibility studies on risperidone-loaded solid lipid nanoparticles (SLN): high pressure homogenization *versus* ultrasound. Colloid. Surface B, 2011, 86 (1), 158-165.

44. Pandey, R.; Khuller, G. Antitubercular inhaled therapy: opportunities, progress and challenges. J. Antimicrob. Chemoth., 2005, 55 (4), 430-435.

45. Jensen, L.; Magnussson, E.; Gunnarsson, L.; Vermehren, C.; Nielsen, H.; Petersson, K. Corticosteroid solubility and lipid polarity control release from solid lipid nanoparticles. Int. J. Pharm., 2010, 390 (1), 53-60.

46. Fathi, M.; Mozafari, M.; Mohebbi, M. Nanoencapsulation of food ingredients using lipid based delivery systems. Trends Food Sci. Tech., 2012, 23 (1), 13-27.

47. Müller, R.H.; Mäder, K.; Gohla, S. Solid lipid nanoparticles (SLN) for controlled drug delivery - a review of the state of the art. Eur. J. Pharm. Biopharm., 2000, 50 (1), 161-177.

48. Üner, M.; Yener, G. Importance of solid lipid nanoparticles (SLN) in various administration routes and future perspectives. Int. J. Nanomed., 2007, 2 (3), 289-300.

49. Müller, R.; Radtke, M.; Wissing, S. Solid lipid nanoparticles (SLN) and nanostructured lipid carriers (NLC) in cosmetic and dermatological preparations. Adv. Drug Deliv. Rev., 2002, 54 (1), 131-155.

50. Liu, J.; Gong, T.; Fu, H.; Wang, C.; Wang, X.; Chen, Q.; Zhang, Q.; He, Q.; Zhang, Z. Solid lipid nanoparticles for pulmonary delivery of insulin. Int. J. Pharm., 2008, 356 (1), 333-344.

51. Pandey, R.; Khuller, G. Solid lipid particle-based inhalable sustained drug delivery system against experimental tuberculosis. Tuberculosis, 2005, 85 (4), 227-234.

52. Videira, M.; Botelho, M.; Santos, A.; Gouveia, L.; Pedroso de Lima, J.; Almeida, A. Lymphatic uptake of pulmonary delivered radiolabelled solid lipid nanoparticles. J. Drug Target., 2002, 10 (8), 607-613.

53. Videira, M.; Gano, L.; Santos, C.; Neves, M.; Almeida, A. Lymphatic uptake of lipid nanoparticles following endotracheal administration. J. Microencapsul., 2006, 23 (8), 855-862.

54. Westesen, K.; Siekmann, B.; Koch, M.H. Investigations on the physical state of lipid nanoparticles by synchrotron radiation X-ray diffraction. Int. J. Pharm., 1993, 93 (1), 189-199.

55. Mehnert, W.; Mäder, K. Solid lipid nanoparticles: production, characterization and applications. Adv. Drug Deliv. Rev., 2001, 47 (2), 165-196.

56. Bunjes, H.; Westesen, K.; Koch, M.H. Crystallization tendency and polymorphic transitions in triglyceride nanoparticles. Int. J. Pharm., 1996, 129 (1), 159-173.

57. Wissing, S.; Müller, R. Solid lipid nanoparticles as carrier for sunscreens: *in vitro* release and *in vivo* skin penetration. J. Control. Release, 2002, 81 (3), 225-233.

58. Freitas, C.; Müller, R. Correlation between long-term stability of solid lipid nanoparticles (SLN™) and crystallinity of the lipid phase. Eur. J. Pharm. Biopharm., 1999, 47 (2), 125-132.

59. Hagemann, J. Thermal behavior and polymorphism of acylglycerides. In: N Garti KS, Ed.In: Crystallization and polymorphism of fats and fatty acids. New York: Marcel Dekker; 1988. p. 97-137.

60. Hernqvist, L. Crystal structures of fats and fatty acids. In: N Garti KS, Ed.In: Crystallization and polymorphism of fats and fatty acids. New York: Marcel Dekker; 1988. p. 97-137.

61. Jenning, V.; Gysler, A.; Schäfer-Korting, M.; Gohla, S.H. Vitamin A loaded solid lipid nanoparticles for topical use: occlusive properties and drug targeting to the upper skin. Eur. J. Pharm. Biopharm., 2000, 49 (3), 211-218.

62. Müller, R.; Radtke, M.; Wissing, S. Nanostructured lipid matrices for improved microencapsulation of drugs. Int. J. Pharm., 2002, 242 (1), 121-128.

63. Radtke, M.; Muller, R. Comparison of structural properties of solid lipid nanoparticles (SLN) versus other lipid particles. Proc. Int. Symp. Control. Rel. Bioact. Mater., 2000, 27 (1), 309-310.

64. Olbrich, C.; Gessner, A.; Kayser, O.; Müller, R.H. Lipid-drug-conjugate (LDC) nanoparticles as novel carrier system for the hydrophilic antitrypanosomal drug diminazenediaceturate. J. Drug Target., 2002, 10 (5), 387-396.

65. Attama, A.; Momoh, M.; Builders, P. Chapter 5 - Lipid nanoparticulate drug delivery systems: a revolution in dosage form design and development. In: Demir A, Ed.In: Recent Advances in Novel Drug Carrier Systems. Croatia: InTech; 2012. p. 107-140.

66. Almeida, A.J.; Runge, S.; Müller, R.H. Peptide-loaded solid lipid nanoparticles (SLN): influence of production parameters. Int. J. Pharm., 1997, 149 (2), 255-265.

67. Beloqui, A.; Solinís, M.Á.; Rodríguez-Gascón, A.; Almeida, A.J.; Préat, V. Nanostructured Lipid Carriers: promising drug delivery systems for future clinics. Nanomed.: Nanotechnol., 2016, 12 (1), 143–161.

68. Dingler, A.; Blum, R.; Niehus, H.; Muller, R.; Gohla, S. Solid lipid nanoparticles (SLN^{TM}/Lipopearls^{TM}) a pharmaceutical and cosmetic carrier for the application of vitamin E in dermal products. J. Microencapsul., 1999, 16 (6), 751-767.

69. Patel, S.; Chavhan, S.; Soni, H.; Babbar, A.; Mathur, R.; Mishra, A.; Sawant, K. Brain targeting of risperidone-loaded solid lipid nanoparticles by intranasal route. J. Drug Target., 2011, 19 (6), 468-474.

70. Severino, P.; Andreani, T.; Macedo, A.S.; Fangueiro, J.F.; Santana, M.H.A.; Silva, A.M.; Souto, E.B. Current state-of-art and new trends on lipid nanoparticles (SLN and NLC) for oral drug delivery. J. Drug Deliv., 2011, 2012 (1), 1-10.

71. Heiati, H.; Tawashi, R.; Phillips, N. Drug retention and stability of solid lipid nanoparticles containing azidothymidine palmitate after autoclaving, storage and lyophilization. J. Microencapsul., 1998, 15 (2), 173-184.

72. Yassin, A.; Anwer, M.K.; Mowafy, H.A.; El-Bagory, I.M.; Bayomi, M.A.; Alsarra, I.A. Optimization of 5-fluorouracil solid-lipid nanoparticles: a preliminary study to treat colon cancer. Int. J. Med. Sci., 2010, 7 (6), 398-408.

73. Tsai, M.J.; Huang, Y.B.; Wu, P.C.; Fu, Y.S.; Kao, Y.R.; Fang, J.Y.; Tsai, Y.H. Oral apomorphine delivery from solid lipid nanoparticleswith different monostearate emulsifiers: pharmacokinetic and behavioral evaluations. J. Pharm. Sci., 2011, 100 (2), 547-557.

74. Teeranachaideekul, V.; Souto, E.B.; Müller, R.H.; Junyaprasert, V.B. Physicochemical characterization and *in vitro* release studies of ascorbyl palmitate-loaded semi-solid nanostructured lipid carriers (NLC gels). J. Microencapsul., 2008, 25 (2), 111-120.

75. Priano, L.; Zara, G.P.; El-Assawy, N.; Cattaldo, S.; Muntoni, E.; Milano, E.; Serpe, L.; Musicanti, C.; Pérot, C.; Gasco, M.R. Baclofen-loaded solid lipid nanoparticles: preparation, electrophysiological assessment of efficacy, pharmacokinetic and tissue distribution in rats after intraperitoneal administration. Eur. J. Pharm. Biopharm., 2011, 79 (1), 135-141.

76. Kržič, M.; Šentjurc, M.; Kristl, J. Improved skin oxygenation after benzyl nicotinate application in different carriers as measured by EPR oximetry *in vivo*. J. Control. Release, 2001, 70 (1), 203-211.

77. Martins, S.; Silva, A.; Ferreira, D.; Souto, E. Improving oral absorption of samon calcitonin by trimyristin lipid nanoparticles. J. Biomed. Nanotechnol., 2009, 5 (1), 76-83.

78. Zhang, X.; Pan, W.; Gan, L.; Zhu, C.; Gan, Y.; Nie, S. Preparation of a dispersible PEGylate nanostructured lipid carriers (NLC) loaded with 10-hydroxycamptothecin by spray-drying. Chem. Pharm. Bull., 2008, 56 (12), 1645-1650.

79. Huang, Z.-r.; Hua, S.-c.; Yang, Y.-l.; Fang, J.-y. Development and evaluation of lipid nanoparticles for camptothecin delivery: a comparison of solid lipid nanoparticles, nanostructured lipid carriers, and lipid emulsion. Acta Pharm. Sinic., 2008, 29 (9), 1094-1102.

80. Manjunath, K.; Venkateswarlu, V. Pharmacokinetics, tissue distribution and bioavailability of clozapine solid lipid nanoparticles after intravenous and intraduodenal administration. J. Control. Release, 2005, 107 (2), 215-228.

81. Sawant, K.K.; Varia, J.K.; Dodiya, S.S. Cyclosporine a loaded solid lipid nanoparticles: optimization of formulation, process variable and characterization. Cur. Drug Deliv., 2008, 5 (1), 64-69.

82. Müller, R.; Runge, S.; Ravelli, V.; Thünemann, A.; Mehnert, W.; Souto, E. Cyclosporine-loaded solid lipid nanoparticles (SLN®): Drug-lipid physicochemical interactions and characterization of drug incorporation. Eur. J. Pharm. Biopharm., 2008, 68 (3), 535-544.

83. Sharma, P.; Dube, B.; Sawant, K. Synthesis of cytarabine lipid drug conjugate for treatment of meningeal leukemia: development, characterization and *in vitro* cell line studies. J. Biomed. Nanotechnol., 2012, 8 (6), 928-937.

84. Chen, G.; Hou, S.; Hu, P.; Hu, Q.; Guo, D.; Xiao, Y. *In vitro* dexamethasone release from nanoparticles and its pharmacokinetics in the inner ear after administration of the drug-loaded nanoparticles via the round window. J. South. Med., 2008, 28 (6), 1022-1024.

85. Abdelbary, G.; Fahmy, R.H. Diazepam-loaded solid lipid nanoparticles: design and characterization. AAPS PharmSciTech, 2009, 10 (1), 211-219.

86. Olbrich, C.; Gessner, A.; Schröder, W.; Kayser, O.; Müller, R.H. Lipid-drug conjugate nanoparticles of the hydrophilic drug diminazene - cytotoxicity testing and mouse serum adsorption. J. Control. Release, 2004, 96 (3), 425-435.

87. Kang, K.W.; Chun, M.-K.; Kim, O.; Subedi, R.K.; Ahn, S.-G.; Yoon, J.-H.; Choi, H.-K. Doxorubicin-loaded solid lipid nanoparticles to overcome multidrug resistance in cancer therapy. Nanomed.: Nanotechnol., 2010, 6 (2), 210-213.

88. Hu, F.; Hong, Y.; Yuan, H. Preparation and characterization of solid lipid nanoparticles containing peptide. Int. J. Pharm., 2004, 273 (1), 29-35.

89. Potta, S.G.; Minemi, S.; Nukala, R.K.; Peinado, C.; Lamprou, D.A.; Urquhart, A.; Douroumis, D. Preparation and characterization of ibuprofen solid lipid nanoparticles with enhanced solubility. J. Microencapsul., 2011, 28 (1), 74-81.

90. Ma, P.; Dong, X.; Swadley, C.L.; Gupte, A.; Leggas, M.; Ledebur, H.C.; Mumper, R.J. Development of idarubicin and doxorubicin solid lipid nanoparticles to overcome Pgp-mediated multiple drug resistance in leukemia. J. Biomed. Nanotechnol., 2009, 5 (2), 151-161.

91. Yang, R.; Gao, R.; Li, F.; He, H.; Tang, X. The influence of lipid characteristics on the formation, *in vitro* release, and *in vivo* absorption of protein-loaded SLN prepared by the double emulsion process. Drug Dev. Ind. Pharm., 2011, 37 (2), 139-148.

92. Kheradmandnia, S.; Vasheghani-Farahani, E.; Nosrati, M.; Atyabi, F. Preparation and characterization of ketoprofen-loaded solid lipid nanoparticles made from beeswax and carnauba wax. Nanomed.: Nanotechnol., 2010, 6 (6), 753-759.

93. Alex, M.A.; Chacko, A.; Jose, S.; Souto, E. Lopinavir loaded solid lipid nanoparticles (SLN) for intestinal lymphatic targeting. Eur. J. Pharm. Sci., 2011, 42 (1), 11-18.

94. Paliwal, R.; Rai, S.; Vyas, S.P. Lipid drug conjugate (LDC) nanoparticles as autolymphotrophs for oral delivery of methotrexate. J. Biomed. Nanotechnol., 2011, 7 (1), 130-131.

95. Patravale, V.; Ambarkhane, A. Study of solid lipid nanoparticles with respect to particle size distribution and drug loading. Int. J. Pharm., 2003, 58 (6), 392-395.

96. Lv, Q.; Yu, A.; Xi, Y.; Li, H.; Song, Z.; Cui, J.; Cao, F.; Zhai, G. Development and evaluation of penciclovir-loaded solid lipid nanoparticles for topical delivery. Int. J. Pharm., 2009, 372 (1), 191-198.

97. Yuan, H.; Wang, L.-L.; Du, Y.-Z.; You, J.; Hu, F.-Q.; Zeng, S. Preparation and characteristics of nanostructured lipid carriers for control-releasing progesterone by melt-emulsification. Colloid. Surface B, 2007, 60 (2), 174-179.

98. Cavalli, R.; Peira, E.; Caputo, O.; Gasco, M.R. Solid lipid nanoparticles as carriers of hydrocortisone and progesterone complexes with β-cyclodextrins. Int. J. Pharm., 1999, 182 (1), 59-69.

99. Rawat, M.K.; Jain, A.; Singh, S. *In vivo* and cytotoxicity evaluation of repaglinide-loaded binary solid lipid nanoparticles after oral administration to rats. J. Pharm. Sci., 2011, 100 (6), 2406-2417.

100. Rawat, M.K.; Jain, A.; Singh, S. Studies on binary lipid matrix based solid lipid nanoparticles of repaglinide: *in vitro* and *in vivo* evaluation. J. Pharm. Sci., 2011, 100 (6), 2366-2378.

101. Hong, Y.; Hu, F.; Yuan, H. Effect of PEG2000 on drug delivery characterization from solid lipid nanoparticles. Int. J. Pharm., 2006, 61 (4), 312-315.

102. Xu, X.-m.; Wang, Y.-s.; Chen, R.-y.; Feng, C.-l.; Yao, F.; Tong, S.-s.; Wang, L.; Yamashita, F.; Yu, J.-n. Formulation and pharmacokinetic evaluation of tetracycline-loaded solid lipid nanoparticles for subcutaneous injection in mice. Chem. Pharm. Bull., 2011, 59 (2), 260-265.

103. Xu, C.-f.; Wang, J. Delivery systems for siRNA drug development in cancer therapy. Asian J. Pharm. Sci., 2015, 10 (1), 1-12.

104. Kanasty, R.; Dorkin, J.R.; Vegas, A.; Anderson, D. Delivery materials for siRNA therapeutics. Nat. Mater., 2013, 12 (11), 967-977.

105. Smith, P. Peptide delivery via the pulmonary route: a valid approach for local and systemic delivery. J. Control. Release, 1997, 46 (1), 99-106.

106. Almeida, A.J.; Grenha, A. Technosphere®: an inhalation system for pulmonary delivery of biopharmaceuticals. In: Neves J SB, Ed.In: Mucosal Delivery of

Biopharmaceuticals: Biology, Challenges and Strategies. New York: Springer; 2014. p. 483-498.

107. Taylor, K. Pulmonary drug delivery. In: Aulton M, Ed.In: Pharmaceutics: The Science of Dosage Form Design. Edinburgh, UK: Churchill Livingstone; 2002. p. 473 - 488.

108. Bowey, K.; Neufeld, R. Systemic and mucosal delivery of drugs within polymeric microparticles produced by spray-drying. BioDrugs, 2010, 24 (6), 359-377.

109. Dombu, C.; Betbeder, D. Airway delivery of peptides and proteins using nanoparticles. Biomaterials, 2013, 34 (2), 516-525.

110. Al-Qadi, S.; Grenha, A.; Carrión-Recio, D.; Seijo, B.; Remuñán-López, C. Microencapsulated chitosan nanoparticles for pulmonary protein delivery: *in vivo* evaluation of insulin-loaded formulations. J. Control. Release, 2012, 157 (3), 383-390.

111. Andrade, F.; Rafael, D.; Videira, M.; Ferreira, D.; Sosnik, A.; Sarmento, B. Nanotechnology and pulmonary delivery to overcome resistance in infectious diseases. Adv. Drug Deliv. Rev., 2013, 65 (13), 1816-1827.

112. Ungaro, F.; d'Angelo, I.; Miro, A.; La Rotonda, M.; Quaglia, F. Engineered PLGA nano- and micro-carriers for pulmonary delivery: challenges and promises. J. Pharm. Pharmacol., 2012, 64 (9), 1217-1235.

113. Dombu, C.; Betberder, D. Airway delivery of peptides and proteins using nanoparticles. Biomaterials, 2013, 34 (2), 516-525.

114. Sham, J.; Zhang, Y.; Finlay, W.; Roa, W.; Löbenberg, R. Formulation and characterization of spray-dried powders containing nanoparticles for aerosol delivery to the lung. Int. J. Pharm., 2004, 269 (2), 457-467.

115. Kawashima, Y.; Yamamoto, H.; Takeuchi, H.; Fujioka, S.; Hino, T. Pulmonary delivery of insulin with nebulized DL-lactide/glycolide copolymer (PLGA) nanospheres to prolong hypoglycemic effect. J. Control. Release, 1999, 62 (1), 279-287.

116. Zhang, Q.; Shen, Z.; Nagai, T. Prolonged hypoglycemic effect of insulin-loaded polybutylcyanoacrylate nanoparticles after pulmonary administration to normal rats. Int. J. Pharm., 2001, 218 (1), 75-80.

117. Walters, R.H.; Bhatnagar, B.; Tchessalov, S.; Izutsu, K.I.; Tsumoto, K.; Ohtake, S. Next generation drying technologies for pharmaceutical applications. J. Pharm. Sci., 2014, 103 (9), 2673-2695.

118. Yang, W.; Peters, J.; Williams III, R. Inhaled nanoparticles - a current review. Int. J. Pharm., 2008, 356 (1), 239-247.

119. Telko, M.; Hickey, A. Dry powder inhaler formulation. Resp. Care, 2005, 50 (9), 1209-1227.

120. Cheow, W.; Hadinoto, K. Preparations of dry-powder therapeutic nanoparticle aerosols for inhaled drug delivery. Earozoru Kenkyu, 2010, 25 (2), 155-165.

121. Merkel, O.M.; Zheng, M.; Debus, H.; Kissel, T. Pulmonary gene delivery using polymeric nonviral vectors. Bioconjugate Chem., 2012, 23 (1), 3-20.

122. Lam, J.; Liang, W.; Chan, H. Pulmonary delivery of therapeutic siRNA. Adv. Drug Deliv. Rev., 2012, 64 (1), 1-15.

123. Fröhlich, E.; Salar-Behzadi, S. Toxicological Assessment of Inhaled Nanoparticles: Role of *in Vivo*, *ex Vivo*, *in Vitro*, and *in Silico* Studies. Int. J. Mol. Sci., 2014, 15 (3), 4795-4822.

124. Patton, J.S.; Byron, P.R. Inhaling medicines: delivering drugs to the body through the lungs. Nat. Rev. Drug Discov., 2007, 6 (1), 67-74.

125. Pacławski, A.; Szlęk, J.; Lau, R.; Jachowicz, R.; Mendyk, A. Empirical modeling of the fine particle fraction for carrier-based pulmonary delivery formulations. Int. J. Nanomed., 2015, 10 801.

126. Nahar, K.; Gupta, N.; Gauvin, R.; Absar, S.; Patel, B.; Gupta, V.; Khademhosseini, A.; Ahsan, F. *In vitro*, *in vivo* and *ex vivo* models for studying particle deposition and drug absorption of inhaled pharmaceuticals. Eur. J. Pharm. Sci., 2013, 49 (5), 805-818.

127. Marple, V.; Roberts, D.; Romay, F.; Miller, N.; Truman, K.; Van Oort, M.; Olsson, B.; Holroyd, M.; Mitchell, J.; Hochrainer, D. Next generation pharmaceutical impactor (A new impactor for pharmaceutical inhaler testing). Part I: Desig. Trop. J. Pharm. Res., 2003, 16 (3), 283-299.

128. Dunbar, C.; Mitchell, J. Analysis of cascade impactor mass distributions. J. Aerosol Med., 2005, 18 (4), 439-451.

129. Grenha, A.; Al-Qadi, S.; Seijo, B.; Remuñán-López, C. The potential of chitosan for pulmonary drug delivery. J. Drug Deliv. Sci. Tec., 2010, 20 (1), 33-43.

130. Taylor, G.; Kellaway, I. Chapter 10: Pulmonary Drug Delivery. In: Hillery A, Lloyd A, Swarbrick J, editors.In: Drug Delivery and Targeting. London: Taylor & Francis; 2001. p. 269-300.

131. Sturm, R. Deposition and cellular interaction of cancer-inducing particles in the human respiratory tract: Theoretical approaches and experimental data. Thoracic cancer, 2010, 1 (1), 141–152.

132. Oberdörster, G.; Oberdörster, E.; Oberdörster, J. Nanotoxicology: an emerging discipline evolving from studies of ultrafine particles. Environ. Health Persp., 2005, 113 (7), 823-839.

133. Chow, A.H.; Tong, H.H.; Chattopadhyay, P.; Shekunov, B.Y. Particle engineering for pulmonary drug delivery. Pharmaceut. Res., 2007, 24 (3), 411-437.

134. Mansour, H.; Rhee, Y.; Wu, X. Nanomedicine in pulmonary delivery. Int. J. Nanomed., 2009, 4 (1), 299-319.

135. Percy, S., Improvement in drying and concentrating liquid substances by atomizing. US Patent 125406 A. 1872.

136. Cal, K.; Sollohub, K. Spray drying technique. I: Hardware and process parameters. J. Pharm. Sci., 2010, 99 (2), 575-586.

137. Chow, A.; Tong, H.; Chattopadhyay, P.; Shekunov, B. Particle engineering for pulmonary drug delivery. Pharmaceut. Res., 2007, 24 (3), 411-437.

138. Brar, S.; Verma, M.; Tyagi, R.; Surampalli, R. Engineered nanoparticles in wastewater and wastewater sludge – Evidence and impacts. Waste Manage., 2010, 30 (3), 504-520.

139. Heurtault, B.; Saulnier, P.; Pech, B.; Proust, J.; Benoit, J. Physico-chemical stability of colloidal lipid particles. Biomaterials, 2003, 24 (23), 4283-4300.

140. Li, X.; Anton, N.; Arpagaus, C.; Belleteix, F.; Vandamme, T. Nanoparticles by spray-drying using innovative new technology: The Büchi Nano-Spray-Dryer B-90. J. Control. Release, 2010, 147 (2), 304-310.

141. Healy, A.M.; Amaro, M.I.; Paluch, K.J.; Tajber, L. Dry powders for oral inhalation free of lactose carrier particles. Adv. Drug Deliv. Rev., 2014, 75 (1), 32-52.

142. Katteboinaa, S. Approaches for the development of solid self-emulsifying drug delivery systems and dosage forms. Asian J. Pharm. Sci., 2009, 4 (4), 240-253.

143. Lee, S.; Heng, D.; Ng, W.; Chan, H.; Tan, R. Nano-spray-drying: a novel method for preparing protein nanoparticles for protein therapy. Int. J. Pharm., 2011, 403 (1), 192-200.

144. Beck-Broichsitter, M.; Schweiger, C.; Schmehl, T.; Gessler, T.; Seeger, W.; Kissel, T. Characterization of novel spray-dried polymeric particles for controlled pulmonary drug delivery. J. Control. Release, 2012, 158 (2), 329-335.

145. Vehring, R.; Foss, W.R.; Lechuga-Ballesteros, D. Particle formation in spray drying. J. Aerosol Sci., 2007, 38 (7), 728-746.

146. Vicente, J.; Pinto, J.; Menezes, J.; Gaspar, F. Fundamental analysis of particle formation in spray drying. Powder Technol., 2013, 247 1-7.

147. Feng, A.; Boraey, M.; Gwin, M.; Finlay, P.; Kuehl, P.; Vehring, R. Mechanistic models facilitate efficient development of leucine containing microparticles for pulmonary drug delivery. Int. J. Pharm., 2011, 409 (1), 156-163.

148. Gonnissen, Y.; Remon, J.; Vervaet, C. Development of directly compressible powders via co-spray-drying. Eur. J. Pharm. Biopharm., 2007, 67 (1), 220-226.

149. Freitas, C.; Müller, R. Spray-drying of solid lipid nanoparticles (SLN^{TM}). Eur. J. Pharm. Biopharm., 1998, 46 (2), 145-151.

150. Kawashima, Y.; Serigano, T.; Hino, T.; Yamamoto, H.; Takeuchi, H. A new powder design method to improve inhalation efficiency of pranlukast hydrate dry powder aerosols by surface modification with hydroxypropylmethylcellulose phthalate nanospheres. Pharmaceut. Res., 1998, 15 (11), 1748-1752.

151. Tsapis, N.; Bennett, D.; Jackson, B.; Weitz, D.A.; Edwards, D. Trojan particles: large porous carriers of nanoparticles for drug delivery. Proc. Natl. Acad. Sci. USA, 2002, 99 (19), 12001-12005.

152. Sham, J.O.-H.; Zhang, Y.; Finlay, W.H.; Roa, W.H.; Löbenberg, R. Formulation and characterization of spray-dried powders containing nanoparticles for aerosol delivery to the lung. Int. J. Pharm., 2004, 269 (2), 457-467.

153. Cook, R.O.; Pannu, R.K.; Kellaway, I.W. Novel sustained release microspheres for pulmonary drug delivery. J. Control. Release, 2005, 104 (1), 79-90.

154. Grenha, A.; Seijo, B.; Remuñán-López, C. Microencapsulated chitosan nanoparticles for lung protein delivery. Eur. J. Pharm. Sci., 2005, 25 (4), 427-437.

155. Grenha, A.; Remuñán-López, C.; Carvalho, E.L.; Seijo, B. Microspheres containing lipid/chitosan nanoparticles complexes for pulmonary delivery of therapeutic proteins. Eur. J. Pharm. Biopharm., 2008, 69 (1), 83-93.

156. Al-Qadi, S.; Grenha, A.; Remuñán-López, C. Microspheres loaded with polysaccharide nanoparticles for pulmonary delivery: Preparation, structure and surface analysis. Carbohyd. Polym., 2011, 86 (1), 25-34.

157. Rodrigues, S.; Cordeiro, C.; Seijo, B.; Remuñán-López, C.; Grenha, A. Hybrid nanosystems based on natural polymers as protein carriers for respiratory delivery: stability and toxicological evaluation. Carbohyd. Polym., 2015, 123 (1), 369-380.

158. Kunda, N.K.; Alfagih, I.M.; Dennison, S.R.; Somavarapu, S.; Merchant, Z.; Hutcheon, G.A.; Saleem, I.Y. Dry powder pulmonary delivery of cationic PGA-co-PDL nanoparticles with surface adsorbed model protein. Int. J. Pharm., 2015, 492 (1), 213-222.

159. Chougule, M.; Padhi, B.; Misra, A. Development of spray dried liposomal dry powder inhaler of dapsone. AAPS PharmSciTech, 2008, 9 (1), 47-53.

160. Chougule, M.B.; Padhi, B.K.; Misra, A. Nano-liposomal dry powder inhaler of amiloride hydrochloride. J. Nanosci. Nanotechno., 2006, 6 (9-10), 3001-3009.

161. Lo, Y.-l.; Tsai, J.-c.; Kuo, J.-h. Liposomes and disaccharides as carriers in spray-dried powder formulations of superoxide dismutase. J. Control. Release, 2004, 94 (2), 259-272.

162. Colonna, C.; Conti, B.; Genta, I.; Alpar, O. Non-viral dried powders for respiratory gene delivery prepared by cationic and chitosan loaded liposomes. Int. J. Pharm., 2008, 364 (1), 108-118.

163. Tewa-Tagne, P.; Briançon, S.; Fessi, H. Preparation of redispersible dry nanocapsules by means of spray-drying: development and characterisation. Eur. J. Pharm. Sci., 2007, 30 (2), 124-135.

164. Tomoda, K.; Ohkoshi, T.; Kawai, Y.; Nishiwaki, M.; Nakajima, T.; Makino, K. Preparation and properties of inhalable nanocomposite particles: effects of the temperature at a spray-dryer inlet upon the properties of particles. Colloid. Surface B, 2008, 61 (2), 138-144.

165. Ohashi, K.; Kabasawa, T.; Ozeki, T.; Okada, H. One-step preparation of rifampicin/poly (lactic-co-glycolic acid) nanoparticle-containing mannitol microspheres using a four-fluid nozzle spray drier for inhalation therapy of tuberculosis. J. Control. Release, 2009, 135 (1), 19-24.

166. Li, Y.; Sun, X.; Gong, T.; Liu, J.; Zuo, J.; Zhang, Z. Inhalable microparticles as carriers for pulmonary delivery of thymopentin-loaded solid lipid nanoparticles. Pharmaceut. Res., 2010, 27 (9), 1977-1986.

167. Pourshahab, P.S.; Gilani, K.; Moazeni, E.; Eslahi, H.; Fazeli, M.R.; Jamalifar, H. Preparation and characterization of spray dried inhalable powders containing chitosan nanoparticles for pulmonary delivery of isoniazid. J. Microencapsul., 2011, 28 (7), 605-613.

168. Jensen, D.K.; Jensen, L.B.; Koocheki, S.; Bengtson, L.; Cun, D.; Nielsen, H.M.; Foged, C. Design of an inhalable dry powder formulation of DOTAP-modified PLGA nanoparticles loaded with siRNA. J. Control. Release, 2012, 157 (1), 141-148.

169. Ungaro, F.; d'Angelo, I.; Coletta, C.; d'Emmanuele di Villa Bianca, R.; Sorrentino, R.; Perfetto, B.; Tufano, M.; Miro, A.; La Rotonda, M.; Quaglia, F. Dry powders based on PLGA nanoparticles for pulmonary delivery of antibiotics: modulation of encapsulation efficiency, release rate and lung deposition pattern by hydrophilic polymers. J. Control. Release, 2012, 157 (1), 149-159.

170. Ely, L.; Roa, W.; Finlay, W.H.; Löbenberg, R. Effervescent dry powder for respiratory drug delivery. Eur. J. Pharm. Biopharm., 2007, 65 (3), 346-353.

171. Hadinoto, K.; Phanapavudhikul, P.; Kewu, Z.; Tan, R.B. Dry powder aerosol delivery of large hollow nanoparticulate aggregates as prospective carriers of nanoparticulate drugs: effects of phospholipids. Int. J. Pharm., 2007, 333 (1), 187-198.

172. Hadinoto, K.; Zhu, K.; Tan, R.B. Drug release study of large hollow nanoparticulate aggregates carrier particles for pulmonary delivery. Int. J. Pharm., 2007, 341 (1), 195-206.

173. Hadinoto, K.; Phanapavudhikul, P.; Kewu, Z.; Tan, R.B. Novel formulation of large hollow nanoparticles aggregates as potential carriers in inhaled delivery of nanoparticulate drugs. Ind. Eng. Chem. Res., 2006, 45 (10), 3697-3706.

174. Goldbach, P.; Brochart, H.; Stamm, A. Spray-drying of liposomes for a pulmonary administration. II. Retention of encapsulated materials. Drug Dev. Ind. Pharm., 1993, 19 (19), 2623-2636.

175. Sung, J.C.; Padilla, D.J.; Garcia-Contreras, L.; VerBerkmoes, J.L.; Durbin, D.; Peloquin, C.A.; Elbert, K.J.; Hickey, A.J.; Edwards, D.A. Formulation and pharmacokinetics of self-assembled rifampicin nanoparticle systems for pulmonary delivery. Pharmaceut. Res., 2009, 26 (8), 1847-1855.

176. Li, X.; Guo, Q.; Zheng, X.; Kong, X.; Shi, S.; Chen, L.; Zhao, X.; Wei, Y.; Qian, Z. Preparation of honokiol-loaded chitosan microparticles via spray-drying method intended for pulmonary delivery. Drug Deliv., 2009, 16 (3), 160-166.

177. El-Sherbiny, I.M.; Smyth, H.D. Controlled release pulmonary administration of curcumin using swellable biocompatible microparticles. Mol. Pharm., 2011, 9 (2), 269-280.

178. Papadimitriou, S.; Bikiaris, D. Novel self-assembled core-shell nanoparticles based on crystalline amorphous moieties of aliphatic copolyesters for efficient controlled drug release. J. Control. Release, 2009, 138 (2), 177-184.

179. Cheow, W.S.; Ng, M.L.L.; Kho, K.; Hadinoto, K. Spray-freeze-drying production of thermally sensitive polymeric nanoparticle aggregates for inhaled drug delivery: effect of freeze-drying adjuvants. Int. J. Pharm., 2011, 404 (1), 289-300.

180. Nguyen, X.C.; Herberger, J.D.; Burke, P.A. Protein powders for encapsulation: a comparison of spray-freeze-drying and spray-drying of darbepoetin alfa. Pharmaceut. Res., 2004, 21 (3), 507-514.

181. Azarmi, S.; Tao, X.; Chen, H.; Wang, Z.; Finlay, W.H.; Löbenberg, R.; Roa, W.H. Formulation and cytotoxicity of doxorubicin nanoparticles carried by dry powder aerosol particles. Int. J. Pharm., 2006, 319 (1), 155-161.

182. Sweeney, L.G.; Wang, Z.; Loebenberg, R.; Wong, J.P.; Lange, C.F.; Finlay, W.H. Spray-freeze-dried liposomal ciprofloxacin powder for inhaled aerosol drug delivery. Int. J. Pharm., 2005, 305 (1), 180-185.

183. Bi, R.; Shao, W.; Wang, Q.; Zhang, N. Spray-freeze-dried dry powder inhalation of insulin-loaded liposomes for enhanced pulmonary delivery. J. Drug Target., 2008, 16 (9), 639-648.

184. Bi, R.; Shao, W.; Wang, Q.; Zhang, N. Solid lipid nanoparticles as insulin inhalation carriers for enhanced pulmonary delivery. J. Biomed. Nanotechnol., 2009, 5 (1), 84-92.

185. Ali, M.E.; Lamprecht, A. Spray-freeze-drying for dry powder inhalation of nanoparticles. Eur. J. Pharm. Biopharm., 2014, 87 (3), 510-517.

186. Rehman, M.; Shekunov, B.Y.; York, P.; Lechuga-Ballesteros, D.; Miller, D.P.; Tan, T.; Colthorpe, P. Optimisation of powders for pulmonary delivery using supercritical fluid technology. Eur. J. Pharm. Sci., 2004, 22 (1), 1-17.

187. Malcolmson, R.J.; Embleton, J.K. Dry powder formulations for pulmonary delivery. Pharm. Sci. Technol. To., 1998, 1 (9), 394-398.

188. Feeley, J.; York, P.; Sumby, B.; Dicks, H. Determination of surface properties and flow characteristics of salbutamol sulphate, before and after micronisation. Int. J. Pharm., 1998, 172 (1), 89-96.

189. Pilcer, G.; Vanderbist, F.; Amighi, K. Preparation and characterization of spray-dried tobramycin powders containing nanoparticles for pulmonary delivery. Int. J. Pharm., 2009, 365 (1), 162-169.

190. York, P.; Hanna, M. Salmeterol xinafoate with controlled particle size. Google Patents; 1998.

191. Fages, J.; Lochard, H.; Letourneau, J.-J.; Sauceau, M.; Rodier, E. Particle generation for pharmaceutical applications using supercritical fluid technology. Powder Technol., 2004, 141 (3), 219-226.

192. Shekunov, B.; Chattopadhyay, B.; Seitzinger, J., editors. Supercritical fluid processing techniques: comparing the products. Proceedings of the Conference on Respiratory Drug Delivery, Palm Springs, California; 2004.

193. Lobo, J.M.; Schiavone, H.; Palakodaty, S.; York, P.; Clark, A.; Tzannis, S.T. SCF-engineered powders for delivery of budesonide from passive DPI devices. J. Pharm. Sci., 2005, 94 (10), 2276-2288.

194. Amidi, M.; Pellikaan, H.C.; de Boer, A.H.; Crommelin, D.J.; Hennink, W.E.; Jiskoot, W. Preparation and physicochemical characterization of supercritically dried insulin-loaded microparticles for pulmonary delivery. Eur. J. Pharm. Biopharm., 2008, 68 (2), 191-200.

195. Schiavone, H.; Palakodaty, S.; Clark, A.; York, P.; Tzannis, S.T. Evaluation of SCF-engineered particle-based lactose blends in passive dry powder inhalers. Int. J. Pharm., 2004, 281 (1), 55-66.

196. Wang, Y.; Kho, K.; Cheow, W.; Hadinoto, K. A comparison between spray-drying and spray-freeze-drying for dry powder inhaler formulation of drug-loaded lipid-polymer hybrid nanoparticles. Int. J. Pharm., 2012, 424 (1), 98-106.

197. Misra, A.; Hickey, A.; Rossi, C.; Borchard, G.; Terada, H.; Makino, K.; Fourie, P.; Colombo, P. Inhaled drug therapy for treatment of tuberculosis. Tuberculosis, 2011, 91 (1), 71-81.

198. Sebti, T.; Amighi, K. Preparation and *in vitro* evaluation of lipidic carriers and fillers for inhalation. Eur. J. Pharm. Biopharm., 2006, 63 (1), 51-58.

This page was intentionally left blank.

Chapter 2

Rifabutin-loaded solid lipid nanoparticles for inhaled antitubercular therapy: physicochemical and *in vitro* studies

This chapter is based on the following publication:
Gaspar DP, Faria V, Gonçalves LMD, Taboada P, Remuñán-López C and Almeida AJ. *Rifabutin-loaded solid lipid nanoparticles for inhaled antitubercular therapy: Physicochemical and in vitro studies*. International Journal of Pharmaceutics. 2016, 497 (1-2), 199-209.

This page was intentionally left blank.

Abstract

Systemic administration of antitubercular drugs can be complicated by off-target toxicity to cells and tissues that are not infected by *Mycobacterium tuberculosis*. Delivery of antitubercular drugs via nanoparticles directly to the infected cells has the potential to maximize efficacy and minimize toxicity. The present work demonstrates the potential of solid lipid nanoparticles (SLN) as a delivery platform for rifabutin (RFB). Two different RFB-SLN formulations were produced using glyceryl dibehenate or glyceryl tristearate as lipid components. Full characterization was performed in terms of particle size, encapsulation and loading efficiency, morphology by transmission electron microscopy and differential scanning calorimetry studies. Physical stability was evaluated when formulations were stored at 5±3°C and in the freeze-dried form. Formulations were stable throughout lyophilisation without significant variations on physicochemical properties and RFB losses. The SLN showed to be able to endure harsh temperature conditions as demonstrated by dynamic light scattering. Release studies revealed that RFB was almost completely released from SLN. *In vitro* studies with THP1 cells differentiated in macrophages showing a nanoparticle uptake of 46±3% and 26±9% for glyceryl dibehenate and glyceryl tristearate SLN, respectively. Cell viability studies using relevant lung cell lines (A549 and Calu-3) revealed low cytotoxicity for the SLN, suggesting these could be new potential vehicles for pulmonary delivery of antitubercular drugs.

Graphical abstract

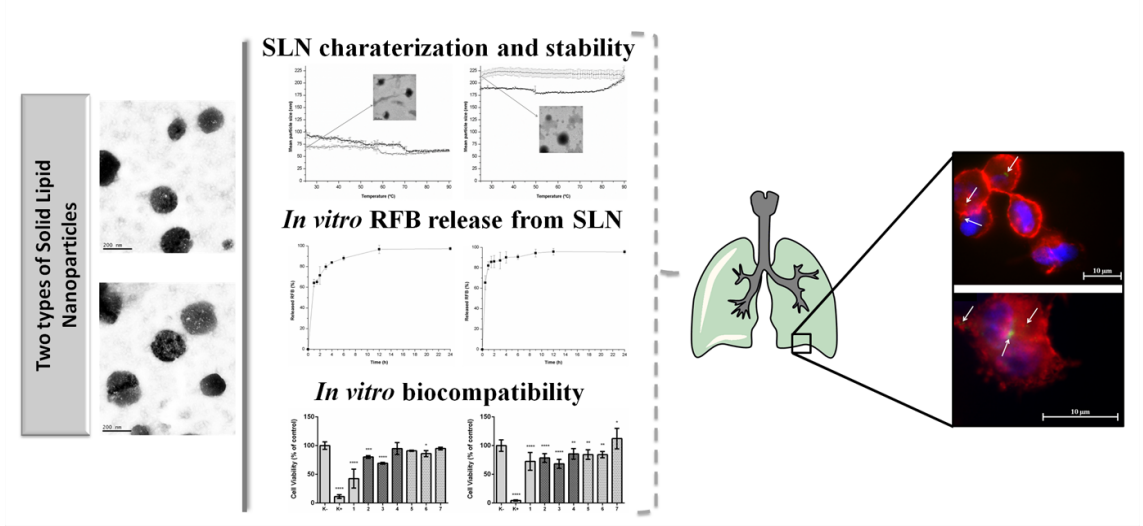

This page was intentionally left blank.

2.1. Introduction

Rifabutin (RFB) has activity against mycobacteria including atypical organisms such as *Mycobacterium avium* and *M. intracellulare*, also referred to as *M. avium-intracellulare* complex (MAC). It is used as an alternative to macrolides, being generally more active *in vitro* than rifampicin against rifampicin-susceptible isolates of *M. tuberculosis*, and also for the prophylaxis of MAC infection in immunocompromised patients [1].

Pulmonary TB remains the commonest form of this disease and the development of methods for delivering anti-tubercular drugs directly to the lung via the respiratory route is a rational therapeutic goal. The obvious advantages of inhaled therapy include direct drug delivery to the diseased organ, targeting to alveolar macrophages harbouring the *M. tuberculosis*, reduced risk of systemic toxicity and improved patient compliance [2]. As *M. tuberculosis* resides and multiplies within host mononuclear phagocytes, which internalize particles efficiently, encapsulation of antitubercular drugs within nanoparticles offers a mechanism for specific targeting of infected cells. Indeed, nanoparticles are taken up by the mononuclear phagocyte system and accumulate in macrophages, being ideally suited to treat *M. tuberculosis*. An additional advantage of nanoparticles delivery of antitubercular drugs is that it shields the drug from degradation or modification prior to delivery of the drug to infected tissues [3, 4].

SLN are colloidal lipid-based carriers prepared with lipids that are solid at room and body temperatures, and with surfactants generally recognized as safe, which are used to stabilize the nanocarriers avoiding aggregation [5, 6]. They have received increased attention over the last decade, presenting good physical stability, providing drug protection and allowing controlled and targeted drug release. SLN can be produced without using organic solvents, minimizing the toxicological risk and are easy to scale up and sterilize, thus fulfilling the requirements for an optimum particulate carrier system [7-9]. Previous studies performed in our laboratories showed ^{99m}Tc-radiolabelled SLN could be successfully aerosolized and delivered by inhalation. The authors proposed the same strategy for the treatment of lung cancer using SLN containing paclitaxel being demonstrated that this system provides a target administration, which is expected to avoid a high concentration of the drug at non-target tissues, reducing toxicity and increasing the drug's therapeutic index [10].

In fact, the concept of delivering antitubercular drug through the aerosol route is not new. In earlier studies, microparticles encapsulating rifampicin or rifampicin plus isoniazid were used for this purpose [11, 12]. More recently, inhalable polymeric nanoparticles and liposomes were shown to be efficient antitubercular drug carriers. However, the advantage of using SLN over the use of liposomes is their long-term stability as well as superior drug incorporation efficiency. However, SLN have not yet been fully explored for the respiratory delivery of antitubercular drugs. In fact, the SLN nebulization is a new and upcoming area of research [2]. Therefore, the aim of this work was to encapsulate RFB in SLN formulations and demonstrate its suitability for pulmonary administration. The study involved a full SLN physicochemical characterization, as well as the stability studies of SLN in liquid suspension and in freeze-dried form during 12 months. *In vitro* evaluation included cytotoxicity analysis using relevant lung cell lines and the uptake evaluation by human monocytes.

2.2. Materials

RFB was acquired from CHEMOS GmbH (Germany). Glyceryl dibehenate (m.p. 70°C) was a kind gift from Gattefossé (France). Glyceryl tristearate (m.p. 72-75°C), 3-(4,5-dimethyl-2-thiazolyl)-2,5-diphenyl-2H-tetrazolium bromide (MTT), propidium iodide, dimethylsulfoxide (DMSO), phorbol 12-myristate 13-acetate (PMA) and paraformaldehyde were purchased from Sigma-Aldrich (USA). Tween® 80 (polysorbate 80) was obtained from Merck (Kenilworth, USA). Lung surfactant (Curosurf®) was a generous gift from Angelini Farmacêutica, Lda. (Portugal). For the viability studies, three cell lines were used: A549 (human alveolar lung carcinoma cell line, ATCC® CCL-185™), Calu-3 (human lung adenocarcinoma from tracheobronchial epithelium cell line, ATCC® HTB-55™) and THP1 cells (human monocytic cell line, ATCC® TIB-202™). DAPI, the culture medium and their supplements were acquired from Life Technologies (UK). Phosphate buffered saline (PBS, pH 7.4) was purchased from Invitrogen™. Purified water was obtained by inverse osmosis (Millipore, Elix 3) with a 0.45 μm pore filter. All other reagents were of analytical grade and were used without further purification.

2.3. Methods

2.3.1. RFB solubility studies

In a first stage, the solubility of RFB in the molten lipids (glyceryl dibehenate and glyceryl tristearate) was determined using a slight modification of a previously described method [13]. Briefly, the solid lipids were melted at a temperature 10°C above their respective m.p. (glyceryl dibehenate has a m.p. of 70°C and glyceryl tristearate between 72-75°C), in a controlled temperature water bath. Small amounts of RFB were then successively added until the saturation of the lipid was achieved. This occurred when excess of solid RFB persisted for more than 8 h. Each determination was carried out in triplicate (n=3).

2.3.2. Formulation of SLN

The preparation of SLN was made using glyceryl dibehenate or glyceryl tristearate as the lipid component and Tween® 80 as a surfactant, using a modification of a previously described-hot high shear homogenization (HSH) method [14]. Briefly, the lipid phase was melted at a temperature 10°C above its m.p.. RFB was added to the melted lipid until complete dissolution. An aqueous phase was prepared by dissolving Tween® 80 in purified water and heated to the same temperature of the oil phase. Then, the hot aqueous phase was added to lipid phase and homogenization was carried out using a high-shear laboratory mixer (Silverson SL2, UK) at 12300 rpm for 10 min, in a water bath to keep the melting temperature of the lipids. The SLN dispersions were finally obtained by allowing the hot nanoemulsion to cool in an ice bath, with gentle agitation for 5 min. Each formulation was carried out in triplicate (n=3). The final dispersions were packaged in sterile glass vials, closed with bromobutyl rubber stoppers, sealed with aluminium seal, and stored at 5±3°C until further use.

2.3.3. Characterization of SLN

2.3.3.1. Particle size, surface charge and physical stability

The average particle size was analysed by photon correlation spectroscopy (PCS) using a Zetasizer Nano S (Malvern Instruments, UK). Samples were kept in polystyrene cuvettes

and the measurements were made at 25.0±0.1°C after appropriate dilution in 0.45 μm-pore filtered purified water (1:100). Results were expressed as average particle size and polydispersity index (PI). Surface charge was determined through particle mobility in an electric field to calculate the zeta potential of SLN using a Zetasizer Nano Z (Malvern Instruments, UK). For this purpose, samples were placed in a specific cuvette where a potential of ±150 mV was established after appropriate dilution of the samples in filtered purified water. For all the measurements, at least three replicate samples were determined.

2.3.3.2. Encapsulation efficiency and drug loading

After preparation, non-incorporated RFB was separated from the SLN dispersions by size exclusion chromatography on Sephadex G-25/PD-10 columns. The RFB incorporation in SLN was determined after dissolving the nanoparticles with acetonitrile, which promoted the precipitation of the lipid phase. The encapsulated RFB remained in the supernatant, which was separated by centrifugation. The amount of free drug in the aqueous phase was measured in the supernatant using UV-Visible spectrophotometry, at λ_{max} of 320 nm, in a microplate spectrophotometer reader (FLUOstar Omega, BMGLabtech, Germany). The supernatant of unloaded nanoparticles was used as basic correction. This quantification method was actually validated based on the international guideline *ICH Topic Q2(R1) (CPMP/ICH/381/95), Validation of Analytical Procedures*, showing sensitivity and precision adequate to the concentration range used in this investigation. The linearity was established between 0.375 and 0.00037 mg/mL with a standard error of the method of 0.0034 and a 5% relative standard deviation. Intraday precision for the standard controls prepared at 0.375 and 0.094 mg/mL was less than 5% relative standard deviation. The limit of quantification and detection were 0.034 mg/mL and 0.011 mg/mL, respectively, with 95% of confidence.

The RFB EE and DL were calculated according to the following equations:

$$\mathrm{EE}(\%) = \frac{\mathrm{W}_{\mathrm{loaded\ drug}}}{\mathrm{W}_{\mathrm{initial\ drug}}} \times 100 \qquad \text{(Eq. 2.1)}$$

$$\mathrm{DL}(\%) = \frac{\mathrm{W}_{\mathrm{loaded\ drug}}}{\mathrm{W}_{\mathrm{lipid}}} \times 100 \qquad \text{(Eq. 2.2)}$$

where $W_{initial\ drug}$ is the weight of the drug used, $W_{loaded\ drug}$ is the weight of encapsulated drug that was detected in the supernatant after SLN purification, solubilization and centrifugation and W_{lipid} represents the weight of the lipid vehicle.

2.3.3.3. Stability studies

Stability of SLN suspensions was evaluated in different conditions: the aqueous suspension of SLN at 5±3°C and its freeze-dried form at room temperature in a dessicator. For stability in suspension, SLN were stored at 5±3°C and mean particle diameter, PI and zeta potential were determined after 6 and 12 months of storage. The average particle size was analysed by PCS using a Zetasizer Nano S (Malvern Instruments, UK) as described in section 2.2.3.1. Besides, for detection of larger sized particles, i.e., outside the measuring range of PCS, laser diffractometry (LD) was employed using a Malvern Mastersizer 2000 (Malvern Instruments, UK). In this equipment, the size distribution measurements were achieved five times for individual samples and at least three replicate samples were done (n=3). Stability evaluation was also performed in terms of EE and DL after separation of non-incorporated RFB by size exclusion chromatography, as described above.

The effect of freeze-drying was also assessed. For that, after preparation, SLN formulations were divided into two aliquots of equal volume. One aliquot was frozen overnight and freeze-dried for 24 h (Christ Alfa 1-4, Osterode am Harz, Germany) while the other one (reference) was kept at 5±3°C for comparative evaluation of the physicochemical properties (particle diameter, PI and surface charge as well as EE and DL).

2.3.3.4. Transmission electron microscopy analysis (TEM)

The morphological analysis of SLN was conducted by TEM. The samples were stained with phosphotungstic acid at 2% (w/v) during 2 min and fixed on racks of copper covered by a membrane of carbon for observation. Afterwards, they were analysed with a JEOL Microscopy (JEM 2010, Japan) at 120 kV, and the images were acquired through a Gatan Orius™ camera.

2.3.3.5. Thermal analysis using dynamic light scattering (DLS)

The influence of temperature on the physical stability of SLN suspensions was assessed using- DLS (Zetasizer Nano S; Malvern Instruments, UK). Samples were appropriately diluted with purified water (1:100) in a quartz cell and particle size analysis was performed while heating the sample from 25°C up to 90°C at a rate of 0.5°C/min and subsequently followed by cooling from 90°C to 25°C at a rate of 0.5°C/min. Particle size measurements were made every 0.5°C. For each sample, measurements were carried out in triplicate (n=3). Morphology of SLN after these thermal studies was assessed by TEM, as previously described.

2.3.3.6. Differential scanning calorimetry (DSC) studies

Measurements were performed on a calorimeter DSC Q200 (TA Instruments, DE, USA). The SLN dispersions (empty and loaded with RFB) and bulk materials (glyceryl dibehenate, glyceryl tristearate, Tween® 80 and RFB) were accurately weighted into aluminium pans, which were hermetically sealed and measured against an empty reference pan. The pan was heated and the thermograms were recorded at temperature range from -20°C to 240°C at a heating rate of 10°C/min. The heat flow was measured.

2.3.4. *In vitro* cell viability studies

The cytotoxicity of SLN formulations was assessed using MTT reduction [7] and propidium iodide exclusion assays. MTT is a yellow, water-soluble tetrazolium dye that is converted by viable cells to a water-insoluble and purple compound, formazan [15]. Cell viability was assessed in A549 and Calu-3 after 24 h of incubation of the cell lines with the different formulations. The Calu-3 and A549 respiratory epithelial cell lines have been frequently used in this context to evaluate the behaviour of systems aimed at respiratory drug delivery, either nasal or pulmonary [16]. The day before the experiment, A549 and Calu-3 cell lines were seeded in sterile flat bottom 96 well tissue culture plates (Greiner, Germany), in RPMI 1640 culture medium, supplemented with 10% foetal serum bovine, 100 units/m of penicillin G (sodium salt), 100 μg/mL of streptomycin sulfate and 2 mM L-glutamine, at a cell density of $1x10^5$ cells/mL, and 100 μL per well. Cells were incubated at 37ºC and 5% CO_2. On the next day, the medium of the cell lines A549 and

Calu-3 cells was replaced by fresh medium containing the different samples to be analysed. Each sample was tested in six wells per plate. In negative control (K-), cells were incubated with culture medium and, in positive control (K+), sodium dodecyl sulphate (SDS) was added at 1 mg/mL in order to promote the cell lyses. After 24 h of incubation, medium was replaced by 0.3 mM propidium iodide in culture medium (stock solution 1.5 mM in DMSO, diluted with culture medium 1:5). Fluorescence was measured (excitation, 485 nm; emission, 590 nm) in microplate reader (FLUOstar Omega, BMGLabtech, Germany), and then, the MTT assay was performed. Medium was replaced by medium containing 0.25 mg/mL MTT. The cells were further incubated for 3 h. On the plates that contain reduced MTT, the media was removed and the intracellular formazan crystals were solubilized and extracted with 100 µL DMSO. After 15 min at room temperature, the absorbance was measured at 570 nm in a microplate reader (FLUOstar Omega, BMGLabtech, Germany). The relative cell viability (%) compared to control cells was calculated for the MTT assay using the following equation:

$$\text{Cell Viability (\% of control)} = \frac{\text{Abs}_{\text{sample}}}{\text{Abs}_{\text{control}}} \times 100 \qquad \text{(Eq. 2.3)}$$

where $\text{Abs}_{\text{sample}}$ is the absorbance value obtained for cells treated with nanoparticles and $\text{Abs}_{\text{control}}$ is the absorbance value obtained for cells incubated with culture medium.

And for propidium iodide by:

$$\text{Cell Viability (relative to control)} = \frac{\text{Fluorescence}_{\text{sample}}}{\text{Fluorescence}_{\text{control}}} \qquad \text{(Eq. 2.4)}$$

where $\text{Fluorescence}_{\text{sample}}$ is the relative fluorescence unit (URF) values obtained for cells treated with nanoparticles and $\text{Fluorescence}_{\text{control}}$ is the URF values obtained for cells incubated with culture medium.

2.3.5. Quantitative SLN uptake assessment

To assess SLN-cell interactions, SLN were labelled by incorporating coumarin-6 after lipid melting. THP1 cell line was grown in 96 well plates at a cell density of $2.5\text{x}10^5$ cells/mL. Cells were incubated at 37ºC and 5% CO_2. Then, the THP1 cell line was differentiated to macrophages for 3 days with 200 nM of PMA before exposition to the samples. After 3 days, the culture medium was replaced by 100 µL of coumarin-6 loaded nanoparticles in the test wells, in order to obtain a final SLN concentration of 0.75

mg/mL. Fluorescence measurements were performed at excitation wavelength of 485 nm and emission 520 nm. These determinations were performed immediately after particles addition and after several incubation times (1 h and 24 h at 37°C, 5% CO_2) after 3 washing steps with 250 µL of PBS containing 20 mM glycine at pH 7.4 pre-warmed at 37°C. The PBS solution was removed and the cells were disrupted with 100 µL of 1% Triton X-100 solution and the fluorescence was again measured to determine the internalized amount of particles. The particles internalized were determined as a percentage of the initial amount feed of cells. Using particle fluorescence as a function of their concentration, it was possible to determine the amount of particles internalized by cells.

2.3.6. Fluorescence Microscopy

Cell cultures were performed at same conditions as described in section 2.3.4, in terms of incubation times of particles tested and cell density. Cells grown on 12 multi-well plates containing sterile glass slides (Greiner, Germany). After the time of incubation with particles, cells were rinsed 3 times with 10 mM PBS containing 20 mM glycine at pH 7.4 before and after being fixed for 15 min at room temperature in dark with a 4% (w/v) paraformaldehyde. After cell fixation, and, for actin staining with Rhodamine phalloidin, cells were permeabilized with 0.1% Triton X-100 for 4 min, then cells were rinsed 3 times with 10 mM PBS containing 20 mM glycine at pH 7.4. The 6.6 µM phalloidin-TRITC solution in 10 mM PBS was added to the cells for 30 min at room temperature. After cells rinsed 3 times with 10 mM PBS containing 20 mM glycine at pH 7.4, and air dried, cell slides were mounted in fluorescent mounting medium ProLong® Gold antifade reagent with DAPI and their fluorescence was observed and recorded on an Axioscop 40 fluorescence microscope (Carl Zeiss, Germany) equipped with an Axiocam HRc (Carl Zeiss, Germany) camera. Images were processed with the software AxioVision Rel. 4.8.1 (Carl Zeiss, Germany).

2.3.7. *In vitro* RFB release studies

Prior to the release studies, the nanodispersions were desalted on Sephadex G-25 medium pre-filled PD-10 columns (GE Healthcare Life Sciences). The release of RFB was carried

out by incubating the nanoparticles in a release medium comprising 10 mM PBS pH 7.4 and 0.1% of pulmonary surfactant (Curosurf®) (0.75 mg of nanoparticles in 1 mL of the release medium), with horizontal shaking (300 rpm) at 37°C. At appropriate time intervals, individual samples were centrifuged (Allegra™ 64R centrifuge, Beckman Coulter) at 30000×g for 30 min at 4°C. The amount of released RFB was evaluated in the supernatants by spectrophotometry in a microplate reader (FLUOstar Omega, BMG Labtech, Germany) at 320 nm (n=3).

In order to investigate the mechanism of RFB release from glyceryl dibehenate and glyceryl tristearate SLN, the obtained release data were analyzed with different models including: zero-order (Eq. 2.5), first-order (Eq. 2.6), Higuchi (Eq. 2.7) and Korsmeyer–Peppas (Eq. 2.8) [17]:

$$M_t = M_0 + k_0 t \quad \text{(Eq. 2.5)}$$

$$\log M_t = \log M_0 + \frac{k_1}{2.303} t \quad \text{(Eq. 2.6)}$$

$$M_t = M_0 + k_H t^{1/2} \quad \text{(Eq. 2.7)}$$

$$M_t = k_{KP} t^n \quad \text{(Eq. 2.8)}$$

where M_0 is the initial amount of RFB, M_t is the cumulative amount of drug release at time t, k_0 is the zero-order release constant, k_1 is the first-order release constant, k_H is the Higuchi constant, k_{KP} is the Korsmeyer–Peppas constant and n is an exponent characterizing the release mechanism. The model that best fits the experimental data was selected based on the highest determination coefficient (r^2) values. The OriginPro8 software was used to perform the data treatment.

2.3.8. Statistical analysis

Statistical analysis of the experimental data was performed using a one-way analysis of variance (one-way ANOVA) and differences between groups were tested by a one-way ANOVA with Dunnet's post hoc test with GraphPad Prism version 6.0 (GraphPad Software, San Diego, CA). Data were expressed as mean±SD or 95% confidence interval. A p<0.05 value was considered significant. All data are shown as mean±SD.

2.4. Results and Discussion

2.4.1. SLN characterization

Delivery of antitubercular drugs by nanoparticles offers potential advantages over free drug, including the potential to target specifically the tissues and cells that are infected by *M. tuberculosis*, thereby increasing therapeutic efficacy and decreasing systemic toxicity, as well as the capacity for prolonged drug release, allowing less-frequent administration [3]. In this context, two different SLN compositions loaded with RFB were prepared using different lipids (glyceryl dibehenate and glyceryl tristearate), and Tween® 80 as the surfactant component. The resultant SLN presented particle size distributions within the nanometre range with PI values < 0.2 (Table 1). Negative zeta potential values of -17 mV and -18 mV were observed for glyceryl dibehenate and glyceryl tristearate SLN, respectively. Although below the critical zeta potential for stability in terms of purely electrostatic repulsions, these values still indicate a good colloidal stability of the nanoparticles suspensions considering the sterically stabilizing effect of Tween® 80 [18].

The RFB was incorporated in both lipid formulations at theoretical amounts of 10.0% and 7.3% (w/w) relative to glyceryl dibehenate and glyceryl tristearate, respectively. These concentrations were selected based on preliminary solubility studies and correspond to the maximum solubility of RFB in the molten lipids. High RFB incorporation, as expressed by EE and DL, was obtained for both formulations, confirming similar results described in the literature for other lipids as hard fat suppository bases [19], tripalmitin [7] and glyceryl palmitostearate [20]. The EE values obtained for RFB were 89.9±5.1% for glyceryl dibehenate SLN and 81.0±9.6% for glyceryl tristearate SLN.

Moreover, comparison of blank SLN with those loaded with RFB reveals drug incorporation into SLN led to an increase in zeta potential, which may be explained by the fact that RFB is a strong base with a dissociation constant (pKa) of 8.62 and, therefore, predominantly negative at the formulation pH value (pH 7-8). No significant variations on size and PI were observed after RFB inclusion in the formulations as compared to empty SLN. Again, the SLN suspensions remained fairly homogeneous with no significant aggregate formation. Microscopy studies by TEM confirmed the particle size distributions previously established from the PCS analysis. The spherical nanostructure of SLN is also evident in TEM micrographs as well as the compact appearance, which is similar to unloaded nanoparticles (Figure 2.1).

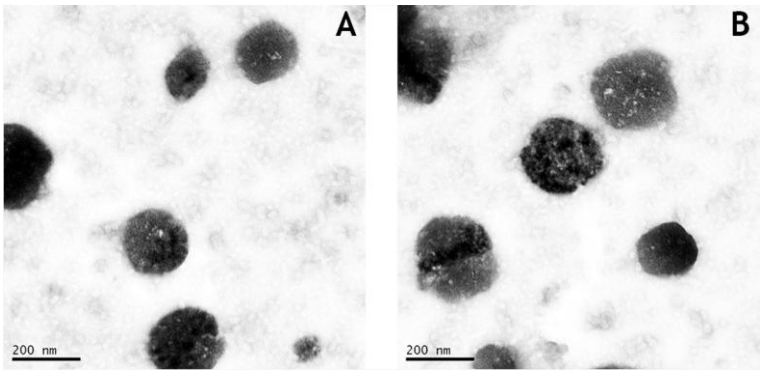

Figure 2.1: TEM micrographs of RFB-loaded SLN based on (A) glyceryl dibehenate and (B) glyceryl tristearate (scale bar: 200 nm).

2.4.2. Stability studies

When nanocarriers are formulated as aqueous suspensions, both physical (aggregation/ particle fusion) and chemical instability phenomena are known to appear at some point, limiting nanoparticles applications. Regarding the present work, it is important to recall that a pulmonary formulation of nanoparticles may involve the lyophilisation of the nanoparticles suspensions, which facilitates administration and can be beneficial for storage [21]. The ability of the SLN matrix to retain RFB and keep the physical properties during storage was assessed both on nanoparticles suspensions at 5±3°C and after lyophilisation after 6 and 12 months. The stability-indicating parameters were particle mean diameter, PI, surface charge and DL (Table 2.1). The physical properties (particle size, PI and surface charge) of the empty and RFB-loaded SLN suspensions stored at 5±3°C remained almost unchanged for up to 12 months, indicating there was no tendency to form aggregates being then the dispersions stable. However, by LD analysis it was possible to observe the presence of some aggregates after 12 months (Figure 2.2B). On the other hand, over the time there was a considerable decrease in RFB content, which may be due to polymorphic transitions of the lipid matrices with subsequent drug expulsion, as described elsewhere [22, 23].

Lyophilisation is being widely used to overcome physical instability of nanosuspensions by reducing the amount of water, which improves the physical and chemical stability of the nanosystems [21]. In the present work, SLN were lyophilised and then rehydrated, which can induce changes in particle size, although formulations remained within the

nano-range scale allowing their use in further studies (Table 2.1). This increase in particle size of lyophilised SLN may be due to the absence of a cryoprotectant during lyophilisation. However, LD analyses did not reveal the presence of aggregates after 12 months of formulation (Figure 2.2D). Despite of this size increase, there was a lower decrease in RFB content when compared to that of SLN that were kept in suspension at 5±3°C. Zeta potential and PI values did not evidence significant alterations after lyophilisation in any tested conditions. Previous stability studies from our laboratories also showed that SLN can be freeze-dried without significant variations in physicochemical properties or significant drug losses throughout the process [7]. Lyophilisation appears in this context as a very adequate choice for ensuring a mild drying procedure while preserving stability even without the use of cryoprotectants.

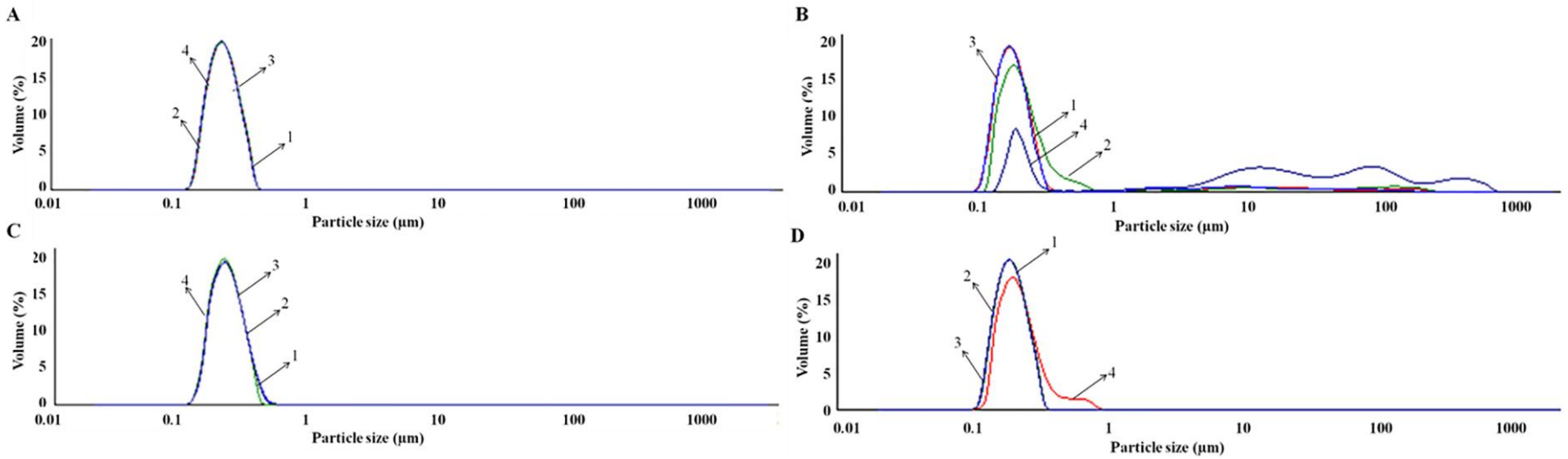

Figure 2.2: Particle size distribution of SLN after formulation (A) and 12 months of storage (B) at 5±3°C in suspension and in freeze-dried form after formulation (C) and 12 months of storage (D): (1) empty glyceryl dibehenate SLN, (2) empty glyceryl tristearate SLN, (3) RFB loaded-glyceryl dibehenate SLN and (4) RFB loaded-glyceryl tristearate SLN.

Table 2.1: Physicochemical properties of: (A) empty glyceryl dibehenate SLN, (B) RFB-loaded glyceryl dibehenate SLN, (C) empty glyceryl tristearate SLN and (D) RFB-loaded glyceryl tristearate SLN freshly prepared and after 6 and 12 months of storage in suspension at 5±3°C and in lyophilised form (mean±SD, *n*=3).

		SLN Suspension at 5±3°C				Lyophilised SLN			
		A	**B**	**C**	**D**	**A**	**B**	**C**	**D**
∅ (nm)	**Month 0**	99±4	108±5	210±8	191±7	103±4	121±2	219±16	299±10
	Month 6	92±1	102±0	187±1	174±1	96±3	187±2	239±1	291±4
	Month 12	104±8	106±5	210±7	186±12	239±20	223±5	260±11	313±6
PI	**Month 0**	0.12±0.01	0.16±0.03	0.15±0.02	0.17±0.01	0.15±0.02	0.18±0.02	0.19±0.03	0.20±0.02
	Month 6	0.15±0.01	0.16±0.01	0.16±0.01	0.16±0.02	0.13±0.01	0.17±0.03	0.17±0.01	0.19±0.02
	Month 12	0.18±0.02	0.19±0.02	0.18±0.02	0.19±0.04	0.28±0.03	0.17±0.03	0.16±0.02	0.20±0.02
ZP (mV)	**Month 0**	-17.1±0.7	-24.0±0.5	-17.8±0.5	-24.6±0.4	-18.2±0.3	-27.6±0.2	-18.6±0.4	-21.6±0.4
	Month 6	-18.3±0.8	-27.4±0.4	-17.3±0.5	-20.0±0.4	-22.9±0.8	-30.5±1.3	-13.9±0.9	-24.8±0.7
	Month 12	-12.8±0.7	-24.6±2.2	-17.3±2.1	-19.7±0.7	-17.3±0.7	-25.5±1.3	-18.4±1.1	-24.8±0.3
EE (%)	**Month 0**	-	89.9±5.1	-	81.0±9.6	-	70.4±4.5		56.7±2.1
	Month 6	-	36.2±0.3	-	19.9±0.1	-	62.8±3.2	-	53.6±4.3
	Month 12	-	36.3±1.7	-	21.8±3.1	-	68.4±3.2	-	55.9±1.5
DL (%)	**Month 0**	-	9.0±0.5	-	6.0±0.7	-	6.8±0.2	-	4.2±0.4
	Month 6	-	4.0±0.3	-	1.6±0.1	-	6.2±0.9	-	3.9±0.3
	Month 12	-	2.8±0.2	-	2.4±0.2	-	7.2±0.4	-	4.8±0.1

∅: mean particle size; PI: polydispersity index; EE: encapsulation efficiency; DL: drug loading.

2.4.3. DLS thermal analysis

The effect of temperature on particle size of SLN formulations was assessed using DLS, applying a heating ramp from 25°C up to 90°C and then a cooling ramp to the initial temperature (Figure 2.3). This assay allowed to state the psychochemical properties (particle size and PI) when SLN were subjected to a temperature increase followed by a decrease. Nevertheless, DLS studies need to be performed whenever a formulation is intended for further temperature processing. Overall the heating and cooling process induced particle size changes in the SLN prepared with both solid lipids, which behaved in a different manner. In the case of glyceryl dibehenate SLN, a gradual particle size reduction was evident throughout the heating step (from 97 to 71 nm), and the initial particle size was not fully recovered after the cooling phase, in line with previous observations with tripalmitin-based SLN whereby particle size was recovered or even slightly decreased, with variations occurring during process [24]. On the other hand, glyceryl tristearate SLN suffered a slight decrease in particle size during heating followed by a marked increase after 75°C, suggesting some instability at these temperatures. This may occur because glyceryl tristearate is a mixture of mono, di- and triglycerides and not a pure lipid. During the cooling step, particle size stabilizes. The particle size variations were always within the nanosize range, indicating both SLN formulations based on glyceryl dibehenate and glyceryl tristearate may withstand the harsh formulation conditions such as moist-heat sterilization or spray-drying conditions used to prepare microparticles intended for pulmonary delivery, thus confirming previously published results [7, 24].

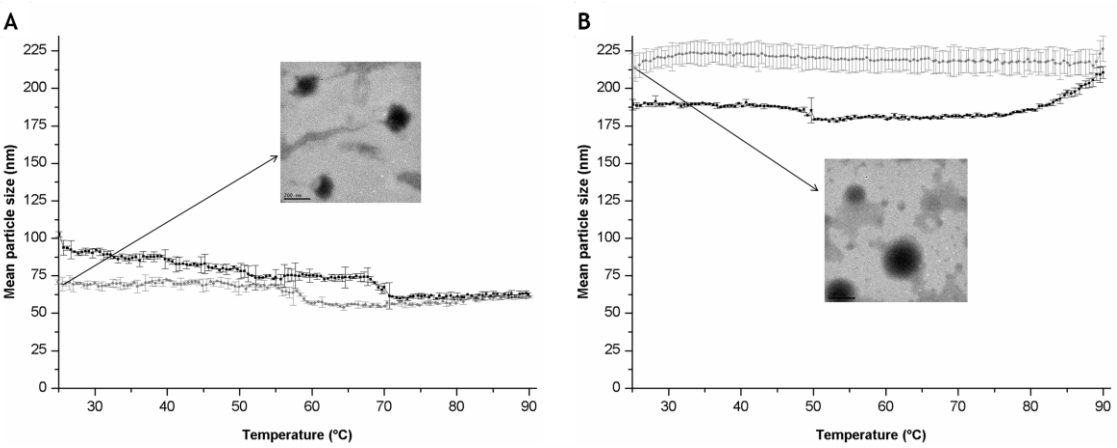

Figure 2.3: DLS thermograms of (A) glyceryl dibehenate SLN and (B) glyceryl tristearate SLN: (■) from 25ºC to 90ºC and (●) from 90ºC to 25ºC (mean±SD, *n*=3), with inset of TEM micrographs of SLN after thermal analysis (scale bar: 200 nm).

2.4.4. DSC analysis

DSC analysis is a powerful technique that was carried out with the aim to observe the physical thermodynamic variations of the samples related to morphological changes when they are submitted at a temperature ramp throughout time. In other words, thermal analysis determines the temperature and heat flow associated with material transitions as a function of time and temperature. It also allows viewing the crystalline state of the drug after being encapsulated in a ternary system (drug-surfactant-lipid). Figure 2.4 shows the thermograms of pure RFB, glyceryl dibehenate, glyceryl tristearate, Tween® 80 and SLN, either empty or incorporating RFB. The thermograms of pure lipids showed melting peaks of 74°C and 60°C for glyceryl dibehenate and glyceryl tristearate, respectively. Pure RFB showed a melting endotherm at approximately 149°C. All these values are in agreement with those reported in the literature. Concerning RFB, the thermogram also showed complete degradation after the m.p. was reached. However, the thermograms of both freeze-dried RFB-SLN preparations did not show the melting peak of RFB, which can be ascribed to the amorphous or molecularly dispersed structure of the RFB in the lipid matrix. In the preparation method, RFB was dissolved in the molten lipids and, subsequently, the surfactant was added. This allowed the homogeneous dispersion of drug in the lipid. Furthermore, it has been reported that in the homogenization process, such as that herein used, the presence of surfactants and the rapid quenching of the

microemulsion may not allow the drug to crystallize [7, 23]. In all formulations, the m.p. of the lipids was depressed when compared to the m.p. of the bulk lipids (71°C for glyceryl dibehenate SLN, either empty or loaded with RFB and 59°C for glyceryl tristearate SLN, either empty and loaded with RFB). This was attributed to the creation of lattice defects onto the lipid matrices following a decrease in their crystallinity in comparison to their bulk counterparts. For less ordered crystals or amorphous solids, the melting of the substance requires much less energy than crystalline substances that need to overcome lattice forces. This m.p. depression might also be due to small particle size (nano) which significantly increases their surface area or to the presence of surfactants [7, 25]. Despite the reduction on the lipid m.p. in the SLN formulations, no significant effect was observed on lipid matrix thermal behaviour pattern after incorporation of RFB.

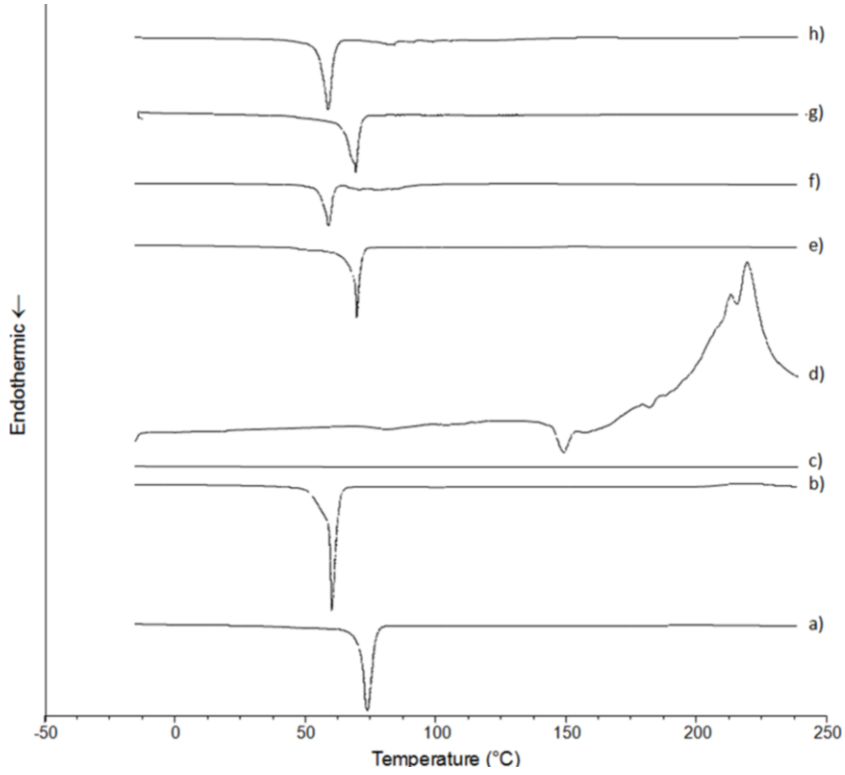

Figure 2.4: DSC thermograms of: (a) glyceryl dibehenate, (b) glyceryl tristearate, (c) Tween® 80, (d) RFB, (e) empty glyceryl dibehenate SLN, (f) empty glyceryl tristearate SLN, (g) RFB-glyceryl dibehenate SLN and (h) RFB-glyceryl tristearate SLN.

2.4.5. *In vitro* cell viability studies

Evaluating the biocompatibility of drug delivery formulations is nowadays a mandatory aspect to address. While an accurate determination of the toxicity of a formulation can only be determined *in vivo*, a variety of *in vitro* toxicological assays, performed in adequately selected cell lines, might provide very useful information and are widely accepted as first indicators. Current international guidelines require the evaluation to be contextualised with a specific route of administration and dose of the material [26].

To address the above mentioned issues, the evaluation of the biocompatibility of SLN was performed by means of two different assays, i.e. the metabolic activity (MTT) and the cell membrane integrity through propidium iodide assay. The SLN were prepared from biocompatible lipids, so better tolerability with respect to polymeric nanoparticles can be hypothesized. In addition, triglycerides, fatty acids or waxes are known to release natural occurring degradation by products [27]. To investigate the potential cytotoxicity of glyceryl dibehenate and glyceryl tristearate SLN, empty and loaded with RFB, the cell viability when in contact with SLN was evaluated using selected lung cell lines (A549 and Calu-3) as they are representative of the respiratory epithelia. Calu-3 is an immortalised cell line obtained from lung adenocarcinoma and has been extensively used in the study of formulations designed for either nasal or pulmonary drug delivery, as it is considered a model of the epithelium of both regions, whereas A549 is a cell line representative of the alveolar epithelium, obtained from human alveolar adenocarcinoma [21].

The MTT assay provides an evaluation of the cell metabolic activity upon exposure to the samples and has been used very frequently in the assessment of drug delivery carriers biocompatibility [28]. It evaluates the ability of the cells to reduce the MTT reagent to tetrazolium salts, an action that is dependent on mitochondrial metabolism. A reduction of cellular metabolic activity is generally accepted as an early indicator of cellular damage [29]. In this work, A549 and Calu-3 cells were cultured and exposed to SLN for a prolonged period (24 h). After this incubation period, no evidence of acute cytotoxicity was observed for the nanoparticles (with and without RFB) at the concentration used for transfection. Over 80% cell viability was observed in A549 and Calu-3 cell lines for both nanodispersions when compared to a negative control consisting of cells incubated only with fresh medium (Figure 2.5).

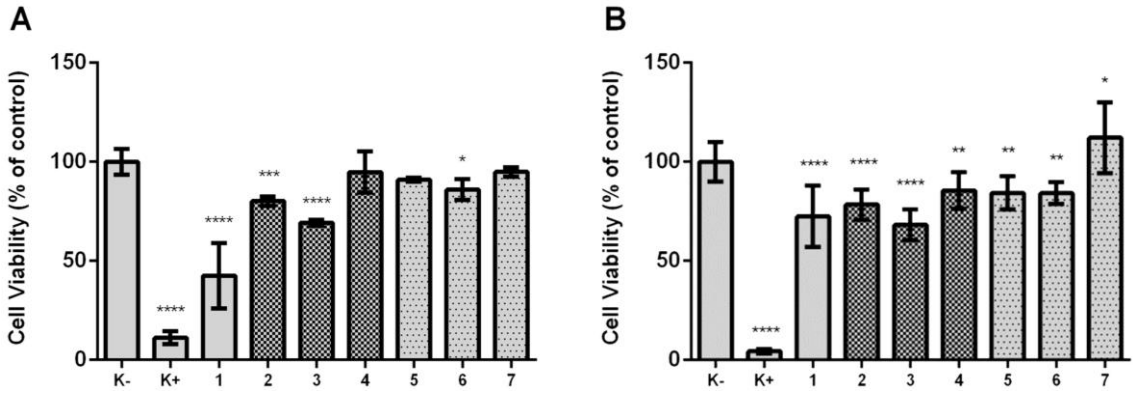

Figure 2.5: Relative cell viability of (A) A549 and (B) Calu-3 cell lines measured by the MTT reduction. (K-) negative control (culture medium); (K+) positive control (SDS, 1 mg/mL); (1) Tween® 80; (2) empty glyceryl dibehenate SLN; (3) RFB loaded-glyceryl dibehenate SLN; (4) RFB solution at 75 µg/mL; (5) empty glyceryl tristearate SLN; (6) RFB loaded-glyceryl tristearate SLN and (7) RFB solution at 75 µg/mL. The nanoparticles concentration is 0.75 mg/mL in all samples. Results are expressed as mean±SD (n=6). Statistical analysis between the control group (K-) and other groups was performed using one-way ANOVA with Dunnet's post hoc test (*p<0.05, **p<0.01, ***p<0.001 and ****p<0.0001).

Moreover, the cells in contact with SLN had higher viability than that of the positive control, where cells were in contact with SDS, an anionic surfactant that promotes cell lysis. Therefore, as a cell viability of 70% is the threshold beyond which a cytotoxic effect is considered to occur according to ISO 10993-5, the observed effects are devoid of physiological relevance (ISO, 2009). This indicates that Calu-3 and A549 cells do not evidence a particular sensitivity to any of the tested samples, either pure RFB or nanoparticles-based formulations, at the tested concentrations. The decrease in cell viability (≈20%) was an expected finding, because SLN were formulated using Tween® 80 and surfactants are considered to be decisive in SLN toxicity [30]. These findings are also in good agreement with other studies reporting an increased cytotoxicity of Tween® 80 in combination with nanoparticles [31, 32]. Nevertheless, the SLN cytotoxicity is relatively low in general when compared to polymeric nanoparticles, particularly those produced with polyalkylcyanoacrylates or PLGA [33, 34]. Furthermore, the incorporation of RFB in SLN did not promote major differences in cell viability when compared to

blank formulations. These findings, in both respiratory cell lines, are considered good indicators of biocompatibility.

On the other hand, propidium iodide serves as a dead cell indicator since this dye monitors losses in membrane integrity [35]. Thus, the retention values of propidium iodide in positive control were high, since these cells were not viable, with a damaged cell membrane promoting dye uptake (> 2 URF for glyceryl dibehenate SLN and > 1.5 URF for glyceryl tristearate SLN). On the other hand, in the negative control, cells were only incubated with fresh medium, being viable, with intact cell membranes and consequently presented low values of propidium iodide uptake (≈ 1 URF) [36]. Moreover, Figure 2.6 also shows that the cell membranes that were in contact with the formulations were also intact because the values of propidium iodide assay are approximately equal to the negative control (≈1 URF for all formulations), concluding that these cells had not disrupted plasma membranes.

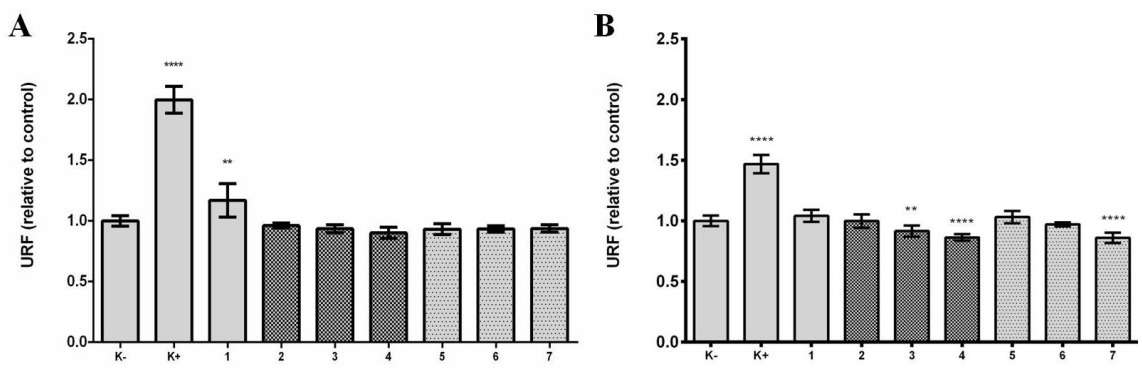

Figure 2.6: Propidium iodide uptake by (A) A549 and (B) Calu-3 cell lines. (K-) negative control (culture medium); (K+) positive control (SDS, 1 mg/mL); (1) Tween® 80; (2) empty glyceryl dibehenate SLN; (3) RFB loaded-glyceryl dibehenate SLN; (4) RFB solution at 75 µg/mL; (5) empty glyceryl tristearate SLN; (6) RFB loaded-glyceryl tristearate SLN and (7) RFB solution at 75 µg/mL. The nanoparticles concentration is 0.75 mg/mL in all samples. Results are expressed as mean±SD (n=6). Statistical analysis between the control group (K-) and other groups was performed using one-way ANOVA with Dunnet's post hoc test (**p<0.01 and ****p<0.0001).

The findings obtained in this work for all nanoparticles-based formulations in both respiratory cell lines are considered good indicators of biocompatibility. However, the evaluation of a biocompatibility profile demands the use of complementary assays to assess other aspects of cell response, which are certainly of importance to establish a final tendency.

2.4.6. Intracellular SLN uptake studies

It is well known that macrophages are predominantly involved in the uptake of nanoparticles, leading to their degradation. The rate of phagocytosis is largely determined by the physicochemical properties of the particle, such as size, surface modification, surface charge and hydrophobicity. Augmented particulate hydrophobicity is known to increase the uptake by forming hydrophobic interactions with the cell surface and, moreover, cationic surface charge is desirable as it promotes interaction of the nanoparticles with cells and, hence, increases the rate and extent of internalization [37, 38]. When nanoparticles are administered *in vivo*, they are rapidly taken up by macrophages. This tendency of nanoparticles is an advantage in the treatment of intracellular infections involving this type of cells, such as TB. The main mechanism by which SLN are captured by phagocytic cells follows several steps: (i) stable adsorption onto the cell membrane, (ii) vesicle internalization through an energy-dependent mechanism, (iii) fusion of the endocytic vesicles with the particles and (iv) degradation of the nanoparticles by lysosomal enzymes, releasing the drug encapsulated within them [33]. In order to demonstrate that glyceryl dibehenate SLN and glyceryl tristearate SLN can be adopted as a platform for delivering anti-TB drugs in human macrophages, both formulations were incubated with PMA-differentiated human macrophage-like THP1 cells. For this purpose, SLN containing the fluorescent label coumarin-6 were incubated with the previous cells at 0.75 mg/mL at 37ºC for 1 h and 24 h. Results showed SLN were efficiently internalized by these cells (Figure 2.7). Fluorescence microscopy was used to follow the intracellular trafficking of coumarin-6-labeled nanoparticles and their uptake by human THP1 cells. At 1 h after addition of the SLN to macrophages, 25.9±8.6% of RFB loaded-glyceryl dibehenate SLN and 6.3±0.9% of RFB loaded-glyceryl tristearate SLN were internalized in THP1 cells. As expected, this uptake was higher after 24 h of incubation, with 46.3±3.0% and 25.6±9.3% respectively for RFB loaded-SLN based

glyceryl dibehenate and glyceryl tristearate, indicating that nanoparticles are clearly taken up by macrophages. These uptake differences between glyceryl dibehenate and glyceryl tristearate SLN are related with particle sizes, since glyceryl dibehenate SLN (≈100 nm) have a smaller size than those of glyceryl tristearate (≈200 nm) and so they are more readily phagocytized [39]. Indeed, this high uptake is important, because, since *M. tuberculosis* is an intracellular parasite, the SLN formulations herein described are expected to be internalized by the macrophages where the acidic/enzymatic conditions inside the phagolysosome will be sufficient to release the drug from the nanoparticles and make it available to act upon the bacteria.

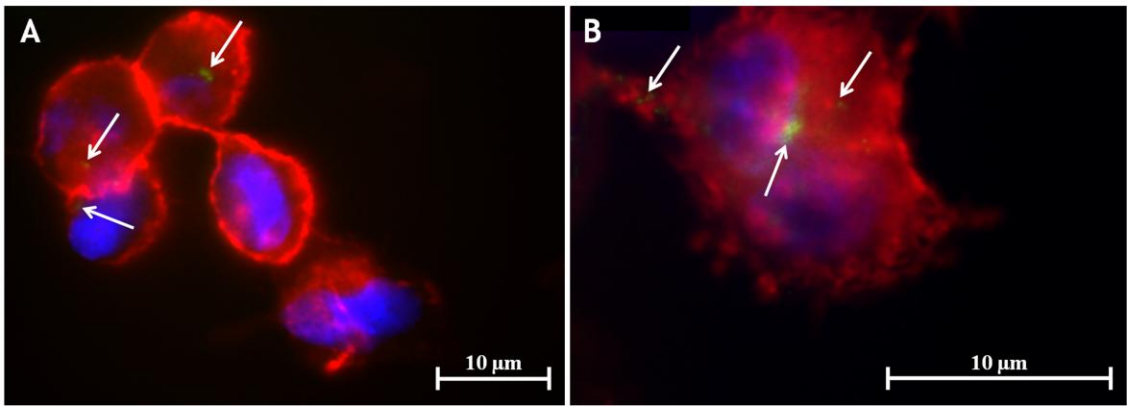

Figure 2.7: Fluorescence micrographs of (A) glyceryl dibehenate and (B) glyceryl tristearate SLN uptake in macrophages. SLN were labeled with coumarin-6 (green, arrows), rhodamine phalloidin was used as a marker of actin (red) and nuclei were stained with DAPI dye (blue) (scale bar: 10 µm).

2.4.7. *In vitro* RFB release studies from SLN

To investigate the ability of the designed SLN to act as drug reservoirs, glyceryl dibehenate and glyceryl tristearate SLN were loaded with RFB, which is used for the treatment of mycobacterial infections caused by *M. tuberculosis* [40]. Release studies were performed using 0.1% of lung surfactant in the release medium with the purpose to mimic the lung environment as well as to increase RFB solubility in the release medium. Both *in vitro* RFB release profiles from SLN presented a drug release profile where almost all encapsulated RFB was released (97.4±1.3% for glyceryl dibehenate SLN and

95.6±1.7% for glyceryl tristearate SLN) over 24 h (Figure 2.8). The drug release from the nanoparticles appeared to have two components with an initial fast release of about 65% at the first sampling time of 30 min. This was followed by a slower exponential release of the remaining drug over the next 12 h. The rapid initial release of RFB was probably due to drug molecules which were adsorbed or close to the surface of SLN, as well as the large surface to volume ratio of the nanoparticles geometry [41]. Overall, upon addition of the nanosuspensions to the release medium, RFB partitioned rapidly into the release medium accounting for the "*burst effect*" observed. On the other hand, the exponential delayed release may be attributed to diffusion of the dissolved drug within the core of the nanoparticles into the dissolution medium. As all drug content was released within 12 h, these systems have great advantages for short-term drug release applications.

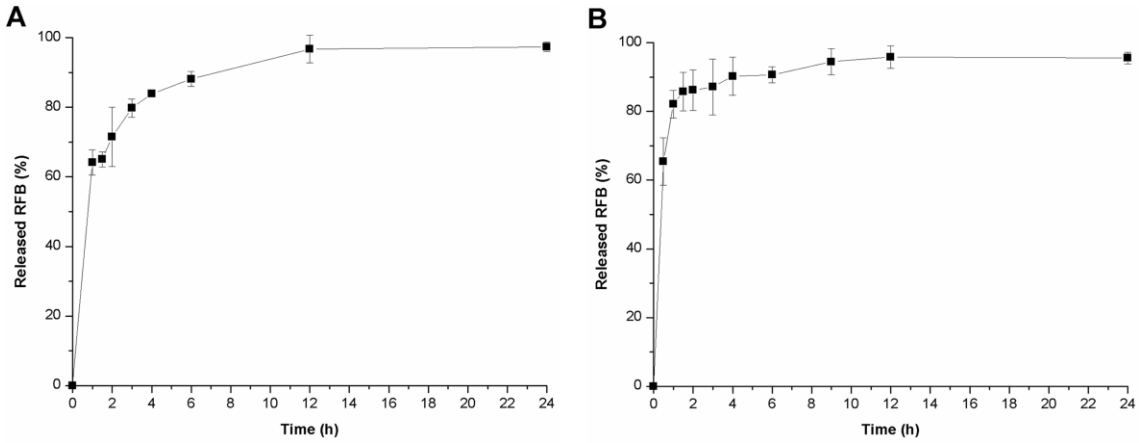

Figure 2.8: Release profiles of RFB from (A) glyceryl dibehenate and (B) glyceryl tristearate SLN in 10 mM PBS pH 7.4 and 0.1% of lung surfactant, at 37°C (mean±SD, *n*=3).

The drug release kinetics was characterized by fitting the experimental data with the standard release equations (eq. 2.5–2.8). According to the r^2 values in Table 2.2, the best fit for both types of SLN was with the Korsmeyer–Peppas model, which was applied as the mechanism of drug release and is used when more than one type of mechanism is involved. Both systems showed a *n* value smaller than 0.43 indicating that the release rate

was also significantly dependent on the rate of RFB diffusion (Fickian diffusion) through the crosslinked lipid networks.

To tailor the release profiles to an appropriate efficiency for certain applications, it would be necessary to change the formulation of the liquid precursor (e.g. concentration of surfactants) to modify the structure of the particles in order to control drug release by increasing the structural complexity of the particles, namely, by the production of multilayer spherical systems where non-loaded layers may act as barriers to control the release of drugs immobilized in the inner layers.

Table 2.2: Mathematical models and respective parameters (correlation coefficients and release constants) obtained from the fitting of the experimental data corresponding to a RFB release from: (A) glyceryl dibehenate SLN and (B) glyceryl tristearate SLN.

	Zero-order		First-order		Higuchi		Korsmeyer-Peppas		
	r^2	k_0 (µg/h)	r^2	k_1 (h^{-1})	r^2	k_H ($h^{-0.5}$)	r^2	k_{KP} (h^n)	n
A	0.343	2.261	0.611	0.017	0.632	16.264	0.922	1.814	0.148
B	0.196	1.716	0.363	0.009	0.434	13.074	0.759	1.895	0.082

r^2: determination coefficient; k_0: zero-order release constant; k_1: first-order release constant; k_H: Higuchi constant; k_{KP}: Korsmeyer–Peppas constant; n: release mechanism exponent

2.5. Conclusions

Stable SLN formulations prepared with two different lipid compositions were optimized revealing high entrapment efficiencies of RFB close to the drug solubility in the molten lipids were obtained. The drug RFB was dissolved in the lipid matrix of the nanoparticles as shown by DSC analysis, while the formulations presented a remarkable physical stability, being able to endure temperature changes up to 90ºC, recovering their particle size and morphology. The nanoparticles were easily internalized by human monocytes, which is an important feature because *M. tuberculosis* is an intracellular parasite. After SLN incubation with lung cells, no evidence of acute cytotoxicity was observed, thus confirming that lipid nanoparticles are potential carrier systems for pulmonary delivery of anti-TB drugs.

2.6. References

1. Adams, I.B.; Schafer, J.J.; Roberts, A.L.; Short, W.R. *Mycobacterium avium* complex (MAC) immune reconstitution syndrome (IRIS) with reduced susceptibility to ethambutol in an HIV-infected patient case report and review of the literature. Ann. Pharmacother., 2014, 48 (9), 1219-1224

2. Pandey, R.; Khuller, G. Solid lipid particle-based inhalable sustained drug delivery system against experimental tuberculosis. Tuberculosis, 2005, 85 (4), 227-234.

3. Clemens, D.; Lee, B.; Xue, M.; Thomas, C.; Meng, H.; Ferris, D.; Nel, A.; Zink, J.; Horwitz, M. Targeted intracellular delivery of antituberculosis drugs to *Mycobacterium tuberculosis*-infected macrophages via functionalized mesoporous silica nanoparticles. Antimicrob. Agents Ch., 2012, 56 (5), 2535-2545.

4. Pandey, R.; Ahmad, Z. Nanomedicine and experimental tuberculosis: facts, flaws, and future. Nanomed.: Nanotechnol., 2011, 7 (3), 259-272.

5. Das, S.; Chaudhury, A. Recent advances in lipid nanoparticle formulations with solid matrix for oral drug delivery. AAPS PharmSciTech, 2011, 12 (1), 62-76.

6. Silva, A.; González-Mira, E.; García, M.; Egea, M.; Fonseca, J.; Silva, R.; Santos, D.; Souto, E.; Ferreira, D. Preparation, characterization and biocompatibility studies on risperidone-loaded solid lipid nanoparticles (SLN): high pressure homogenization *versus* ultrasound. Colloid. Surface B, 2011, 86 (1), 158-165.

7. Lopes, R.; Eleutério, C.; Gonçalves, L.; Cruz, M.; Almeida, A. Lipid nanoparticles containing oryzalin for the treatment of leishmaniasis. Eur. J. Pharm. Sci., 2012, 45 (4), 442-450.

8. Vitorino, C.; Carvalho, F.; Almeida, A.; Sousa, J.; Pais, A. The size of solid lipid nanoparticles: An interpretation from experimental design. Colloid. Surface B, 2011, 84 (1), 117-130.

9. Cipolla, D.; Shekunov, B.; Blanchard, J.; Hickey, A. Lipid-based carriers for pulmonary products: Preclinical development and case studies in humans. Adv. Drug Deliv. Rev., 2014, 75 (1), 53-80.

10. Videira, M.; Almeida, A.J.; Fabra, À. Preclinical evaluation of a pulmonary delivered paclitaxel-loaded lipid nanocarrier antitumor effect. Nanomed.: Nanotechnol., 2012, 8 (7), 1208-1215.

11. Suarez, S.; O'Hara, P.; Kazantseva, M.; Newcomer, C.E.; Hopfer, R.; McMurray, D.N.; Hickey, A.J. Airways delivery of rifampicin microparticles for the treatment of tuberculosis. J. Antimicrob. Chemoth., 2001, 48 (3), 431-434.

12. Sharma, R.; Saxena, D.; Dwivedi, A.K.; Misra, A. Inhalable microparticles containing drug combinations to target alveolar macrophages for treatment of pulmonary tuberculosis. Pharmaceut. Res., 2001, 18 (10), 1405-1410.

13. Vitorino, C.; Almeida, J.; Gonçalves, L.; Almeida, A.; Sousa, J.; Pais, A. Co-encapsulating nanostructured lipid carriers for transdermal application: From experimental design to the molecular detail. J. Control. Release, 2013, 167 (3), 301–314.

14. Estella-Hermoso de Mendoza, A.; Campanero, M.A.; Lana, H.; Villa-Pulgarin, J.A.; de la Iglesia-Vicente, J.; Mollinedo, F.; Blanco-Prieto, M.J. Complete inhibition of extranodal dissemination of lymphoma by edelfosine-loaded lipid nanoparticles. Nanomedicine, 2012, 7 (5), 679-690.

15. Mehanna, C.; Baudouin, C.; Brignole-Baudouin, F. Spectrofluorometry assays for oxidative stress and apoptosis, with cell viability on the same microplates: A multiparametric analysis and quality control. Toxicol. *in vitro*, 2011, 25 (5), 1089-1096.

16. Grenha, A.; Seijo, B.; Serra, C.; Remuñán-López, C. Chitosan nanoparticle-loaded mannitol microspheres: structure and surface characterization. Biomacromolecules, 2007, 8 (7), 2072-2079.

17. Aydin, R.; Pulat, M. 5-Fluorouracil encapsulated chitosan nanoparticles for pH-stimulated drug delivery: evaluation of controlled release kinetics. J. Nanomater., 2012, 2012 (313961), 42-52.

18. Freitas, C.; Müller, R.H. Effect of light and temperature on zeta potential and physical stability in solid lipid nanoparticle (SLN™) dispersions. Int. J. Pharm., 1998, 168 (2), 221-229.

19. Ruktanonchai, U.; Sakulkhu, U.; Bejrapha, P.; Opanasopit, P.; Bunyapraphatsara, N.; Junyaprasert, V.; Puttipipatkhachorn, S. Effect of lipid types on physicochemical

characteristics, stability and antioxidant activity of gamma-oryzanol-loaded lipid nanoparticles. J. Microencapsul., 2009, 26 (7), 614-626.

20. Vivek, K.; Reddy, H.; Murthy, R. Investigations of the effect of the lipid matrix on drug entrapment, *in vitro* release, and physical stability of olanzapine-loaded solid lipid nanoparticles. AAPS PharmSciTech, 2007, 8 (4), 16-24.

21. Rodrigues, S.; Cordeiro, C.; Seijo, B.; Remuñán-López, C.; Grenha, A. Hybrid nanosystems based on natural polymers as protein carriers for respiratory delivery: Stability and toxicological evaluation. Carbohyd. Polym., 2015, 123 (1), 369–380.

22. Wissing, S.; Kayser, O.; Müller, R. Solid lipid nanoparticles for parenteral drug delivery. Adv. Drug Deliv. Rev., 2004, 56 (9), 1257-1272.

23. Venkateswarlu, V.; Manjunath, K. Preparation, characterization and *in vitro* release kinetics of clozapine solid lipid nanoparticles. J. Control. Release, 2004, 95 (3), 627-638.

24. Mancini, G.; Lopes, R.M.; Clemente, P.; Raposo, S.; Gonçalves, L.; Bica, A.; Ribeiro, H.M.; Almeida, A.J. Lecithin and parabens play a crucial role in tripalmitin-based lipid nanoparticle stabilization throughout moist heat sterilization and freeze-drying. Eur. J. Lipid Sci. Tech., 2015, 117 (12), 1947-1959.

25. Bunjes, H.; Koch, M. Saturated phospholipids promote crystallization but slow down polymorphic transitions in triglyceride nanoparticles. J. Control. Release, 2005, 107 (2), 229-243.

26. Gaspar, R.; Duncan, R. Polymeric carriers: preclinical safety and the regulatory implications for design and development of polymer therapeutics. Adv. Drug Deliv. Rev., 2009, 61 (13), 1220-1231.

27. Wang, F.; Cao, J.; Hao, J.; Liu, K. Pharmacokinetics, tissue distribution and relative bioavailability of geniposide-solid lipid nanoparticles following oral administration. J. Microencapsul., 2014, 31 (4), 382-389.

28. Cadete, A.; Figueiredo, L.; Lopes, R.; Calado, C.C.R.; Almeida, A.J.; Gonçalves, L.M.D. Development and characterization of a new plasmid delivery system based on chitosan - sodium deoxycholate nanoparticles. Eur. J. Pharm. Sci., 2012, 45 (4), 451-458.

29. Scherließ, R. The MTT assay as tool to evaluate and compare excipient toxicity *in vitro* on respiratory epithelial cells. Int. J. Pharm., 2011, 411 (1), 98-105.

30. Doktorovova, S.; Souto, E.; Silva, A. Nanotoxicology applied to solid lipid nanoparticles and nanostructured lipid carriers - A systematic review of *in vitro* data. Eur. J. Pharm. Biopharm., 2014, 87 (1), 1-18.

31. Schöler, N.; Olbrich, C.; Tabatt, K.; Müller, R.; Hahn, H.; Liesenfeld, O. Surfactant, but not the size of solid lipid nanoparticles (SLN) influences viability and cytokine production of macrophages. Int. J. Pharm., 2001, 221 (1), 57-67.

32. Olivier, J.; Fenart, L.; Chauvet, R.; Pariat, C.; Cecchelli, R.; Couet, W. Indirect evidence that drug brain targeting using polysorbate 80-coated polybutylcyanoacrylate nanoparticles is related to toxicity. Pharmaceut. Res., 1999, 16 (12), 1836-1842.

33. Briones, E.; Isabel Colino, C.; Lanao, J. Delivery systems to increase the selectivity of antibiotics in phagocytic cells. J. Control. Release, 2008, 125 (3), 210-227.

34. Müller, R.; Maaβen, S.; Weyhers, H.; Specht, F.; Lucks, J. Cytotoxicity of magnetite-loaded polylactide, polylactide/glycolide particles and solid lipid nanoparticles. Int. J. Pharm., 1996, 138 (1), 85-94.

35. Shi, L.; Günther, S.; Hübschmann, T.; Wick, L.; Harms, H.; Müller, S. Limits of propidium iodide as a cell viability indicator for environmental bacteria. Cytom. Part A, 2007, 71 (8), 592-598.

36. Hanley, C.; Layne, J.; Punnoose, A.; Reddy, K.; Coombs, I.; Coombs, A.; Feris, K.; Wingett, D. Preferential killing of cancer cells and activated human T cells using ZnO nanoparticles. Nanotechnology, 2008, 19 (29), 1-10.

37. Chellat, F.; Merhi, Y.; Moreau, A.; Yahia, L.H. Therapeutic potential of nanoparticulate systems for macrophage targeting. Biomaterials, 2005, 26 (35), 7260-7275.

38. Kumari, A.; Yadav, S.; Yadav, S. Biodegradable polymeric nanoparticles based drug delivery systems. Colloid. Surface B, 2010, 75 (1), 1-18.

39. Shann, S.; Lau, C.; Thomas, S.; Jerome, W.; Maron, D.; Dickerson, J.; Hubbell, J.; Giorgio, T. Size-and charge-dependent non-specific uptake of PEGylated nanoparticles by macrophages. Int. J. Nanomed., 2012, 7 (1), 799-813.

40. Gaspar, M.; Cruz, A.; Penha, A.; Reymao, J.; Sousa, A.; Eleutério, C.; Domingues, S.; Fraga, A.; Cruz, M.; Pedrosa, J. Rifabutin encapsulated in liposomes exhibits increased therapeutic activity in a model of disseminated tuberculosis. Int. J. Antimicrob. Ag., 2008, 31 (1), 37-45.

41. Govender, T.; Stolnik, S.; Garnett, M.; Illum, L.; Davis, S. PLGA nanoparticles prepared by nanoprecipitation: drug loading and release studies of a water soluble drug. J. Control. Release, 1999, 57 (2), 171-185.

This page was intentionally left blank.

Chapter 3

Microencapsulated solid lipid nanoparticles as a hybrid platform for pulmonary antibiotic delivery

This chapter is based on the following publication:
Gaspar DP, Gaspar MM, Eleutério CV, Grenha A, Blanco M, Gonçalves LMD, Taboada P, Almeida AJ and Remuñán-López C. *Microencapsulated solid lipid nanoparticles as a hybrid platform for pulmonary antibiotic delivery. Submitted.*

This page was intentionally left blank.

Abstract

Solid lipid nanoparticles (SLN) containing rifabutin (RFB), with pulmonary administration purposes, were developed through a technique that avoids the use of organic solvents or sonication. In order to facilitate their pulmonary delivery, the RFB-loaded SLN were included in microspheres of appropriate size using suitable excipients (mannitol and trehalose) through a spray-drying technique. Confocal analysis microscopy showed that microspheres are spherical and that SLN were efficiently microencapsulated and homogenously distributed throughout the microsphere matrices. The aerodynamic diameters observed an optimal distribution for reaching the alveolar region. The dry powder's performance during aerosolization and the *in vitro* drug deposition were tested using a twin-impinger approach, which confirmed that the microspheres can reach the deep lung. Isothermal titration calorimetry revealed that SLN had higher affinity for mannitol than for trehalose. Upon microsphere dissolution in aqueous media, SLN were readily recovered, maintaining their physicochemical properties. When these dry powders reach the deep lung, microspheres are expected to readily dissolve, delivering the SLN which, in turn, will release RFB. The *in vivo* biodistribution of microencapsulated RFB-SLN demonstrated that the antibiotic achieved the tested organs 15 and 30 min post pulmonary administration. Their antimycobacterial activity was also evaluated in a murine model of infection with a *Mycobacterium tuberculosis* strain H37Rv resulting in an enhancement of activity against *M. tuberculosis* infection compared to non-treated animals. These results suggest that RFB-SLN microencapsulation is a promising approach for the treatment of tuberculosis.

Graphical abstract

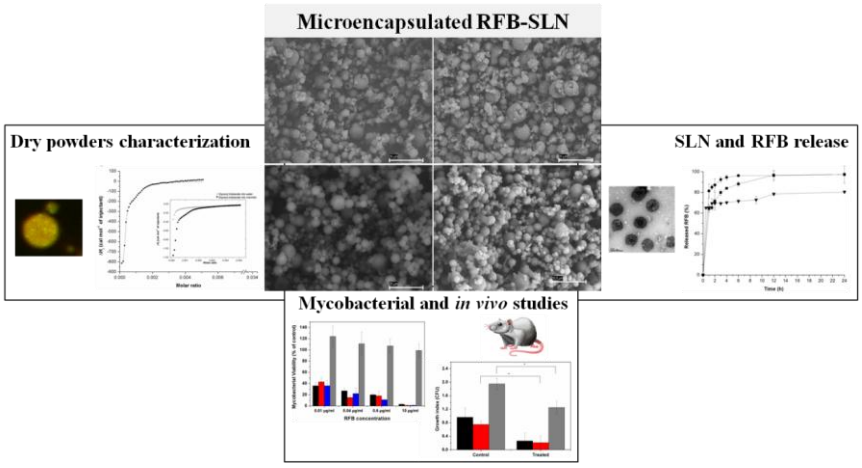

This page was intentionally left blank.

3.1. Introduction

The lung is an attractive target for the treatment of respiratory diseases due to easy self-administration of inhalable aerosols and direct delivery to the site of action [1]. Pulmonary administration is very interesting for locally treating pulmonary TB, which is the most common form of TB, since the alveolar macrophages host a large number of the bacilli [2]. Effective chemotherapy of TB involves daily oral administration of two or more drugs for a period of six months or longer [3]. Moreover, most orally delivered anti-TB drugs currently in use fail to reach high drug concentrations in the lung, since drugs can be degraded before reaching their target site [4]. Hence, targeting drugs to the alveolar macrophages by inhalation may offer the advantage that the drug is administered directly to the site of action and, as a result, the lag time before onset of action is shorter. In addition, direct drug delivery to the lung could potentially lead to a reduction in the therapeutic dose, which could further reduce systemic concentrations and the incidence of adverse events and drug interactions [5].

Nanoparticles of different compositions have been proposed to deliver drugs to the lung epithelium, having marginal side effects compared to the free drug [2, 6, 7]. Among these, SLN can be produced without using organic solvents and can incorporate hydrophobic or hydrophilic drugs, thus fulfilling the requirements for an optimum particulate drug carrier system for the pulmonary route [8]. Although SLN have already been efficiently aerosolized, reaching the deep lung region [9], some instability phenomena common to nanosized systems, such as particle-particle interactions and poor delivery efficiency due to exhalation of low-inertia nanoparticles, could not be precluded. In previous studies dealing with polymeric nanoparticles intended for inhalation, their microencapsulation in micron-sized powder carriers using suitable spray-drying techniques has been proposed [6, 10]. This has resulted in improved handling and aerosolization of nanoparticles through enhanced powder stability and acquisition of aerodynamic properties that lead to an efficient lung delivery. In addition, inhalable powders have also demonstrated to be superior over their liquid counterparts with regard to enhanced absorption and bioavailability of active ingredients [11]. The so formed microparticles present a suitable d_{aer}, relating to particle aerodynamic behaviour and lung deposition. Aerosols with optimal properties must contain particles that are neither too small, risking exhalation, nor too large, which are likely to deposit in the upper airways. The optimal d_{aer} for reaching the alveolar region has been intended to be between 1 and 5

μm. [12]. Besides, the nanoparticle-containing microparticles must readily deliver the primary nanoparticles upon depositing in the lung interstitial fluid, which should retain their benefits as highly potent carriers for biopharmaceuticals [13, 14]. For this purpose, the spray-drying process typically employs a wide range of inert pharmaceutical excipients, which are approved by the regulatory authorities and act as drying adjuvants that protect the structural integrity of the nanoparticles, avoiding coalescence upon exposure to high temperature during the spray-drying process and during subsequent storage [14].

The aim of this study was to obtain microencapsulated SLN powders adequate for the pulmonary administration of the anti-TB drug RFB. Herein we report the preparation of two types of RFB-loaded SLN based on glyceryl dibehenate and glyceryl tristearate (biocompatible and biodegradable solid lipids exhibiting high m.p.). Thereafter, these SLN were microencapsulated in mannitol and trehalose microspheres by spray-drying to acquire adequate morphological and aerodynamic properties for lung deposition. Structural and aerodynamic characterization of these micro-powders loaded with SLN were performed using scanning electron microscopy (SEM), confocal laser scanning microscopy (CLSM) and aerodynamic sampling using a twin-impinger. Physical characterization of the powders was performed by isothermal titration calorimetry (ITC). SLN recovery from microspheres and RFB release from microencapsulated SLN were also assessed. *In vitro* antimycobacterial activity of RFB formulations was evaluated by a (3- (4,5-dimethylthiazol-2-yl) - 5 - (3-carboxymethoxyphenyl) - 2 - (4-sulfophenyl) - 2H - tetrazolium) (MTS) reduction assay. The *in vivo* biodistribution profile of microencapsulated RFB-SLN was analyzed following 15 and 30 min post pulmonary administration. Their antimycobacterial activity was also evaluated in a murine model of infection with a *M. tuberculosis* strain H37Rv.

3.2. Materials

3.2.1. Chemicals

RFB was acquired from CHEMOS GmbH (Germany). Glyceryl dibehenate was a kind gift from Gattefossé (France). Glyceryl tristearate, mannitol and D-(+)-trehalose dihydrate were purchased from Sigma-Aldrich (Spain). Tween® 80 (polysorbate 80) was obtained from J. Vaz Pereira, S.A. (Portugal). Lung surfactant (Curosurf®) was a

generous gift from Angelini Farmacêutica, Lda. (Portugal). PBS, pH 7.4 was acquired from Invitrogen™. Bodipy® 630/650-X was obtained from Molecular Probes® (Netherlands). Purified water was obtained by inverse osmosis (Millipore, Elix 3) with a 0.45 μm pore filter. Middlebrook 7H9 broth and 7H11 agar, BACTO Middlebrook and albumin-dextrose-catalase enrichments were obtained from Difco Laboratories (Detroit, USA). Reagents for the MTS assay were purchased from Promega (WI, USA). All other reagents were of analytical grade and were used without further purification.

3.2.2. Animals

BALB/c mice (6–8 weeks old, 25-30 g) were obtained from the Gulbenkian Institute of Science (Oeiras, Portugal). The animals were kept under standard hygiene conditions, fed commercial chow and given acidified drinking water *ad libitum*. All animal experiments were carried out with the permission of the local ethical committees of the Faculty of Pharmacy and of the Institute of Molecular Medicine in accordance with the EU Directive (2010/63/UE) and Portuguese laws (DR 113/2013, 2880/2015 and 260/2016).

3.2.3. Mycobacterial strains

For *in vitro* studies, the *M. avium* strain DSMZ 44157 from Leibniz-Institute, Germany was used. For *in vivo* studies, the *M. tuberculosis* strain H37Rv was used. Quantification of inocula was performed as described previously by Gaspar *et al.* [15].

3.3. Methods

3.3.1. Preparation of RFB-loaded SLN

RFB-loaded glyceryl dibehenate and glyceryl tristearate SLN were prepared using a hot HSH, as previously described in Chapter 2, section 2.3.2..

3.3.2. Characterization of RFB-loaded SLN

Size and zeta potential of RFB-loaded SLN were characterized by PCS using a Zetasizer Nano S and Z (Malvern Instruments, UK) respectively, as reported in Chapter 2, section 2.3.3.1.. Briefly, samples were kept in polystyrene cuvettes and the measurements were

made at 25.0±0.1°C after their appropriate dilutions (1:100) with filtered (0.45 μm) purified water and, then, they were analyzed at a 173° scattering angle. Surface charge was determined through particle mobility in an electric field to calculate the zeta potential of SLN. For that, samples were placed in a specific cuvette where a potential of ±150 mV was established after their appropriate dilution with filtered purified water. Particle size distribution and morphology were also confirmed by atomic force microscopy (AFM). Noncontact AFM in air was performed with a XEI-100 instrument from Park Systems, operating with decoupled XY (50 Å ~50 μm^2) and Z-scanners (12 μm). SLN formulations were diluted (1:250) in Milli-Q water and deposited on freshly cleaved muscovite mica for 20 min. After subsequent washes, the samples were allowed to air dry at room conditions. Samples were mounted on top of magnetic discs and imaged by using microfabricated crystal silicon probes with a spring constant of 40 N/m and a resonant frequency of 300 kHz (ACTA, AppNano). The XYZ-accuracy was checked once a day by means of a silicon grating (TGXYZ02, from Mikromasch), ensuring a nominal height deviation lower than 2% at the highest scan size. To eliminate imaging artifacts, the scan direction was varied, ensuring a true image. The images were obtained from at least three macroscopically separated areas on each sample. All images were processed using procedures for plane-fit and flatten in the WSxM 4.0 Develop 11.4 software50 without any filtering. Surface topography and roughness were determined from 10 Å ~10 μm^2 images. All experiments were carried out at room temperature.

3.3.3. Determination of association efficiency and drug loading of RFB

The EE and DL of RFB were also determined, as previously reported in Chapter 2, section 2.3.3.2.. Briefly, non-associated RFB was separated from the SLN by size exclusion chromatography on Sephadex G-25/PD-10 columns. The amount of RFB associated to SLN was determined after dissolving the nanoparticles with acetonitrile, which promoted the precipitation of the lipid phase. The encapsulated RFB remained in the supernatant, which was separated by centrifugation (30 min at 12300 rpm). The amount of drug was measured by UV-Visible spectrophotometry, at λmax of 320 nm, in a microplate spectrophotometer reader (FLUOstar Omega, BMGLabtech, Germany). The supernatant of unloaded nanoparticles was used as basic correction. All experiments were carried out in triplicate (n=3). The RFB EE and DL were calculated according to the following equations:

$$EE(\%) = \frac{W_{loaded\ drug}}{W_{initial\ drug}} \times 100 \quad \text{(Eq. 3.1)}$$

$$DL(\%) = \frac{W_{loaded\ drug}}{W_{lipid}} \times 100 \quad \text{(Eq. 3.2)}$$

where $W_{initial\ drug}$ is the weight of the drug used, $W_{loaded\ drug}$ is the weight of encapsulated drug that was detected in the supernatant after SLN purification, solubilization and centrifugation and W_{lipid} represents the weight of the lipid vehicle.

3.3.4. Preparation of dry powders containing SLN

The RFB-SLN dispersions were suspended in aqueous spray-drying excipient solutions, at a 1:3 SLN:excipient mass ratio, containing 20% and 22% w/v of mannitol and 15% and 17% w/v of trehalose for glyceryl dibehenate and glyceryl tristearate SLN, respectively. Dry powders were obtained by spray-drying the suspensions using a laboratory-scale spray-dryer (Büchi® Mini spray-dryer, B-290, Switzerland). The spray-drying conditions were: two fluids external 0.7 mm nozzle, feed rate varied from 2.3 to 8.5 mL/min (depending on the spray-dried suspension), air flow of 400 L/h and T_{inlet} of 103±2°C, resulting in an T_{outlet} between 63°C and 70°C. The aspirator rates were kept constant at 100% and 70% for SLN suspensions in mannitol and trehalose, respectively. The produced spray-dried powders were collected and stored in a dessicator at room temperature until further use. For CLSM studies, the SLN and excipients were previously stained with fluorescent labels to allow visualization by confocal microscopy. SLN were labeled with coumarin-6 during their formulation (40 µL of a coumarin-6 solution was added to the melted lipid). Mannitol and trehalose were stained with the fluorophore Bodipy®, which was added to the spray-drying excipient solution (500 µL of a 1 mg/mL solution of Bodipy® in DMSO) and kept under magnetic stirring for 2 h before spray-drying. The spray-drying production yields (PY) were calculated by gravimetry, comparing the initial total solids amount with the resultant powder amount after spray-drying, as follows:

$$PY(\%) = \frac{\text{Weight of the resultant spraydrying powder (microspheres)}}{\text{Weight of initial total solids (SLN+spraydrying excipients)}} \times 100 \quad \text{Eq. (3.3)}$$

3.3.5. Characterization of microspheres size, morphology and moisture content

Particle size and morphology of the spray-dried powders were assayed using SEM. The dry powder samples were mounted on an aluminium stub using a double-side adhesive tape, covered with a 200 nm thick gold-palladium film using an Emitech K550 (London, UK) sputter coater and analyzed using a Zeiss Evo LS15 (UK) microscope, working at an accelerating voltage of 20 kV and at various amplifications. The SEM micrographs were used to calculate the mean particle size, which was estimated as the Feret's diameter and measured as the mean of 300 particle measurements (n=300) [6].

The moisture content of the spray-dried powders was determined by calculating the loss of weight upon drying from 25°C to 105°C, using an electronic moisture balance (Shimadzu, EB-280 MOC, Japan), according to the Ph. Eur. (2.2.32. Loss on drying). The percentage of the initial weight that was lost during the heating process was ascribed to the moisture content of the powders. Measurements were carried out in triplicate.

3.3.6. Structural characterization of SLN-loaded microspheres using CLSM

The internal structures of SLN-loaded microspheres were observed using CLSM with an AOBS SP5X microscope (Leica GmbH, Germany), which collects images using different detectors for fluorescent signals upon irradiation with a white light laser. Small aliquots of the dry powders comprised of coumarin-6-labelled SLN encapsulated in Bodipy®-labelled excipient microspheres (mannitol and trehalose) were placed on a glass slide, and a drop of immersion oil was added to avoid particle displacement during viewing. Laser excitation wavelengths of 470 and 633 nm were used to scan the powder, and fluorescent emissions from coumarin-6 (emission λ=480-555 nm) and Bodipy® (emission λ=650-700 nm) were collected using separate channels. Images were acquired with a magnification of 63X, using an oil immersion objective (HCX PL APO CS). The gray scale images obtained from each scan were pseudo-coloured green (coumarin-6) and red (Bodipy®) and overlapped afterwards (LAS AF, Leica Confocal Software, Leica GmbH, Germany) to obtain a multicoloured image.

3.3.7. Determination of the dry powders flow properties

The real density (real ρ) of the dry powders was measured using a helium pycnometer (AccuPyc 1330, Micrometrics Ltd, Dunstable, UK) at room temperature (*n*=3). The apparent density or tapped density (apparent ρ) was determined under defined conditions of the apparent volumes, before and after settling (Stav 2003, JEF Germany). The latter was obtained by measuring the volume of a known weight of the dry powder in a 10 mL test-tube after mechanical tapping (1250 taps), according to the Ph. Eur. (2.9.34. Bulk density and tapped density of powders) (*n*=3). Using density measurements, it was possible to calculate the Carr's index and Hausner ratio, which are considered as appropriate methods of evaluating flow properties of solids. The d_{aer}, Carr's index and Hausner ratio of spray-dried particles were calculated based on the following equations 3.4, 3.5 and 3.6, respectively:

$$d_{aer}(\mu m) = d_{geo}\sqrt{\frac{\rho_e}{\lambda \rho_s}} \quad \text{(Eq. 3.4)}$$

where d_{geo} is the particle geometric diameter, ρ_s is 1 g/cm^3, ρ_e is the effective particle density in the same unit as ρ_s and λ is the dynamic shape factor of the particle. This shape factor is theoretically defined as 1 for spherical particles.

$$\text{Carr's index (\%)} = \frac{100 \times (V_0 - V_f)}{V_0} \quad \text{(Eq. 3.5)}$$

$$\text{Hausner ratio} = \frac{V_0}{V_f} \quad \text{(Eq. 3.6)}$$

where V_o is the unsettled apparent volume and V_f is the final tapped volume.

3.3.8. Isothermal titration calorimetry of SLN and spray-drying excipients

Binding studies between SLN and spray-drying excipients were performed using a VP-ITC titration microcalorimeter from MicroCal Inc., (Northampton, MA) with a cell volume of 1.436 mL at 25°C. Samples were degassed in a ThermoVac system (MicroCal) prior to use. The sample cell was filled with the sugar solution containing either mannitol (1160 or 1280 mM when injecting glyceryl dibehenate and glyceryl tristearate SLN, respectively) or trehalose (397 or 450 mM) and the reference cell with a buffer solution. The SLN solution (64.7 and 31.4 mM for glyceryl dibehenate and glyceryl tristearate, respectively) was introduced into the thermostated cell by means of a syringe and stirred

at 286 rpm, which ensured rapid agitation without foaming on solutions. Each titration consisted of an initial 2 μL injection (neglected in the analysis) followed by 55 subsequent 5 μL injections programmed to occur at 400 s intervals, sufficient for the heat signal to return to the baseline. The results of the ITC experiments, in terms of the heat of injection normalized by the SLN concentration added per each injection (Q^*), were presented as a function of the SLN to excipient molar ratio. The heats of dilution from titrations of SLN suspension into buffer were subtracted from the heats obtained from titrations of the SLN suspensions into the sugar solution to obtain the net binding heats. All experiments were carried out at least in duplicate and the reproducibility was within ±3%. Raw data of binding were analyzed as described previously [16] on the basis of a set of two identical binding sites model by using the Affinimiter software. The two identical binding sites model employs the following fitting equation that incorporates Langmuir isotherm binding equilibria for two independent types of association, where Q^* is the heat per injection, n_i the binding stoichiometry, Θ_i the fractional sites of macromolecule occupied by ligand, M the macromolecule concentration, ΔH_i the enthalpy of interaction and V the cell volume.

$$Q* = MV(n_1\Theta_1\Delta H_1 + n_2\Theta_2\Delta H_2) \qquad \text{Eq. (3.7)}$$

where the sub-indices 1 and 2 stand for the two sets of sites.

One can solve for Θ_1 and Θ_2 using the equilibria equations for binding constants K_1 and K_2, with X being the total concentration of ligand and $[X]$ the concentration of unbound ligand:

$$K_1 = \frac{\Theta_1}{(1-\Theta_1)[X]} \quad \text{and} \quad K_2 = \frac{\Theta_2}{(1-\Theta_2)[X]} \quad \text{with} \quad [X] = X - M(n_1\Theta_1 + n_2\Theta_2) \qquad \text{Eq. (3.8)}$$

To reach an accurate fit of all floating parameters to these data, multiple assays were performed starting from random initial parameters. The same values were reached at the minimum χ^2 regardless of the values of initialization. Finally, changes in free energy ΔG_i and entropy of binding ΔS_i for each site were calculated from the fitted parameter values according to the following standard, thermodynamic relations:

$$\Delta G_i = -R_g T \ln K_i \qquad\qquad \Delta G_i = \Delta H_i - T\Delta S_i \qquad \text{Eq. (3.9)}$$

where R_g is the universal gas constant.

3.3.9. *In vitro* deposition of dry powders using a twin-stage liquid impinger

Hard capsule shells made of hydroxypropyl methylcellulose (HPMC) were manually filled up with 40.0±0.2 mg of each dry powder and introduced in a Rotahaler® device. The aerodynamic characteristics of inhalable complexes were assessed through a TSLI (TSI, Copley Instruments, UK). Briefly, the TSLI equipment was divided in four compartments, corresponding to: (i) device+capsules (D+C); (ii) mouth+throat (M+T); (iii) medium compartment (MC) and (iv) lung. According to the Ph. Eur. (2.9.18. Preparations for inhalation: aerodynamic assessment of fine particles, Aparatus A – glass impinger), 7 and 30 mL of ethanol were added to MC and lung compartments, respectively. The content of each capsule was discharged through a flow rate of 60±5 L/min during 15 s (5 s×3). The lower impingement chamber of the apparatus is so designed at an air flow rate of 60 L/min and an effective mean d_{aer} particle cut-off size of ≈6.4 μm. Indeed, drug deposition in this chamber, which simulates the alveoli, was of interest to us. The TSLI was disassembled and all the compartments were carefully washed with ethanol and separately collected to conical flasks up to final volume of 50 mL. Samples were filtered and RFB content in each compartment determined by spectrophotometry in a microplate reader (FLUOstar Omega, BMG Labtech, Germany) at 320 nm (*n*=3).

3.3.10. SLN recovery from microspheres

The spray-dried powders were incubated in 10 mM isotonic PBS pH 7.4 with 0.1% of lung surfactant (Curosurf®) under mild magnetic stirring at 37°C for 90 min. After this time, the mean particle size and zeta potential of the recovered SLN were analyzed using a Zetasizer Nano S and Z (Malvern Instruments, UK), respectively. The morphology was observed by TEM. The average particle size was analyzed by PCS and the surface charge was determined through particle mobility in an electric field to calculate the zeta potential of SLN, as described in detail in section 3.3.2.. On the other hand, the morphological analysis of SLN after being recovered from microspheres was conducted by TEM. Briefly, the samples were stained with phosphotungstic acid at 2% (w/v) during 2 min and fixed on racks of copper covered by a membrane of carbon for observation. Afterwards, the samples were analyzed on a JEOL Microscopy (JEM 2010, Japan) at 120 kV and the images were acquired through a Gatan Orius™ camera.

3.3.11. *In vitro* RFB release from microencapsulated RFB-loaded SLN

The release of RFB was carried out by incubating the SLN (≈0.75 mg) and the dry powders (100±5 mg) in 1 mL of a medium comprised by 10 mM isotonic PBS pH 7.4 with 0.1% of lung surfactant (Curosurf®), under horizontal shaking (300 rpm) at 37°C. At appropriate time intervals, individual samples were taken and centrifuged in a high speed centrifuge (Allegra™ 64R centrifuge, Beckman Coulter) at 30000×g for 30 min at 4°C. The amount of released RFB was evaluated in the supernatants by spectrophotometry in a microplate reader (FLUOstar Omega, BMG Labtech, Germany) at 320 nm (*n*=3).

3.3.12. *In vitro* activity of RFB formulations against *M. avium* strain DSMZ 44157 by MTS assay

The susceptibility of *M. avium* strain to RFB formulations was assessed by adding 10 µL of inocula at a concentration of 10^9 colony-forming units (CFU)/mL to 96 well plates containing the formulations diluted in 7H9 broth with albumin-dextrose-catalase supplement (six replicate samples). RFB formulations under study, at a concentration of 10 µg/mL, were added to the first well making serial two-fold dilutions up to 12 wells with 7H9 broth supplemented. Wells only with the supplemented 7H9 broth were used as negative controls. After inoculation, the plates were incubated for 10 days at 37ºC and 5% CO_2 in a humidified atmosphere. After the incubation period, 20 µL of the MTS was added to all wells, plates were incubated at 37ºC for 3 h and the absorbances were measured at 490 nm in a microplate reader Model 680 (Bio-Rad, CA, USA).

3.3.13. *In vivo* fate of RFB formulations

3.3.13.1. Biodistribution studies

Mice received inhaled RFB formulations using a simple apparatus based on a 15 mL centrifuge tube where the dry powder was inserted. A small hole was done in the bottom of the tube allowing the powder delivery to mouse. A manual pump connected to the upper part of the tube allowed the production of a turbulent air stream for fluidizing the powder. Each mouse was restrained in a 50 mL tube where a small hole in the bottom was done. This lower part of the 50 mL tube was connected to the 15 mL tube using a baby

bottle teat. The tested formulation was RFB-glyceryl dibehenate SLN microencapsulated in mannitol and RFB-mannitol microspheres as control. Forty mg of each dry powder were put in the device and each animal received the formulation by inhalation during 2 min. Fifteen and 30 min following administration (four animals per time point), mice were anaesthetised with isoflurane, blood was collected from the retinal blood vessels into heparinised tubes and stored at -30°C. Animals were then, sacrificed by cervical dislocation and lung, spleen and liver were removed and stored at -70°C.

3.3.13.2. RFB extraction from blood and tissues

RFB levels in blood and tissues were determined by high-performance liquid chromatography (HPLC) after an extraction procedure described in Gaspar *et al.* [17]. This quantification method was validated showing sensitivity and precision adequate to the concentration range used in this study. The linearity was established between 5.60 and 0.25 µg/mL with a 5% relative standard deviation. The quantification and detection limits were 0.380 and 0.125 µg/mL, respectively, with 95% of confidence. Briefly, 500 µL of blood were mixed with 250 µL of potassium dihydrogen phosphate buffer 0.05 M and sodium acetate 0.05 M (pH adjusted to 4.0 with acetic acid) and extracted twice with 1 mL of a dichloromethane:isooctane mixture (2:3, v/v) under stirring at room temperature (15 min), followed by a centrifugation step at 1200×g for 10 min (Beckman Instruments, Inc.). Liver, lung and spleen tissues were thawed and aliquots of ca. 100 mg were weighed out for each sample and extracted twice with 2300 µL of dichloromethane:isooctane mixture by mechanical shaking for 30 min at room temperature, followed by a centrifugation step at 1200×g for 10 min in a centrifuge. The organic extracts were pooled and evaporated to dryness under nitrogen. The residue was dissolved in 500 µL of mobile phase, filtered and then injected into the HPLC system. To determine the efficiency of the extraction procedures, a known amount of RFB was added to blood and solid tissues removed from mice that had not received RFB administration and then submitted to the same above-mentioned extraction protocol.

3.3.13.3. Determination of RFB by HPLC

Plasma and tissue levels of RFB were determined by HPLC according to Gaspar *et al.* [17]. Briefly, the HPLC system consisted of a System Gold (Beckman Instruments, Inc.),

a Midas Spark 1.1 autoinjector and a Diode-Array 168 detector (Beckman Instruments, Inc.). The wavelength of this detector was set to 275 nm. The analytical column was a LiChroCART® (250-4.6), Purospher® Star RP-8 (5 µm) (Merck, Darmstadt, Germany). The mobile phase consisted of potassium dihydrogen phosphate 0.05 M and sodium acetate 0.05 M (pH adjusted to 4.0 with acetic acid)-acetonitrile (53:47, v/v) with a flow rate of 1 mL/min at 25°C.

3.3.13.4. Preparation of standard solutions for HPLC

Standard solutions of RFB (100 µg/mL) were prepared by weighing the appropriate amount of bulk RFB and dissolving it in mobile phase. Further stock solutions were made by diluting the initial stock standard solutions with mobile phase. Calibration curves, ranging from 0.25 to 5.0 µg/mL with a loop of 100 µL, were used for the quantification of RFB in plasma and tissues. A stock solution of 1.0 µg/mL was stored at -30°C and a sample of this stock solution was always injected together with the analyzed samples to verify the precision of the obtained concentrations of RFB in samples and controls from their peak area concentration response.

3.3.14. Biological evaluation in a *M. tuberculosis* infection model: experimental infection, treatment and bacterial counts

BALB/c mice were injected intravenously with 5×10^4 CFU of *M. tuberculosis* H37Rv. Treatment started 2 weeks after infection induction and mice received the tested formulation (RFB-glyceryl dibehenate SLN microencapsulated in mannitol) using the same simple apparatus described in section 3.3.13.1.. Forty mg of dry powder were put in the device and each mice received the formulation by inhalation during 2 min. Administrations were performed in a total number of 10 for two weeks. Two days after the last administration, mice were sacrificed, liver, spleen and lung were aseptically removed, homogenized, serially diluted in 0.04% Tween® 80 and plated onto Middlebrook 7H11 agar medium supplemented with OADC for CFU countings. One group of mice infected and non-treated was sacrificed at the beginning of treatment and another one at the end. The CFU counts in liver, spleen and lung were analyzed. Colonies were counted after 21 days of incubation at 37ºC with 5% CO_2. From CFU counts, the

growth index was calculated using the difference between the $\log_{10}$ CFU at the end of treatment and the $\log_{10}$ CFU at the beginning of treatment [18].

3.3.15. Statistical analysis

Statistical analysis of the experimental data was performed using a one-way analysis of variance (one-way ANOVA) and differences between groups were tested by a one-way ANOVA with Dunnet's post hoc test with GraphPad Prism version 6.0 (GraphPad Software, San Diego, CA). Data were expressed as mean±SD or 95% confidence interval. A $p<0.05$ value was considered significant. All data are shown as mean±SD.

3.4. Results and Discussion

3.4.1. SLN formulation and characterization

SLN have emerged as an alternative to liposomes and polymeric nanoparticles mainly due to their easy scale-up, good stability and biocompatibility, while providing drug protection and sustained release [8]. Herein, two different SLN formulations loaded with RFB were prepared using different lipids (glyceryl dibehenate and glyceryl tristearate), and Tween® 80 as the surfactant component, using a hot HSH technique, as previously described in Chapter 2. Both SLN formulations presented particle size distributions within the nanometer range (108±5 nm for RFB-glyceryl dibehenate SLN and 191±7 nm for RFB-glyceryl tristearate SLN) with suitable polydispersity index values (< 0.2). Furthermore, negative zeta potential values (ca. -18 mV) and high EE were obtained for both formulations (89.9±5.1% and 81.0±9.6% for glyceryl dibehenate and glyceryl tristearate SLN, respectively). Regarding DL results, the obtained values were 9.0±0.5% for glyceryl dibehenate SLN and 6.0±0.7 for glyceryl tristearate SLN.

Concerning AFM analysis of RFB-loaded SLN, the microphotographs showed isolated discoid structures, revealing a spherical appearance of both types of SLN. A detailed inspection of the cross-section profiles (Figure 3.1A) showed the diameter of the RFB-SLN corresponds to the width of the peak at the base of the graphic. The regular trace of the graphs indicates that particles present low surface roughness. After measuring the width from each cross-section, a width frequency count histogram (Figure 3.1B) was built. The results acquired from the width histogram, after applying the Gaussian model,

showed that RFB-SLN are homogenous formulations, with similar size distinguishable subpopulations with similar average cross-sectional widths. Overall, particle sizes obtained using AFM images are similar to those established from the PCS analysis. The full characterization of these SLN had been reported in Chapter 2.

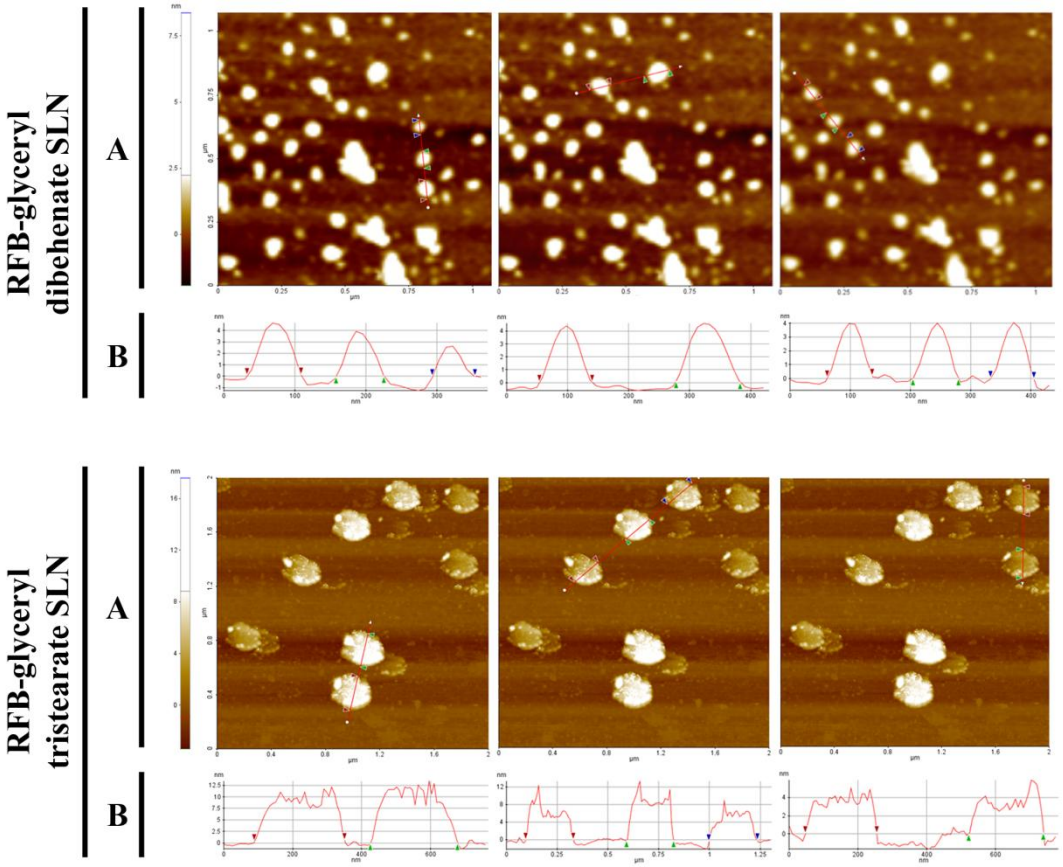

Figure 3.1: AFM images of the optimized RFB-glyceryl dibehenate and RFB-glyceryl tristearate SLN: (A) cross-section height profiles and (B) histograms of width frequency counts performed to quantitatively measuring the width of the particles.

3.4.2. Dry powder preparation and characterization

Pulmonary administration of therapeutic SLN is an attractive concept. However, their direct aerosolization may result in poor delivery efficiency due to exhalation of the low-inertia nanoparticles [19-21]. The inclusion of nanoparticles in a microparticulated system became a promising alternative to deliver them to the deep lung [6, 10], while avoiding the stability problems of liquid formulations. In this context, previously optimized RFB-

loaded SLN were microencapsulated using a spray-drying process with two different inert and FDA-approved excipients, the polyol mannitol and the disaccharide trehalose, at a 1:3 SLN:excipient ratio. The used excipients are known to enhance aerosolization performance, as well as to reduce moisture content. The SLN microencapsulation process was performed in a one-step spray-drying process after an initial screening of different SLN/excipient mass ratios, excipient concentrations and spray-drying conditions, seeking for the production of dry powders with the most suitable characteristics for pulmonary delivery. Hence, T_{inlet}, which in turn determines T_{outlet}, needs to be higher than the boiling point of water to evaporate the excipient drops but it cannot be too high in order to avoid SLN melting. So, T_{inlet} was established to be 103°C. In addition, a screening of spray-drying conditions (e.g., aspirator and pump) using several mannitol and trehalose concentrations indicated that the optimum excipient concentration for glyceryl tristearate SLN (22% and 17% w/w for mannitol and trehalose, respectively) was higher than those used for glyceryl dibehenate SLN (20% and 15% w/w for mannitol and trehalose, respectively). This is due to the fact that glyceryl tristearate is a lipid that presents a lower m.p. than glyceryl dibehenate and thus, SLN based on glyceryl tristearate require a larger quantity of excipient to protect them from the high temperatures during the spray-drying process.

The spray-drying processes presented acceptable PY values (approximately 50%, Table 3.1) for both SLN, in line with data reported elsewhere for spray-drying using similar excipients [6, 11]. It should be emphasised that lab-scale spray-drying processes typically present lower PY values – in comparison to large-scale spray-drying processes – due to higher wall deposits, since air residence times and radial distances from the atomiser to the drying chamber wall are shorter [22].

Successful delivery of inhaled particles is governed by the deposition pattern. This is mainly controlled by particle size and density that strongly influence the dispersion and sedimentation properties of the powder [23, 24]. The d_{aer} along with the densities (real ρ and apparent ρ) and Feret's diameters of the dry powders are depicted in Table 3.1. The microspheres' d_{aer} (between 4.33 and 5.16 μm) and densities (real ρ of approximately 1.5 g/cm^3 and tap $\rho < 0.6$ g/cm^3) are within the optimal particle range for deposition in the deep lung. Similar results were obtained by Grenha *et al*. [6] and Al-qadi *et al.* [25] for systems consisting in microencapsulated chitosan nanoparticles for pulmonary administration of insulin.

The Carr's index and the Hausner ratio, which can be used as indirect measures of the interparticulate forces within each powder, were calculated from the poured and apparent ρ using equations 3.5 and 3.6 (above), and are also listed in Table 3.1. According to the results, all formulations presented high Carr's index (≥20) and Hausner ratio (≥1.35) values, predicting poor flowability of powders according to Ph. Eur. (2.9.36. Powder Flow). However, despite being extensively used to predict the quality of powders regarding flowability and deposition, precaution must be taken during the interpretation of Carr's index and Hausner ratio because it has been reported that microcapsules prepared by spray- and freeze-drying may have poor or very poor flowability, probably due to some residual moisture content and their small size [26, 27].

Table 3.1: Physical and aerodynamic properties of SLN-loaded dry powders: glyceryl dibehenate SLN microencapsulated in mannitol (A), glyceryl tristearate SLN microencapsulated in mannitol (B), glyceryl dibehenate SLN microencapsulated in trehalose (C) and glyceryl tristearate SLN microencapsulated in trehalose (D) (mean±SD, *n*=3).

Dry Powders	Process yield (%)	Feret's diameter (μm, *n*=300)	Real density (g/cm^3)	Apparent density (g/cm^3)	Aerodynamic diameter (μm)	Carr's index (%)	Hausner ratio	Moisture residual content (%)
A	60.5±2.5	4.87±1.61	1.47±0.00	0.62±0.01	4.75±0.52	38.7±4.6	1.6±0.1	0.57±0.02
B	47.0±1.1	5.54±1.79	1.46±0.00	0.59±0.01	5.16±0.88	38.3±0.6	1.6±0.0	0.01±0.01
C	52.4±7.0	4.75±1.10	1.46±0.00	0.48±0.02	4.56±0.75	40.3±1.5	1.7±0.0	1.67±0.04
D	56.4±2.5	4.50±1.60	1.50±0.00	0.45±0.04	4.33±0.81	36.0±3.0	1.6±0.1	1.66±0.05

Regarding the moisture content of the powders, a factor that has a major impact on it is the T_{outlet} during spray-drying, whereby a lower moisture content is associated to a higher T_{outlet} value [28]. In this study, the obtained T_{outlet} values were ca. 61°C and 56°C for the microencapsulation process of glyceryl dibehenate and glyceryl tristearate SLN in mannitol and 65°C and 67°C for the spray-drying of glyceryl dibehenate and glyceryl tristearate SLN in trehalose microspheres. However, a correlation between the residual moisture content and the T_{outlet} was not found. The differences in moisture contents of the spray-dried powder can be related to the excipient properties, as reported elsewhere [28]. The low moisture content of the spray-dried mannitol particles was explained by their

crystalline state. In addition, this compound possesses a low MW and a good drying aptitude contrarily to trehalose which is characterized by a high MW [28].

The shape and morphology of particles produced by spray-drying are mainly determined by the rate of droplet evaporation and the composition [28]. Figure 3.2 shows the morphology of SLN-loaded mannitol and trehalose microspheres. In general, microspheres had a spherical shape with well-defined limits, although some mannitol microspheres showed a slightly convoluted morphology (Figure 3.2A and B).

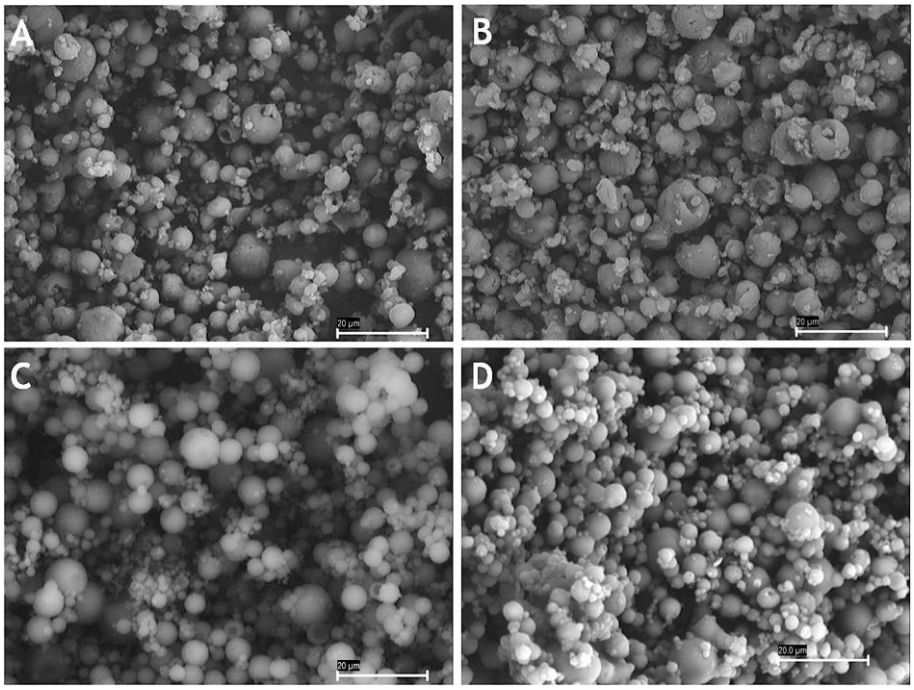

Figure 3.2: SEM micrographs of dry powders: mannitol microspheres containing (A) glyceryl dibehenate SLN and (B) glyceryl tristearate SLN, and trehalose microspheres containing (C) glyceryl dibehenate SLN and (D) glyceryl tristearate SLN (scale bar: 20 µm).

3.4.3. Structural characterization of SLN-loaded microspheres using CLSM

The application of CLSM permitted elucidating the microsphere structure and the SLN distribution within the microspheres, using double fluorescent labelling (i.e. green coumarin-6 for SLN and red Bodipy® for the spray-drying excipient). According to the images depicted in Figure 3.3, glyceryl dibehenate and glyceryl tristearate SLN

formulations stained with coumarin-6 were efficiently incorporated into the mannitol and trehalose microspheres obtained by spray-drying process, being homogenously distributed throughout the matrix of both types of microspheres.

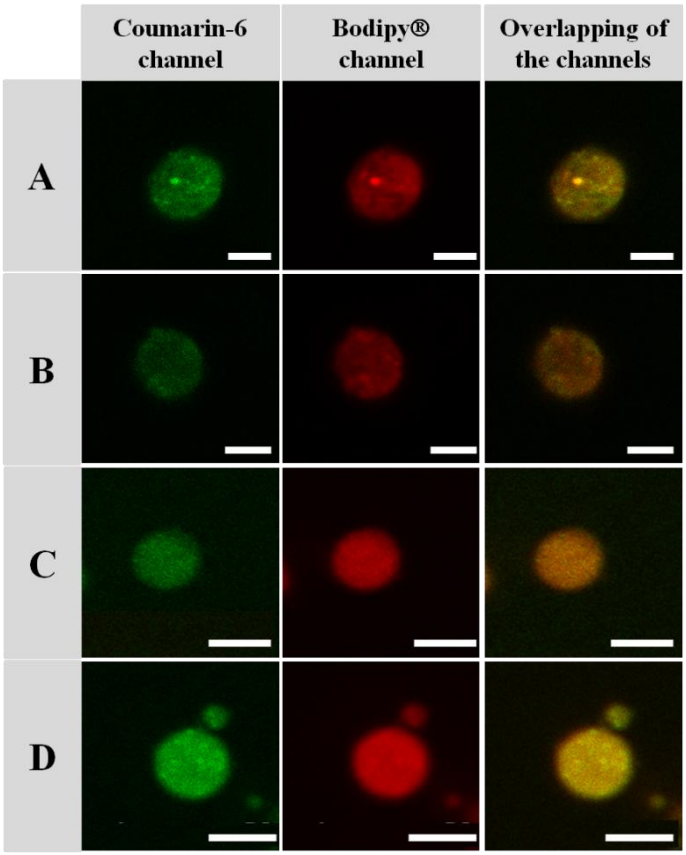

Figure 3.3: Confocal imaging of dry powders: mannitol microspheres containing (A) glyceryl dibehenate SLN and (B) glyceryl tristearate SLN and trehalose microspheres containing (C) glyceryl dibehenate SLN and (D) glyceryl tristearate SLN. SLN were labeled with coumarin-6 (green channel) and excipients were stained with Bodipy® (red channel) (scale bar: 5 µm).

These matrix type structures are different from those obtained by Grenha *et al.* [29] and Al-qadi *et al.* [25] after the incorporation of chitosan nanoparticles in mannitol microparticles, which resulted in microcapsule-like structure consisting of a mannitol matrix containing the nanoparticles, which is surrounded by an outer mannitol shell. This shell around the matrix was not observed in the present study. It may be hypothesized that

these structural differences may happen due to two factors. First, T_{inlet} was different in both studies, in the current work it was 103°C, while in Grenha *et al.* and Al-qadi *et al.* studies was 170°C. So, this high T_{inlet} allowed a high drying ratio of mannitol molecules in microspheres' shell. On the other hand, the used excipient concentrations were also different in both studies, being higher in the present work and, consequently, with a higher viscosity solution. Thus, water molecules had more difficult to diffuse during the drying step, while in Grenha *et al.*, the excipient solution was less concentrated and excipient molecules had a high trend to follow the water diffusion to out of the particles, remaining at the microspheres' shell after drying process.

3.4.4. Determination of SLN binding affinity to microspheres by ITC

As commented previously, the spray-drying process of SLN with the two excipients, mannitol and trehalose, led to the formation of microspheres with distinct morphological particularities. Hence, to gain further knowledge about the origin of such differences, the nature of the interactions established between SLN and the excipients used in the spray-drying process was investigated using ITC. This technique enables to probe the thermodynamics of nanocarrier-excipient interactions, which are quantitatively measured as a change in the system energy triggered by molecule binding/dissociation, perturbations of the solvent around the binding site, by structural changes in the target binding site and/or ligand binding mode. All alterations in the system's thermodynamic parameters, including the binding affinity/dissociation constants at a given temperature, reaction stoichiometry, as well as enthalpic and entropic contributions to the binding are evaluated [30]. The association of SLN mannitol and trehalose was studied by titration of SLN suspensions onto each excipient solution at the same concentrations used in the spray-drying process. Figure 3.4 shows the net enthalpy of injection of SLN into the excipient solution (after subtraction of the heat evolved after the titration of SLN suspension into water) as a function of the SLN/excipient molar ratio for both types of SLN. The inset in Figure 3.4C shows the raw enthalpies of titration of glyceryl tristearate onto mannitol and water.

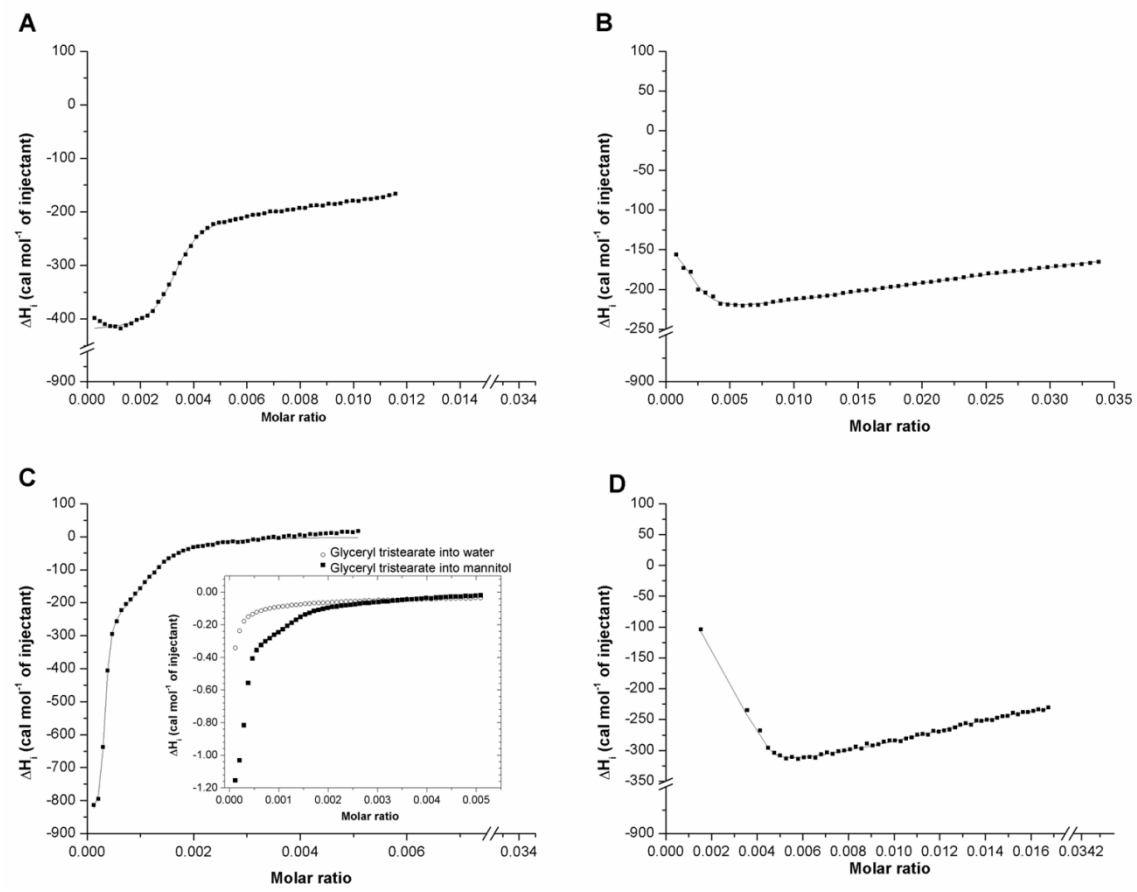

Figure 3.4: Heats of interaction of glyceryl dibehenate SLN with (A) mannitol and (B) trehalose and glyceryl tristearate SLN with (C) mannitol and (D) trehalose solutions. Each dot on the curve corresponds to the heat of reaction following 2 µL injection every 400 s at 25°C (cell volume=1.436 mL). The solid lines represent the fitting to experimental data.

In the case of mannitol (Figures 3.4A and C), the enthalpy of interaction (ΔH_i^i, the superscript denoting the binding site) with SLN is rather more negative than that of trehalose (Figures 3.4B and D), and hence the complexation process is exothermic and becomes progressively less negative as the SLN/mannitol molar ratio increases, as observed for other systems such as protein-drug and polyelectrolyte-polyelectrolyte systems [31]. The negative ΔH_i^i values can be originated from extensive hydrogen bonding network formation between fatty acids comprising both types of SLN and hydroxyl groups of mannitol. Increase in SLN concentration leads to a progressive increase of ΔH_i^i (less exothermic) due to surface dehydration of SLN and excipient

molecules upon mutual interaction, although contributions from a certain SLN charge shielding and excipient's molecular rearrangements upon excipient adsorption onto SLN surfaces could not be neglected. Finally, a plateau region is reached which corresponds to simple SLN dilution effects at molar ratios ca. 0.0025 and 0.005 for glyceryl tristearate and glyceryl dibehenate SLN, respectively.

On the other hand, titrations of SLN into trehalose solution (Figures 3.4B and D) led to a different profile. There exists firstly a progressive exothermic decrease in ΔH_i^i at low SLN/trehalose molar ratios until reaching an exothermic minimum (at ca. 0.0055 for both types of SLN) followed by an additional averaged endothermic event leading to less negative ΔH_i^i values. In this case, a plateau region is not observed probably because this would take place at larger SLN/trehalose molar ratios exceeding those here analyzed which reproduce the concentrations used in the spray-drying process, as mentioned above. The first exothermic decrease and subsequent minimum can be associated to dipole-dipole interactions between water molecules oriented favourable on adjacent SLN thanks to the presence of trehalose molecules at low SLN concentrations, as also suggested for other systems [32]. In contrast, subsequent addition of SLN would lead to an enhancement of trehalose and SLN dehydration to promote extensive trehalose binding to all injected SLN favouring mutual interactions, giving to progressive larger ΔH_i^i values. The potential contribution of hydrophobic interactions between disaccharide rings and conformational rearrangements of trehalose molecules onto SLN surface might play an additional role and can contribute to ΔH_i^i values.

Regarding the thermodynamic characterization, Table 3.2 summarizes the enthalpy, entropy, binding constant and the stoichiometry of SLN-excipients interaction derived on the basis of the two-binding-site model. As observed, binding of glyceryl tristearate SLN with both excipients involved binding constants in the order of 10^5 and 10^3 M^{-1} for the first and second class of binding sites, respectively, two orders of magnitude larger than those observed for glyceryl dibehenate ones (10^3-10^4 and 10^1-10^2 M^{-1}). Such differences may probably arise from the relatively lower hydrophobic character and some steric restrictions of the former lipid which facilitates the interaction with the excipients via dipole-dipole interactions. Nevertheless, the magnitude of binding constants and their variability is rather similar to those previously obtained when analyzing, for example, the interactions between saccharides with proteins, such as lectins [33] and functionalized latex nanoparticles [34].

Table 3.2: Enthalpy (ΔH_i^i), entropy (ΔS_i^i), binding constant (K^i) and stoichiometry (n^i) of the interaction of glyceryl dibehenate and glyceryl tristearate SLN with mannitol and trehalose at 25°C (mean±SD, n=3).

Spray-drying excipient	Type of SLN	ΔH_i^i (cal/mol)	ΔS_i^i (cal/mol)	10^{-3} K^i (M^{-1})	10^2 n^i
Mannitol	Glyceryl dibehenate	-423±4 -243±2	94±3 29±2	93±5 0±0	0±0 2±0
	Glyceryl tristearate	-852±6 -290±3	109±8 70±3	664±16 5±0	0±0 0±0
Trehalose	Glyceryl dibehenate	-130±1 -199±9	72±3 23±4	6±0 0±0	0±0 3±0
	Glyceryl tristearate	-351±45 -358±1	103±7 58±2	278±20 1±0	0±0 2±0

Values in each column from top to bottom correspond to the first and second class of binding sites (i=1, 2).

In addition, the stoichiometry of binding is fractional, corresponding to the interaction of multivalent substrate/ligands, such as SLN, for which $1/n^i$ would provide the functional valence of the nanocarriers to the excipients [35]. Concerning the enthalpy of interaction, their relatively small exothermic values agree with the potential predominance of hydrogen bonding between excipients and nanoparticles. Moreover, some electrostatic repulsion between SLN and small dispersion forces of attraction occurring in solution (such as dehydration processes and molecular rearrangements) leads to ΔH_i^i values slightly larger for glyceryl tristearate than for glyceryl dibehenate SLN in both excipients. In spite of the negative values ΔH_i^i, SLN-excipients complexation was proven to be entropically driven as observed from the relatively large and positive entropy changes, in agreement with strong changes in solvation. In particular, release of water molecules to the solvent either hydrogen bonded to polar groups of the excipient molecules and SLN surfaces or ordered at the interface of SLN apolar groups upon intermolecular interaction [36].

In summary, it can be deduced from thermodynamic data that interactions of both kinds of SLN with mannitol are more energetic (more exothermic) and with higher affinity than for trehalose, in agreement with a larger hydration shell and interaction strength with water of the latter saccharide. This behaviour could imply a greater ability of trehalose to encapsulate SLN in more rigid and packed structures requiring lower concentrations than other excipients, as corroborated by SEM and spray-drying experimental data.

3.4.5. *In vitro* deposition studies

The TSLI, that simulates the respiratory tract, was used to evaluate the *in vitro* performance during aerosolization and drug deposition of each formulation. It has an aerodynamic particle cut-off of 6.4 μm for the lower impingement chamber, which mimics the alveoli. Thus, the drug deposited in this chamber correlates to the amount of drug which will probably get deposited in the terminal lung units. A Rotahaler® device was chosen for these experiments due to its simple construction, allowing comparison of the dispersibility of loaded powders. Mass deposition of the spray-dried formulation in the DPI and on each stage of the TSLI were measured by spectrophotometry following their dissolution in ethanol and expressed as a percentage of the total RFB mass recovered. In general, the percentage of each component deposited on a specific TSLI stage or in the DPI device varied with respect to particle size of the sample. The aerodynamic behaviour of the different evaluated powder formulations is shown in Figure 3.5. Overall, approximately 30% of RFB percentage was retained in the D+C for all tested dry powders. A possible explanation for this result might be the inadequacy of the device or capsule used or/and the cohesive/adhesive properties of the powders, which can limit the process. A small fraction of RFB (< 15%) was retained in the upper (M+T) and medium chamber (MC). Regarding the RFB contents that reached the lung compartment, ≈ 50% of the total administered drug *per* dry powder can be detected in the lower compartment of the TSLI equipment. This can indicate that when these RFB-SLN-loaded microspheres are administered *in vivo*, 51.6±8.0% and 51.3±2.9% of the RFB loaded in glyceryl tristearate SLN microencapsulated in mannitol and in trehalose, respectively, could reach the deep lung. These amounts are higher than those corresponding to the same antibiotic loaded in glyceryl dibehenate SLN microencapsulated in mannitol and in trehalose (44.1±2.1% and 45.4±0.4%, respectively).

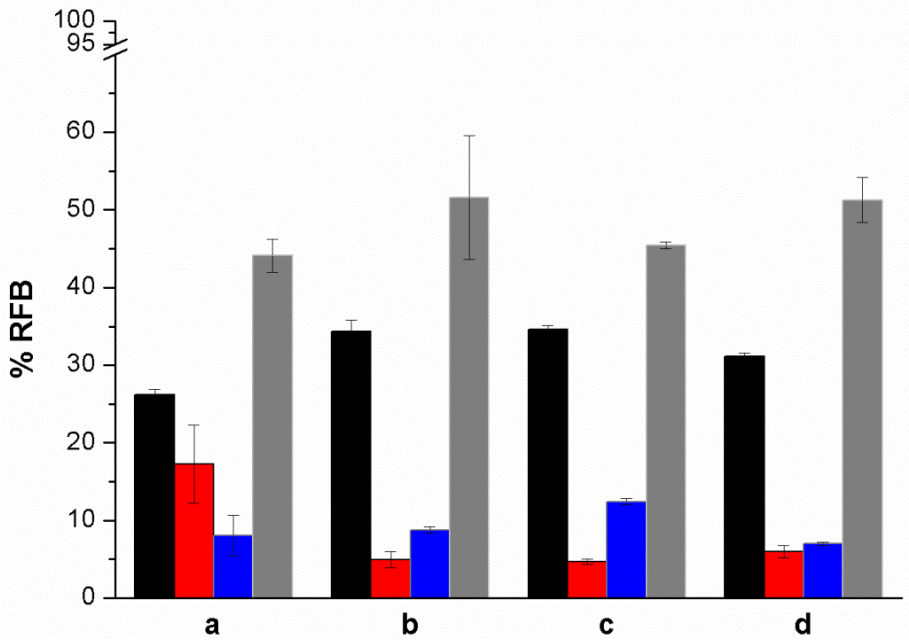

Figure 3.5: *In vitro* deposition of the spray-dried microsphere powders: (a) mannitol microspheres containing glyceryl dibehenate SLN; (b) mannitol microspheres containing glyceryl tristearate SLN; (c) trehalose microspheres containing glyceryl dibehenate SLN; (d) trehalose microspheres containing glyceryl tristearate SLN. (■) device+capsules (D+C); (■) mouth+throat (M+T); (■) medium compartment (MC) and (■) lung compartment (mean±SD, *n*=3).

3.4.6. SLN recovery from microspheres

To preserve their advantages as colloidal carriers after microencapsulation, SLN must be readily delivered from microspheres following their *in vivo* pulmonary administration, maintaining their original size and zeta potential. The excipient molecules are expected to protect the SLN from spray-drying, not only from the heat but also preventing particle/particle interactions that might be able to involve their aggregation and avoid their deposition and delivery in the deep lung [6, 28]. Since the excipients used in the microencapsulation process are freely soluble in aqueous medium, it is possible to easily recover the microencapsulated SLN in aqueous media [6]. Recovery studies were performed by incubating the dry powders in isotonic PBS pH 7.4 with 0.1% lung surfactant in order to mimic the lung environment. The mean particle size and surface charge of SLN, before spray-drying and after recovery from dry powders, were compared. It is possible to state that there was a change in the size of the recovered

glyceryl dibehenate SLN when compared with initial records (Table 3.3), since it was observed a size increase of 2.3-fold for recovery from trehalose microspheres compared to 1.7-fold for mannitol microspheres. On the other hand, glyceryl tristearate SLN maintained their initial sizes. In addition, it is also possible to observe that, in some cases, there was an inefficient dissolution process of the carrier particles (mainly in trehalose microspheres) (Figure 3.6) at the assayed incubation time (90 min); the presence of some "excipient bridges" can still be observed, similar to that described elsewhere [14]. Nevertheless, in spite of the enlargement presented by glyceryl dibehenate nanoparticles, they are still in the nano-range, being the increase irrelevant for our purposes. The enlargement of nanoparticle size after spray-drying has also been reported for powders prepared with chitosan [6] and gelatin [13] nanoparticles and was attributed to eventual changes in conformation due to the thermal conditions of the spray-drying process. Furthermore, a lower zeta potential was observed for the reconstituted SLN as compared to the fresh ones probably due to the fact that the release medium was composed by PBS with lung surfactant. This surfactant is constituted by proteins that when adhered to the surface of the SLN promoted this reduction in the zeta potential. Consequently, from this assay, we could expect that after reaching the deep lung, mannitol and trehalose microspheres will be quickly dissolved in the lung aqueous covered epithelium and release the RFB-loaded SLN.

Table 3.3: Mean size (∅) and zeta potential (ZP) of SLN after recovery from dry powders in isotonic PBS pH 7.4 with 0.1% lung surfactant (mean±SD, *n*=3).

Microspheres	SLN	Glyceryl dibehenate SLN		Glyceryl tristearate SLN	
		∅ (nm)	ZP (mV)	∅ (nm)	ZP (mV)
	Fresh	99±4	-18±1	210±8	-18±1
Mannitol	Recovered	168±2	-12±3	196±7	-10±1
	Mean Δ_1	1.7	0.7	0.9	0.6
Trehalose	Recovered	229±13	-9±1	224±12	-9±1
	Mean Δ_2	2.3	0.5	1.1	0.5

Δ_1: size or zeta potential of recovered nanoparticles from mannitol microspheres / size or zeta potential of fresh nanoparticles

Δ_2: size or zeta potential of recovered nanoparticles from trehalose microspheres / size or zeta potential of fresh nanoparticles

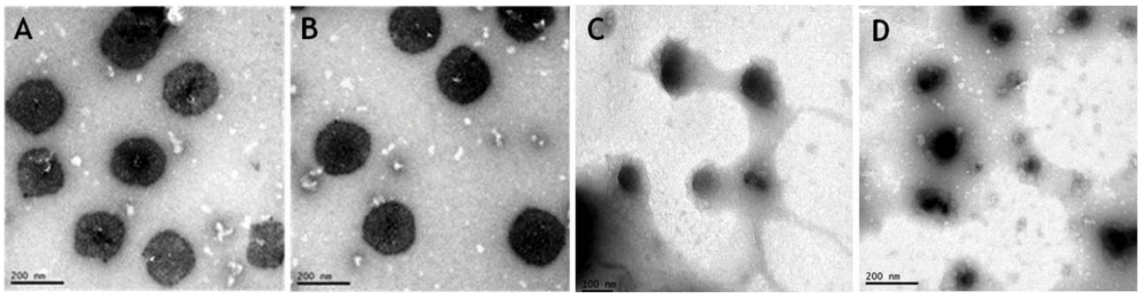

Figure 3.6: TEM micrographs of: (A) glyceryl dibehenate SLN and (B) glyceryl tristearate SLN after recovery from mannitol microspheres; and (C) glyceryl dibehenate SLN and (D) glyceryl tristearate SLN after recovery from trehalose microspheres.

3.4.7. *In vitro* RFB release studies

The employed excipients (mannitol and trehalose) are soluble in aqueous medium and allowed nanoparticle easy delivery as discussed in the previous section, resulting in a nanoparticle suspension with the native characteristics. Thus, results suggest that after reaching the deep lung, microspheres will be quickly dissolved in the lung aqueous covered epithelium, releasing the nanoparticles [6, 11]. Figure 3.7 depicts the release profile of RFB from SLN and dry powders in PBS pH 7.4 and 0.1% lung surfactant at 37°C as previously described. Indeed, the RFB release profile from SLN and from SLN microencapsulated in mannitol and trehalose revealed a fast drug release within the first hour for both particulate systems followed by a controlled and more sustained release over a prolonged period of time (24 h). However, the RFB release from trehalose microspheres for both SLN formulations was incomplete probably due to the fact that trehalose microspheres did not dissolve totally, as discussed before (Figure 3.6C and D), thus hampering the RFB release (80.4±1.2% for RFB release from glyceryl dibehenate microencapsulated in trehalose and 86.6±0.0% for RFB release from glyceryl tristearate microencapsulated in trehalose).

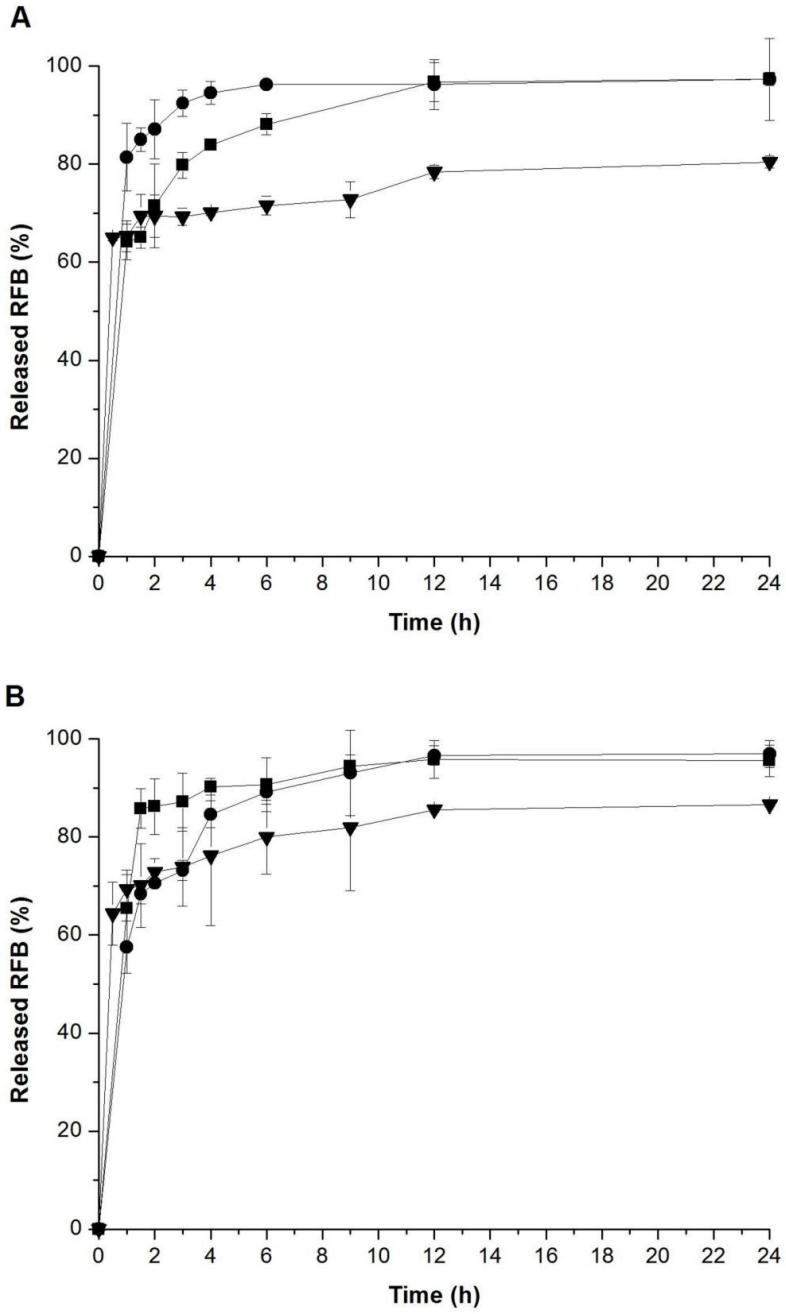

Figure 3.7: Release profiles of RFB from (A): (■) glyceryl dibehenate SLN, (●) glyceryl dibehenate SLN microencapsulated in mannitol and (▼) glyceryl dibehenate SLN microencapsulated in trehalose; and (B): (■) glyceryl tristearate SLN, (●) glyceryl tristearate SLN microencapsulated in mannitol and (▼) glyceryl tristearate SLN microencapsulated in trehalose. These release studies were performed in 10 mM isotonic PBS pH 7.4 and 0.1% of lung surfactant at 37°C (mean±SD, *n*=3).

3.4.8. *In vitro* antimycobacterial activity of RFB formulations by MTS assay

A high number of biological assays are currently in use for evaluating the susceptibility of mycobacteria to formulations of interest, ranging from classical disk diffusion and broth dilution assays to radiorespirometric (BACTEC), dye-based and fluorescent/luminescence methodologies. In particular, the use of oxidation/reduction indicator dyes such as Alamar Blue, MTT or MTS, allowing the fluorimetric or spectrophotometric quantification of the respective reduced forms constitute accurate and reproducible methods for mycobacterial viability evaluation without the need of radioisotopes or costly materials and equipment [37]. In the present work, the susceptibility of *M. avium* strain to different RFB formulations was evaluated by the MTS assay. The intention was to validate if RFB antimycobacterial activity was preserved after incorporation in glyceryl dibehenate SLN or following their encapsulation in mannitol microparticles. As the previous experiments allowed to anticipate similar characteristics of the SLN prepared with both lipids as well as both kind of microspheres, for further studies only the microencapsulated RFB-glyceryl dibehenate SLN in mannitol were analyzed. RFB formulations were tested at concentrations ranging from 0.005 to 10 µg/mL in the free form, loaded in glyceryl dibehenate SLN and loaded in glyceryl dibehenate SLN microencapsulated in mannitol. Moreover, the influence of mannitol, present in the microspheres, on mycobacterial growth was also evaluated constituting the empty mannitol microspheres. Figure 3.8 shows the viability of the *M. avium inoculum* 10 days after incubation with the selected formulations. For all tested RFB formulations, the increase on the antibiotic concentration resulted in a reduction on the mycobacterial viability. In addition, for the same concentration no statistically significant differences were observed for the three types of RFB formulations and empty mannitol microspheres did not display any antimycobacterial effect as viability was always superior to 100%. Taking into account the obtained results, the antimycobacterial activity is due to RFB and not from the raw materials that formed the formulations (i.e. from mannitol). Moreover, RFB was able to keep its antimycobacterial effect after being encapsulated in SLN and followed by microencapsulation through spray-drying technique. Indeed, RFB withstands the harsh physical conditions present in both production techniques, i.e. HSH and spray-drying.

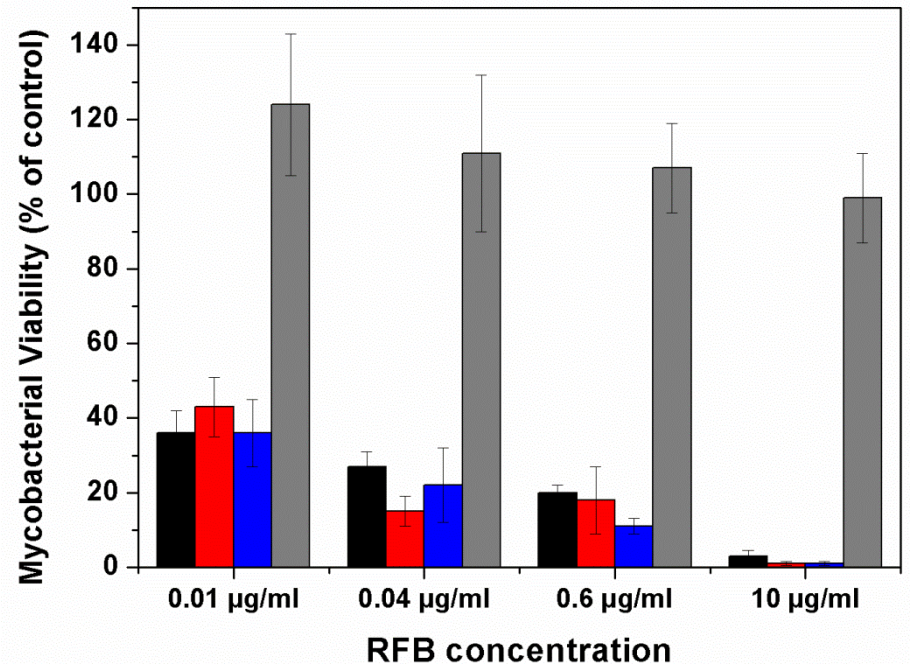

Figure 3.8: *In vitro* antimycobacterial activity of RFB formulations by MTS assay: (■) RFB in free form, (■) RFB-loaded glyceryl dibehenate SLN, (■) RFB-loaded glyceryl dibehenate SLN microencapsulated in mannitol and (■) empty mannitol microspheres (mean±SD, *n*=6).

3.4.9. *In vivo* fate of RFB formulations: biodistribution studies

Biodistribution studies of microencapsulated RFB-glyceryl dibehenate SLN in mannitol following pulmonary administration were performed and the amount of non-metabolized antibiotic in the spleen, liver, lung and blood was determined by HPLC after an extraction procedure previously described (Figure 3.9). RFB microencapsulated in mannitol was used as a control.

For both formulations under study, the pulmonary administration allowed an accumulation of the antibiotic mainly in lung, spleen and blood. Higher amounts of RFB incorporated in mannitol microencapsulated SLN were observed in lung when compared with RFB in mannitol microspheres. In addition, RFB amounts increased after 30 min of pulmonary administration, from 0.87±0.23 µg/g to 1.37±0.47 µg/g of lung regarding RFB-loaded glyceryl dibehenate SLN microencapsulated in mannitol and from 0.29±0.14 µg/g to 0.49±0.21 µg/g of lung concerning RFB in mannitol microspheres. The same profile was obtained for RFB levels in blood. An increase was observed for both

formulations with time, from 0.97±0.09 μg/g to 1.39±0.09 μg/g of blood for RFB-loaded glyceryl dibehenate SLN microencapsulated in mannitol and from 0.70±0.47 μg/g to 1.05±0.32 μg/g of blood for RFB in mannitol microspheres. The liver constituted the organ where low RFB levels were achieved for both dry powder formulations. The obtained results are in accordance with literature as inhaled microparticles were able to reach systemic circulation [38, 39]. Overall, regarding the amount of the antibiotic, low levels of non-metabolized RFB were obtained in the studied organs. However the RFB loading in SLN and, subsequently, in microspheres was very low and so other strategies to enhance the DL should be addressed.

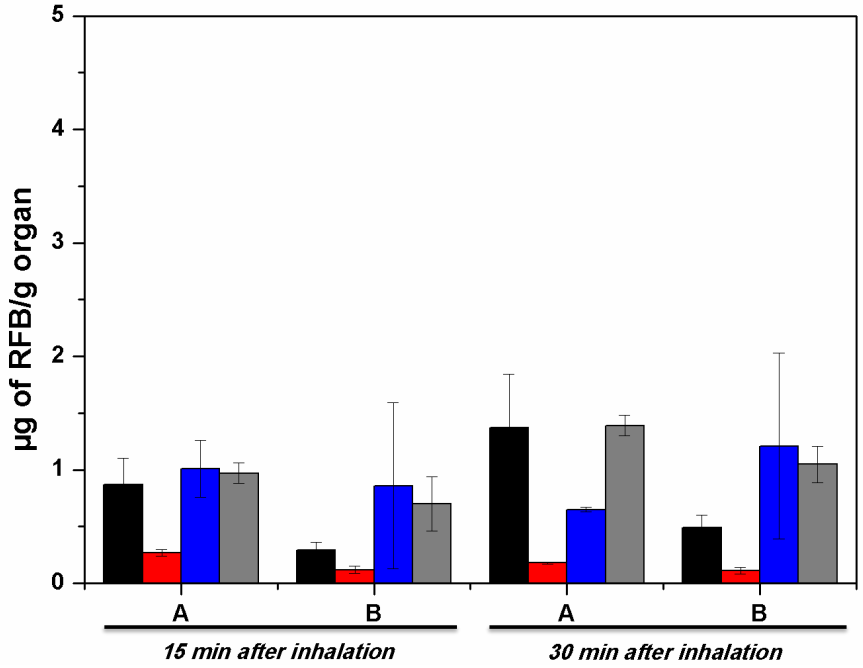

Figure 3.9: Biodistribution of (A) RFB-glyceryl dibehenate SLN microencapsulated in mannitol and (B) RFB microencapsulated in mannitol as measured by non-metabolised RFB in BALB/c mice in (■) lung, (■) liver, (■) spleen and (■) total blood following pulmonary administration. Mice were sacrificed after 15 and 30 min of administration (mean±SD, *n*=4 mice per selected time).

3.4.10. Biological evaluation of RFB-SLN in mannitol microparticles in a murine model of *M. tuberculosis*

In spite of the low levels of RFB achieved after pulmonary administration, the biological evaluation in a *M. tuberculosis* murine model of infection was performed. The therapeutic activity of RFB-glyceryl dibehenate SLN microencapsulated in mannitol was evaluated in mice infected intravenously with 4.7 log10 CFU of *M. tuberculosis* and compared with infected and non-treated mice (control group). From CFU counts in liver, spleen and lung, the growth index was calculated as previously described. At the beginning of treatment, bacillary burdens had increased in all organs and a group of infected mice was sacrificed and the log10 CFU average in liver, spleen and lung was 5.1, 5.2 and 3.9, respectively. Figure 3.10 shows the growth index values for control and treated groups.

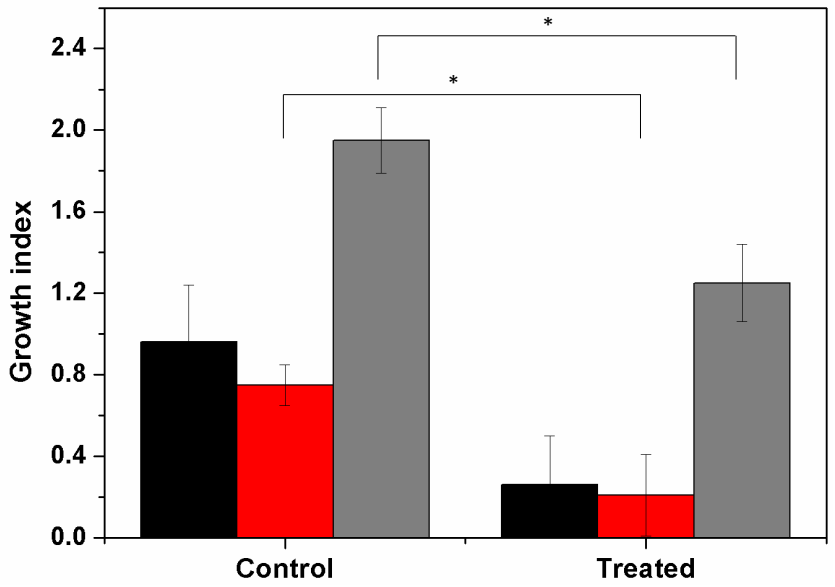

Figure 3.10: Influence of pulmonary administration of RFB-glyceryl dibehenate SLN microencapsulated in mannitol on the growth index of *M. tuberculosis* in (■) liver, (■) spleen and (■) lung of BALB/c mice. The *M. tuberculosis* strain used in this animal model was the H37Rv. Each mouse was intravenously infected with $5x10^4$ CFU of the *inoculum*. Treatment started two weeks after infection induction. Mice received the formulation under study five times a week for two weeks (mean±SD, n=5). Statistical analysis between the control (infected and non-treated) and treated groups, for each organ was performed using one-way ANOVA with Dunnet's post hoc test (*p<0.05).

The displayed results showed relevant decrease on the growth index values in the liver (from 0.96±0.28 to 0.26±0.24), spleen (from 0.75±0.10 to 0.21±0.20) and lung (from 1.95±0.16 to 1.25±0.19) to control group and treated mice, respectively. The values indicated that RFB formulation was able to reduce the bacterial loads in all analyzed organs. Overall, conjugating these results with biodistribution data, it is possible to sustain that, despite the low non-metabolized RFB levels observed after pulmonary administration, these microencapsulated SLN were able to reduce the bacterial loads in liver, spleen and lung.

3.5. Conclusions

In this work, RFB-loaded glyceryl dibehenate and glyceryl tristearate SLN were successfully incorporated in mannitol and trehalose microspheres by means of a spray-drying process, resulting in dry powders with suitable properties for pulmonary administration. This method allows to overcome stability issues of liquid nanoparticle formulations, as well as to reach deep lung deposition upon inhalation. The inert excipients, mannitol and trehalose, serve as thermoprotectants, resulting in dry powders consisting in microencapsulated SLN, with adequate morphological and aerodynamic properties. The structural examination by SEM and CLSM indicated that microspheres are spherical with well-defined limits and that SLN were efficiently encapsulated in the microspheres, being homogeneously distributed within the whole microparticles. These observations confirm the efficiency of the microencapsulation method, according to the formulation and process conditions employed in this work. Physical characterization by ITC demonstrated that SLN have higher affinity for mannitol than for trehalose during the spray-drying process, favouring the interactions between SLN and mannitol. Through *in vitro* deposition studies, it was demonstrated that a considerable portion of dry powders can reach the lung. Mannitol and trehalose microspheres were readily dissolved and the SLN redispersion was immediate, providing a high *in vitro* RFB release (>95% for SLN and SLN-mannitol microspheres and ca. 80% for SLN microencapsulated in trehalose over 24 h). *In vitro* results confirmed that the micro-nanoformulations kept the antimycobacterial activity of RFB. *In vivo* studies demonstrated that the dry powder was an effective formulation to deliver RFB to the lung, although relevant quantities were also detected in liver and spleen. The RFB in microencapsulated-glyceryl dibehenate SLN reduced the growth index of the *M. tuberculosis* infection in all studied organs compared

to non-treated animals. Thereby, it was confirmed that these microencapsulated SLN are a promising platform for pulmonary delivery of therapeutic antibiotics for the treatment of mycobacterial infections in the lung, contributing to improved chemotherapy of TB.

3.6. References

1. Patton, J.S.; Platz, R.M. (D) Routes of delivery: Case studies: (2) Pulmonary delivery of peptides and proteins for systemic action. Adv. Drug Deliv. Rev., 1992, 8 (2-3), 179-196.

2. Suarez, S.; O'Hara, P.; Kazantseva, M.; Newcomer, C.E.; Hopfer, R.; McMurray, D.N.; Hickey, A.J. Respirable PLGA microspheres containing rifampicin for the treatment of tuberculosis: screening in an infectious disease model. Pharmaceut. Res., 2001, 18 (9), 1315-1319.

3. Misra, A.; Hickey, A.; Rossi, C.; Borchard, G.; Terada, H.; Makino, K.; Fourie, P.; Colombo, P. Inhaled drug therapy for treatment of tuberculosis. Tuberculosis, 2011, 91 (1), 71-81.

4. Adi, H.; Young, P.M.; Chan, H.-K.; Agus, H.; Traini, D. Co-spray-dried mannitol–ciprofloxacin dry powder inhaler formulation for cystic fibrosis and chronic obstructive pulmonary disease. Eur. J. Pharm. Sci., 2010, 40 (3), 239-247.

5. Cruz, L.; Fattal, E.; Tasso, L.; Freitas, G.C.; Carregaro, A.B.; Guterres, S.S.; Pohlmann, A.R.; Tsapis, N. Formulation and *in vivo* evaluation of sodium alendronate spray-dried microparticles intended for lung delivery. J. Control. Release, 2011, 152 (3), 370-375.

6. Grenha, A.; Seijo, B.; Remuñán-López, C. Microencapsulated chitosan nanoparticles for lung protein delivery. Eur. J. Pharm. Sci., 2005, 25 (4), 427-437.

7. Al-Qadi, S.; Alatorre-Meda, M.; Zaghloul, E.; Taboada, P.; Remunán-López, C. Chitosan–hyaluronic acid nanoparticles for gene silencing: The role of hyaluronic acid on the nanoparticles' formation and activity. Colloid. Surface B, 2013, 103 (1), 615-623.

8. Almeida, A.; Souto, E. Solid lipid nanoparticles as a drug delivery system for peptides and proteins. Adv. Drug Deliv. Rev., 2007, 59 (6), 478-490.

9. Videira, M.; Almeida, A.J.; Fabra, À. Preclinical evaluation of a pulmonary delivered paclitaxel-loaded lipid nanocarrier antitumor effect. Nanomed.: Nanotechnol., 2012, 8 (7), 1208-1215.

10. Al-Qadi, S.; Remuñán-López, C. A micro- and nano-structured drug carrier based on biocompatible, hybrid polymeric nanoparticles for potential application in dry powder inhalation therapy. Polymer, 2014, 55 (16), 4012-4021.

11. Al-Qadi, S.; Grenha, A.; Carrión-Recio, D.; Seijo, B.; Remuñán-López, C. Microencapsulated chitosan nanoparticles for pulmonary protein delivery: *in vivo* evaluation of insulin-loaded formulations. J. Control. Release, 2012, 157 (3), 383-390.

12. Mortensen, N.; Durham, P.; Hickey, A. The role of particle physico-chemical properties in pulmonary drug delivery for tuberculosis therapy. J. Microencapsul., 2014, 31 (8), 785-795.

13. Sham, J.-H.; Zhang, Y.; Finlay, W.; Roa, W.; Löbenberg, R. Formulation and characterization of spray-dried powders containing nanoparticles for aerosol delivery to the lung. Int. J. Pharm., 2004, 269 (2), 457-467.

14. Cheow, W.; Hadinoto, K. Preparations of dry-powder therapeutic nanoparticle aerosols for inhaled drug delivery. J. Aerosol Res., 2010, 25 (2), 155-165.

15. Gaspar, M.M.; Neves, S.; Portaels, F.; Pedrosa, J.; Silva, M.T.; Cruz, M.E.M. Therapeutic efficacy of liposomal rifabutin in a Mycobacterium avium model of infection. Antimicrob. Agents Ch., 2000, 44 (9), 2424-2430.

16. Kim, W.; Yamasaki, Y.; Kataoka, K. Development of a fitting model suitable for the isothermal titration calorimetric curve of DNA with cationic ligands. J. Phys. Chem. B, 2006, 110 (22), 10919-10925.

17. Gaspar, M.; Cruz, A.; Penha, A.; Reymao, J.; Sousa, A.; Eleutério, C.; Domingues, S.; Fraga, A.; Longatto Filho, A.; Cruz, M. Rifabutin encapsulated in liposomes exhibits increased therapeutic activity in a model of disseminated tuberculosis. Int. J. Antimicrob. Ag., 2008, 31 (1), 37-45.

18. Gaspar, M.M.; Calado, S.; Pereira, J.; Ferronha, H.; Correia, I.; Castro, H.; Tomás, A.M.; Cruz, M.E.M. Targeted delivery of paromomycin in murine infectious diseases through association to nano lipid systems. Nanomed.: Nanotechnol., 2015, 11 (7), 1851-1860.

19. Finlay, W.; Stapleton, K.; Zuberbuhler, P. Fine particle fraction as a measure of mass depositing in the lung during inhalation of nearly isotonic nebulized aerosols. Journal of aerosol science, 1997, 28 (7), 1301-1309.

20. Heyder, J.; Gebhart, J.; Rudolf, G.; Schiller, C.F.; Stahlhofen, W. Deposition of particles in the human respiratory tract in the size range 0.005–15 μm. J. Aerosol Sci, 1986, 17 (5), 811-825.

21. Finlay, W.; Gehmlich, M. Inertial sizing of aerosol inhaled from two dry powder inhalers with realistic breath patterns versus constant flow rates. Int. J. Pharm., 2000, 210 (1), 83-95.

22. Gonnissen, Y.; Remon, J.; Vervaet, C. Development of directly compressible powders via co-spray-drying. Eur. J. Pharm. Biopharm., 2007, 67 (1), 220-226.

23. Bosquillon, C.; Lombry, C.; Preat, V.; Vanbever, R. Influence of formulation excipients and physical characteristics of inhalation dry powders on their aerosolization performance. J. Control. Release, 2001, 70 (3), 329-339.

24. You, Y.; Zhao, M.; Liu, G.; Tang, X. Physical characteristics and aerosolization performance of insulin dry powders for inhalation prepared by a spray drying method. J. Pharm. Pharmacol., 2007, 59 (7), 927-934.

25. Al-Qadi, S.; Grenha, A.; Remuñán-López, C. Microspheres loaded with polysaccharide nanoparticles for pulmonary delivery: Preparation, structure and surface analysis. Carbohyd. Polym., 2011, 86 (1), 25-34.

26. Hassan, M.S.; Lau, R.W.M. Effect of particle shape on dry particle inhalation: study of flowability, aerosolization, and deposition properties. AAPS PharmSciTech, 2009, 10 (4), 1252-1262.

27. Kaialy, W.; Martin, G.P.; Ticehurst, M.D.; Royall, P.; Mohammad, M.A.; Murphy, J.; Nokhodchi, A. Characterisation and deposition studies of recrystallised lactose from binary mixtures of ethanol/butanol for improved drug delivery from dry powder inhalers. AAPS J., 2011, 13 (1), 30-43.

28. Tewa-Tagne, P.; Briançon, S.; Fessi, H. Preparation of redispersible dry nanocapsules by means of spray-drying: development and characterisation. Eur. J. Pharm. Sci., 2007, 30 (2), 124-135.

29. Grenha, A.; Seijo, B.; Serra, C.; Remuñán-López, C. Chitosan nanoparticle-loaded mannitol microspheres: structure and surface characterization. Biomacromolecules, 2007, 8 (7), 2072-2079.

30. Wiseman, T.; Williston, S.; Brandts, J.; Lin, L. Rapid measurement of binding constants and heats of binding using a new titration calorimeter. Anal. Biochem., 1989, 179 (1), 131-137.

31. Taboada, P.; Fernández, Y.; Mosquera, V. Interactions of two amphiphilic penicillins with myoglobin in aqueous buffered solutions: a thermodynamic and spectroscopy study. Biomacromolecules, 2004, 5 (6), 2201-2211.

32. Castro, E.; Taboada, P.; Mosquera, V. Behavior of a styrene oxide-ethylene oxide diblock copolymer/surfactant system: a thermodynamic and spectroscopy study. J. Phys. Chem. B, 2005, 109 (12), 5592-5599.

33. Dam, T.K.; Gerken, T.A.; Cavada, B.S.; Nascimento, K.S.; Moura, T.R.; Brewer, C.F. Binding studies of α-GalNAc-specific lectins to the α-GalNAc (Tn-antigen) form of porcine submaxillary mucin and its smaller fragments. J. Biol. Chem., 2007, 282 (38), 28256-28263.

34. Schumacher, S.; Katterle, M.; Hettrich, C.; Paulke, B.-R.; Hall, D.G.; Scheller, F.W.; Gajovic-Eichelmann, N. Label-free detection of enhanced saccharide binding at pH 7.4 to nanoparticulate benzoboroxole based receptor units. J. Mol. Recognit., 2011, 24 (6), 953-959.

35. Dam, T.K.; Brewer, C.F. Thermodynamic studies of lectin-carbohydrate interactions by isothermal titration calorimetry. Chem. Rev., 2002, 102 (2), 387-430.

36. Srinivasachari, S.; Liu, Y.; Prevette, L.E.; Reineke, T.M. Effects of trehalose click polymer length on pDNA complex stability and delivery efficacy. Biomaterials, 2007, 28 (18), 2885-2898.

37. Sánchez, J.G.B.; Kouznetsov, V.V. Antimycobacterial susceptibility testing methods for natural products research. Braz. J. Microbiol., 2010, 41 (2), 270-277.

38. Verma, R.K.; Mukker, J.K.; Singh, R.S.P.; Kumar, K.; Verma, P.R.P.; Misra, A. Partial biodistribution and pharmacokinetics of isoniazid and rifabutin following pulmonary delivery of inhalable microparticles to rhesus macaques. Mol. Pharm., 2012, 9 (4), 1011-1016.

39. Verma, R.K.; Kaur, J.; Kumar, K.; Yadav, A.B.; Misra, A. Intracellular time course, pharmacokinetics, and biodistribution of isoniazid and rifabutin following pulmonary delivery of inhalable microparticles to mice. Antimicrob. Agents Ch., 2008, 52 (9), 3195-3201.

This page was intentionally left blank.

Chapter 4

Microencapsulated SLN: an innovative strategy for pulmonary protein delivery

This chapter is based on the following publication:
Gaspar DP, Serra C, Lino PR, Gonçalves LMD, Taboada P, Remuñán-López C and Almeida AJ. *Microencapsulated SLN: an innovative strategy for pulmonary protein delivery*. International Journal of Pharmaceutics.2017, 516 (1-2), 231–246.

This page was intentionally left blank.

Abstract

Associating protein with nanoparticles is an interesting strategy to improve their bioavailability and biological activity. Solid lipid nanoparticles (SLN) have been sought as carriers for therapeutic proteins transport to the lung epithelium. Nevertheless, because of their low inertia, nanoparticles intended for pulmonary application usually escape from lung deposition. To overcome this problem, the production of spray-dried powders containing nanoparticles has been recently reported. Herein we developed new hybrid microencapsulated SLN for pulmonary administration, containing a model protein (papain, PAP). PAP was adsorbed onto glyceryl dibehenate and glyceryl tristearate SLN. Physical characterization using transmission electron microscopy, Fourier transform infrared spectroscopy and differential scanning calorimetry confirmed the interaction between PAP and SLN corroborating that the protein was efficiently adsorbed at SLN's surface. PAP adsorption onto SLN (PAP-SLN) slightly increased particle size, while decreasing the SLN negative surface charge. The adsorption process followed a Freundlich type of adsorption isotherm. Nanoformulations were then spray-dried, originating spherical microparticles with suitable aerodynamic characteristics. Full characterization of microparticles was performed using scanning electron microscopy, X-ray photoelectron spectroscopy and isothermal titration calorimetry. PAP was released from dry powders in a higher extent when compared with non spray-dried SLN. Nevertheless, protein stability was kept throughout microsphere production, as assessed by SDS-PAGE.

Graphical abstract

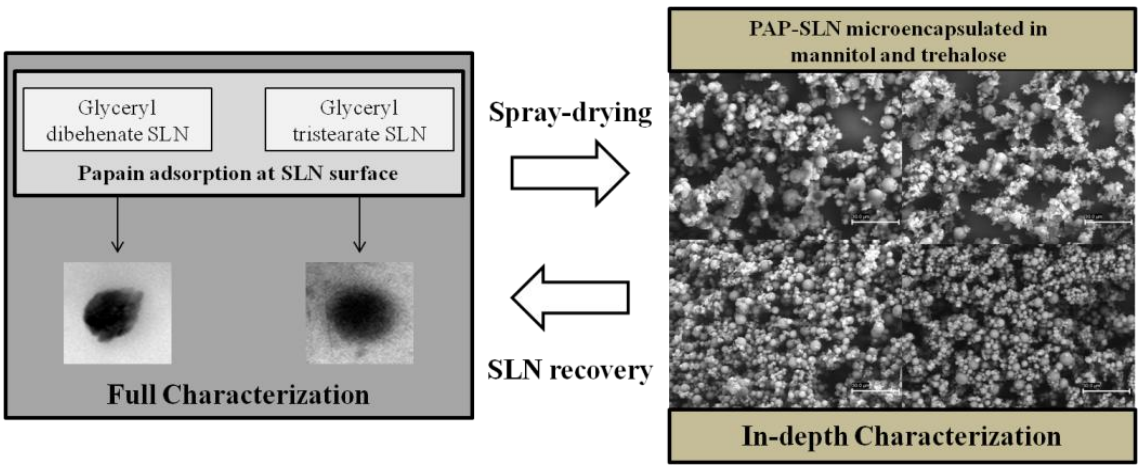

This page was intentionally left blank.

4.1. Introduction

Being highly vulnerable molecules, proteins usually present short *in vivo* half-lives either at the site of administration or in every anatomical location on their way to the site of pharmacological action. Regardless the administration route, many therapeutic proteins do not possess the required physicochemical properties to be absorbed and reach or enter target cells, needing delivery and targeting systems to overcome these limitations and improve drug performance [1].

Soon after their first description by the research groups of R.H. Müller and M.R. Gasco, SLN have been sought as alternative carriers for therapeutic peptides, proteins and antigens [1]. These molecules may be incorporated in SLN and further administered by parenteral routes or by alternative routes such as oral, nasal and pulmonary. However, the smaller the particle diameter, the more difficult it becomes to achieve high drug encapsulation efficiency and a good sustained release effect. To circumvent this problem, the proteins can be adsorbed onto the particle surface rather than encapsulated within. Due to their amphipathic nature, proteins are known to adsorb, accumulating at solid-liquid interfaces where the rate and extent of protein adsorption are influenced by the properties of the protein and its concentration in solution, by the characteristics of the adsorption matrix [2]. Adsorption of proteins onto particles often comprises various steps or stages: (i) transport of the protein from the bulk solution into the interfacial region, (ii) attachment of the protein at the sorbent surface and (iii) the relaxation of the protein on the surface, i.e., optimization of the protein-surface interaction [3, 4]. In protein adsorption studies, particle properties such as electrical charge density and hydrophobicity as well as environmental conditions like pH, temperature and ionic strength are often taken as experimental variables [5]. However, loss of activity of protein molecules during adsorption and release from particle surfaces is often mentioned as an example of the change in the structure of adsorbed proteins [1].

Although nanoparticles have been proposed as valuable vehicles for efficient drug transport to the lung epithelium, their utility for pulmonary application is severely hindered because of their low inertia due to their excessively small dimensions and mass, which causes them to escape from lung deposition and be predominantly exhaled. Furthermore, their small size often leads to aggregation, making physical handling of nanoparticles difficult in liquid and dry powder forms. To solve these limitations, nanoparticles may be microencapsulated using spray-drying techniques thus forming

powders suitable for inhalation, which will quickly dissolve in the lung epithelium [6, 7]. This process has the advantages of being simple, continuous, easily up scaled and cost-effective. Moreover, it has been shown that spray-dried heat sensitive molecules are exposed to high temperatures for only a few milliseconds to seconds in the spray-drying chamber, thus minimizing temperature-related stability problems [8]. During the spraying process, stability issues may also arise as a result of shear forces, which increase the kinetic energy of the system, leading to an intensification of particle collisions. These phenomena can be decreased by the addition of protectants, excipients generally recognized as safe, inert and non-toxic, for example sugars such as lactose and mannitol, or polymers that are located between the particles, or by decreasing the particle concentration in the sprayed liquid [6, 7]. Microencapsulation improved nanoparticles handling and aerosolization performance, enhanced stability and acquisition of aerodynamic properties, which resulted in an efficient lung delivery [6].

In the previous chapters, we described the development of SLN intended for anti-TB drug pulmonary administration, formulated with glyceryl dibehenate and glyceryl tristearate and prepared, using a hot HSH, which were successfully microencapsulated in mannitol and trehalose microparticles. The purpose of the present work was to explore the application of such procedure to protein drugs, producing powders for inhalation based on the microencapsulation of protein-containing SLN. A model protein was loaded onto previously prepared SLN using adsorption to avoid the harsh conditions involved in SLN preparation. The nanoparticles were then suitably microencapsulated in mannitol and trehalose microspheres using spray-drying and evaluated throughout the procedure. The effects of production parameters as well as the effects of excipients on the integrity of the protein were assessed. Papain (PAP), a commonly used and well characterized protease, was selected as a model protein, allowing the assessment of changes in the molecule integrity and stability [9]. The studies included the full physicochemical, pharmaceutical and *in vitro* biological characterization of PAP-SLN and dry powders.

4.2. Materials

Glyceryl dibehenate, m.p. 70°C, was a gift from Gattefossé (France). Tween® 80 (polysorbate 80) was obtained from J. Vaz Pereira, S.A. (Portugal). Glyceryl tristearate (m.p. 72-75°C), mannitol, D-(+)-trehalose dihydrate, SDS and PBS were purchased from

Sigma-Aldrich (USA). PAP from *Carica papaya* (MW ≈23 kDa; ≥3 units/mg protein) was acquired from Fluka (Sigma-Aldrich). Lung surfactant (Curosurf®) was a generous gift from Angelini Farmacêutica, Lda. (Portugal). Purified water was obtained by inverse osmosis (Millipore, Elix 3) with a 0.45 μm pore filter. All other reagents were of analytical grade and were used without further purification.

4.3. Methods

4.3.1. Nanoparticle preparation

Glyceryl dibehenate and glyceryl tristearate SLN were prepared using a hot HSH, as described previously in Chapter 2, section 2.3.2.. Briefly, the lipid phase was melted at a temperature 10°C above its m.p.. A hot aqueous phase consisting of Tween® 80 in purified water was added to lipid phase and homogenized using a high-shear laboratory mixer (Silverson SL2, UK) at 12300 rpm for 10 min. The SLN dispersions were allowed to cool in an ice bath, with gentle agitation during 5 min. The final dispersions were stored at 5±3°C until further use. Each formulation was carried out in triplicate (*n*=3).

4.3.2. Protein adsorption

PAP adsorption onto SLN was carried out as described elsewhere [10, 11]. Briefly, the SLN (30 mg) were incubated overnight with a protein solution (0.197 mg/mL to 1.083 mg/mL) in PBS pH 7.4, at 37ºC, with gentle horizontal shaking. SLN incubated with PBS, without PAP, were used as a control. After incubation, unadsorbed protein was separated from SLN using ultrafiltration membranes (Sartorius AG, Germany; cut-off of 100 kDa,) at 15000×g for 30 min at 4°C in a high-speed centrifuge (Allegra™ 64R centrifuge, Beckman Coulter). The degree of adsorption was calculated indirectly by determining the amount of protein remaining in the supernatant by the BCA protein assay (Pierce, USA), using a microplate reader (FLUOstar Omega, BMG Labtech, Germany), at 562 nm (*n*=3).

Protein adsorption kinetics of PAP was evaluated using the Langmuir and Freundlich models, as previously described [11]. Briefly, the Langmuir model can be expressed by:

$$\frac{C_e}{Q_e} = \frac{C_e}{Q_m} + \frac{1}{Q_m K_L} \qquad \text{(Eq. 4.1)}$$

where C_e is the concentration in equilibrium (μg/mL), Q_e is the amount of protein adsorbed (μg/mg) and Q_m is the maximum adsorption capacity (μg/mg), which is the plateau surface concentration. K_L is a Langmuir constant related to the adsorption capacity. This theory refers that the adsorbed protein layer is confined to a monolayer, where the adsorbate solution is very dilute and all sites available for adsorption are energetically equivalent and there are no lateral interactions between adsorbate molecules. Usually the deviations from this hypothesis are attributed to the formation of multilayers and are treated by the Freundlich equation, which does not predict a limiting value for adsorption and can be expressed by:

$$\log Q_e = \log K_F + \frac{1}{n} \log C_e \qquad \text{(Eq. 4.2)}$$

where K_F is the Freundlich constant for the system, whose index n is usually < 1, so that the amount adsorbed increases less rapidly than the concentration. This model predicts infinite adsorption at infinite concentration. The main assumptions are: the adsorbed layer is not confined to a monolayer and lateral interactions between adsorbate molecules may be possible.

4.3.3. Nanoparticle size and surface charge

The average particle size of SLN before and after PAP adsorption was analyzed by PCS using a Zetasizer Nano S (Malvern Instruments, UK). Zeta potential determination was performed by anemometry using a Zetasizer Nano Z (Malvern Instruments, UK). Both procedures were previously described in Chapter 2, section 2.3.3.1..

4.3.4. Transmission electron microscopy

The morphological analysis of nanoparticles was performed by TEM, following the same specifications as detailed in Chapter 2, section 2.3.3.4..

4.3.5. Fourier transform infrared spectroscopy (FTIR)

FTIR spectra of PAP, glyceryl dibehenate, glyceryl tristearate and PAP-adsorbed SLN were obtained using a Fourier transform infrared spectrometer (IRAffinity-1, Shimadzu, Kyoto, Japan). Samples equivalent to 2 mg were mixed with KBr (about 30 mg) and

ground into a fine powder using an agate mortar, before compressing into the KBr disk under a press at 10,000 psi. Baseline was corrected and the samples were scanned against a blank KBr pellet background at a wave number ranging from 4000 to 400 cm^{-1} with a resolution of 2.0 cm^{-1}, with 30 scans. The characteristic peaks were recorded.

4.3.6. Thermal analysis

4.3.6.1. Differential scanning calorimetry

Measurements were performed on a calorimeter DSC Q200 (TA Instruments, DE, USA). The SLN dispersions (both blank and PAP-adsorbed nanoparticles) and bulk materials (glyceryl dibehenate, glyceryl tristearate, Tween® 80 and PAP) were accurately weighted into aluminium pans (ca. 2 mg), which were hermetically sealed and measured against an empty reference pan. The pan was heated and the thermograms were recorded at temperature range from -20°C to 240°C, at a heating rate of 10°C/min. The heat flow was measured.

4.3.6.2. Dynamic light scattering

The influence of temperature on the physical stability of PAP-SLN suspensions was assessed using-DLS (Zetasizer Nano S; Malvern Instruments, UK) as previously reported in Chapter 2, section 2.3.3.5.. A PAP solution in PBS was kept at 37°C for 2 h and analyzed by DLS as a control of PAP stability during the adsorption process. For each sample, measurements were carried out in triplicate.

4.3.7. Spray-drying process of SLN

The PAP-SLN formulations were incubated with aqueous spray-drying excipients solutions containing 20 and 22% w/v of mannitol and 15 and 17% w/v of trehalose for SLN based on glyceryl dibehenate and glyceryl tristearate respectively, selected according to previous studies, and using the same SLN:excipient mass ratio (1:3). The suspensions were spray-dried (Büchi® Mini spray-dryer, B-290, Switzerland) to produce dry powders in the same conditions that detailed in Chapter 3, section 3.3.4..

The spray-drying PY was calculated by gravimetry, comparing the initial amount of total solids with the amount of resultant powder after spray-drying, through the following equation:

$$\text{PY}\ (\%) = \frac{\text{Weight of the resultant powder after spray-drying}}{\text{Weight of solids totals}} \times 100 \qquad \text{(Eq. 4.3)}$$

4.3.8. Microsphere size, shape and moisture content

Particle morphology and residual moisture content of the spray-dried powders were evaluated using SEM and an electronic moisture balance respectively, as previously described in Chapter 3, section 3.3.5..

4.3.9. Isothermal titration calorimetry

Binding studies were performed using a VP-ITC titration microcalorimeter from MicroCal Inc., (Northampton, MA) with a cell volume of 1.436 mL at 25°C. Samples were degassed in a ThermoVac system (MicroCal) prior to use. The sample cell was filled with the sugar solution containing either mannitol (1160 or 1280 mM when injecting glyceryl dibehenate and glyceryl tristearate SLN, respectively) or trehalose (397 or 450 mM) and the reference cell with buffer solution only. The PAP-SLN solution (64.7 and 31.4 mM for glyceryl dibehenate and glyceryl tristearate, respectively) was introduced into the thermostated cell by means of a syringe and stirred at 286 rpm, which ensured rapid mixing but did not cause foaming on solutions. The following procedure was fully described in Chapter 3, section 3.3.8..

4.3.10. X-ray photoelectron spectroscopy (XPS)

The surfaces of microencapsulated glyceryl dibehenate nanoparticles in mannitol and trehalose, and blank microspheres were analyzed by XPS. Raw material glyceryl dibehenate was also analyzed as a control. XPS analysis was performed using a Thermo Scientific K-Alpha ESCA instrument (VG Escalab 250 iXL ESCA, VG Scientific, UK), equipped with aluminium Ka monochromatized radiation at 1486.6 eV X-ray source. The X-ray monochromatic spots were 400 μm in diameter and the correspondingly sampling area was 0.35 mm^2. Due to the non-conductor nature of samples, it was necessary to use

an electron flood gun to minimize surface charging. Neutralization of the surface charge was performed using both a low energy flood gun (electrons in the range 0 to 14 eV) and a low energy argon ions gun. The XPS measurements were carried out using monochromatic Al-K radiation ($\lambda\nu$ = 1486.6 eV). Photoelectrons were collected from a take-off angle of 90° relative to the sample surface. The measurement was carried out in a Constant Analyzer Energy mode with a 100 eV pass energy for survey spectra and 20 eV pass energy for high resolution spectra. Charge referencing was achieved by setting the lower binding energy C1s photopeak at 285.0 eV C1s hydrocarbon peak. Residual vacuum in the analysis chamber was maintained at around $6x10^{-9}$ mbar. Surface elemental composition was determined using the standard scofield photoemission cross sections.

4.3.11. Powder flow properties

The real ρ of the dry powders was measured using a helium pycnometer (AccuPyc 1330, Micrometrics Ltd, Dunstable, UK) at room temperature (*n*=3). The apparent ρ was determined before and after settling the samples (1250 taps) using a stampf volumeter (Stav 2003, JEF Germany). The d_{aer}, Carr's index and Hausner ratio of spray-dried particles were also calculated based on the equations 3.4, 3.5 and 3.6 respectively, depicted in Chapter 3, section 3.3.7..

4.3.12. Aerodynamic assessment of fine particles

The aerodynamic characteristics of inhaled complexes were assessed through a TSLI (TSI, Copley Instruments, UK), corresponding to the Ph. Eur. (2.9.18. Preparations for inhalation: aerodynamic assessment of fine particles, Apparatus A - glass impinger), according to the procedure reported in Chapter 3, section 3.3.9.. After that, the TSLI was disassembled and all the compartments were carefully washed with 10 mM PBS pH 7.4 and separately collected to conical flasks up to final volume of 50 mL. Samples were filtered and PAP content in each compartment was determined by the MicroBCA protein assay (Pierce, USA) measuring the absorbances by spectrophotometry in a microplate reader (FLUOstar Omega, BMG Labtech, Germany) at 562 nm (*n*=6).

4.3.13. SLN recovery from microspheres

Since the excipients used for microsphere preparation are freely soluble in aqueous media, it is possible to recover the microencapsulated SLN, mimicking what happens when the dry powders reach the deep lung. For that purpose, the spray-dried powders were incubated in 10 mM PBS pH 7.4 with 0.1% of lung surfactant (Curosurf®) under mild magnetic stirring at 37°C for 90 min. After that time, the physicochemical properties and morphology of the recovered SLN were analyzed by PCS and TEM as above described.

4.3.14. *In vitro* release studies

Release was determined by incubating the nanoparticles (≈0.3 mg SLN/mL) or the dry powders (≈2 mg microspheres/mL) in 1 mL of isotonic PBS, as reported elsewhere [7], with horizontal shaking (300 rpm), at 37°C. At pre-established periods of time, aliquots of 500 µL of the supernatant were taken out and replaced with equal volume of fresh medium to maintain the volume constant during the release study. The amount of released protein was evaluated in the supernatants by the MicroBCA protein assay (Pierce, USA) measuring the absorbances by spectrophotometry in a microplate reader (FLUOstar Omega, BMG Labtech, Germany) at 562 nm (n=3).

4.3.15. Assessment of PAP integrity

Structural integrity of PAP throughout the adsorption process and after release from SLN and dry powders was assessed by SDS-PAGE [12]. In brief, suitable volumes of samples, in order to obtain a PAP quantity of 7.5 µg per sample, were denatured for 5 min in sample buffer (NuPAGE® Technical Guide, Life Technologies, USA). Afterwards, samples were loaded into each well and analyzed by SDS-PAGE on a NuPAGE® Novex 12% Bis-Tris Gel (Life Technologies, USA) on NuPAGE® MES SDS Running Buffer for ≈1 h at 135 mA. Proteins were visualized by Coomassie blue staining (SimplyBlue™ SafeStain solution, Life Technologies, USA).

4.3.16. Proteinase assays with fluorogenic peptide substrates

Assays were carried out in 200 μL assay buffer (10 mM PBS, pH 7.4, 5 mM DTT) containing 20 μL of PAP activated in assay buffer at 5 μg/mL [13]. Reactions were initiated by the addition of 50 μM fluorogenic substrate (Z-Leu-Leu-Arg-AMC, from Bachem, Germany) and activity was monitored (excitation 355 nm; emission 460 nm) for 30 min, at 37°C on a Fluorescence Microplate Reader (FLUOstar Omega, BMGLabtech, Germany). For all assays, saturated substrate concentration was used, throughout, in order to obtain linear fluorescence curves. The assays were performed in triplicate.

4.4. Results and Discussion

4.4.1. PAP-SLN characterization

Therapeutic protein formulation is highly dependent on protein stability. Preventing degradation, denaturation and aggregation is critical to ensure the maintenance of physicochemical and biological properties of protein drugs [1]. Loading nanoparticulate carriers with proteins using adsorption has become an important formulation tool in the biomedical field. It is also an alternative to common encapsulation procedures, avoiding harsh formulation conditions, such as the use of organic solvents, high shear agitation, or high-pressure homogenization [1]. In the present work, the model protein drug (PAP) was adsorbed onto SLN to avoid its possible degradation caused by the high temperatures involved in the glyceryl dibehenate and glyceryl tristearate SLN formulation, which occurs at ±80°C for the lipid melting. PAP contains 345 amino acid residues, and consists of a signal sequence (1-18), a propeptide (19-133) and a mature peptide (134-345). It is a cysteine protease with strong biological activity, which is isolated from the latex of the *Carica papaya* fruit. The enzyme has a large spectrum of action, being involved in the degradation of myofibrillar proteins and collagen [9].

As a first formulation step, the stability of PAP in solution was studied by DLS for 2 h at 37°C to mimic the adsorption process. These results predict that PAP is stable in PBS at 37°C, since its initial mean size (3.7±0.2 nm) did not change during the 2 h period (4.1±0.5 nm after 2 h).

The adsorption of increasing amounts of PAP onto SLN led to an increase of mean particle diameter in both formulations but the PI remained within the optimal range for

SLN, suggesting the nanoparticle populations remained fairly homogeneous (Figure 4.1A and B). For the SLN prepared with glyceryl tristearate, there was an abrupt size increase at higher PAP concentrations, which may indicate the formation of aggregates favored by protein binding between different particles. TEM analysis confirmed the sizes established from the PCS analysis and showed fairly round particles with a dynamic layer of proteins adsorbed into nanoparticles surface (inset of Figure 4.1A and B).

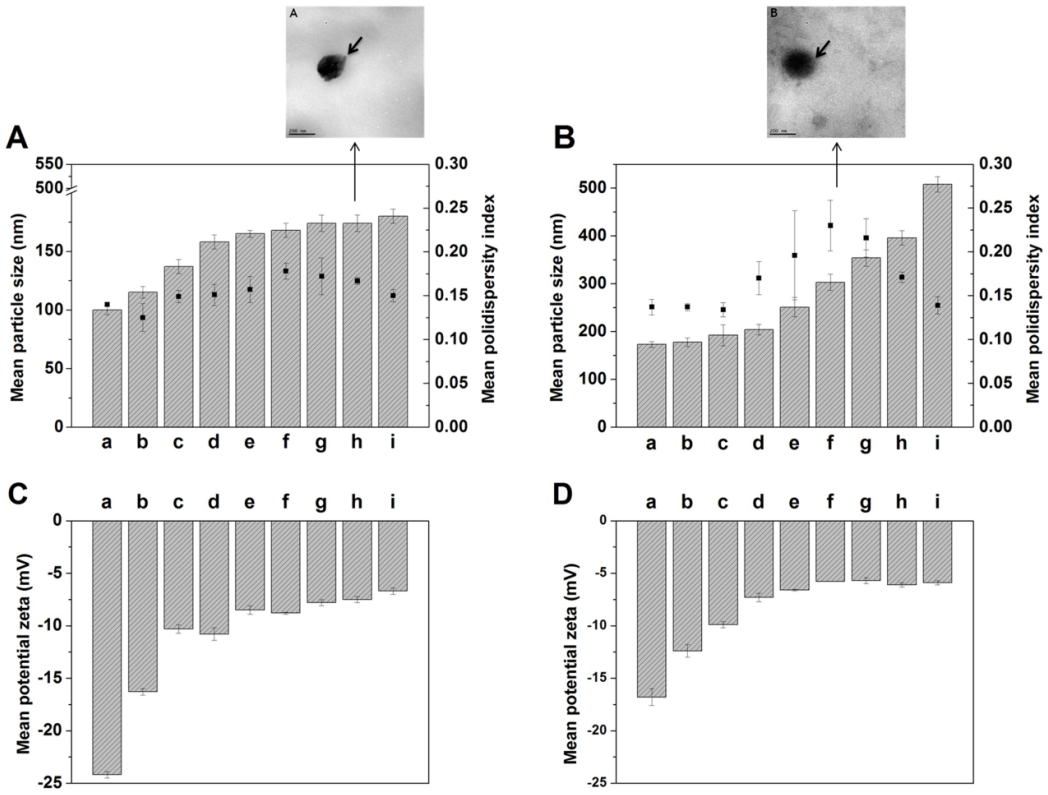

Figure 4.1: Mean size and PI of glyceryl dibehenate (A) and glyceryl tristearate (B) SLN containing different concentrations of PAP adsorbed onto the SLN surface. The bars represent the mean size and the symbols (■) correspond to the PI. Charge of glyceryl dibehenate (C) and glyceryl tristearate (D) SLN containing different concentrations of PAP adsorbed onto the surface. (a) blank SLN; SLN incubated with (b) 0.197 mg/mL; (c) 0.361 mg/mL; (d) 0.619 mg/mL; (e) 0.722 mg/mL; (f) 0.812 mg/mL; (g) 0.963 mg/mL; (h) 1.026 mg/mL and (i) 1.083 mg/mL of PAP (SLN weight≈30 mg) (mean±SD, *n*=3). TEM micrographs of PAP-SLN prepared using: (A) glyceryl dibehenate and (B) glyceryl tristearate. The arrows correspond to the layer of proteins around SLN (scale bar: 200 µm).

Not surprisingly, PAP adsorption onto SLN resulted in a decrease of zeta potential when compared to the respective blank controls (Figure 4.1C and D). Protein adsorption at interfaces is generally considered as being through hydrophobic interactions and hydrogen bonds between the molecules of the adsorbate and the adsorbent [2]. In this study, some electrostatic interactions may not be precluded since the isoelectric point of PAP is 8.8 so, at physiological pH value, it is positively charged while the SLN have a negative surface charge (-24.2±0.3 mV for blank glyceryl dibehenate SLN and -16.8±0.8 mV for blank glyceryl tristearate SLN). When all the SLN surface is covered with protein molecules, the potential zeta stabilizes around -6.7±0.3 mV for glyceryl dibehenate SLN (Figure 4.1C) and -5.9±0.2 mV for glyceryl tristearate SLN (Figure 4.1D), confirming the previous findings [11], where similar findings were obtained with other nanoparticulate systems and proteins.

4.4.2. Characterization of the adsorption process

As adsorption from solution depends on solute concentration, the final composition of the formulation will also depend on the concentration of protein added to the nanoparticles (Table 4.1). Results from PAP adsorption onto SLN show adsorbed amounts were up to 51% (w/w) and 41% (w/w) of the initial amount, for glyceryl dibehenate SLN and glyceryl tristearate SLN, respectively, corresponding to maximum adsorption efficiencies of 3.69±0.39% and 2.94±0.08% (w/w). So, PAP seems to have a high affinity for both triacylglycerols.

Table 4.1: Adsorption efficiency of PAP onto SLN.

PAP (mg/mL)	Amount adsorbed (% w/w) in final spheres composition	
	Glyceryl dibehenate SLN	Glyceryl tristearate SLN
0.197	0.10±0.03	0.21±0.04
0.361	0.39±0.08	0.34±0.08
0.619	1.42±0.11	0.98±0.11
0.722	1.61±0.22	1.35±0.04
0.812	2.17±0.17	1.70±0.18
0.963	2.90±0.24	2.45±0.10
1.026	2.94±0.45	2.48±0.11
1.083	3.69±0.39	2.94±0.08

The protein effectively adsorbed from solution onto particle surface can be described by several models, including those of Langmuir and Freundlich, providing information on how molecules bind to the surface. The PAP adsorption followed the empirical Freundlich type of isotherm for both SLN compositions ($r^2 \geq 0.982$), over the concentration range studied (Table 4.2), corroborating our previous results whereby a complex protein mixtures was adsorbed onto nanoparticles [11]. In such cases adsorption results from the competition of many different protein molecules to the particles' surface. In addition, the interactions protein–protein, which are likely to occur with complex protein mixtures, are not considered by the Langmuir monolayer theory. In fact, the enzyme used in the present study is not a pure protein (supplier's specifications). In addition, the SLN size increased with the increase of PAP amounts in both formulations (Figure 4.1A, B), as well as the gradual increase of adsorption efficiency (Table 4.1), also supports this theory of multilayer PAP adsorption. Apparently the adsorption occurs as a result of three phenomena: (i) protein-lipid interaction, i.e., adsorption of protein onto the lipid surface; (ii) protein-protein interaction on the lipid surface, in which adsorption of protein onto lipid was followed by adsorption onto previously adsorbed protein layer, this resulted in formation of multilayer, and (iii) adsorption onto lipid at high protein concentrations wherein self-association of PAP molecules (protein-protein interaction) preceded adsorption onto the lipid resulting in multilayer formation [14]. Further studies were performed using PAP-adsorbed SLN obtained at PAP concentrations of 1.026 mg/mL for glyceryl dibehenate and 0.812 mg/mL for glyceryl tristearate. These concentrations were chosen taking into account the amount of protein adsorbed and nanoparticle size. Since the adsorption process follows the equation of Freundlich, the isotherms do not reach a clear plateau and the mathematical model does not predict a limiting value for adsorption. So these concentrations make a balance between the amount of PAP adsorbed and the other physicochemical properties resulted from the interaction, such as size, PI and surface charge.

Table 4.2: Langmuir and Freundlich parameters for PAP adsorption onto SLN.

	Langmuir isotherm			Freundlich isotherm		
	r^2	K_L	Q_m	r^2	K_F	n
Glyceryl dibehenate SLN	0.871	2.87×10^{-4}	14.49	0.985	4.78×10^{-5}	0.52
Glyceryl tristearate SLN	0.917	1.07×10^{-3}	8.08	0.982	10.03×10^{-5}	0.56

r^2: correlation coefficient; K_L: Langmuir constant related to the adsorption capacity; Q_m: maximum adsorption capacity; K_F: Freundlich constant and n: is the slope of the straight line.

4.4.3. Fourier transform infrared spectroscopy analysis

The Fourier transform infrared spectra of raw materials (glyceryl dibehenate, glyceryl tristearate and PAP) and optimized blank and PAP-adsorbed glyceryl dibehenate and glyceryl tristearate SLN are shown in Figure 4.2. Both lipids showed peaks corresponding to C=O stretching (1635 cm^{-1}) and aliphatic C–H stretching (near of 2800 cm^{-1}). The reduction (in case of glyceryl dibehenate SLN) or disappearance (regarding glyceryl tristearate SLN) of these lipids absorption bands on SLN spectra could be attributed to the smaller amounts of lipid used. PAP also showed a predominant band, as a hump, at 3750-2350 cm^{-1}. In literature it is described that raw PAP must have a peak at 3300 cm^{-1} due to the N–H stretch of a secondary N–substituted amide, p-substituted aromatic out of plane C–H deformation of an aromatic residue of tryptophan or tyrosine at 868 cm^{-1} and 850 cm^{-1}, with C=O stretch of a carboxylate anion and an amide group at 1654.2 cm^{-1} and strong peaks between 1150–1050 cm^{-1} and 705-570 cm^{-1} due to C–S stretch of sulfides and disulfides. However, this peak was not observed, probably due to residual moisture content in the sample. The spectra of the PAP-adsorbed nanoparticles showed slight peaks at 3380 cm^{-1} for the substituted secondary amide, 875 cm^{-1} due to the substituted aromatic ring, and 1145 cm^{-1} and 600 cm^{-1} due to C–S stretch of sulfides and disulfides, confirming the adsorption of the enzyme. However, further physical characterization of the surface of PAP-adsorbed nanoparticles is still needed to confirm these observations.

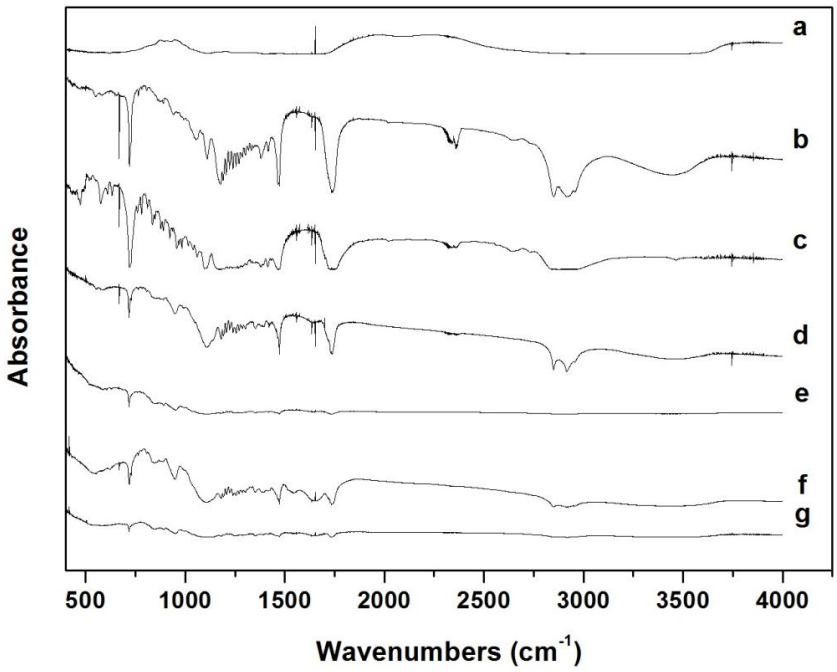

Figure 4.2: The FTIR spectra of: (a) PAP powder; (b) glyceryl dibehenate; (c) glyceryl tristearate; (d) optimized formulations of blank glyceryl dibehenate and (e) glyceryl tristearate SLN and optimized formulations of PAP adsorbed on (f) glyceryl dibehenate and (g) glyceryl tristearate SLN.

4.4.4. Differential scanning calorimetry

The DSC thermograms of PAP, glyceryl dibehenate, glyceryl tristearate, Tween® 80 and blank and PAP-adsorbed SLN of glyceryl dibehenate and glyceryl tristearate are shown in Figure 4.3. The thermograms obtained with the three excipients (glyceryl dibehenate, glyceryl tristearate and Tween® 80) matched their normal thermal behavior as previously described in Chapter 2, section 2.4.4., particularly the broad endotherm peak at 74°C and 60°C for the triacylglycerols, glyceryl dibehenate and glyceryl tristearate respectively (Figure 4.3a, b and c). The native protein showed two endothermic peaks, at 90.49°C and 198.97°C (Figure 4.3d). It has been reported that the DSC profile of PAP is characterized by a peak at ≈83°C and another peak at ≈89°C, corresponding to unfolding of two domains [15]. Although some differences can be due to the presence of impurities (as shown by SDS-PAGE analysis), only the second endothermic could be detected, while the peak at 198.97°C is probably due to thermal protein degradation. The DSC thermograms of PAP-adsorbed SLN were similar to those of the respective lipids, but the

melting peaks were shifted to lower temperatures due to the presence of PAP. No thermal events similar to those of pure PAP were detected, suggesting the adsorbed enzyme is in an amorphous state.

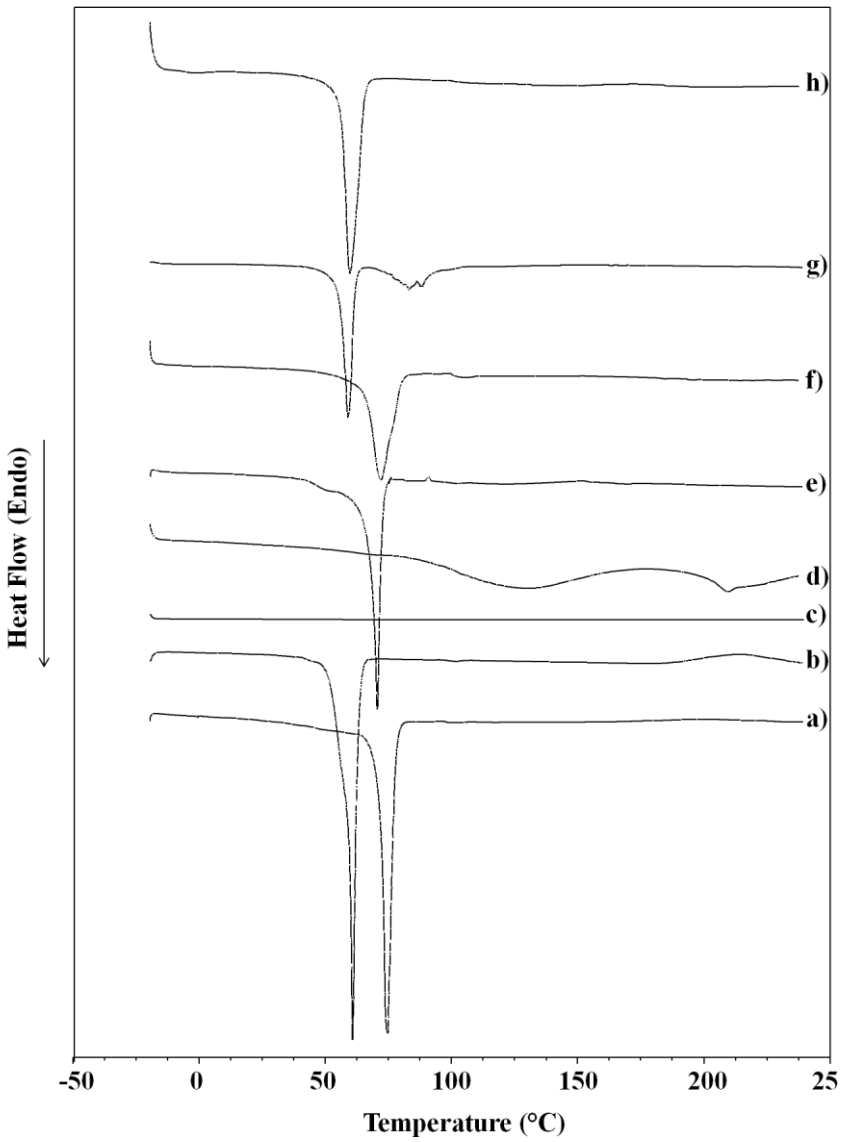

Figure 4.3: DSC thermograms of: (a) glyceryl dibehenate; (b) glyceryl tristearate; (c) Tween® 80; (d) PAP; (e) blank glyceryl dibehenate SLN; (f) PAP-glyceryl dibehenate SLN; (g) blank glyceryl tristearate SLN and (h) PAP-glyceryl tristearate SLN.

4.4.5. Dynamic light scattering

The effect of temperature on particle size of PAP-SLN was assessed throughout a heating ramp from 25°C up to 90°C and then a cooling ramp to the initial temperature (Figure 4.4). This study allowed studying the physicochemical properties when SLN suspensions were subjected to severe temperature variations, being useful whenever a formulation is intended for further temperature processing. Firstly, a 0.06 mg/mL PAP solution was subjected a heating ramp from 25°C up to 90°C and then a cooling ramp to 25°C. The respective data are depicted in Figure 4.4A showing protein aggregation above 80°C, which was not reversed upon cooling. The heating process induced particle size changes in the SLN prepared with both solid lipids, although the particle size variations were always within the nanosize range. In the case of glyceryl dibehenate SLN, a gradual particle size increase was observed after ≈70°C reaching 556 nm, demonstrating the formation of protein aggregates (Figure 4.4B). The PAP aggregation masked the glyceryl dibehenate m.p. (70°C). Moreover, the initial particle size was not fully recovered after the cooling phase, in line with previous studies conducted with SLN of similar composition in Chapter 2, section 2.4.3.. On the other hand, glyceryl tristearate SLN suffered a slight decrease in particle size during heating, at a temperature close to the lipid's m.p.. However, after 80°C, there was a slight increase, suggesting some instability above this temperature, which can be due to protein aggregation as happened with glyceryl dibehenate SLN (Figure 4.4C). During the cooling step, particle size stabilizes reaching the initial particle size (291 nm), indicating a protein stabilizing effect of both SLN formulations.

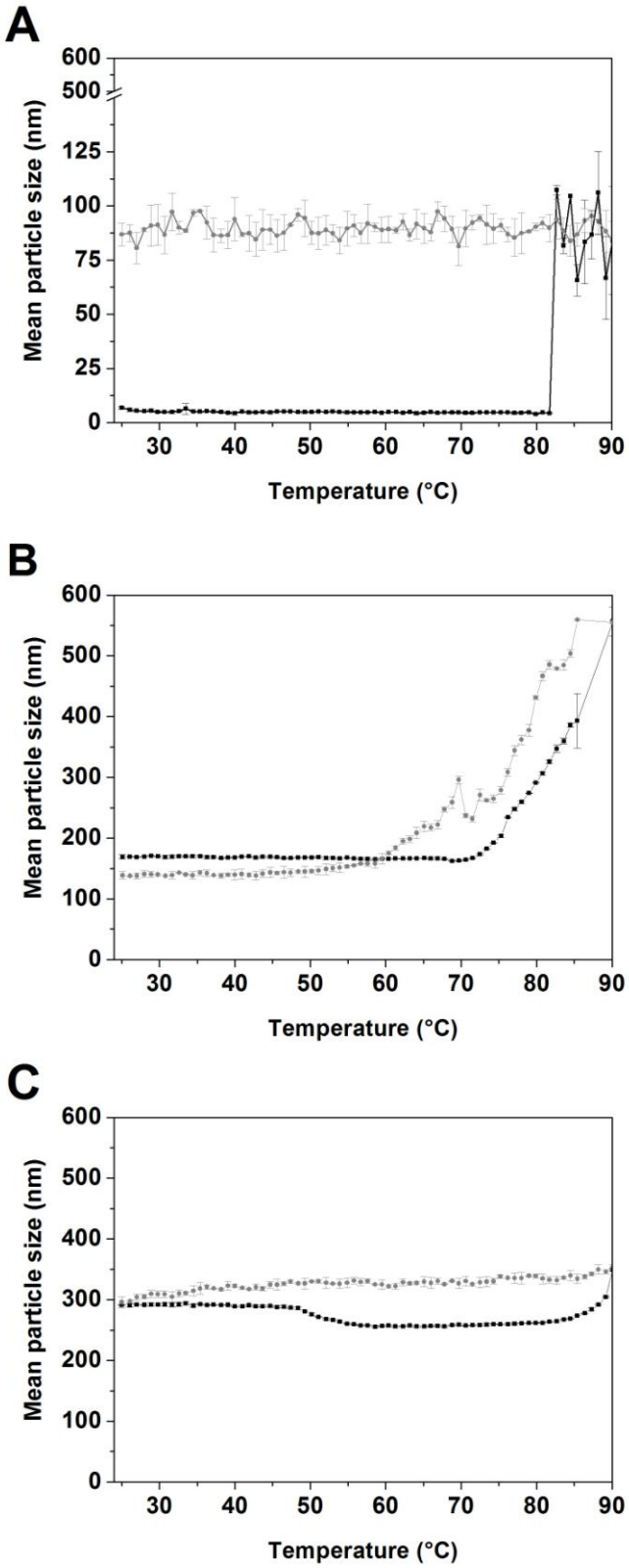

Figure 4.4: DLS thermograms of (A) PAP, (B) glyceryl dibehenate and (C) glyceryl tristearate SLN with PAP adsorbed: (■) from 25°C to 90°C and (●) from 90°C to 25°C (mean±SD, *n*=3).

4.4.6. SLN microencapsulation by spray-drying

The delivery of nanoparticles to the lung is difficult, if not impractical, due to their reduced size and low inertia [7]. To overcome these limitations, PAP-SLN were encapsulated within microspheres made of mannitol or trehalose, as an attempt to improve aerosolization, by conferring adequate aerodynamic properties for suitable particle deposition and drug delivery in the lung. In addition, it was expected these excipients would have a general stabilizing effect on PAP-SLN formulations. Mannitol and trehalose are FDA and EMA approved excipients for pulmonary delivery used in osmotic adjustment in injectable preparations, as well as bulking agents in freeze-drying and various dry powder formulations contributing to the enhanced aerosolization performance [16]. In addition, as polyols they also play an important role on the stabilization of relevant therapeutic proteins throughout pharmaceutical processing [17], including spray-drying [7, 18].

Spray-drying is an evaporation technique where the aqueous solvent is removed very quickly due to heat energy provided in the spray-drier. Both SLN formulations were spray-dried with the two excipients in a one-step spray-drying process with acceptable yields around 45-55% (w/w). The enzyme PAP was associated to the SLN before spray-drying and it was expected that PAP bioactivity would be retained at the spray-drying conditions used in this experiment [18]. In a similar work, an antibody (IgG1) was co-spray-dried with mannitol as a stabilizer and a subsequent analysis of the protein secondary structure concluded that protein bioactivity was retained since the secondary structure was not significantly altered by the procedure [19]. The resulting nanostructured microparticles were observed using SEM evidencing spherical morphology with well-defined limits (Figure 4.5).

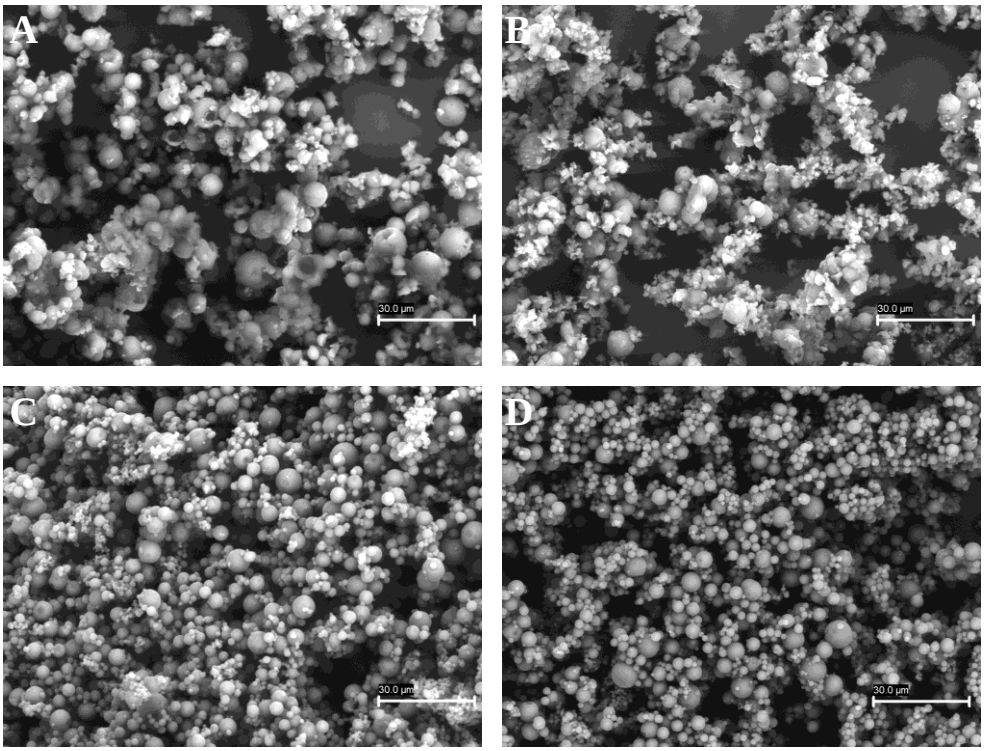

Figure 4.5: SEM micrographs of dry powders: mannitol microspheres containing (A) PAP-glyceryl dibehenate SLN and (B) PAP-glyceryl tristearate SLN; trehalose microspheres containing (C) PAP-glyceryl dibehenate SLN and (D) PAP-glyceryl tristearate SLN (scale bar: 30 µm).

Morphology is an important parameter when formulating powders for inhalation, essentially because particle shape and aggregation, which may interfere in the flow properties. However, the aerodynamic characteristics are the limiting parameters to succeed in pulmonary delivery. Generally, the d_{aer}, which is a combination of the particle size and density, influences the dispersion and sedimentation patterns, and should vary between 1 and 5, to allow an optimal alveolar deposition [20]. In this study, PAP-SLN-loaded mannitol and trehalose microspheres exhibited a real ρ between 1.43-1.81 g/cm^3, corresponding to an d_{aer} around 5-6 µm (Table 4.3), which confers suitable characteristics to achieve deep lung deposition.

As density influences flowability, the Hausner ratio and Carr's index were calculated as measures of the flow properties of the powders (Table 4.3). A Hausner ratio of < 1.25 indicates a free flowing powder, whereas > 1.25 indicates poor flow ability. On the other hand, the smaller the Carr's Index the better the flow properties. The Carr's index and the

Hausner ratio of all dry powders were greater than 23% and 1.25, respectively, suggesting the developed powders possessed extremely poor flow property according to Ph. Eur. (2.9.36. Powder Flow), but further data revealed that the microspheres were able to aerosolize suitably. Despite being extensively used to predict the quality of powders regarding flowability and deposition, precaution must be taken when analyzing the Carr's index and the Hausner ratio, since for some powders a direct correlation between these parameters and higher fine particle fraction was not observed [21]. Furthermore, it has been reported that microspheres prepared by spray- and freeze-drying have poor or very poor flowability, probably due to some residual moisture content and, as verified in the present study.

Table 4.3: Physical and aerodynamic properties of: (A) PAP-glyceryl dibehenate SLN and (B) PAP-glyceryl tristearate SLN microencapsulated in mannitol; (C) PAP-glyceryl dibehenate SLN and (D) PAP-glyceryl tristearate SLN microencapsulated in trehalose (mean±SD, *n*=3).

Dry Powders	Process yield (%)	Feret's diameter (μm, *n*=300)	Real density (g/cm^3)	Apparent density (g/cm^3)	Aerodynamic diameter (μm)	Carr's index (%)	Hausner ratio	Moisture residual content (%)
A	50.7±5.1	5.34±0.94	1.47±0.00	0.59±0.01	6.47±1.14	42.0±2.0	1.7±0.1	0.58±0.03
B	54.3±5.9	5.46±1.16	1.64±0.00	0.57±0.05	6.99±1.48	41.3±3.8	1.7±0.1	0.42±0.03
C	47.1±4.6	4.45±1.57	1.81±0.00	0.44±0.03	5.99±2.11	29.3±7.6	1.4±0.2	1.78±0.02
D	46.7±0.9	4.40±1.23	1.43±0.00	0.40±0.02	5.27±1.47	36.0±5.0	1.6±0.1	1.74±0.01

4.4.7. Analysis of excipients and PAP-SLN binding affinity and their influence in microspheres formation by ITC

The spray-drying of PAP-SLN with the two excipients led to the formation of nanostructured microspheres. Hence, ITC assays were performed with PAP-SLN and mannitol and trehalose to get further knowledge about the microspheres structure and the nature of the interactions established between PAP-SLN and both excipients during the spray-drying process. This is an extremely sensitive technique that probes the thermodynamics of PAP-SLN-spray-drying excipients (mannitol and trehalose) interactions, which are quantitatively measured as a change in the system energy. Figure 4.6 shows the heat of injection normalized by the PAP-SLN amount added per injection, ΔH_i^i, as a function of the PAP-SLN to excipients molar ratio after subtraction of the heat

evolved after the titration of PAP-SLN suspension into water. The thermodynamic parameters (enthalpies, entropies, binding constants and stoichiometries) obtained from the fitting are shown in Table 4.4. For all combinations of PAP-SLN and excipients, deviations from SLN titration curve into water denote that the interaction between the excipient and SLN occurs even at the lowest concentration tested.

Titrations of PAP-glyceryl dibehenate SLN into mannitol solution led to a biphasic profile (Figure 4.6A). Firstly, there was a progressive exothermic decrease in ΔH_i^i at low PAP-SLN/mannitol molar ratios until reaches an exothermic minimum (≈ 0.002). In a second stage, further addition of PAP-SLN drew a progressively increase in the heat absorbed leading to less negative ΔH_i^i values. The exothermic decrease and subsequent minimum at low PAP-SLN/mannitol molar ratios can be related to the establishment of strong dipole-dipole interactions between water molecules that were oriented favourable on adjacent PAP-SLN, as also suggested for polymer-protein [22], and hydrogen bonding formation between hydroxyl groups of fatty acids and protein molecules with those of mannitol. Moreover, a potential exothermic contribution stemming from some PAP release from the surface of PAP-SLN cannot be excluded. In fact, exothermic heats are diminished upon titration PAP-SLN onto a mannitol with PAP solution mixture (data not shown), with the shape profile largely maintained. Additional titrations (>0.002) of PAP-glyceryl dibehenate SLN onto mannitol led to a progressive increase of ΔH_i^i (less exothermic) thanks to an enhancement of mannitol and PAP-SLN dehydration to support the excipient binding to all PAP-SLN, favoring mutual interactions. Nevertheless, the potential contributions of hydrophobic interactions between mannitol molecules and/or with PAP/SLN, charge shielding effects and/or excipient's molecular rearrangements upon excipient adsorption onto SLN surfaces could not be neglected.

On the other hand, titrations of PAP-adsorbed glyceryl dibehenate SLN onto trehalose (Figure 4.6B) led to a similar profile as PAP-SLN/mannitol titrations except for the absence of the initial exothermic decrease and subsequent minimum. Instead, an exothermic plateau is observed up to a PAP-SLN/trehalose molar ratio of ≈ 0.012. This exothermic plateau region might be originated from, on one hand, fewer or at least less energetic interactions between this saccharide and PAP-SLN than mannitol ones, as observed from Figure 4.6A. The non-reducing character of trehalose would hinder direct binding of aldehyde or ketone end groups to the lysine or arginine residues of the protein. On the other hand, the flexible nature of the disaccharide molecule would enable the

rotation of the monosaccharide moieties around the glycosidic oxygen, which would favor the formation of a stable hydration layer, providing a further stabilization of PAP onto the SLN surface and decreasing their potential release. After the plateau region, the potential contribution of hydrophobic interactions between the disaccharide rings and conformational rearrangements of trehalose molecules, in particular, to give small aggregates onto SLN surface might play an additional role and could contribute to the observed less exothermic ΔH_i^i values in the presence of PAP-adsorbed SLN. For both interactions of mannitol and trehalose with PAP-glyceryl dibehenate SLN, a final plateau region is not observed probably because this would take place at larger PAP-SLN/trehalose molar ratios exceeding those here analyzed, which reproduce the concentrations used in the spray-drying process.

The interaction between PAP-adsorbed glyceryl tristearate SLN and the two saccharides led to rather different titration profiles than those observed for PAP-glyceryl dibehenate ones. In particular, for both PAP-glyceryl tristearate SLN titrated onto mannitol (Figure 4.6C) and trehalose (Figure 4.6D), positive ΔH_i^i values are observed in the whole concentration range analyzed. In particular, at very low PAP-SLN/saccharide molar ratios (0.00034 and 0.0012 for mannitol and trehalose, respectively), an abrupt decrease in the endothermic ΔH_i^i values is observed, which is followed by a more sustained one. In fact, for trehalose a quasi-plateau region can be envisaged at high PAP-glyceryl tristearate SLN/saccharide molar ratios. These endothermic values suggest that the interaction between PAP-glyceryl tristearate SLN and saccharides are entropically driven denoting the rupture of water solvation upon complex formation, which became progressively less important as more PAP-adsorbed SLN are present in the concentrated saccharide solution thanks to the establishment of extensive hydrogen bonding with the latter molecules being predominant. This is specially observed for the PAP-adsorbed glyceryl tristearate SLN/mannitol system, from which an additional contribution through some hydrophobic interactions between mannitol, with long hydrocarbon radicals in their molecular structure and PAP-glyceryl tristearate SLN may be present. On the other hand, the lower (less endothermic) ΔH_i^i values for trehalose might arise from the certain stabilization of PAP on the SLN surfaces impeding their release, and hence contributing less to the overall thermodynamic process, as mentioned previously.

The experimental data were fitted to a three-independent sites binding model, except for the PAP-glyceryl dibehenate SLN/trehalose system, which was fitted to a two-biding site

model. Binding of PAP-glyceryl dibehenate SLN with both excipients involved binding constants of up to ca. 10^8 M^{-1}, one order of magnitude larger than those observed for glyceryl tristearate ones. Protein release may be the reason which impedes the fitting of experimental data to a less complex model as in the case of pure SLN onto excipients which was modeled by a two-binding site model. Also the presence of the protein on the SLN surface modified the heat profiles (from endothermic to exothermic) for the PAP-adsorbed glyceryl tristearate SLN upon interaction with both excipients if compared to those SLN without surface-adsorbed protein. Moreover, the magnitude of binding constants and their variability are also larger than those of bare SLN.

Concerning the enthalpy of interaction, the relatively small exothermic values found for PAP-glyceryl dibehenate SLN agrees with the potential predominance of hydrogen bonding upon interaction with both excipients. In contrast, interactions of PAP-glyceryl tristearate SLN with excipients involve positive ΔH_i^i values indicating a predominance of the rupture of water solvation layer and dispersion forces upon interaction. Nevertheless, SLN-excipients complexation was proven to be enthalpic drive at most driven as observed from the relatively large and negative entropy changes (except for PAP-adsorbed glyceryl tristearate SLN first binding site interacting with mannitol), in agreement with strong hydrogen bonding, and probably, protein release to the solution. In fact, the present behavior is opposite to that observed for the titration of bare SLN onto the excipients, in which the complexation process was exclusively entropy-driven.

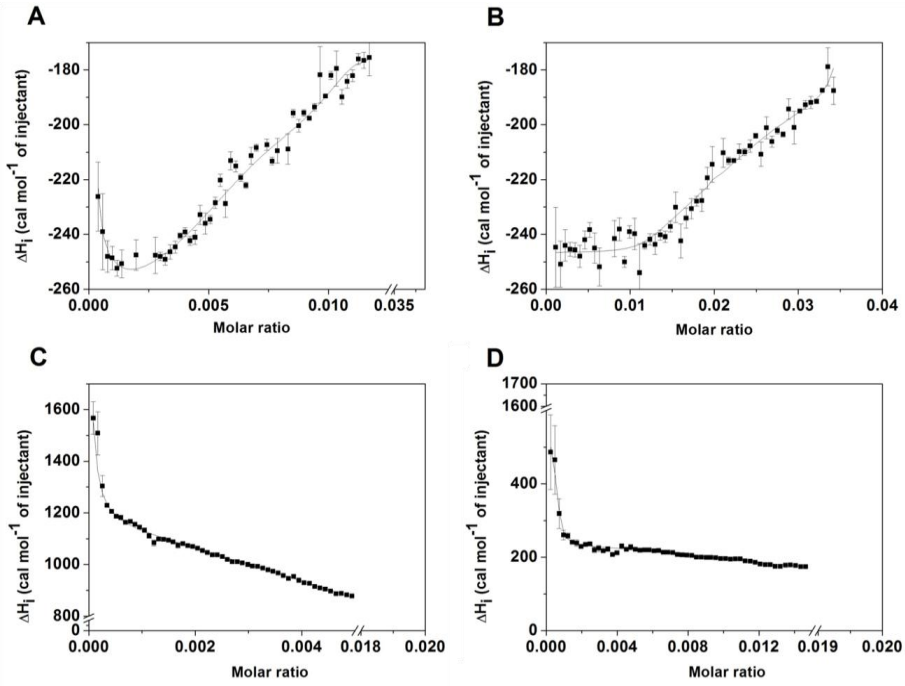

Figure 4.6: Isothermal titration calorimetry of PAP-adsorbed onto glyceryl dibehenate SLN into (A) mannitol and (B) trehalose; PAP-adsorbed onto glyceryl tristearate SLN into (C) mannitol and (D) trehalose. Each dot on the curve corresponds to the heat of reaction following 5 µL injection every 400 s at 25°C (cell volume = 1.436 mL).

Table 4.4: Enthalpy (ΔH_i^i), entropy (ΔS_i^i), binding constant (K^i) and stoichiometry (n^i) of the interaction of PAP-adsorbed onto glyceryl dibehenate and glyceryl tristearate SLN with spray-drying excipients, mannitol and trehalose, at 25°C (mean±SD, *n*=3).

Excipient	PAP-SLN	$10^{-2}\ \Delta H_i^i$ (cal/mol)	ΔS_i^i (cal/mol)	$10^{-5}\ K^i$ (M^{-1})	$10^2\ n^i$
Mannitol	Glyceryl dibehenate	-7.3±0.2	-168.0±37.0	8140.0±2865.0	1.8±0.5
		-1.5±318.0	-183.0±49.0	37419.0±1410.0	0.0±0.0
		-1.9±24.0	-89.0±22.0	0.5±0.1	0.0±0.0
	Glyceryl tristearate	1589.0±111.0	408.0±91.0	33.0±10.0	0.0±0.0
		-536.0±50.0	-245.0±66.0	0.0±0.0	12.1±0.1
		43.0±3.0	-57.0±23.0	0.1±0.0	97.1±0.1
Trehalose	Glyceryl dibehenate	-2.5±0.3	-158.0±45.0	1724.0±895.0	1.2±0.0
		-2.5±0.3	-134.0±61.0	96.0±5.0	2.4±0.0
	Glyceryl tristearate	5.6±0.2	-144.0±38.0	445.0±56.0	0.1±0.0
		1.4±0.6	-64.0±13.0	0.0±0.0	17.7±1.2
		2.5±0.4	-100.0±21.0	1.8±0.2	1.2±0.1

Values in each column from top to bottom correspond to the first, second and third class of binding sites (*i*=1, 2, 3). In the case of PAP-glyceryl dibehenate SLN microencapsulated in trehalose, we only have the first and second class of binding sites, because it generally used the lowest amount of fitting parameters.

4.4.8. Microspheres surface analysis using XPS

The application of XPS in the characterization of drug delivery systems arises from the ability of this technique to provide quantitative and qualitative information of surface composition. Upon exposure of the sample to a X-ray beam, the binding energies of characteristically emitted photoelectrons are measured, providing information on the elements from which they originate, as well as their chemical bonding. This is particularly relevant for the interpretation of drug location in the formulation, release and stability [6]. As the previous experiments, particularly ITC, allow anticipating a similar behavior during spray-drying of the SLN prepared with both lipids, only the microspheres containing glyceryl dibehenate SLN were analyzed by XPS. Table 4.5 displays the percentage of each chemical element present in the samples of controls (glyceryl dibehenate and PAP), nanoparticles and dry powders. The analysis of controls revealed the expected elements, such as carbon (C), oxigen (O), nitrogen (N) and sulfur (S).

Table 4.5: Surface elemental composition of mannitol and trehalose microspheres containing glyceryl dibehenate-SLN, as determined by XPS.

Samples	Element (atomic percentage, %)						
	C	O	N	S	Si	O/C Ratio	N/C Ratio
Glyceryl dibehenate	92.80	7.20	0	0	0	0.08	0
PAP	63.98	22.63	11.95	1.44	0	0.35	0.19
Mannitol	54.60	45.40	0	0	0	0.83	0
Trehalose	54.39	45.61	0	0	0	0.84	0
Blank SLN	91.26	8.37	0	0	0	0.10	0
PAP-SLN	89.66	9.35	0.99	0	0	0.10	0.11
Mannitol microspheres	59.10	39.69	0	0	1.10	0.67	0
Blank SLN microencapsulated in mannitol	68.12	31.88	0	0	0	0.47	0
PAP-SLN microencapsulated in mannitol	66.31	32.88	0.47	0.23	0.33	0.49	0
Trehalose microspheres	58.76	40.39	0	0	0.85	0.69	0
Blank SLN microencapsulated in trehalose	67.12	32.88	0	0	0	0.49	0
PAP-SLN microencapsulated in trehalose	70.59	28.66	0.76	0	0	0.41	0.01

Glyceryl dibehenate presents a high atomic percentage of C and a low O percentage. On the other hand, PAP is the only compound that contains N in a considerable amount (>11%) and S in its composition. Regarding the glyceryl dibehenate SLN, there was a variation when compared with the respective lipid raw material (control), with a slight

increase in the O percentage (from 7.20% to 8.37%), probably due to the presence of Tween® 80 as surfactant in formulation. In contrast, the N signal in the PAP-nanoparticles spectrum persisted after the sputter cycle with a relatively high value, suggesting that it is chemically bonded and could be ascribed to PAP adsorption at SLN surface. Concerning mannitol microspheres containing blank glyceryl dibehenate SLN, a modification in chemistry composition was noticed, with an increase in C percentage. An explanation for this feature is the presence of SLN at microspheres surface and the possibility of measurement of some photoelectrons from glyceryl dibehenate SLN. Our assumption of efficient nanoparticle microencapsulation can be further reinforced by the presence of N at the surface of microspheres loaded with PAP-SLN, which effectively indicated that there were PAP-SLN at the microspheres surface. It should be noticed that a signal for Si was identified in some spectra, which could be originated from the silicon wafer used as a sample support during the analysis.

These results were also confirmed by deconvolution analysis of the spectra in which the high resolution spectra of carbon (C1s) signals, showing an envelope, were curve fitted using the Gaussian distribution into a series of peaks corresponding to different functional groups. The reference peak at the lowest binding energy (285.0 eV) was assigned to carbon atoms linked to other carbon and hydrogen atoms. Table 4.6 summarizes the relative peak area of each carbon environment. The peak areas (%) and relative intensities of C–C (285 eV), C–O (286.4 eV) and C=O (288 eV) were nearly similar in mannitol and trehalose microspheres and microencapsulated nanoparticles. More importantly, the peak of O–C=O (289 eV), unique for glyceryl dibehenate, was detected in the spectra of SLN and SLN-trehalose microspheres but not in the SLN-mannitol microspheres, probably due to a phenomenon that occurred during spray-drying. The analysis of deconvoluted C1s high resolution spectra confirmed that SLN are entirely encapsulated in mannitol and trehalose microspheres.

Table 4.6: The relative peak area (%) of each carbon environment for blank and PAP-adsorbed glyceryl dibehenate SLN, mannitol and trehalose microspheres and microencapsulated SLN.

Samples	C–C/C–H 285 (eV)	C–O 286.4 (eV)	C=O 288 (eV)	O–C=O 289 (eV)
Glyceryl dibehenate	88.52	7.27	0	4.20
PAP	47.48	26.27	26.25	0
Mannitol	12.90	80.82	6.26	0
Trehalose	7.27	71.48	20.94	0
Blank SLN	78.94	17.46	0	3.60
PAP-SLN	74.09	17.29	0	3.67
Mannitol microspheres	26.66	67.98	5.36	0
Blank SLN microencapsulated in mannitol	41.38	53.51	5.11	0
PAP-SLN microencapsulated in mannitol	35.96	60.05	3.99	0
Trehalose microspheres	23.64	57.36	17.29	1.71
Blank SLN microencapsulated in trehalose	25.61	31.35	8.97	1.21
PAP-SLN microencapsulated in trehalose	45.74	41.31	11.53	1.42

4.4.9. *In vitro* deposition studies

The performance during aerosolization and drug deposition of each formulation were evaluated using the TSLI apparatus, with an aerodynamic particle cut off of 6.4 μm for the lower impingement chamber, which mimics the terminal lung units (i.e., the alveoli). Thus, the drug deposited in this chamber correlates to the amount of drug which will probably get deposited in the terminal lung units, whereas the drug deposited in the upper chamber represents the amount of drug deposited in the tracheo-bronchial tree and the oropharynx. A Rotahaler® device was chosen for these experiments due to its simple structure. Mass deposition of the spray-dried formulation in the inhaler and on each stage of the TSLI were measured and expressed as a percentage of the total PAP mass recovered. In general, the percentage of either component deposited on a specific TSLI stage or in the DPI device varied with respect to particle size of the sample. For all tested formulations >90% of the protein was delivered from the capsules. As illustrated (Figure 4.7), all formulations showed higher mouth deposition when compared to the other compartments, probably due to the fact of the higher Feret's diameter of microparticles calculated previously using SEM (Figure 4.5) and confirmed by d_{aer} measurement (Table 4.3). However, for all dry powders, a significantly higher percentage of PAP was

deposited in the lower chamber (lung compartment), which demonstrated PAP-SLN dry powders could be distributed in the deep lung.

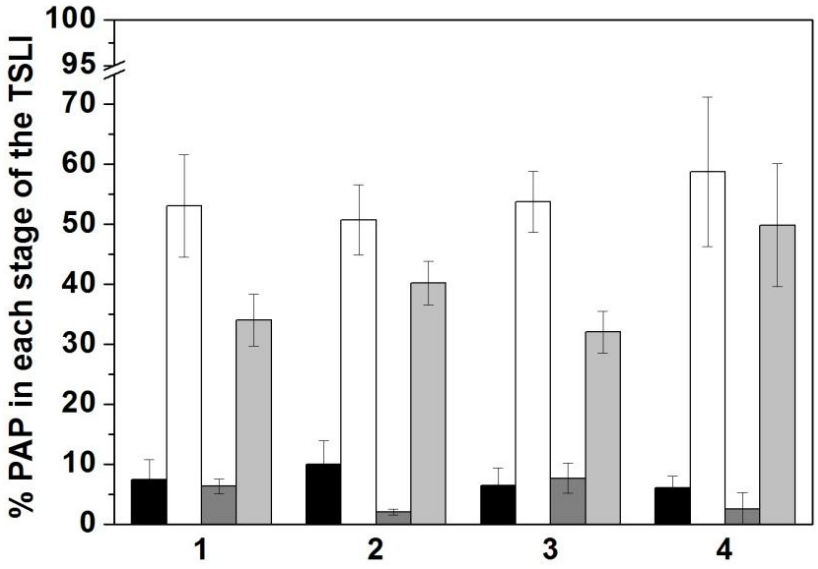

Figure 4.7: *In vitro* deposition of the spray-dried microsphere powders containing PAP-SLN. (1) Mannitol microspheres containing glyceryl dibehenate SLN; (2) mannitol microspheres containing glyceryl tristearate SLN; (3) trehalose microspheres containing glyceryl dibehenate SLN, and (4) trehalose microspheres containing glyceryl tristearate SLN. (■) device+capsules (D+C); (□) mouth+throat (M+T); (■) medium compartment (MC) and (■) lung compartment (mean±SD, *n*=6).

4.4.10. SLN recovery from microspheres

In order to maintain the advantages of the nanoparticulate formulation, the SLN should be recovered immediately after microsphere dissolution in an adequate medium, while preserving their original properties. The used excipients are expected to protect the SLN during spray-drying, not only from the heat during spray-drying process but also against nanoparticles aggregation. Thus, after SLN reconstitution, they should keep their innate physicochemical characteristics, such as mean particle size, PI and surface charge. In this context, recovery studies should also mimic the *in vivo* conditions that dry powders will meet when administered by the pulmonary route. For this purpose, the experiments were performed using 10 mM PBS pH 7.4 with 0.1% of lung surfactant. The SLN main

characteristics after recovery from dry powders were then compared with those determined before spray-drying (Table 4.7). The recovered particles had similar diameters and PI when compared to those obtained with freshly prepared ones. This fact confirmed the hypothesis that both mannitol and trehalose protect SLN from some harsh conditions involved in the microencapsulation process, preventing, for example, particle melting or aggregation. The stabilizing effect of the excipients was further proved by TEM analysis of SLN recovered from the dry powders, which showed no aspect or particle size changes (Figure 4.8). Nevertheless, zeta potential increased in both SLN formulations, particularly in the glyceryl tristearate nanoparticles, probably due to some PAP release during the assay.

Table 4.7: Mean SLN size (∅), polydispersity index (PI) and zeta potential (ZP) after recovery from dry powders (mean±SD, *n*=3).

Microspheres	SLN	Glyceryl dibehenate SLN			Glyceryl tristearate SLN		
		∅ (nm)	PI	ZP (mV)	∅ (nm)	PI	ZP (mV)
	Fresh	174±7	0.167±0.004	-7.5±0.3	508±16	0.230±0.029	-5.8±0.0
Mannitol	Recovered	163±6	0.209±0.027	-10.7±1.1	541±4	0.237±0.001	-19.3±0.4
	Mean Δ_1	0.9	1.3	1.4	1.1	1.0	3.3
Trehalose	Recovered	182±8	0.229±0.031	-12.8±1.2	478±7	0.319±0.085	-17.3±1.4
	Mean Δ_2	1.0	1.4	1.7	0.9	1.4	3.0

Δ_1: size or zeta potential of recovered nanoparticles from mannitol microspheres / size or zeta potential of fresh nanoparticles

Δ_2: size or zeta potential of recovered nanoparticles from trehalose microspheres / size or zeta potential of fresh nanoparticles

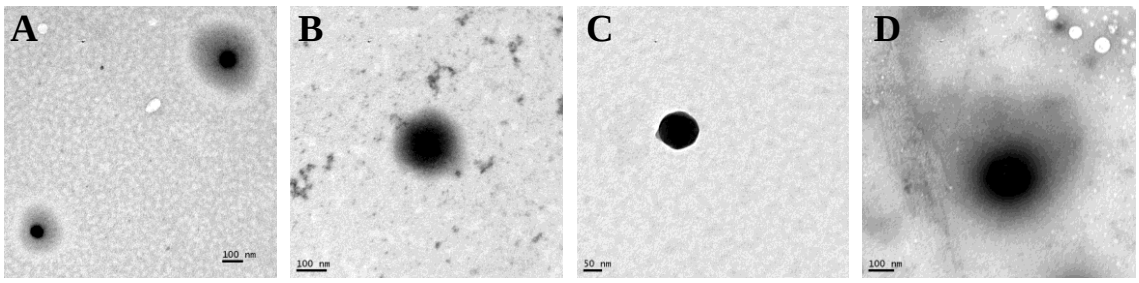

Figure 4.8: TEM micrographs of (A) glyceryl dibehenate SLN and (B) glyceryl tristearate SLN after recovery from mannitol microspheres; (C) glyceryl dibehenate SLN and (D) glyceryl tristearate SLN after recovery from trehalose microspheres.

4.4.11. *In vitro* release studies

The PAP *in vitro* release profiles from both SLN formulations (Figure 4.9) indicated a relatively slow and incomplete release, which could be explain by the interactions between the protein and the surface, because in some cases the presence of strong enough hydrophobic interactions and hydrogen bonds would result in some irreversible adsorption taking place. Furthermore, as protein molecules are attached to the adsorbent at several contact points, release would imply the simultaneous detachment of all these bonds, which is statistically improbable [2]. As mannitol and trehalose are freely soluble in aqueous media, the SLN are immediately delivered. Therefore, it was expected that the release profiles of PAP from dry powders were similar to those obtained from non-microencapsulated SLN, as reported elsewhere for insulin-loaded chitosan nanoparticles microencapsulated in mannitol [7]. However, it did not occur in the present study because PAP release from the several dry powders was higher when compared the release from non-microencapsulated SLN. These studies clearly showed that PAP could withstand spray-drying conditions, which are usually harsh for protein molecules, either by its association with the SLN, or by the protective effect of mannitol or trehalose [17, 23]. The increase in protein release may be due to a solubilising effect of the polyols (mannitol or trehalose) used as microencapsulation excipients. Interestingly, the protein was adsorbed onto the glyceryl dibehenate SLN's surface, it presented a higher release rate from trehalose microspheres than from mannitol microspheres. In turn, when the protein adsorbed onto the glyceryl tristearate SLN's surface, it presented a higher release rate from mannitol microspheres than from trehalose microspheres. This phenomenon is explained by the binding constants (K^i) determined during the ITC analyses (Table 4.4). Higher values were obtained for glyceryl dibehenate SLN microencapsulated in mannitol and glyceryl tristearate SLN in trehalose. So, as PAP release is mainly due to a desorption mechanism, it will be more delayed in the formulations presenting higher binding constants.

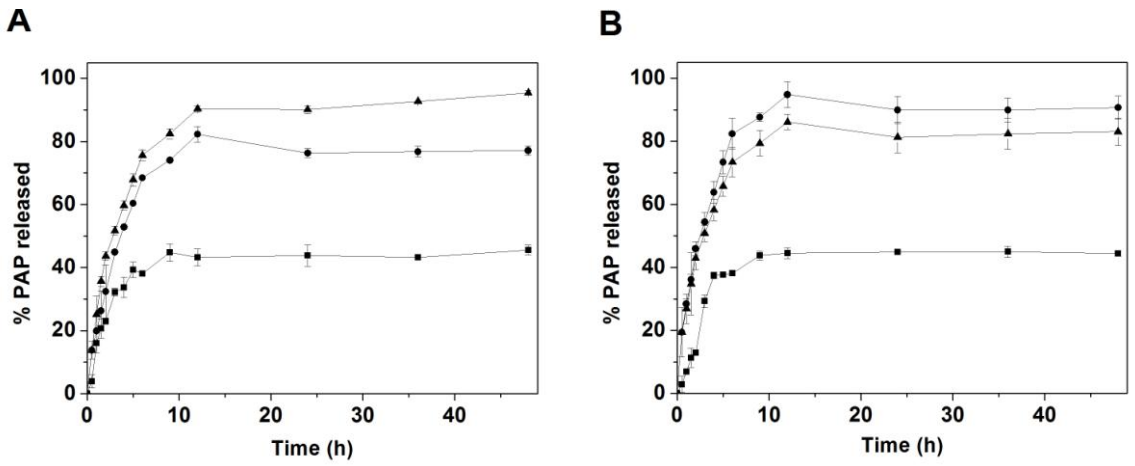

Figure 4.9: Release profiles of PAP from (A) glyceryl dibehenate SLN and (B) glyceryl tristearate SLN, in isotonic PBS pH 7.4/37°C (mean±SD, *n*=3). (■) SLN; (●) SLN microencapsulated in mannitol; (▲) SLN microencapsulated in trehalose.

4.4.12. Protein stability

Adsorption of proteins at solid-liquid interfaces may affect their secondary and tertiary structures and, consequently, disturbing the biological function. There is consequently concern about the possibility of irreversibly damaging the protein during the formulation procedures. Although adsorption was used to associate proteins to nanocarriers in order to avoid protein exposition to harsh thermal conditions in SLN formulation, structural changes and loss of activity during adsorption and release may also occur. The stability of the enzyme was investigated by SDS-PAGE after adsorption onto nanoparticles and after release from SLN and microencapsulated SLN. No changes in the migration of the protein could be detected (Figure 4.10) when compared with the native protein. However, the additional bands seen in all wells confirm presence of impurities in the original PAP.

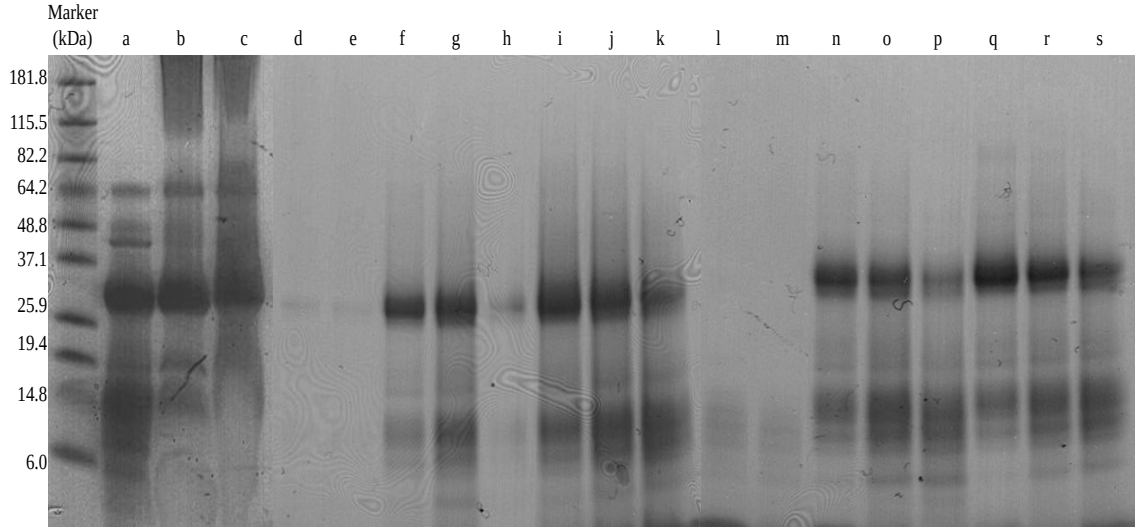

Figure 4.10: SDS-PAGE of PAP before and after adsorption and release (NuPAGE® Novex 12% Bis-Tris Gel). Lanes: (a) Native PAP; (b) PAP solution after adsorption onto glyceryl dibehenate SLN; (c) PAP solution after adsorption onto glyceryl tristearate SLN; PAP released from glyceryl dibehenate SLN after: (d) 1 h; (e) 2 h; (f) 6 h and (g) 9 h; PAP released from glyceryl dibehenate SLN microencapsulated in mannitol after: (h) 1 h and (i) 9 h and microencapsulated in trehalose after: (j) 1 h and (k) 9 h; PAP released from glyceryl tristearate SLN after: (l) 1 h; (m) 2 h; (n) 6 h and (o) 9 h; PAP released from glyceryl tristearate SLN microencapsulated in mannitol after: (p) 1 h and (q) 9 h and microencapsulated in trehalose after: (r) 1 h and (s) 9 h.

Therefore, according to this method, the adsorption procedure appears not to affect the whole structure of PAP. However, such observation does not necessarily indicate that the PAP molecule retains its biological activity. So, with the aim to evaluate PAP activity after release from SLN and dry powders, the protein was analyzed by a fluorometric assay using a specific substrate. For this purpose, non-microencapsulated SLN and both dry powders were incubated in the release medium in the same conditions that previously described. After 12h of incubation, samples were centrifuged and the activity of released PAP was determined (Table 4.8). Results show that >90% of PAP was active in all glyceryl tristearate-based formulations, and >80% in all glyceryl dibehenate-based formulations, allowing to conclude that PAP formulation in SLN using an adsorption procedure and the subsequent microencapsulation of SLN in polyols matrix by a spray-

drying technique contribute to preserving protein stability throughout harsh pharmaceutical procedures.

Table 4.8: Enzymatic activity of PAP from SLN, mannitol microspheres and trehalose microspheres after incubation with a specific fluorogenic substrate (Z-Leu-Leu-Arg-AMC) (mean±SD, *n*=3).

Samples		Total PAP concentration (µg/mL)	Enzymatically active PAP (µg/mL)	Activity (%)
PAP-glyceryl dibehenate SLN	SLN	152.6 ± 7.4	128.6 ± 11.0	84.2±13.3
	SLN microencapsulated in mannitol	182.5 ± 9.3	171.0 ± 10.4	93.6±14.0
	SLN microencapsulated in trehalose	235.8 ± 15.7	183.3 ± 9.0	77.7±18.1
PAP-glyceryl tristearate SLN	SLN	34.9 ± 1.8	31.2 ± 1.9	89.4±2.6
	SLN microencapsulated in mannitol	73.1 ± 10.2	64.9 ± 3.4	88.8±10.8
	SLN microencapsulated in trehalose	48.7 ± 0.9	48.8 ± 2.0	100.2±2.2

4.5. Conclusions

This study demonstrates the suitability of glyceryl dibehenate and glyceryl tristearate SLN as carriers for an application in pulmonary protein delivery. A model protein (PAP) was suitably adsorbed onto SLN, following a Freundlich type of adsorption isotherm over the concentration range studied, suggesting protein multilayers on the SLN surface through the electrostatic interaction between amino groups of PAP and the negative charged sites of SLN, as confirmed by FTIR, DSC and XPS. PAP-containing SLN were successfully incorporated in mannitol and trehalose microspheres by means of a spray-drying process, resulting in dry powders with acceptable characteristics for lung deposition. The protein released from dry powders retained its enzymatic activity. Altogether, these results are an encouraging indicator of the utility of microencapsulated SLN as protein carriers for pulmonary delivery, making them suitable candidates for this application.

4.6. References

1. Almeida, A.; Souto, E. Solid lipid nanoparticles as a drug delivery system for peptides and proteins. Adv. Drug Deliv. Rev., 2007, 59 (6), 478-490.

2. Alpar, H.; Almeida, A. Identification of some of the physico-chemical characteristics of microspheres which influence the induction of the immune response following mucosal delivery. Eur. J. Pharm. Biopharm., 1994, 40 (4), 198-202.

3. Norde, W. Interaction of proteins with polymeric and other colloids. In: Asua J, Ed.In: Polymeric dispersions: principles and applications. Navarra: Springer; 1997. p. 541-555.

4. Hu, J.; Li, S.; Liu, B. Adsorption of BSA onto sulfonated microspheres. Biochem. Eng. J., 2005, 23 (3), 259-263.

5. Arai, T.; Norde, W. The behavior of some model proteins at solid-liquid interfaces 1. Adsorption from single protein solutions. Colloid. Surface, 1990, 51 (1), 1-15.

6. Al-Qadi, S.; Grenha, A.; Remuñán-López, C. Microspheres loaded with polysaccharide nanoparticles for pulmonary delivery: Preparation, structure and surface analysis. Carbohyd. Polym., 2011, 86 (1), 25-34.

7. Grenha, A.; Seijo, B.; Remuñán-López, C. Microencapsulated chitosan nanoparticles for lung protein delivery. Eur. J. Pharm. Sci., 2005, 25 (4), 427-437.

8. Sham, J.O.-H.; Zhang, Y.; Finlay, W.H.; Roa, W.H.; Löbenberg, R. Formulation and characterization of spray-dried powders containing nanoparticles for aerosol delivery to the lung. Int. J. Pharm., 2004, 269 (2), 457-467.

9. Manosroi, A.; Chankhampan, C.; Manosroi, W.; Manosroi, J. Transdermal absorption enhancement of papain loaded in elastic niosomes incorporated in gel for scar treatment. Eur. J. Pharm. Sci., 2013, 48 (3), 474-483.

10. Almeida, A.; Alpar, H.; Brown, M. Immune response to nasal delivery of antigenically intact tetanus toxoid associated with poly (L-lactic acid) microspheres in rats, rabbits and guinea-pigs. J. Pharm. Pharmacol., 1993, 45 (3), 198-203.

11. Florindo, H.; Pandit, S.; Goncalves, L.; Alpar, H.; Almeida, A. Surface modified polymeric nanoparticles for immunisation against equine strangles. Int. J. Pharm., 2010, 390 (1), 25-31.

12. Florindo, H.; Pandit, S.; Lacerda, L.; Gonçalves, L.; Alpar, H.; Almeida, A. The enhancement of the immune response against *S. equi* antigens through the intranasal administration of poly-ε-caprolactone-based nanoparticles. Biomaterials, 2009, 30 (5), 879-891.

13. Caldeira, R.; Gonçalves, L.; Martins, T.; Silveira, H.; Novo, C.; Rosário, V.; Domingos, A. *Plasmodium chabaudi*: Expression of active recombinant chabaupain-1 and localization studies in *Anopheles* sp. Exp. Parasitol., 2009, 122 (2), 97-105.

14. Calis, S.; Jeyanthi, R.; Tsai, T.; Mehta, R.C.; DeLuca, P.P. Adsorption of salmon calcitonin to PLGA microspheres. Pharmaceut. Res., 1995, 12 (7), 1072-1076.

15. Kaul, P.; Sathish, H.; Prakash, V. Effect of metal ions on the structure and activity of papain from *Carica papaya*. Nahrung, 2002, 46 (1), 2-6.

16. Kaialy, W.; Momin, M.; Ticehurst, M.; Murphy, J.; Nokhodchi, A. Engineered mannitol as an alternative carrier to enhance deep lung penetration of salbutamol sulphate from dry powder inhaler. Colloid. Surface B, 2010, 79 (2), 345-356.

17. Nascimento, C.; Leandro, J.; Lino, P.R.; Ramos, L.; Almeida, A.J.; de Almeida, I.T.; Leandro, P. Polyol additives modulate the *in vitro* stability and activity of recombinant human phenylalanine hydroxylase. Appl. Biochem. Biotech., 2010, 162 (1), 192-207.

18. Al-Qadi, S.; Grenha, A.; Carrión-Recio, D.; Seijo, B.; Remuñán-López, C. Microencapsulated chitosan nanoparticles for pulmonary protein delivery: *in vivo* evaluation of insulin-loaded formulations. J. Control. Release, 2012, 157 (3), 383-390.

19. Schüle, S.; Frieß, W.; Bechtold-Peters, K.; Garidel, P. Conformational analysis of protein secondary structure during spray-drying of antibody/mannitol formulations. Eur. J. Pharm. Biopharm., 2007, 65 (1), 1-9.

20. Mortensen, N.; Durham, P.; Hickey, A. The role of particle physico-chemical properties in pulmonary drug delivery for tuberculosis therapy. J. Microencapsul., 2014, 31 (8), 785-795.

21. Hassan, M.S.; Lau, R.W.M. Effect of particle shape on dry particle inhalation: study of flowability, aerosolization, and deposition properties. AAPS PharmSciTech, 2009, 10 (4), 1252-1262.

22. Al-Qadi, S.; Alatorre-Meda, M.; Martin-Pastor, M.; Taboada, P.; Remuñán-López, C. The role of hyaluronic acid inclusion on the energetics of encapsulation and release of a protein molecule from chitosan-based nanoparticles. Colloid. Surface B, 2016, 141 (1), 223-232.

23. Kaushik, J.K.; Bhat, R. Why is trehalose an exceptional protein stabilizer? An analysis of the thermal stability of proteins in the presence of the compatible osmolyte trehalose. J. Biol. Chem., 2003, 278 (29), 26458-26465.

Chapter 5

Hybrid pDNA-polycationic nanostructured microparticles for pulmonary delivery of genetic material

This chapter is based on the following publication:
Gaspar DP, Vítor J, Vital J, Leiva MC, Gonçalves LMD, Taboada P, Remuñán-López C and Almeida AJ. *Hybrid pDNA-polycationic nanostructured microparticles for pulmonary delivery of genetic material. Submitted.*

This page was intentionally left blank.

Abstract

Plasmid DNA (pDNA) is a powerful tool for gene therapy but it is rapidly eliminated from the circulation following administration. Therefore, optimized DNA delivery systems are necessary for successful clinical use. Herein, the suitability of cationically modified solid lipid nanoparticles (SLN) as a novel pDNA carrier for the pulmonary route, as well as a transfection agent was investigated. Modified SLN were produced using glyceryl dibehenate or glyceryl tristearate as matrix lipid, Tween® 80 as surfactant and chitosan as surface charge modifier. The SLN were loaded with the model plasmid pEGFP-C1 resulting in nanoparticles of approximately 200 nm, showing zeta potential values around +15mV. Electrophoretic analysis confirmed the stability, integrity and functionality of the loaded pEGFP-C1. The formulations were able to transfect the relevant pulmonary cell lines A549 and Calu-3, while showing low cytotoxicity. Further SLN encapsulation in mannitol and trehalose microspheres, obtained by spray-drying, yielded dry powders suitable for inhalation that protected pDNA against premature degradation.

Graphical abstract

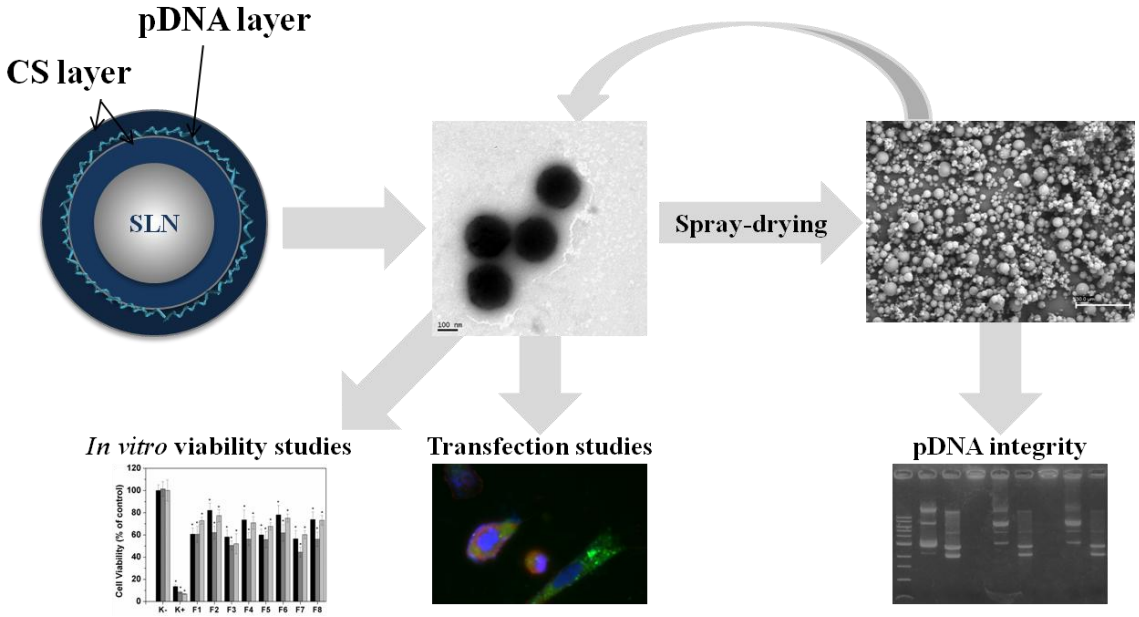

This page was intentionally left blank.

5.1. Introduction

Pulmonary delivery provides a non-invasive route for the administration of biomacromolecules like therapeutic genes, siRNA and proteins. It is therefore a promising approach for new treatments of genetic disorders like cystic fibrosis and other diseases such as asthma, chronic obstructive pulmonary disease, emphysema and lung cancer. The potential of pulmonary gene delivery is reflected in a large number of reports in the literature [1-3]. Theoretically pDNA is a powerful tool for gene therapy because of its easy preparation, great safety and stability. However, DNA is rapidly eliminated from the circulation due to the digestion by nucleases. Consequently, the therapeutic application of these pharmaceuticals is seriously limited. Therefore, the development of optimized delivery systems that can protect pDNA is critical for its success and conventional clinical use [2, 4].

Colloidal carriers seem to be the right choice for gene therapy since they have similar sizes compared to certain viruses, which are the natural but pathogenic gene delivery systems [5, 6]. A number of cationic polymers have been investigated as gene carriers, including polylysine [7], polyethyleneimine [8], polyamidoamine [9], poly (α-(4-aminobutyl)-L-glycolic acid) [10], among others. Nevertheless, an ideal gene carrier has yet to emerge with high efficacy of gene transfer, targeting ability and good biocompatibility [11]. In this context, SLN are an alternative drug delivery system to emulsions, liposomes and polymeric nanoparticles since they can be produced without the use of toxic solvents and large-scale production is possible [12, 13]. Their solid matrix protects active biopharmaceuticals against chemical degradation and allows modulation of drug release profiles [14, 15]. These properties make them a suitable pulmonary drug carrier system [16]. Moreover, SLN of suitable composition have been shown to be well tolerated *in vitro* [17], as well as *in vivo* [18, 19]. In addition, the potential of CS as a polycationic gene carrier has been explored in recent years by several research groups [20-24]. CS is a biodegradable polysaccharide extracted from crustacean shells that has been shown to be non-toxic in a range of toxicity tests, both in experimental animals and humans [22]. It has also been shown to bind effectively DNA and partially protect it from nuclease degradation until it reaches its target, facilitating intracytoplasmatic trafficking to the nucleus by escaping the endosomal and lysosomal systems [11, 25].

Herein, we propose, as a proof of concept, systems for delivery of genetic material by pulmonary route. These systems are composed by hybrid nanocarriers with a core formed

by glyceryl dibehenate and glyceryl tristearate SLN, previously optimized and characterized in Chapter 2, and a shell produced by a CS coating. The genetic material association is done between the positively charged CS with the negatively charged plasmid by electrostatic interaction. It is expected that these systems maintain the plasmid integrity when in contact with nucleases. Afterwards, in order to investigate the potential of these polycationic SLN as a gene delivery system in the form of an inhaled powder, they were subjected to microencapsulation in mannitol or trehalose microspheres in a subsequent spray-drying process. The physicochemical properties of the carriers were characterized and the pDNA integrity tested when incubated with a specific endonuclease. The expression efficiency of pDNA was studied *in vitro* on A549 and Calu-3 pulmonary cell lines. Finally, the aerodynamic properties of the produced microsphere-based dry powders were characterized and an in-depth thermodynamic analysis was also performed using ITC.

5.2. Materials

Glyceryl dibehenate was a kind gift from Gattefossé (France). Tween® 80 (polysorbate 80) was obtained from Merck (Kenilworth, USA). Glyceryl tristearate, CS (low MW), chitosanase from *Streptomyces griseus*, mannitol, D-(+)-trehalose dihydrate, PBS, MTT, propidium iodide, DMSO and paraformaldehyde were purchased from Sigma-Aldrich (USA). BstBI (20000 U/mL), DNase I (2000 U/mL), 1 kb DNA molecular weight marker and CutSmart® buffer were from New England Biolabs Inc. (USA). Agarose L (low electroendosmosis) was from Amersham Biosciences (Uppsala, Sweden). pDNA (pEGFP-C1, GenBank U55763) was a generous gift from Institute of Biopathology and Regenerative Medicine (IBIMER), University of Granada, Spain. Lung surfactant (Curosurf®) was a gift from Angelini Farmacêutica, Lda. (Portugal). For the viability studies, two cell lines were used: A549 (human alveolar lung carcinoma cell line, ATCC® CCL-185™) and Calu-3 (human lung adenocarcinoma from tracheobronchial epithelium cell line, ATCC® HTB-55™). The RPMI 1640 culture medium and their supplements (foetal serum bovine, penicillin G, streptomycin sulphate and L-glutamine) were acquired from Life Technologies (UK). Lipofectamine® 2000 was purchased from Invitrogen™ (Scotland, UK). Purified water was obtained by reverse osmosis and electrodeionisation (Millipore, Elix 3) being afterwards filtered (pore 0.45 μm). Reagents used in DNA

isolation and analysis were of molecular biology grade. All other reagents were of analytical grade and were used without further purification.

5.3. Methods

5.3.1. Bacteria transformation and plasmid purification

NEB® 5-alpha competent *Escherichia coli* DH5α™ was thawed on ice and 0.5 µg of pEGFP-C1 was gently mixed with *E. coli*. After 30 min on ice, *E. coli* was incubated at 42°C for 30 s and then incubated on ice for 5 min. After heat shock, *E. coli* was cultured in Super Optimal broth with Catabolite repression (SOC) medium for 1 h at 37°C and 100 µL was spread on the Lysogeny broth (LB) agar containing 30 µg/mL kanamycin and incubated at 37°C overnight. One colony was incubated in 500 mL of LB with kanamycin and incubated overnight at 37°C. The cells were isolated by centrifugation, the cell pellet was washed with pre-chilled 10 mM PBS pH 7.4 and was frozen until further use. Plasmid purification was performed according the procedure of Maxi Quialfilter Kit (Quiagen, Germany) and confirmed by 0.7% agarose gel containing 0.5 µg/mL ethidium bromide at 175 V for 50 min (Electrophoresis Power Supply, EPS 301, Amersham Pharmacia Biotech). DNA extracts were stored at -20°C for further molecular analyses. The quantification of the extracted DNA was measured using a Nanodrop ND-1000 v3.3.0 spectrophotometer (Nanodrop Technology, Cambridge, UK) at 260 nm.

5.3.2. Preparation of pDNA-polycationic SLN

Empty glyceryl dibehenate and glyceryl tristearate SLN were prepared with Tween® 80 as a surfactant using a hot HSH technique, as described previously in Chapter 2, section 2.3.2.. Briefly, a hot aqueous phase was added to a melted lipid phase and then homogenized using a high-shear laboratory mixer (Silverson SL2, UK). The SLN were obtained by cooling the dispersions in an ice bath. Afterwards, the SLN were coated with a CS solution 0.25% (w/v) in 1% acetic acid (v/v) at a CS:SLN ratio of 1:4 for 1 h at room temperature with a gentle stirring. The pEGFP-C1 (stock solution 5.07 µg/µL) was added to the nanosuspensions after CS coating. Loading capacity was determined by adding increasing amounts of pEGFP-C1 to the CS-coated SLN (from 0% to 100% of pEGFP-C1, where 100% (w:w) of pEGFP-C1 correspond to the total mass of CS in the

system). In other words, 100% (w:w) of pEGFP-C1 corresponds to a mass of 2.5 µg of plasmid. Nanoadsorption of pEGFP-C1 onto the CS-coated SLN (SLN:CS:pDNA) was investigated by gel electrophoresis (0.7% agarose containing 0.5 µg/mL ethidium bromide, at 175 V, 50 min) (Electrophoresis Power Supply, EPS 301, Amersham Pharmacia Biotech), using a 1 kb DNA molecular weight marker. The gel was visualized under an UV Transilluminator 2000 (Bio-Rad Laboratories). The SLN:CS:pDNA were further coated with an external CS layer (SLN:CS:pDNA:CS) in order to improve pEGFP-C1 integrity (Figure 5.1). The final nanodispersions were stored at 5±3°C until further use. Each formulation was carried out in triplicate (*n*=3).

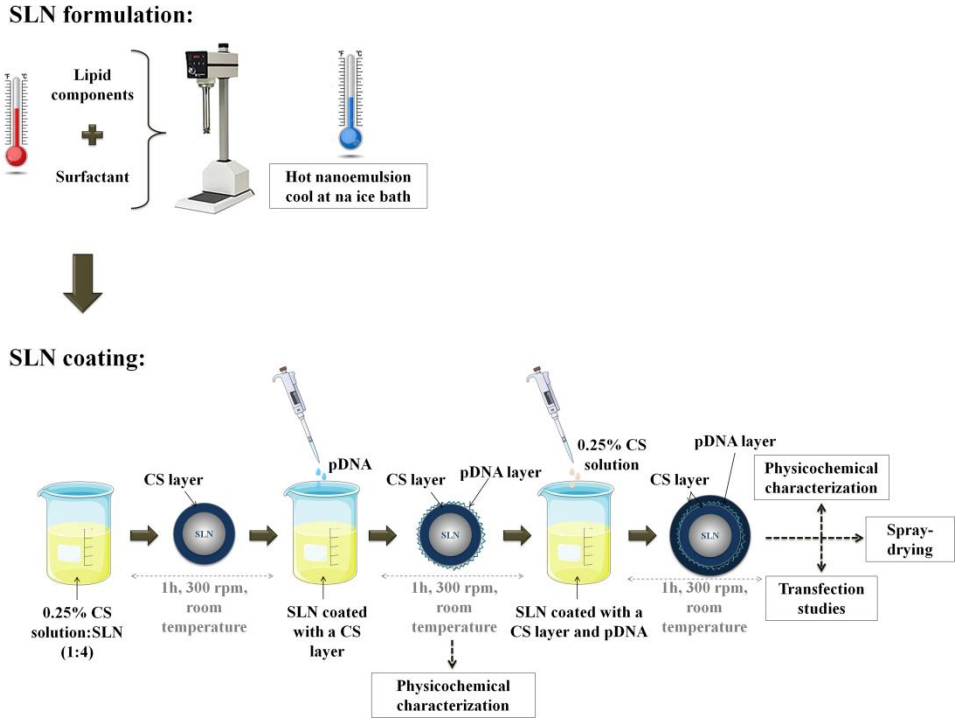

Figure 5.1: Preparation of DNA-containing SLN:CS hybrid nanoparticles.

5.3.3. Nanoparticle characterization

5.3.3.1. Particle size and surface charge

The pDNA-polycationic SLN mean diameter and PI were determined by quasi-elastic laser light scattering in a Malvern Zetasizer Nano S (Malvern Instruments, UK). The zeta potential (surface charge) was determined using laser Doppler anemometry in a Nano Z

(Malvern Instruments, UK). Samples were appropriately diluted in filtered purified water for the measurements. For the measurements, at least three replicate samples were determined.

5.3.3.2. Transmission electron microscopy analysis

The shape and surface morphology of the pDNA-polycationic SLN were observed by TEM. The samples were prepared by fixing a drop of the dispersion onto copper grids with a carbon layer for examination. Subsequently, it was dried with paper filter and treated with 2% (w/v) phosphotungstic acid for 2 min. The grids were then observed in a JEOL Microscopy (JEM 2010, Japan) at 120 kV, coupled to a Gatan Orius™ camera.

5.3.3.3. Thermal analysis using dynamic light scattering

The influence of temperature on the physical stability of pDNA-loaded polycationic SLN either coated with a single or a double CS layer was assessed using DLS (Zetasizer Nano S; Malvern Instruments, UK). Samples were appropriately diluted with filtered purified water (1:100) in a quartz cell and particle size analysis was performed while heating the sample from 25°C up to 90°C, subsequently followed by cooling from 90°C to 25°C at a rate of 0.5°C/min. Particle size measurements were made every 1°C. For each sample, measurements were carried out in triplicate (n=3).

5.3.4. Integrity of pEGFP-C1

Protection of pEGFP-C1 loaded in both types of nanoparticles (SLN:CS:pDNA and SLN:CS:pDNA:CS) was evaluated by enzymatic degradation with BstBI, an endonuclease with two recognition sites on pEGFP-C1 at positions 1357 and 3437. A complete plasmid digestion will produce two DNA fragments with 2080 and 2651 bp. The CS layers of SLN:CS:pDNA:CS were digested through incubation (4 h, 37°C) with chitosanase (10 U/mL in 50 mM acetate buffer pH 5.5) [26]. Afterwards, they were treated with 1 U BstBI/1 µg pDNA for 1 h at 65°C with 1x CutSmart® buffer. The reactions were stopped using a stop solution composed by 50% (v/v) glycerol, 50 mM EDTA and 0.2% (w/v) bromophenol blue. The integrity of pEGFP-C1 was then analysed by gel electrophoresis, as described above, and compared with pEGFP-C1 controls (one

with and another without BstBI treatment). The physicochemical properties (mean particle size, PI and surface charge) of the SLN:CS:pDNA:CS after digestion by chitosanase were also assessed as previously described in section 5.3.3.1..

5.3.5. *In vitro* cell viability studies

The cytotoxicity of nanoformulations was assessed using MTT reduction and propidium iodide assays. The MTT is a yellow, water-soluble tetrazolium dye that is converted by viable cells to a water-insoluble and purple compound, formazan [27]. Cell viability was assessed in A549 and Calu-3 cells after 24, 48 and 72 h of incubation of the cell lines in the presence of the different formulations. The Calu-3 and A549 respiratory epithelial cell lines have been frequently used in this context to evaluate the behaviour of systems aimed to be used as respiratory drug delivery systems, either nasal or pulmonary [28]. The day before the experiment, A549 and Calu-3 cells were seeded in sterile flat bottom 96 well tissue culture plates (Greiner, Germany) in RPMI 1640 culture medium, supplemented with 10% foetal serum bovine, 100 units/mL of penicillin G (sodium salt), 100 µg/mL of streptomycin sulfate and 2 mM L-glutamine, at a cell density of $1x10^5$ cells/mL and $0.5x10^5$ cells/mL for the Calu-3 and A549 cell lines, respectively. Cells were incubated at 37°C on 5% CO_2 atmosphere. On the following day, the culture medium was replaced by fresh one containing the different samples. A negative control (K-), cells only with culture medium, and a positive control (K+), cells with SDS (1 mg/mL) in order to promote lysis, were used. Each sample was tested in six wells per plate. After incubation, culture medium was replaced by 0.3 mM propidium iodide in culture medium (stock solution 1.5 mM in DMSO, diluted with culture medium 1:5). Fluorescence was measured (excitation, 485 nm; emission, 590 nm) in a microplate reader (FLUOstar Omega, BMGLabtech, Germany) and then, the MTT assay was performed. Briefly, existing culture medium was replaced by fresh one containing 0.25 mg/mL MTT. The cells were further incubated for 3 h. The medium was then removed and the intracellular formazan crystals were solubilized and extracted with 100 µL DMSO. After 15 min at room temperature, the absorbance was measured at 570 nm in a microplate reader (FLUOstar Omega, BMGLabtech, Germany). The relative cell viability (%) compared to control cells was calculated for the MTT assay using the following equation:

$$\text{Cell Viability (\% of control)} = \frac{\text{Abs}_{\text{sample}}}{\text{Abs}_{\text{control}}} \times 100 \qquad \text{(Eq. 5.1)}$$

where Abs_{sample} is the absorbance value obtained for cells treated with nanoparticles and $Abs_{control}$ is the absorbance value obtained for cells incubated with culture medium (K-).

For propidium iodide, cell viability was obtained by:

$$\text{Cell Viability (relative to control)} = \frac{\text{Fluorescence}_{\text{sample}}}{\text{Fluorescence}_{\text{control}}} \quad \text{(Eq. 5.2)}$$

where $Fluorescence_{sample}$ is the URF values obtained for cells treated with nanoparticles and $Fluorescence_{control}$ is the URF values obtained for cells incubated with culture medium (K-).

5.3.6. *In vitro* transfection studies

The Calu-3 and A549 respiratory epithelial cell lines were used in transfection assays. They were cultured as a monolayer in RPMI 1640 culture medium, supplemented with 10% foetal serum bovine (Invitrogen, UK), 100 units/mL of penicillin G (sodium salt), 100 μg/mL of streptomycin sulphate (Invitrogen, UK) and 2 mM L-glutamine, at a cell density of $1x10^5$ cells/mL and $0.5x10^5$ cells/mL for Calu-3 and A549 respectively, at 37°C in a humidified atmosphere with 5% CO_2. Cell transfection was performed in 24 well plates (Greiner, Germany) with nanoparticles containing 0.5 μg of pDNA per well encoding a red-shifted variant of wild-type green fluorescent protein (GFP) which has been optimized for brighter fluorescence and higher expression in mammalian cells [29]. Transfection with SLN:CS:pDNA:CS was performed in 500 μL RPMI 1640 culture medium without supplementation for 4 h. The medium pH was adjusted with HEPES buffer to 6.8 as previously described [30], since it is considered as an optimum pH for a high transfection rate. After incubation, 500 μL fresh medium supplemented with 20% foetal serum bovine was added. Lipofectamine® reagent (Invitrogen™) according to the manufacturer's instructions was used as a positive control. Wells only with culture medium, i.e. without nanoparticles, were used as a negative control. After incubation in the presence of the particles (72 h), cells were rinsed 3 times with 10 mM PBS containing 20 mM glycine at pH 7.4 before and after being fixed for 15 min at room temperature in dark with a 4% (w/v) paraformaldehyde solution. After fixation, cells were permeabilized with 0.1% Triton X-100 for 4 min, and then rinsed 3 times with 10 mM PBS containing 20 mM glycine at pH 7.4 for subsequent actin staining with rhodamine phalloidin. The 6.6 mM phalloidin-TRITC solution in 10 mM PBS was added to the cells for 30 min at

room temperature. Afterwards, cells were rinsed 3 times with 10 mM PBS containing 20 mM glycine at pH 7.4, and air dried, cell slides were mounted in fluorescent mounting medium ProLong® Gold antifade reagent with DAPI and their fluorescence was observed and recorded on an Axioscop 40 fluorescence microscope provided with an Axiocam HRc camera (Carl Zeiss, Germany). Images were processed with the software AxioVision Rel. 4.8.1 (Carl Zeiss, Germany).

5.3.7. Microencapsulation of nanoparticles

The nanoformulations were dispersed in aqueous mannitol and trehalose solutions at a 1:3 SLN:excipient ratio and then spray-dried using a laboratory-scale spray-dryer (Büchi® Mini spray-dryer, B-290, Switzerland), as previously reported in Chapters 3 and 4. Briefly, the spray-drying process was operated under the following conditions: a 0.7 mm nozzle, an air flow of 400 L/h and an T_{inlet} maintained at 103±2°C, resulting in an T_{outlet} between 63 and 67°C. The aspirator rates were adjusted to 100% and 70% for mannitol and trehalose microspheres, respectively. At the end, the obtained dry powders were collected and kept in a dessicator until further use.

The spray-drying PY were calculated by gravimetry, comparing the initial amount of total solids with the amount of resultant powder after spray-drying. The PY was calculated using the following equation:

$$PY(\%) = \frac{\text{Weight of the resultant powder after spray-drying}}{\text{Weight of solids totals}} \times 100 \qquad \text{(Eq. 5.3)}$$

5.3.8. Dry powder characterization

5.3.8.1. Particle size, morphological characterization and moisture content

The SEM analysis was performed in order to investigate the morphological characteristics of the spray-dried powders. Prior to analysis, the samples were placed on a double-side carbon tape mounted onto an aluminium stud and was then sputter coated with gold using an Emitech K550 (London, England) sputter in order to make it conducting. SEM images were recorded on a Zeiss Evo LS15 (UK) SEM, with an acceleration voltage of 20 kV. The SEM micrographs were used to calculate mean particle size, which was estimated as the Feret's diameter by measuring the mean of 300 particle measurements (*n*=300). The

moisture content of the spray-dried powders was determined by loss on drying from 25°C to 105°C, using an electronic moisture balance (Shimadzu, EB-280 MOC, Japan), according to the Ph. Eur. (2.2.32. Loss on drying). The percentage of the initial dry powder weight that was lost during the heating process was ascribed to the moisture content of the powders. Measurements were carried out in triplicate.

5.3.8.2. Aerodynamic properties determination

The real ρ of the dry powders was measured using a helium pycnometer (AccuPyc 1330, Micrometrics Ltd, Dunstable, UK) at room temperature (*n*=3). The apparent ρ was determined under defined conditions of the apparent volumes, before and after settling the samples using a stampf volumeter (Stav 2003, JEF Germany). It was obtained by measuring the volume of a known weight of the dry powders analysed in a 10 mL test-tube after mechanical tapping (1250 taps), according to the Ph. Eur. (2.9.34. Bulk density and tapped density of powders) (*n*=3). The d_{aer}, Carr's index and Hausner ratio of spray-dried particles were calculated based on the following equations 5.4, 5.5 and 5.6, respectively:

$$d_{aer}(\mu m) = d_{geo}\sqrt{\frac{\rho_e}{\lambda \rho_s}} \quad \text{(Eq. 5.4)}$$

where d_{geo} is the particle geometric diameter, ρ_s is 1 g/cm^3, ρ_e is the effective particle density in the same unit as ρ_s and λ is the dynamic shape factor of the particle. This shape factor is defined as the ratio of the drag force of the particle to that of a sphere of equivalent volume and for spherical particles is defined as 1.

$$\text{Carr's index } (\%) = \frac{100 \times (V_0 - V_f)}{V_0} \quad \text{(Eq. 5.5)}$$

$$\text{Hausner ratio} = \frac{V_0}{V_f} \quad \text{(Eq. 5.6)}$$

where V_o is the unsettled apparent volume and V_f is the final tapped volume.

5.3.8.3. Isothermal titration calorimetric studies

Binding studies were performed using a VP-ITC titration microcalorimeter (MicroCal Inc., Northampton, MA) with a cell volume of 1.436 mL at 25°C. First, samples were degassed in a ThermoVac system (MicroCal). The excipient solutions containing either

mannitol (1160 or 1280 mM when injecting glyceryl dibehenate and glyceryl tristearate SLN:CS:pDNA:CS, respectively) or trehalose (397 or 450 mM) was placed in a specific cell, having a reference cell with buffer solution. The thermostated cell was filled with the SLN:CS:pDNA:CS solutions (64.7 and 31.4 mM for glyceryl dibehenate and glyceryl tristearate SLN, respectively) under mild stirring without causing foaming. Each titration consisted of an initial 2 μL injection followed by 55 subsequent 5 μL injections planned to take place at 400 s intervals, sufficient for the heat signal to come back to the baseline. The results of the ITC experiments in terms of the heat of injection normalized by the SLN:CS:pDNA:CS concentration added per each injection (Q^*) were represented as a function of the SLN:CS:pDNA:CS to excipient molar ratio. The dilution heats from SLN:CS:pDNA:CS titrations into buffer solution were subtracted from the heats obtained from SLN:CS:pDNA:CS titrations into the excipient solution in order to get the net binding heats. Binding raw data were determined on the basis of a set of two identical binding sites by using the Affinimiter software as previously reported by Kim *et al.* [31]. Briefly, the two identical binding sites model employs the following fitting equation that encompasses Langmuir isotherm binding equilibria for two independent types of association, according to the following equation:

$$Q *= MV(n_1\Theta_1\Delta H_1 + n_2\Theta_2\Delta H_2) \qquad \text{(Eq. 5.7)}$$

where the sub-indices 1 and 2 stand for the two sets of sites.

One can solve for Θ_1 and Θ_2 using the equilibria equations for binding constants K_1 and K_2, with X being the total concentration of ligand and $[X]$ the concentration of unbound ligand:

$$K_1 = \frac{\Theta_1}{(1-\Theta_1)[X]} \quad \text{and} \quad K_2 = \frac{\Theta_2}{(1-\Theta_2)[X]} \quad \text{with} \quad [X] = X - M(n_1\Theta_1 + n_2\Theta_2) \qquad \text{(Eq. 5.8)}$$

To get an accurate fit, multiple assays were performed starting from random initial parameters. The same values were reached at the minimum χ^2 regardless of the initial values. Alterations in free energy (ΔG_i) and entropy of binding (ΔS_i) for each site were also measured from the fitted parameters according to following thermodynamic equations where R_g is the universal gas constant:

$$\Delta G_i = -R_g T \ln K_i \qquad\qquad \Delta G_i = \Delta H_i - T\Delta S_i \qquad \text{(Eq. 5.9)}$$

All experiments were carried out at least in duplicate with ±3% of reproducibility.

5.3.9. Nanoparticle recovery from microspheres

The microspheres obtained by spray-drying were incubated in 10 mM PBS pH 7.4 with 0.1% of lung surfactant (Curosurf®) under mild magnetic stirring at 37°C for 90 min. The particle size and morphology of the recovered nanoparticles were analysed by PCS and TEM respectively, as described in the previous sections.

5.3.10. Integrity of pEGFP-C1

The integrity of pEGFP-C1 was assessed throughout the spray-drying process. The SLN:CS:pDNA:CS were first recovered from the mannitol and trehalose microspheres in 10 mM PBS pH 7.4 with 0.1% of lung surfactant, as described in section 5.3.9. After a centrifugation step to precipitate any undissolved material, the integrity of pEGFP-C1 associated to the nanosystems was assessed using BstBI digestion, as described in section 5.3.4.. In addition, the pEGFP-C1 integrity in dry powders was also evaluated after incubation with DNase I, an endonuclease that nonspecifically cleaves DNA, following the supplier specifications (New England Biolabs Inc., USA), and taking into account the previous conditions used with BstBI. Briefly, DNase I solution, in the respective reaction buffer, was added to the recovered nanoparticles suspension. The mixture was incubated at 37°C for 1 h, and a 25 µL aliquot of the suspensions was analysed using the above described gel electrophoresis conditions.

5.3.11. Statistical analysis

Statistical analysis of the experimental data was performed using a one-way analysis of variance (one-way ANOVA) and differences between groups were tested by a one-way ANOVA with Dunnet's post hoc test with GraphPad Prism version 6.0 (GraphPad Software, San Diego, CA). Data were expressed as mean±SD or 95% confidence interval. A $p<0.05$ value was considered significant. All data are shown as mean±SD.

5.4. Results and discussion

5.4.1. pDNA-polycationic SLN formulation and characterization

The main purpose of using carriers for gene delivery is to protect and transport the genetic material into the cell and finally into the nuclear compartment while avoiding intracellular degradation [32]. The most frequently strategy for non-viral gene delivery is the formulation of DNA into condensed particles by means of cationic polymers such as CS. Generally, these systems can be formed by electrostatic interaction between oppositely charged macromolecules, e.g. cationic polymers and anionic DNA [22]. In this study, SLN:CS:pDNA were obtained spontaneously by electrostatic interaction upon incubating the pEGFP-C1 with SLN:CS under gentle stirring. The first step was the SLN coating with a CS layer, resulting from the deposition of CS (positively charged polymer) onto the negatively charged SLN surface (ca. -17 mV). The coating of SLN with CS led to an increase in SLN particle size (Table 5.1) with a narrow distribution. As expected, the surface charge of SLN:CS became positive after coating.

Table 5.1: Physical characteristics of plain SLN before and after coating with CS (mean±SD, *n*=3).

SLN	CS Coating	Mean size (nm)	PI	ZP (mV)
A	Without	99±4	0.123±0.009	-17.1±0.7
	With	211±11	0.286±0.008	28.4±0.5
B	Without	191±7	0.165±0.012	-17.8±0.5
	With	297±16	0.252±0.011	32.8±0.6

A: glyceryl dibehenate SLN; B: glyceryl tristearate SLN; PI: polydispersity index, ZP: zeta potential

Afterwards, the SLN:CS were loaded with a model plasmid (pEGFP-C1) by electrostatic interaction with the CS coating layer. The pEGFP-C1, a recombinant EGFP vector is of interest because it can be transfected into mammalian cells using any standard transfection method expressing GFP, a brighter green fluorescence. Moreover, pEGFP-C1 can be easily synthesized through bacteria transformation [33]. Regardless of the initial amount added to the formulation, all the pEGFP-C1 was incorporated into the SLN:CS nanoparticles as shown by agarose gel electrophoresis (Figure 5.2A and B), where free pEGFP-C1 moved at its usual position in the gel while pEGFP-C1 adsorbed onto the nanoparticles did not move from the wells, indicating the SLN:CS were able to retain the

adsorbed pDNA. The greater the amount of plasmid used, the higher intensity of the band was detected in the respective well, as opposed to the wells with unloaded nanoparticles (without pEGFP-C1), which did not show any fluorescence.

Plasmid incorporation caused a certain decrease in particle size and distribution (Table 5.2), which is in agreement with the underlying strong electrostatic interactions between the cationic CS with negatively charged molecules such as DNA [22, 34]. Furthermore, by increasing the amount of plasmid, zeta potential progressively diminished due to the presence of negatively charged pDNA on the nanoparticles surface.

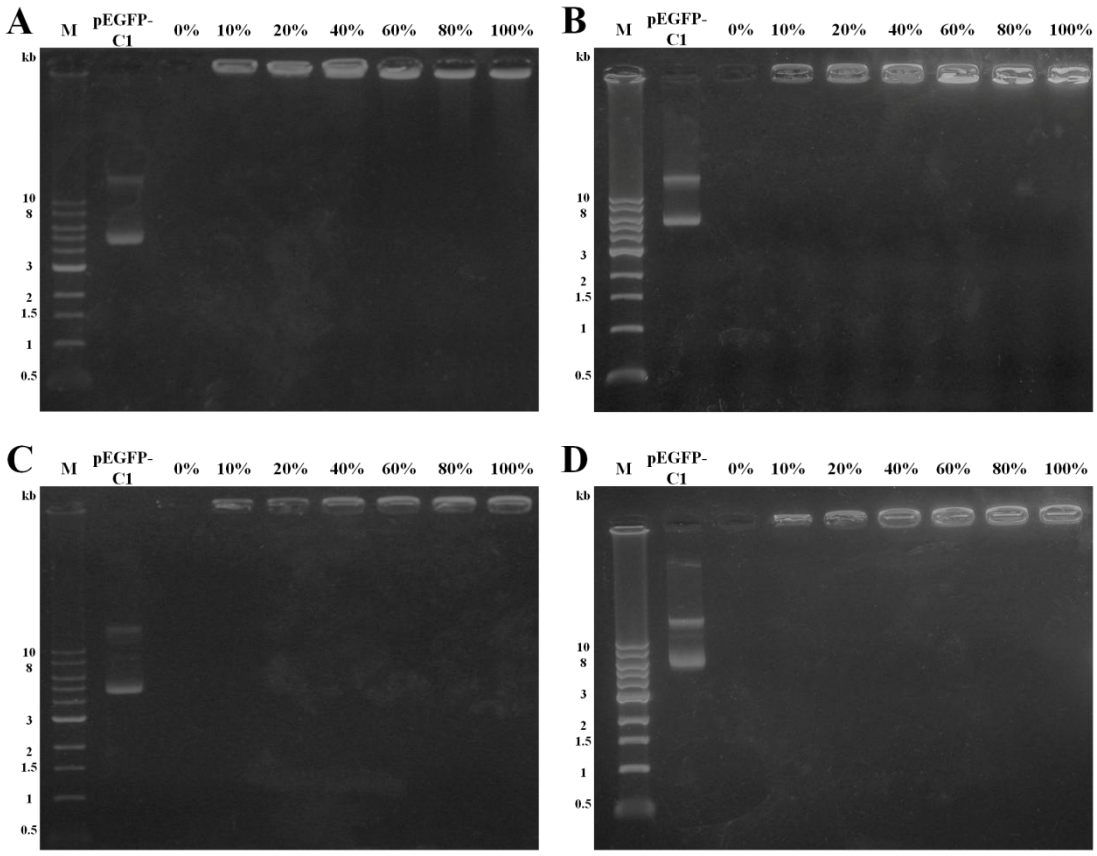

Figure 5.2: Agarose gel electrophoresis (0.7% in TBE) of glyceryl dibehenate (A) and glyceryl tristearate (B) SLN:CS:pDNA and glyceryl dibehenate (C) and glyceryl tristearate (D) SLN:CS:pDNA:CS containing increasing amounts of pEGFP-C1 (from 0 to 100%, w:w). The pEGFP-C1 associated to SLN:CS and SLN:CS:pDNA:CS remained intact. No banding was seen on the gel in both type of particles, indicating pEGFP-C1 was still strongly attached to nanoparticles. M - molecular weight markers.

As the nucleic acid in these formulations may be degraded due to direct exposition to the environment, SLN:CS:pDNA were further coated with a second CS layer, producing the so-called SLN:CS:pDNA:CS. After this second coating, the plasmid remained attached to the nanoparticles, with no band for free pEGFP-C1 observed, and the immobile nanocomplexes remaining in the starting zone of the gel, showing the incorporation efficiency of pEGFP-C1 was 100% for all the tested pDNA quantities (Figure 5.2C and D). Likewise, the greater the amount of plasmid attached to the nanoparticles, the higher the intensity of the band retained in the respective well, whereas the wells with unloaded nanoparticles did not display any fluorescence. The pEGFP-C1:CS mass ratio of 100% (w:w) was, hence, selected for further studies. Figure 5.2 also shows that SLN:CS:pDNA were retained at the positive side of the well while SLN:CS:pDNA:CS are retained at the negative side. This is a consequence of their different surface charges: SLN:CS:pDNA possess a less positive surface charge, so the nanoparticles run to the positive pole, whereas SLN:CS:pDNA:CS are positively charged, tending to migrate to the negative pole.

Table 5.2: Physical characteristics of SLN:CS:pDNA and SLN:CS:pDNA:CS loaded with increasing amounts of pEGFP-C1 (from 0 to 100%, w:w, related to CS mass in the system). Results expressed as mean±SD, *n*=3.

		SLN:CS:pDNA			SLN:CS:pDNA:CS		
SLN	% pEGFP-C1	Ø (nm)	PI	ZP (mV)	Ø (nm)	PI	ZP (mV)
A	0	211±11	0.286±0.008	28.4±0.5	211±11	0.286±0.008	28.4±0.5
	10	198±5	0.271±0.008	14.5±0.6	198±7	0.282±0.009	30.4±3.1
	20	197±7	0.298±0.041	15.6±0.4	204±8	0.291±0.011	30.4±0.8
	40	199±7	0.289±0.012	13.7±0.4	212±5	0.294±0.009	29.2±1.0
	60	197±6	0.271±0.012	12.2±0.7	216±8	0.420±0.009	28.7±0.7
	80	186±5	0.267±0.016	11.9±0.3	198±5	0.275±0.010	27.3±0.7
	100	187±3	0.267±0.011	10.3±1.7	203±10	0.287±0.011	24.9±1.0
B	0	297±16	0.252±0.011	32.8±0.6	297±16	0.252±0.011	32.8±0.6
	10	198±6	0.211±0.014	14.8±0.7	216±8	0.200±0.040	31.9±1.0
	20	224±4	0.181±0.011	12.3±1.1	220±12	0.177±0.028	28.4±1.1
	40	224±5	0.151±0.022	13.6±0.5	228±11	0.178±0.008	28.8±1.2
	60	234±7	0.147±0.021	12.3±0.2	231±13	0.181±0.027	30.2±1.7
	80	227±4	0.176±0.006	13.5±0.8	216±11	0.172±0.010	27.6±0.1
	100	235±5	0.165±0.012	10.7±0.5	220±9	0.166±0.010	28.1±0.3

A: glyceryl dibehenate SLN; B: glyceryl tristearate SLN; PI: polydispersity index, ZP: zeta potential

Regarding nanoparticle size, the coating with a second CS layer did not produce notable changes, remaining within a narrow range, while zeta potential values of SLN:CS:pDNA:CS expectedly became more positive due to the external CS layer (Table 5.2).

TEM images of the SLN:CS:pDNA:CS prepared with both solid lipids are shown in Figure 5.3, where the polymer layers have sufficient electron density to be directly observed through negative staining with phosphotungstic acid. The polymer appears as a grey layer surrounding the denser solid lipid matrix of spherical SLN. The micrographs confirmed the particle size distributions previously established from the PCS studies.

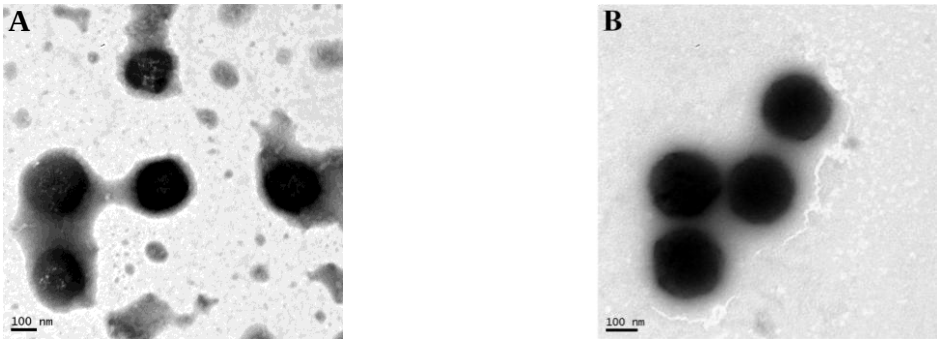

Figure 5.3: TEM micrographs of SLN:CS:pDNA:CS based on (A) glyceryl dibehenate and (B) glyceryl tristearate.

5.4.2. DLS thermal analysis

The effect of temperature on nanoparticle size was assessed using DLS, applying a heating ramp from 25°C up to 90°C and then a cooling ramp to the initial temperature. This assay allowed assessing nanoparticle physical stability by determining particle size variation when the formulations were subjected to a temperature increase followed by a decrease to the initial temperature. These studies are particularly meaningful whenever a formulation is intended for further temperature processing as it occurs during a spray-drying procedure. The heating and cooling ramps induced particle size changes in both SLN:CS:pDNA (Figure 5.4A and B), confirming previous observations reported in Chapter 2, section 2.4.3.. A slight particle size reduction throughout the heating step especially at its m.p. (≈70°C) was evident for glyceryl dibehenate SLN. However, after

the cooling phase, the initial particle size was not fully recovered. The glyceryl tristearate SLN suffered a marked decrease after 50°C, suggesting some instability at high temperatures. During the cooling step, particle size stabilizes. Despite all these variations, the particle size variations of both types of SLN were always within the nanosize range. Interestingly both SLN:CS:pDNA:CS behaved in a different way than SLN:CS:pDNA (Figure 5.4C and D). Regarding glyceryl dibehenate SLN:CS:pDNA:CS, their size was stabilized until ≈60°C after which an abrupt increase took place, returning after to their initial size. For glyceryl tristearate SLN:CS:pDNA:CS, this abrupt increase only occurred at ≈80°C. During the cooling step, both type of particles presented unstable profiles, probably due to the presence of CS. However, pEGFP-C1 remained associated with nanoparticles throughout all the heating and cooling process, i.e. the plasmid was retained in the wells suggesting that its stability and integrity were maintained (Figure 5.4E).

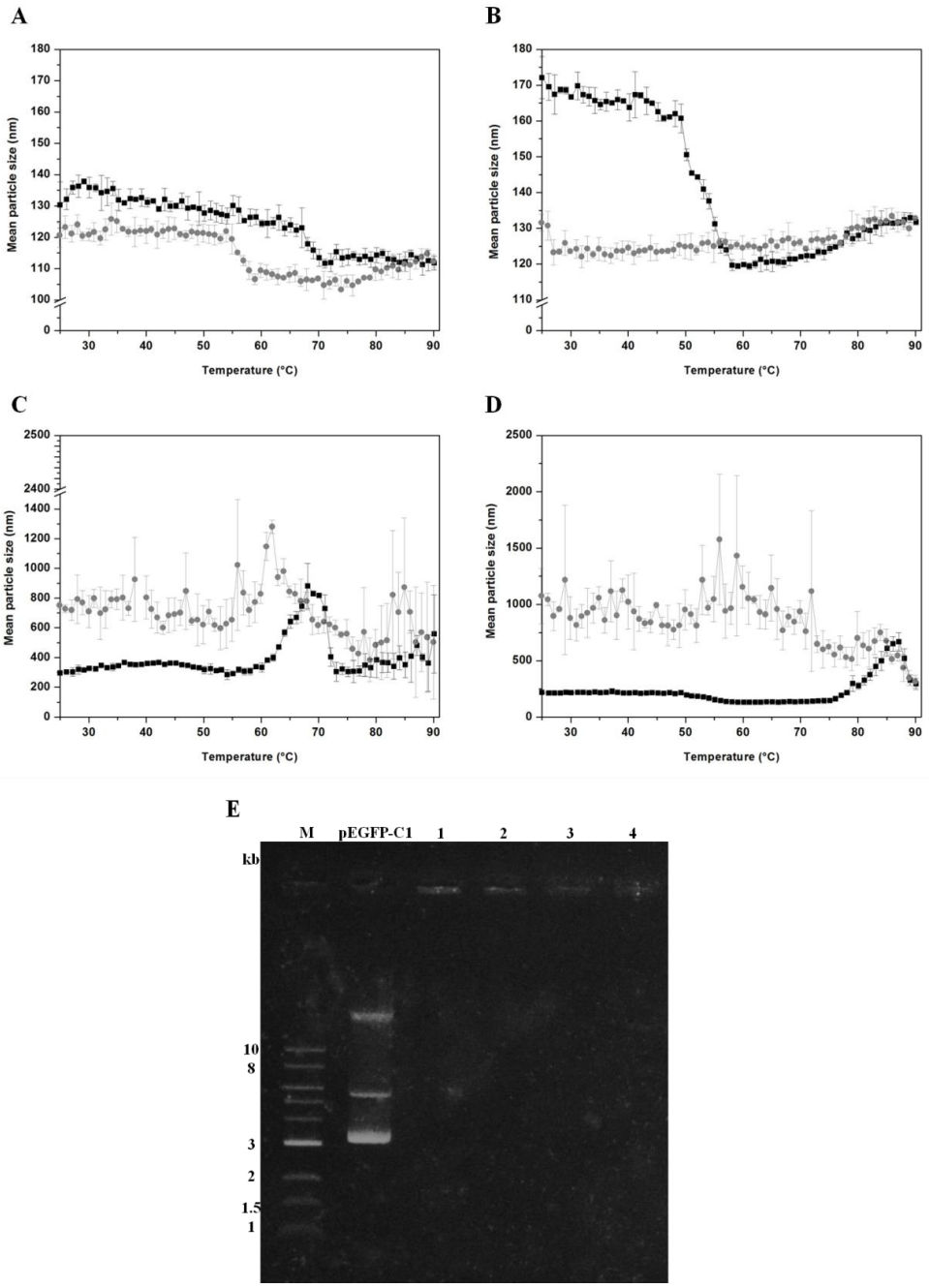

Figure 5.4: Thermal stability of hybrid nanoformulations: DLS thermogram of (A) glyceryl dibehenate SLN:CS:pDNA; (B) glyceryl tristearate SLN:CS:pDNA; (C) glyceryl dibehenate SLN:CS:pDNA:CS; (D) glyceryl tristearate SLN:CS:pDNA:CS (■ - heating step from 25°C to 90°C, ● - cooling step from 90°C to 25°C, mean±SD, *n*=3); (E) Agarose gel electrophoresis (0.7% in TBE) of pEGFP-C1 in (1) glyceryl dibehenate and (2) glyceryl tristearate SLN:CS:pDNA and (3) glyceryl dibehenate and (4) glyceryl tristearate SLN:CS:pDNA:CS after being subjected to DLS heating and cooling (M - molecular weight marker).

5.4.3. Integrity of pEGFP-C1 loaded on nanoparticles

For efficient *in vivo* delivery, particularly in gene therapy applications, the nanoparticulate carrier must be able to protect the genetic material from degradation during its transport to the target cells [35]. The ability of SLN:CS:pDNA and SLN:CS:pDNA:CS nanoparticles to stabilize pEGFP-C1 from endonuclease degradation in the body, as well as inside the cell, was studied using agarose gel electrophoresis. In order to check the level of protection being offered to the pEGFP-C1, the nanoparticles were subjected to an endonuclease treatment consisting of incubation with BstBI (1 U BstBI/1 µg pDNA) at 65°C/1 h in an appropriate buffer. The experimental data showed that naked pEGFP-C1 was partially digested by the endonuclease (Figure 5.5).

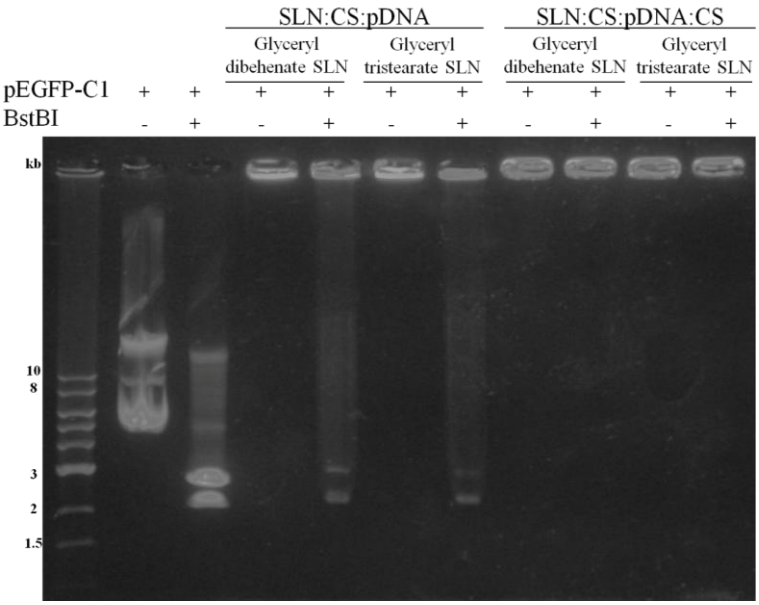

Figure 5.5: Agarose gel electrophoresis (0.7% in TBE) of pEGFP-C1 in glyceryl dibehenate and glyceryl tristearate SLN:CS:pDNA and SLN:CS:pDNA:CS. BstBI caused degradation of naked pEGFP-C1 and pEGFP-C1 associated to SLN:CS, while pEGFP-C1 in SLN:CS:pDNA:CS was protected from degradation and retained in the well.

Moreover, the pEGFP-C1 attached at SLN:CS was largely unprotected as observed by the presence of the two expected oligonucleotide bands (2080 and 2600 bp). In contrast, the plasmid attached to nanoparticles with an outer CS layer was fully protected from digestion (fluorescence observed only in the wells) (Figure 5.5).

The protection conferred by SLN:CS:pDNA:CS was further investigated by incubation of nanoparticles with chitosanase, an enzyme that promotes the endohydrolysis of beta-(1→4)-linkages between D-glucosamine residues in partly acetylated CS, thus destroying the CS layers of the nanoformulations. Then, nanoparticles were incubated with the endonuclease BstBI. The physicochemical properties of nanoparticles after chitosanase digestion were also measured revealing that the initial particle size of SLN was recovered (107±7 nm and 177±8 nm for glyceryl dibehenate and glyceryl tristearate SLN, respectively) with suitable polydispersity. The nanoparticles also recovered their negative surface charge corresponding to the zeta potential of initial SLN (-22±3 mV for glyceryl dibehenate SLN and -17±0 mV for glyceryl tristearate SLN).

Electrophoretic analysis also demonstrated that SLN:CS:pDNA:CS, that were not subjected to BstBI digestion, protected the pEGFP-C1 integrity. Since pEGFP-C1 was released with no signs of degradation from the nanoparticles after CS layers destruction by chitosanase (Figure 5.6), while those subjected to chitosanase and then BstBI treatment, showed the bands resulting of BstBI digestion at 2080 and 2600 bp. However, it is also possible to observe the presence of two additional bands of pEGFP-C1, which may be due to the formation of CS small fragments or even monomers that may remain associated to pEGFP-C1 making it unavailable for BstBI digestion (Figure 5.6, arrows). The small size of these complexes enabled their migration into the agarose gel.

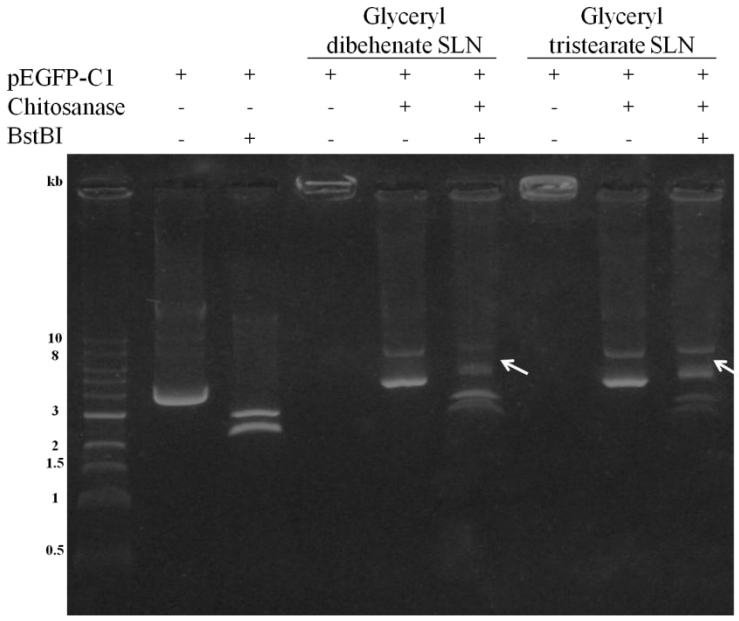

Figure 5.6: Agarose gel electrophoresis (0.7% in TBE) of pEGFP-C1 in glyceryl dibehenate and glyceryl tristearate SLN:CS:pDNA:CS after chitosanase and subsequent endonuclease (BstBI) treatment. Chitosanase promoted pEGFP-C1 dissociation from nanoparticles, making it susceptible to BstBI digestion.

5.4.4. *In vitro* cell viability studies

The biocompatibility of nanoparticles was assessed through cell viability assays performed with relevant pulmonary A549 and Calu-3 cell lines. Both cell lines are suitable models for evaluating biocompatibility of these particles in the pulmonary environment. The Calu-3 is an immortalized cell line obtained from lung adenocarcinoma and has been extensively used in the study of formulations designed for either nasal or pulmonary drug delivery, as it is considered a model of the epithelium of both regions [36]. The A549 cell line is representative of the alveolar epithelium, being obtained from human alveolar adenocarcinoma [36].

The viability of these pulmonary cells incubated with both formulations (SLN:CS:pDNA and SLN:CS:pDNA:CS) at different concentrations was assessed using the MTT proliferation assay. The studies revealed an important difference between negative (live cells, K-) and positive controls (dead cells, K+) at 24, 48 and 72 h of incubation (Figure 5.7A and B). During the first 48 h, there was a decrease in viability of both cell lines induced by the nanoparticle formulations. However, cell viability increased after 72 h.

The general decrease in cell viability observed between 24 and 48 h for all formulations may be explained by the need of an accommodation period by the cells to adapt to new conditions. In previous studies carried out, in Chapter 2, section 2.4.5., with the same cell lines, the glyceryl dibehenate and glyceryl tristearate SLN showed no evidence of acute cytotoxicity. So, the decrease in cell viability herein detected with SLN:CS:pDNA and SLN:CS:pDNA:CS probably occurred due to the presence of the CS in the formulations, which corroborates the findings of Rodrigues *et al.* [37]. As the MTT assay is based on the enzymatic conversion of MTT in the mitochondria, the tested nanoformulations may have inhibited the mitochondrial respiration inducing active oxygen-related cell death and, consequently, the observed cytotoxicity following exposure to the nanoparticles. Moreover, the reactive oxygen species that can be generated within mitochondria can also damage mitochondrial components and therefore a cytotoxicity assay based on mitochondrial respiratory activity would give early signs of toxicity following exposure to a mitochondrial toxicant, such as in MTT assay [38].

In order to validate the MTT results, an additional toxicity test was carried out using the propidium iodide test. This dye does not permeate living cells, being commonly used to detect dead cells in a population since it allows detecting the breakdown of cellular membrane integrity [39]. The retention values of propidium iodide in the positive control (K+) were high, since these cells were not viable, with a damaged cell membrane promoting dye uptake (≈2 URF for both cell lines) (Figure 5.7C and D). On the other hand, cells incubated with only fresh medium (negative control, K-) were viable, with intact cell membranes, and consequently presented low values of propidium iodide uptake (ca. 1 URF). The cell membranes in contact with the formulations remained intact because values of propidium iodide assay were approximately equal to those of the negative control (≈1 URF for all formulations in both cell lines), suggesting the cell membranes were not disrupted irrespective of the nanoparticle concentration used.

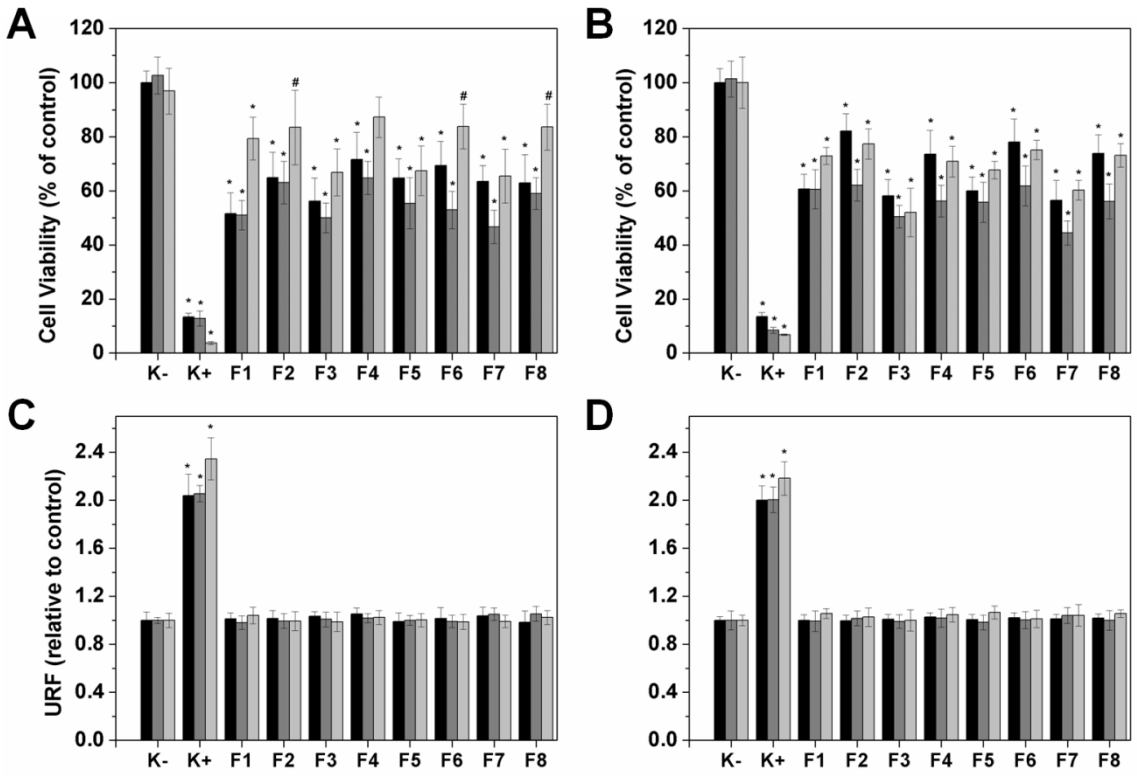

Figure 5.7: Relative cell viability of (A) A549 and (B) Calu-3 cell lines measured by the MTT reduction and propidium iodide uptake by (C) A549 and (D) Calu-3 cell lines at different incubation times: (■) 24, (■) 48 and (■) 72 h. (K-) negative control (culture medium); (K+) positive control (SDS, 1 mg/mL); (F1) glyceryl dibehenate SLN:CS:pDNA and (F2) glyceryl tristearate SLN:CS:pDNA at 0.332 mg/mL; (F3) glyceryl dibehenate SLN:CS:pDNA:CS and (F4) glyceryl tristearate SLN:CS:pDNA:CS at 0.290 mg/mL; (F5) glyceryl dibehenate SLN:CS:pDNA and (F6) glyceryl tristearate SLN:CS:pDNA at 0.166 mg/mL; (F7) glyceryl dibehenate SLN:CS:pDNA:CS and (F8) glyceryl tristearate SLN:CS:pDNA:CS at 0.146 mg/mL. Results are expressed as mean±SD (n=6). Statistical analysis between the control group (K-) and other groups was performed using one-way ANOVA with Dunnet's post hoc test (#p<0.01 and *p<0.0001).

5.4.5. *In vitro* transfection studies

Due to its mucoadhesive and permeation-enhancing properties, CS binds to cell membranes, promoting transcellular and paracellular permeability. Therefore, CS nanoparticles often present high transfection efficiency being successfully used as a non-viral gene delivery system both *in vitro* and *in vivo* [22]. Although the transfection

efficacy is cell line dependent, there are steps common to all cells: (i) binding to cell surface between the positively charged systems and the negatively charged cell membrane receptors by electrostatic interactions, (ii) entry into the cell by following a specific pathway, (iii) release of DNA into the cytoplasm and (iv) passage through the nuclear envelope to reach the cellular machinery for protein synthesis [40, 41] . The transfection capacity of CS-DNA nanoparticles to various cell types, mainly HeLa, HEK293 and COS-1 cells has been described [22, 42].

Transfection of the pulmonary cell lines A549 and Calu-3 with glyceryl dibehenate and glyceryl tristearate SLN:CS:pDNA:CS was established by using the pEGFP-C1 as reporter gene encoding GFP. Likewise, our results suggested that SLN:CS:pDNA:CS were able to effectively transfect both A549 and Calu-3 cell lines (Figure 5.8). The fluorescent GFP molecules were expressed by the transfected pEGFP-C1, being accumulated within the cell and localized in either the cytoplasm (red staining) or perinuclear regions, as evidenced by the green colour in the merged pictures (cell nuclei were blue-stained). It must be emphasized that the levels of transfection were of similar magnitude as those obtained with the commercial agent Lipofectamine®, herein used as a positive control. Negative controls (cells without nanoparticles) were unable to show any fluorescence due to absence of pEGFP-C1. This observation confirmed that the transfection of pulmonary cell lines with pDNA can be effectively carried out by using polycationic SLN as a vehicle, being a promising candidate for successful gene delivery. These results also provided additional evidence about the retention of structural integrity and function of pEGFP-C1 after transfection.

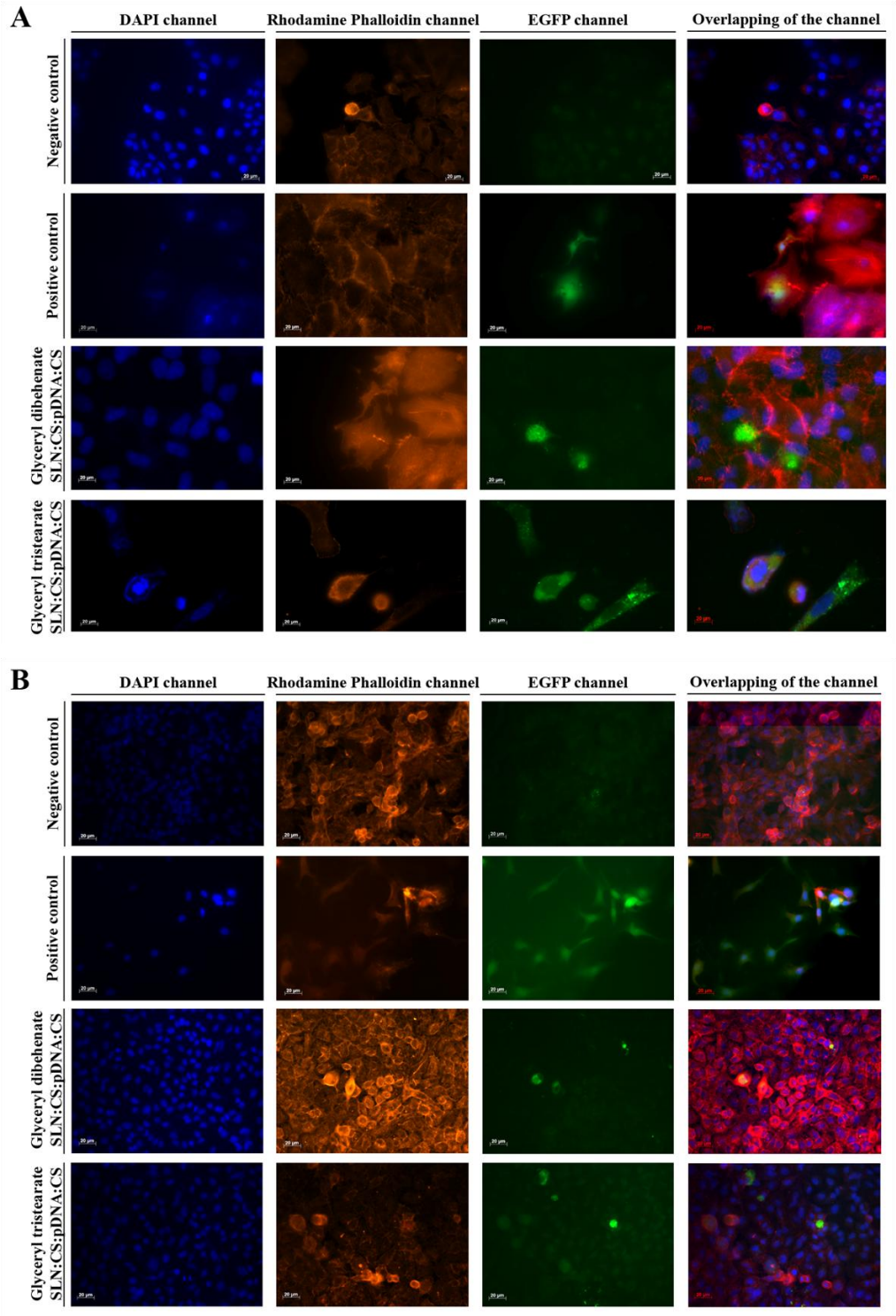

Figure 5.8: Fluorescence microscopy analysis of pEGFP-C1 expression after (A) A549 and (B) Calu-3 cells transfection mediated by SLN:CS:pDNA:CS. (a) nuclei were stained with DAPI (blue); (b) actin were stained with rhodamine phalloidin (red); (c) pEGFP-C1 was expressed as a green fluorescence and (d) overlapping of the three channels (Scale bar: 20 μm).

5.4.6. Microencapsulation of SLN:CS:pDNA:CS nanoparticles

PAP- and RFB-SLN loaded mannitol and trehalose microspheres were previously described, in Chapters 3 and 4, as an outstanding drug delivery system of drugs and proteins by the pulmonary route, given the adequate morphological and aerodynamic characteristics presented by these powders and their ability to release nanoparticles, and consequently the incorporated drug/protein, upon contact with an aqueous medium. So, taking into account this background and highlights the purpose of using these glyceryl dibehenate and glyceryl tristearate SLN:CS:pDNA:CS as gene delivery following pulmonary administration, these hybrid pDNA-polycationic SLN were microencapsulated through a spray-drying procedure. In this work, dry powders were also obtained using mannitol and trehalose as excipients with production yields ranging from 53 to 65% (Table 5.3). Both these excipients were selected as they are approved by regulatory agencies for pulmonary delivery, and so, widely applied in aerosolization.

The d_{aer} is a combination of the particle size, density and shape, influencing the dispersion and sedimentation patterns. Microspheres produced in this work presented a Feret's diameter of ca. 5 and 4 μm for mannitol and trehalose microspheres respectively, real ρ of approximately 1.4 g/cm^3 and a tapped ρ as low as 0.5 g/cm^3 (Table 5.3), which confer an d_{aer} suitable to reach the alveolar area as occurred with the previously reported systems in Chapters 3 and 4, namely RFB- and PAP-SLN incorporated in mannitol and trehalose microspheres. Moreover, flowability has been shown to be a key property of the DPI formulation as it aids in metering, fluidization and dispersion, affecting the emitted dose of a drug from a DPI device and, possibly, the subsequent delivery of that drug to the lung. The flowability indices (Hausner ratio and Carr's index) may be calculated from poured and apparent densities providing a general indication of interparticulate forces. The results indicated poor flowability for dry powders, but further data revealed that the microspheres were able to sufficiently aerosolize and reach the deep lung, as previously described in Chapter 3, section 3.4.5. and Chapter 4, section 4.4.9.. Moreover, the powder residual moisture content varied from 0.55% (for mannitol as excipient) to 1.67% (for trehalose as excipient) (Table 5.3). The final moisture level of the spray-dried powders is mainly determined by the nature of the material due to its interactions with water molecules. Another factor which has a major impact on the moisture level of the powder is the T_{outlet}. Generally, lower moisture content is associated to higher T_{outlet}. In our experiments, a correlation between the powder residual moisture content and the T_{outlet}

was not found. The differences in moisture content of the spray-dried SLN can be related to the drying-aid properties. The low moisture content of the spray-dried mannitol particles was based on their crystalline state. In addition, this compound possesses a low MW and a good drying aptitude contrarily to polymers, which are characterized by high MW such as trehalose.

Table 5.3: Physical and aerodynamic properties of dry powders (mean±SD, *n*=3).

Dry powders	Process yield (%)	Feret's diameter (μm, *n*=300)	Real density (g/cm^3)	Apparent density (g/cm^3)	Aerodynamic diameter (μm)	Carr's index (%)	Hausner ratio	Moisture residual content (%)
A	61.3±5.2	5.44±0.94	1.44±0.00	0.56±0.00	6.53±0.00	51±4	2.1±0.2	0.55±0.03
B	53.0±1.6	5.84±0.70	1.44±0.03	0.50±0.00	7.01±0.08	50±2	2.0±0.1	0.69±0.02
C	65.4±0.9	4.21±0.88	1.43±0.00	0.45±0.04	5.04±0.00	39±4	1.7±0.1	1.32±0.03
D	60.9±2.5	4.08±0.96	1.41±0.01	0.40±0.01	4.85±0.01	43±6	1.8±0.2	1.67±0.01

A: glyceryl dibehenate SLN:CS:pDNA:CS microencapsulated in mannitol; B: glyceryl tristearate SLN:CS:pDNA:CS microencapsulated in mannitol; C: glyceryl dibehenate SLN:CS:pDNA:CS microencapsulated in trehalose; D: glyceryl tristearate SLN:CS:pDNA:CS microencapsulated in trehalose

Although the aerodynamic behaviour of a dry powder intended for pulmonary administration is a key factor for the particles to be successfully inhaled, morphological characteristics may also influence in the powder aggregation and flowing properties [28]. The SEM analysis (Figure 5.9) of the spray-dried powders revealed that microspheres possessed a spherical shape with well-defined limits. However when mannitol was used as excipient, particles look like slightly convoluted (Figure 5.9A and B). Conversely, microspheres based on trehalose presented a smooth surface (Figure 5.9C and D), thus confirming previously reported results in Chapter 3, section 3.4.2 and Chapter 4, section 4.4.6..

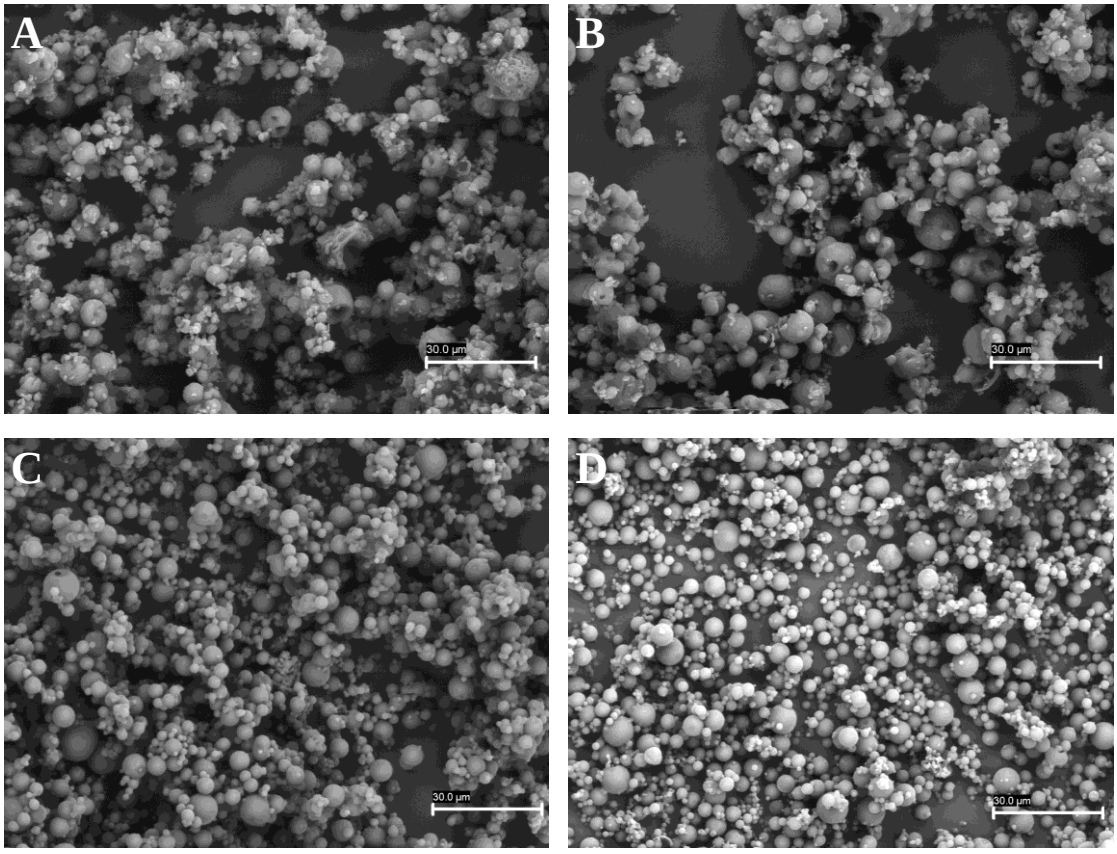

Figure 5.9: SEM micrographs of microspheres obtained by spray-drying: (A) glyceryl dibehenate and (B) glyceryl tristearate SLN:CS:pDNA:CS microencapsulated in mannitol and (C) glyceryl dibehenate and (D) glyceryl tristearate SLN:CS:pDNA:CS microencapsulated in trehalose (scale bar: 30 µm).

5.4.7. ITC analysis of SLN:CS:pDNA:CS binding affinity to excipients

The SLN:CS:pDNA:CS-spray-drying excipients binding strength and complexation thermodynamics along the microspheres formation were characterized by ITC, which quantitatively measured changes in the system's energy. Figure 5.10 depicts the injection heat normalized by the SLN:CS:pDNA:CS concentration added per injection, *Q**, as a function of the nanoparticles to excipients molar ratio after subtraction of the heat evolved after the titration of SLN:CS:pDNA:CS suspension into water.

Titrations of glyceryl dibehenate SLN:CS:pDNA:CS into mannitol (Figure 5.10A) led to a similar profile to that obtained when titrating protein-glyceryl dibehenate into mannitol, as described in Chapter 4, section 4.4.7.. The increase of glyceryl dibehenate SLN:CS:pDNA:CS titrations onto mannitol promoted a progressive increase of ΔH_i^i

(from -155 to -90 cal.mol^{-1} in the tested range of concentrations). As previously explained, this phenomenon was a consequence of an enhancement of mannitol and SLN:CS:pDNA:CS dehydration to support the excipient binding to all nanoparticles. Nonetheless, many factors may influence this condition, such as hydrophobic interactions between mannitol with SLN:CS:pDNA:CS, charge shielding effects and/or excipient's molecular rearrangements upon excipient adsorption onto nanoparticles. Regarding the titrations of glyceryl dibehenate SLN:CS:pDNA:CS onto trehalose (Figure 5.10B), the obtained profile was also very similar to those obtained for titrations between PAP-glyceryl dibehenate SLN and trehalose (as reported in Chapter 4, section 4.4.7.) and glyceryl dibehenate SLN:CS:pDNA:CS into mannitol. The observed gradual ΔH_i^i increase (from -220 to -150 cal.mol^{-1} in the tested concentration range) was probably a result of hydrophobic interactions established between the disaccharide rings and conformational rearrangements of trehalose molecules. The interaction between glyceryl tristearate SLN:CS:pDNA:CS with mannitol (Figure 5.10C) led to positive ΔH_i^i values in the whole concentration tested range. Briefly, at very low nanoparticles/saccharide molar ratios, an abrupt decrease in the endothermic Q^* values was visualized, which was followed by a more gradual one. This endothermic profile was probably caused by the breakdown of water solvation upon complex formation. By observation of the ITC profile from glyceryl tristearate SLN:CS:pDNA:CS with trehalose (Figure 5.10D), it was possible to denote similarities between this profile and those previously obtained by titrating glyceryl dibehenate SLN:CS:pDNA:CS in mannitol and trehalose. The observed exothermic profile (from -360 to -250 cal.mol^{-1} in the tested concentration range) can be originated, as previously explained, from the hydrophobic interaction established between the disaccharide rings of trehalose and their potential conformational rearrangements. Moreover, for all experiments, a final plateau region was not visualized probably as a consequence of the range of SLN:CS:pDNA:CS/excipients molar ratios here tested. However, it is important to emphasize that these used concentration mimics the ones used during the spray-drying process.

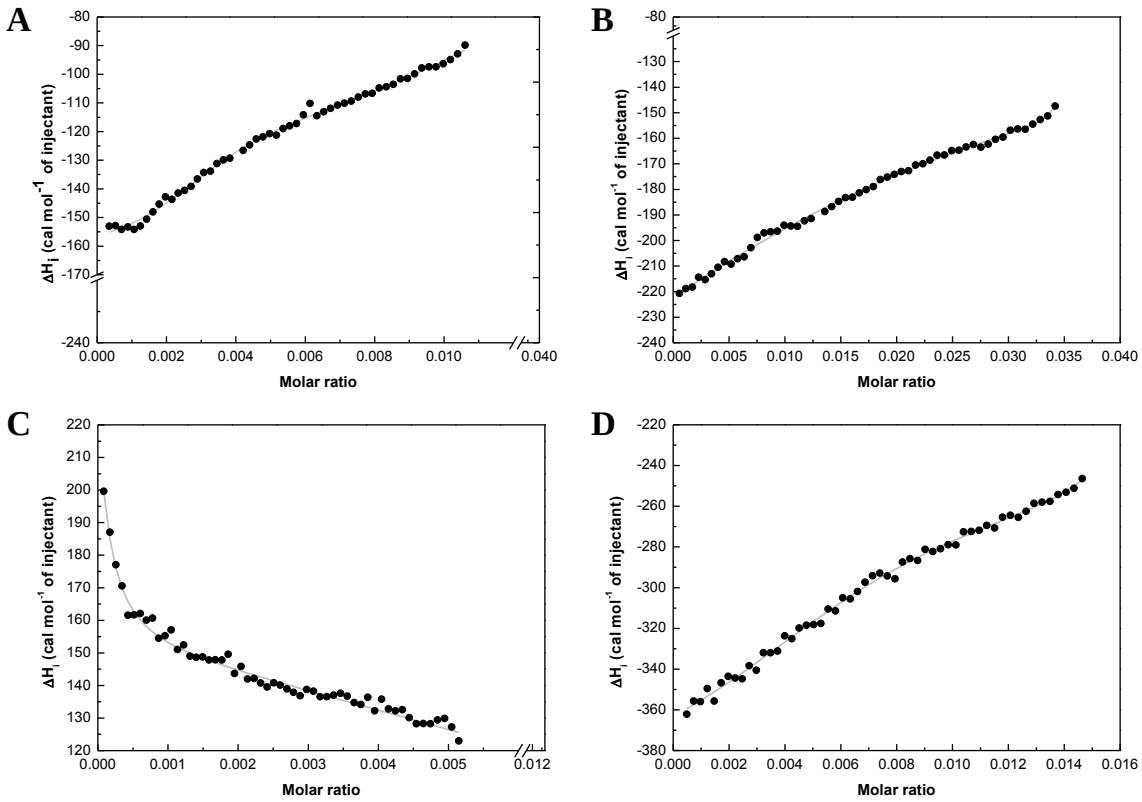

Figure 5.10: Isothermal titration calorimetry of glyceryl dibehenate SLN:CS:pDNA:CS into (A) mannitol and (B) trehalose; glyceryl tristearate SLN:CS:pDNA:CS into (C) mannitol and (D) trehalose. Each dot on the curve corresponds to the heat of reaction following 2 µL injection every 400 s at 25°C (cell volume = 1.436 mL). The solid lines in the plots represent the fitting to experimental data.

Table 5.4 depicts the interaction enthalpy of SLN:CS:pDNA:CS with both spray-drying excipients (mannitol and trehalose). Data demonstrated that SLN:CS:pDNA:CS based on glyceryl dibehenate presented low exothermic values when titrated onto excipients when compared with glyceryl tristearate SLN:CS:pDNA:CS. The same behavior was observed by with PAP-SLN microencapsulated in mannitol and trehalose in Chapter 4, section 4.4.7.. As previously explained, this can be related to the large presence of hydrogen bonding upon interaction between glyceryl dibehenate SLN with both excipients. However, others processes, such as electrostatic repulsions between the nanoparticles, can also influence these data. On the other hand, interaction enthalpies of glyceryl tristearate SLN:CS:pDNA:CS with both excipients presented more positive ΔH_i^i values compared with glyceryl dibehenate SLN:CS:pDNA:CS, reaching true positive ΔH_i^i values for

glyceryl tristearate SLN:CS:pDNA:CS titrated onto mannitol. This evidence indicated that, after interaction between SLN:CS:pDNA:CS and mannitol, the rupture of water solvation layer and/or the presence of dispersion forces took place. In addition, Table 5.4 also reveals that both the entropy change and the binding equilibrium constants resulting from the spray-dried glyceryl dibehenate SLN:CS:pDNA:CS are higher than those from the spray-dried glyceryl tristearate SLN:CS:pDNA:CS one. This characterization demonstrated the spray-drying of glyceryl dibehenate SLN:CS:pDNA:CS into mannitol and trehalose microspheres' formation was a more propitious process (yielding a higher entropy change). These variations may probably take place due to the relatively lower hydrophobic character and some steric restrictions of the nanoparticles, which facilitates the interaction with the spray-drying excipients via dipole-dipole interactions.

Table 5.4: Enthalpy (ΔH_i^i), entropy (ΔS_i^i), binding constant (K^i) and stoichiometry (n^i) of the interaction of glyceryl dibehenate and glyceryl tristearate SLN:CS:pDNA:CS with mannitol and trehalose (spray-drying excipients) at 25°C (mean±SD, n=3).

Spray-drying excipient	SLN:CS:pDNA:CS based on	$10^{-2}\Delta H_i^i$ (cal/mol)	ΔS_i^i (cal/mol)	$10^{-3}\ K^i$ (M^{-1})	$10^3 n^i$
Mannitol	Glyceryl dibehenate	-1.6±0.1	80.9±12.3	18.1±1.8	3.0±0.1
		-1.3±0.1	53.7±9.6	0.7±0.2	13.5±0.8
	Glyceryl tristearate	6.8±1.9	78.2±21.2	9.3±2.1	4.7±0.8
		22.3±2.2	38.1±12.5	0.1±0.1	36.9±11.4
Trehalose	Glyceryl dibehenate	-4.7±0.3	120.6±11.6	2419.0±300.0	6.8±0.4
		-1.1±0.1	116.9±22.4	1336.0±200.0	27.3±1.5
	Glyceryl tristearate	-4.1±0.1	103.5±18.2	304.0±75.0	6.7±0.1
		-2.5±0.1	89.6±15.4	54.3±17.7	16.3±0.6

5.4.8. Nanoparticle recovery from microspheres

The microencapsulated nanoparticles were intended re-disperse as isolate SLN:CS:pDNA:CS when in contact with the lung lining fluid upon rapid excipient (mannitol and trehalose) dissolution. Moreover, these excipients were expected to protect the SLN:CS:pDNA:CS, not only from heat but also against particle/particle interactions able to promote aggregation [43]. Herein, dry powders were incubated in PBS pH 7.4 containing 0.1% lung surfactant with the purpose to mimic the environmental conditions in deep lung. The physicochemical properties (mean particle size, polydispersity and surface charge) and the morphology of the recovered nanoparticles were then analysed

and compared to those of the original (fresh) ones (Table 5.5). The formulations maintained or presented a slight decrease in particle size after recovery from microspheres, keeping an acceptable polydispersity. This may be due to the partial loss of the CS layers that surrounds the SLN, which was supported by the change in zeta potential from positive values before microencapsulation (24.9±1.0 and 28.1±0.3 mV for glyceryl dibehenate and glyceryl tristearate SLN:CS:pDNA:CS respectively) to negative values after recovery. The particle size of all nanoformulations after being recovered obtained by PCS analysis was additionally confirmed by TEM (Figure 5.11).

Table 5.5: Mean nanoparticle size (nm), polydispersity index (PI) and zeta potential (ZP) after recovery from dry powders in PBS pH 7.4 with 0.1% lung surfactant (mean±SD, *n*=3).

	Glyceryl dibehenate SLN:CS:pDNA:CS			Glyceryl tristearate SLN:CS:pDNA:CS		
	∅ (nm)	PI	ZP (mV)	∅ (nm)	PI	ZP (mV)
Fresh SLN:CS:pDNA:CS	203±10	0.287±0.011	24.9±1.0	220±9	0.166±0.010	28.1±0.3
SLN:CS:pDNA:CS recovered from mannitol microspheres	182±4	0.121±0.030	-18.8±1.4	257±5	0.174±0.008	-17.7±1.1
SLN:CS:pDNA:CS recovered from trehalose microspheres	192±9	0.166±0.094	-20.4±0.4	182±6	0.170±0.055	-19.3±2.7

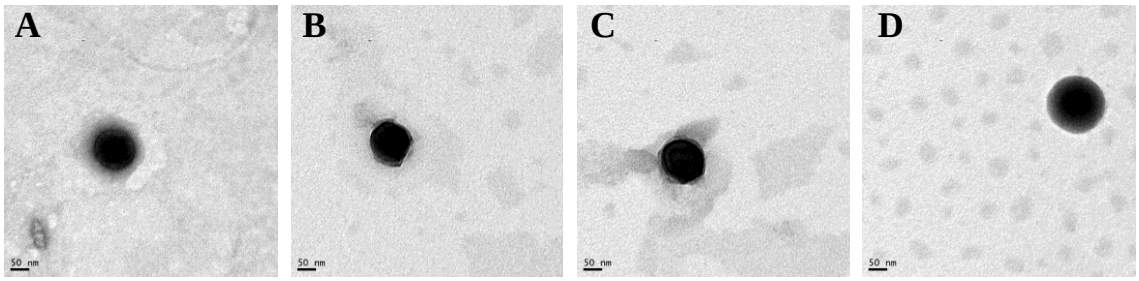

Figure 5.11: TEM micrographs of (A) glyceryl dibehenate and (B) glyceryl tristearate SLN:CS:pDNA:CS recovered from mannitol microspheres; (C) glyceryl dibehenate and (D) glyceryl tristearate SLN recovered from trehalose microspheres (scale bar: 50 nm).

5.4.9. Integrity of pDNA recovered from dry powders

The structural integrity of pEGFP-C1 was assessed after nanoparticle recovery from mannitol and trehalose microspheres. For this purpose, the recovered SLN:CS:pDNA:CS nanoparticles were subjected to the same treatment with chitosanase and, then, with BstBI. Gel electrophoresis confirmed the nanoparticles protected pEGFP-C1 from degradation during the spray-drying procedure (Figure 5.12). This suggests that at the physiological environment, where endonuclease concentration is markedly lower than the tested concentrations, such microencapsulated pDNA-polycationic nanoparticles should provide a significant protection for pEGFP-C1. Finally, these dry powders were also analysed using a specific nuclease, DNase I. The same positive results were obtained after incubation of the microspheres with this nuclease, further supporting that hybrid nanostructured microparticles provided protection to the incorporated pEGFP-C1 against degradation either by BstBI or by DNase I.

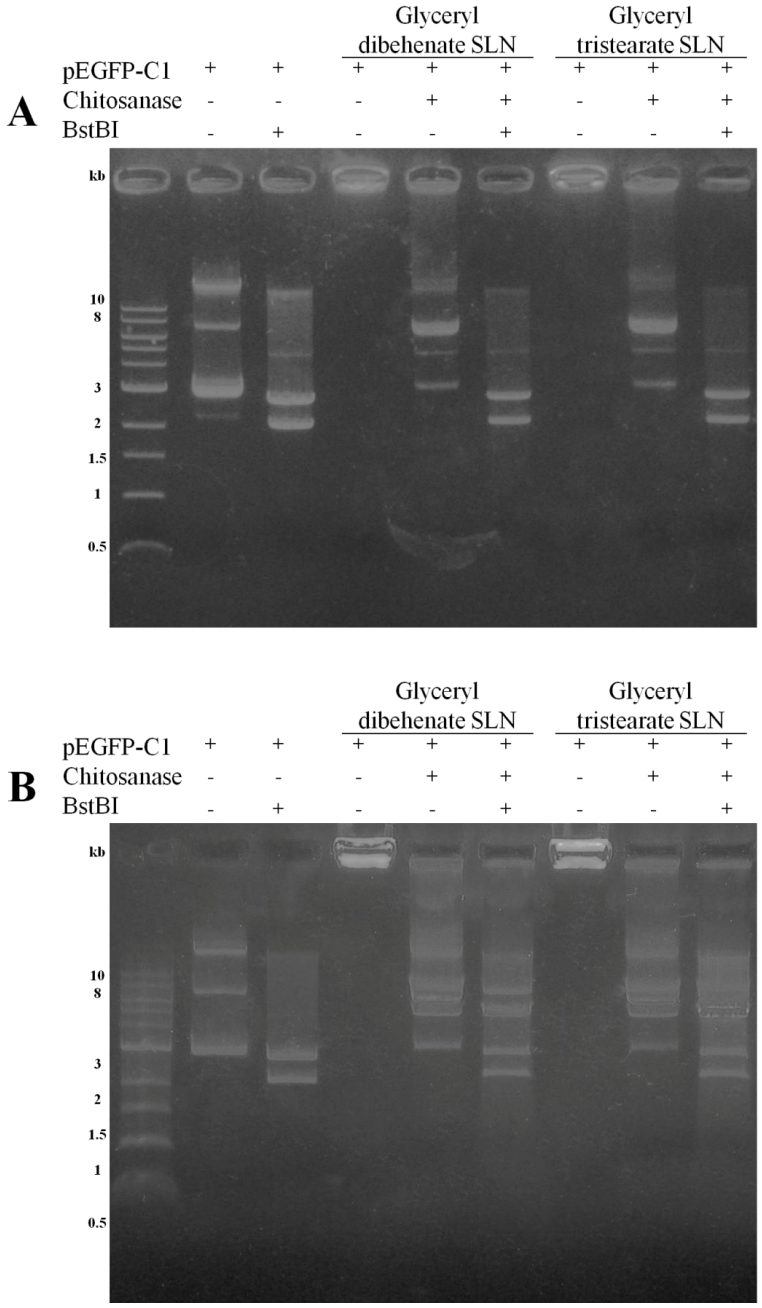

Figure 5.12: Agarose gel electrophoresis (0.7% in TBE) of pEGFP-C1 associated to SLN:CS:pDNA:CS nanocarriers following chitosanase and endonuclease (BstBI) digestions after recovery from (A) mannitol and (B) trehalose microspheres.

5.5. Conclusions

Stable polycationic SLN formulations loaded with pEGFP-C1 were successfully produced, showing a high affinity for the plasmid and providing protection to the

encapsulated pDNA from endonuclease degradation. As the nanoformulations showed low cell cytotoxicity while efficiently transfecting relevant pulmonary cell lines, they are a promising system for gene delivery, able to withstand further formulation into dry powders for inhalation. These were obtained by microencapsulation in mannitol and trehalose through a spray-drying technique, resulting in powders for pulmonary gene delivery containing intact and fully active pEGFP-C1. Finally, results suggested that microencapsulated SLN:CS:pDNA:CS could be a safe and effective vector for gene delivery following pulmonary administration.

5.6. References

1. Garnett, M.C. Gene-delivery systems using cationic polymers. Crit. Rev. Ther. Drug, 1999, 16 (2), 1-61.

2. del Pozo-Rodríguez, A.; Delgado, D.; Solinís, M.Á.; Pedraz, J.L.; Echevarría, E.; Rodríguez, J.M.; Gascón, A.R. Solid lipid nanoparticles as potential tools for gene therapy: *in vivo* protein expression after intravenous administration. Int. J. Pharm., 2010, 385 (1), 157-162.

3. Merkel, O.M.; Zheng, M.; Debus, H.; Kissel, T. Pulmonary gene delivery using polymeric nonviral vectors. Bioconjugate Chem., 2012, 23 (1), 3-20.

4. Liu, F.; Shollenberger, L.M.; Conwell, C.C.; Yuan, X.; Huang, L. Mechanism of naked DNA clearance after intravenous injection. J. Gene Med., 2007, 9 (7), 613-619.

5. Azarmi, S.; Roa, W.H.; Löbenberg, R. Targeted delivery of nanoparticles for the treatment of lung diseases. Adv. Drug Deliv. Rev., 2008, 60 (8), 863-875.

6. Woodle, M.C.; Lu, P.Y. Nanoparticles deliver RNAi therapy. Mater. Today, 2005, 8 (8), 34-41.

7. Choi, Y.H.; Liu, F.; Park, J.S.; Kim, S.W. Lactose-poly (ethylene glycol)-grafted poly-L-lysine as hepatoma cell-targeted gene carrier. Bioconjugate Chem., 1998, 9 (6), 708-718.

8. Boussif, O.; Lezoualc'h, F.; Zanta, M.A.; Mergny, M.D.; Scherman, D.; Demeneix, B.; Behr, J.-P. A versatile vector for gene and oligonucleotide transfer into

cells in culture and *in vivo*: polyethylenimine. Proc. Natl. Acad. Sci. USA, 1995, 92 (16), 7297-7301.

9. Haensler, J.; Szoka Jr, F.C. Polyamidoamine cascade polymers mediate efficient transfection of cells in culture. Bioconjugate Chem., 1993, 4 (5), 372-379.

10. Lim, Y.-B.; Han, S.-O.; Kong, H.-U.; Lee, Y.; Park, J.-S.; Jeong, B.; Kim, S.W. Biodegradable polyester, poly [α-(4-aminobutyl)-L-glycolic acid], as a non-toxic gene carrier. Pharmaceut. Res., 2000, 17 (7), 811-816.

11. Mao, H.-Q.; Roy, K.; Troung-Le, V.L.; Janes, K.A.; Lin, K.Y.; Wang, Y.; August, J.T.; Leong, K.W. Chitosan-DNA nanoparticles as gene carriers: synthesis, characterization and transfection efficiency. J. Control. Release, 2001, 70 (3), 399-421.

12. del Pozo-Rodriguez, A.; Delgado, D.; Solinís, M.A.; Gascon, A.R.; Pedraz, J.L. Solid lipid nanoparticles for retinal gene therapy: transfection and intracellular trafficking in RPE cells. Int. J. Pharm., 2008, 360 (1), 177-183.

13. Müller, R.H.; Mäder, K.; Gohla, S. Solid lipid nanoparticles (SLN) for controlled drug delivery - a review of the state of the art. Eur. J. Pharm. Biopharm., 2000, 50 (1), 161-177.

14. Heiati, H.; Tawashi, R.; Phillips, N.C. Drug retention and stability of solid lipid nanoparticles containing azidothymidine palmitate after autoclaving, storage and lyophilization. J. Microencapsul., 1998, 15 (2), 173-184.

15. zur Mühlen, A.; Schwarz, C.; Mehnert, W. Solid lipid nanoparticles (SLN) for controlled drug delivery-drug release and release mechanism. Eur. J. Pharm. Biopharm., 1998, 45 (2), 149-155.

16. Videira, M.; Almeida, A.J.; Fabra, À. Preclinical evaluation of a pulmonary delivered paclitaxel-loaded lipid nanocarrier antitumor effect. Nanomed.: Nanotechnol., 2012, 8 (7), 1208-1215.

17. Müller, R.H.; Rühl, D.; Runge, S.; Schulze-Forster, K.; Mehnert, W. Cytotoxicity of solid lipid nanoparticles as a function of the lipid matrix and the surfactant. Pharmaceut. Res., 1997, 14 (4), 458-462.

18. Yang, S.C.; Lu, L.F.; Cai, Y.; Zhu, J.B.; Liang, B.W.; Yang, C.Z. Body distribution in mice of intravenously injected camptothecin solid lipid nanoparticles and targeting effect on brain. J. Control. Release, 1999, 59 (3), 299-307.

19. Zara, G.P.; Cavalli, R.; Fundarò, A.; Bargoni, A.; Caputo, O.; Gasco, M.R. Pharmacokinetics of doxorubicin incorporated in solid lipid nanospheres (SLN). Pharmacol. Res., 1999, 40 (3), 281-286.

20. Roy, K.; Mao, H.-Q.; Huang, S.-K.; Leong, K.W. Oral gene delivery with chitosan-DNA nanoparticles generates immunologic protection in a murine model of peanut allergy. Nat. Med., 1999, 5 (4), 387-391.

21. Khatri, K.; Goyal, A.K.; Gupta, P.N.; Mishra, N.; Vyas, S.P. Plasmid DNA loaded chitosan nanoparticles for nasal mucosal immunization against hepatitis B. Int. J. Pharm., 2008, 354 (1), 235-241.

22. Cadete, A.; Figueiredo, L.; Lopes, R.; Calado, C.C.R.; Almeida, A.J.; Gonçalves, L.M.D. Development and characterization of a new plasmid delivery system based on chitosan - sodium deoxycholate nanoparticles. Eur. J. Pharm. Sci., 2012, 45 (4), 451-458.

23. Guliyeva, Ü.; Öner, F.; Özsoy, Ş.; Haziroğlu, R. Chitosan microparticles containing plasmid DNA as potential oral gene delivery system. Eur. J. Pharm. Biopharm., 2006, 62 (1), 17-25.

24. Mansouri, S.; Cuie, Y.; Winnik, F.; Shi, Q.; Lavigne, P.; Benderdour, M.; Beaumont, E.; Fernandes, J.C. Characterization of folate-chitosan-DNA nanoparticles for gene therapy. Biomaterials, 2006, 27 (9), 2060-2065.

25. Mansouri, S.; Lavigne, P.; Corsi, K.; Benderdour, M.; Beaumont, E.; Fernandes, J.C. Chitosan-DNA nanoparticles as non-viral vectors in gene therapy: strategies to improve transfection efficacy. Eur. J. Pharm. Biopharm., 2004, 57 (1), 1-8.

26. Gonçalves, L.M.D.; Cadete, A.; Figueiredo, L.; Calado, C.C.R.; Almeida, A.J., editors. Biodegradable nanoparticles of Alginate and chitosan as non-viral DNA oral delivery system. 1st Portuguese Meeting in Bioengineering (ENBENG); 2011: IEEE.

27. Mehanna, C.; Baudouin, C.; Brignole-Baudouin, F. Spectrofluorometry assays for oxidative stress and apoptosis, with cell viability on the same microplates: A multiparametric analysis and quality control. Toxicol. in vitro, 2011, 25 (5), 1089-1096.

28. Grenha, A.; Seijo, B.; Serra, C.; Remuñán-López, C. Chitosan nanoparticle-loaded mannitol microspheres: structure and surface characterization. Biomacromolecules, 2007, 8 (7), 2072-2079.

29. Inouye, S.; Tsuji, F.I. Aequorea green fluorescent protein. FEBS letters, 1994, 341 (2-3), 277-280.

30. Zhao, X.; Yu, S.-B.; Wu, F.-L.; Mao, Z.-B.; Yu, C.-L. Transfection of primary chondrocytes using chitosan-pEGFP nanoparticles. J. Control. Release, 2006, 112 (2), 223-228.

31. Kim, W.; Yamasaki, Y.; Kataoka, K. Development of a fitting model suitable for the isothermal titration calorimetric curve of DNA with cationic ligands. J. Phys. Chem. B, 2006, 110 (22), 10919-10925.

32. Bisht, S.; Bhakta, G.; Mitra, S.; Maitra, A. pDNA loaded calcium phosphate nanoparticles: highly efficient non-viral vector for gene delivery. Int. J. Pharm., 2005, 288 (1), 157-168.

33. Kremers, G.-J.; Goedhart, J.; van den Heuvel, D.J.; Gerritsen, H.C.; Gadella, T.W.J. Improved green and blue fluorescent proteins for expression in bacteria and mammalian cells. Biochemistry, 2007, 46 (12), 3775-3783.

34. Csaba, N.; Köping-Höggård, M.; Alonso, M.J. Ionically crosslinked chitosan/tripolyphosphate nanoparticles for oligonucleotide and plasmid DNA delivery. Int. J. Pharm., 2009, 382 (1), 205-214.

35. Raviña, M.; Cubillo, E.; Olmeda, D.; Novoa-Carballal, R.; Fernandez-Megia, E.; Riguera, R.; Sánchez, A.; Cano, A.; Alonso, M.J. Hyaluronic acid/chitosan-g-poly (ethylene glycol) nanoparticles for gene therapy: an application for pDNA and siRNA delivery. Pharmaceut. Res., 2010, 27 (12), 2544-2555.

36. Rodrigues, S.; Cordeiro, C.; Seijo, B.; Remuñán-López, C.; Grenha, A. Hybrid nanosystems based on natural polymers as protein carriers for respiratory delivery: stability and toxicological evaluation. Carbohyd. Polym., 2015, 123 (1), 369-380.

37. Rodrigues, S.; Dionísio, M.; López, C.; Grenha, A. Biocompatibility of chitosan carriers with application in drug delivery. J. Funct. Biomater., 2012, 3 (3), 615-641.

38. Fotakis, G.; Timbrell, J.A. *In vitro* cytotoxicity assays: comparison of LDH, neutral red, MTT and protein assay in hepatoma cell lines following exposure to cadmium chloride. Toxicology letters, 2006, 160 (2), 171-177.

39. Shi, L.; Günther, S.; Hübschmann, T.; Wick, L.; Harms, H.; Müller, S. Limits of propidium iodide as a cell viability indicator for environmental bacteria. Cytom. Part A, 2007, 71 (8), 592-598.

40. Gao, X.; Kim, K.-S.; Liu, D. Nonviral gene delivery: what we know and what is next. AAPS J., 2007, 9 (1), E92-E104.

41. Delgado, D.; del Pozo-Rodríguez, A.; Solinís, M.Á.; Rodríguez-Gascón, A. Understanding the mechanism of protamine in solid lipid nanoparticle-based lipofection: the importance of the entry pathway. Eur. J. Pharm. Biopharm., 2011, 79 (3), 495-502.

42. Dastan, T.; Turan, K. *In vitro* characterization and delivery of chitosan-DNA microparticles into mammalian cells. J. Pharm. Pharm. Sci., 2004, 7 (2), 205-214.

43. Tewa-Tagne, P.; Briançon, S.; Fessi, H. Preparation of redispersible dry nanocapsules by means of spray-drying: development and characterisation. Eur. J. Pharm. Sci., 2007, 30 (2), 124-135.

Chapter 6

Concluding remarks and future work

This page was intentionally left blank.

6.1. Conclusions

The work described in this dissertation aimed at developing a novel pulmonary drug delivery system based on an innovative strategy involving hybrid nanostructured microparticles intended for deep-lung delivery of various active agents.

Lipid based carriers, with the main focus on SLN, are a promising nanoparticulate delivery system for the pharmaceutical industry, allowing large scale production, while avoiding the use of organic solvents usually needed for polymeric nanoparticle production. In addition, under optimized condition, SLN can also be freeze-dried and spray-dried to yield stable pharmaceutical powders for inhalation.

The present work also takes advantage of the pulmonary route for treatment of respiratory diseases. Drug inhalation enables a rapid and predictable onset of action and induces fewer side effects compared to other delivery routes, such as the oral administration. However, pulmonary drug delivery must target the deep lung region, which requires the use of particles ranging in d_{aer} from 1 to 5 μm. The control of particle size distribution is critical to achieve an efficient and reproducible pulmonary deposition. For this purpose, SLN were encapsulated in mannitol and trehalose microspheres through a suitable spray-drying technique, resulting in dry powders with the properties required for lung administration.

The SLN based on glyceryl dibehenate and glyceryl tristearate were successfully assessed as potential nanocarriers for the encapsulation and/or incorporation of different active agents, such as a low MW anti-TB drug (RFB), a model protein drug (PAP) and a model nucleic acid (pEGFP-C1). Nanoparticles provided adequate physicochemical properties and afforded stability and protection of the incorporated agent, showing that SLN could act as a suitable and versatile platform for the delivery of several drugs. The SLN-containing microspheres were prepared by spray-drying using pharmaceutically acceptable excipients (mannitol or trehalose) and appropriately characterized in order to comply with the characteristics required for lung administration. Further studies, particularly, *in vitro* and *in vivo* approaches were carried out for the selected microsphere-based systems. The main goals and achievements obtained are summarized as follows.

From a technological standpoint, two different SLN compositions were formulated and optimized using a HSH method as a preparation technique. These SLN presented a high performance in terms of EE and DL regarding RFB and PAP incorporation, being

biocompatible when incubated with relevant pulmonary cell lines (Calu-3 e A549) and being easily taken up by macrophages. This is particularly important since macrophages are the host cells for *M. tuberculosis*, becoming an effective targeted approach to pulmonary TB therapy. Concerning pEGFP-C1 entrapment, the SLN were previously surface-modified with a cationic polymer (CS), allowing DL through electrostatic interactions between the positively charged coating material and the negatively charged DNA, conferring protection against specific endonucleases.

Spray-drying of the SLN with mannitol or trehalose as excipients, resulted in free-flowing dry powders composed by spherical and well-defined nanostructured microparticles, with good handling and aerodynamic properties for lung deposition. For that purpose, the spray-drying process was optimized for aspirator rate, spraying air flow pressure and T_{inlet} parameters. Physicochemical characterization, including density, Carr's index, Hausner ratio and residual moisture content, showed that the developed spray-drying process generated particles for inhalation with uniform particle size distribution and good flow properties. Moreover, this microencapsulation process allowed remaining intact and fully active the pharmaceutics incorporated in the SLN, demonstrating by the *in vitro* activity studies against *M. avium* for RFB formulations, by the SDS-PAGE assay for PAP dry powders and by endonucleases digestion for pEGFP-C1 modified nanocarriers.

Thermodynamic analysis using ITC provided valuable insights into the energetic description of the interaction between SLN and the spray-drying excipients (mannitol and trehalose) and an additional understanding of the *in vitro* release behaviour of RFB and PAP from these SLN. Studies using the two-stage impinger (Ph. Eur. 2.9.18, Apparatus A) show that a high fraction of RFB- and PAP-SLN formulations could reach the airways with a low swallowed fraction. The spray-dried microspheres are expected to dissolve quickly after landing on the aqueous covered epithelium of the lung. *In vitro* results showed that the delivered nanoparticles were released immediately after contact with an aqueous medium containing a lung surfactant, maintaining their original physicochemical properties. In addition, the determination of the *in vitro* RFB and PAP release profiles from the hybrid formulations gives us a good insight on how the particles would behave when administered in an *in vivo* model. Remarkably, it could be observed that almost all the drug was released from SLN and dry powders under the assayed conditions. This sustained release could reduce the number of doses, improving patient compliance.

In vivo experiments were conducted to further analyze the biodistribution of microencapsulated RFB-loaded SLN after pulmonary administration to mice. The studies demonstrated that non-metabolized RFB could achieve the studied organs, reducing the *M. tuberculosis* infection of a murine model compared to untreated control.

As a conclusion, versatile SLN-based drug delivery systems were successfully developed as potential carriers for the encapsulation and/or adsorption of pharmaceuticals with different physicochemical characteristics. Through a spray-drying technique, these nanocarriers were effectively microencapsulated in dry powders form for pulmonary delivery. The development of these hybrid nanostructured microparticles included optimization of composition, manufacturing process, physicochemical characteristics, *in vitro* release, stability studies, cytotoxicity, compatibility, physical interactions analysis between nanoparticles and spray-drying excipients and, finally, aerodynamic and flow performance. Furthermore, this work may provide a promising proof-of-concept for further clinical application in the treatment of lung diseases, such as TB.

6.2. Future work

In the follow up of this work, supplementary *in vivo* experiments involving biodistribution studies and determination of drug concentration in the target organs, as well as the biological evaluation in a *M. tuberculosis* infection model, should be pursued in order to prove the therapeutic efficacy of the developed anti-TB formulations. In this context, bioluminescence imaging studies would be useful to elucidate the nanostructured microparticles distribution along the *pulmonary tree*.

Finally, while an ideal general drug-delivery platform for inhalation may hardly be achieved, hybrid drug delivery systems that incorporate the benefits of various approaches will be tailored to address the needs of specific applications. This appears as an obvious consequence of the knowledge gathered during these studies that clearly point out to the development of a hybrid drug delivery system. Preliminary studies not included in this thesis have already shown the hybrid nanostructured microparticles may integrate both lipophilic (within the SLN) and hydrophilic drugs (in the aqueous phase of the spray-drying excipient) in the same formulation, allowing the co-formulation of hydrophilic and lipophilic drugs, which increases the versatility of this approach.

This page was intentionally left blank.